Copyright is owned by the Author of the thesis. Permission is given for a copy to be downloaded by an individual for the purpose of research and private study only. The thesis may not be reproduced elsewhere without the permission of the Author.

AN INVESTIGATION INTO NON-DESTRUCTIVE TESTING STRATEGIES AND IN-SITU SURFACE FINISH IMPROVEMENT FOR DIRECT METAL PRINTING WITH SS 17-4 PH

A THESIS PRESENTED IN PARTIAL FULFILMENT OF THE REQUIREMENTS FOR

THE DEGREE OF

DOCTOR OF PHILOSOPHY

IN

ENGINEERING

AT MASSEY UNIVERSITY, ALBANY

NEW ZEALAND.

TANISHA PEREIRA

2021

PREFACE

The author declares that this is her own work except where due acknowledgement has been given. It is being submitted for the PhD in Engineering, majoring in Mechatronics to Massey University, New Zealand.

This thesis describes the research carried out by the author at the School of Engineering and Advanced Technology, Massey University, Albany, New Zealand from August 2017 to August 2021, supervised by Prof J. Potgieter, Dr John V. Kennedy, Dr Mathew Legg and Dr Jonathan Zyzalo.

ACKNOWLEDGEMENTS

The completion of this thesis would not have been realized without the support of many amazing people, and I would love to acknowledge the contribution of advice, wisdom, financial aid, and encouragement I received from my friends, family, colleagues, supervisors, funding organizations, and testing facilities around New Zealand.

I would love to equally thank my supervisors Prof J. Potgieter from Massey University and Dr John V. Kennedy from GNS Science, for expertly providing guidance, funding, and insight throughout this project, to help me develop my skills as a researcher. Thank you for the patience, understanding and support you showed me when I was struggling and the constant encouragement and bolstering you provided to help me believe I could finish the PhD. Thank you to my other supervisors Dr Mathew Legg and Dr Jonathan Zyzalo for their assistance and mentoring at different stages of this project.

This experimental work within this thesis would not have been possible without the provision of testing equipment and aid from Massey University (Dr Khalid Arif), GNS Science (Jerome, John, and George), TiDA Ltd (Aamir and Beb), X-Ray Laboratory, University of Auckland, Callaghan Innovation, and the support of the Massey Engineering workshop technicians (Sean Rasmussen, Gabriel Phang, Blair Dixon and Kartikay Lal). Thank you to my summer work students Callum Clark and Christina Eagle for their help with some of the testing.

Primary funding support for this research was provided by NZ Product Accelerator, to whom I am extremely grateful. Additionally, I was unequivocally thankful to the funding I received from the Ken and Elizabeth Powell Bursary, NZ Federation of Graduate Woman North Shore Branch Scholarship, and the Massey University Conference Presentation Grant.

I would like to acknowledge the many current and former Massey University colleagues and friends that I have had the incredible joy and pleasure of working with. Especially, Baden Parr, Asif Rehmani and Dr Mohammed Harris (three of the smartest and hardest working people I got to know), for constantly inspiring me, encouraging me, and helping me to complete my PhD. Thank you to Amy Gardener, Dr Juan Schutte, David Smith, Dr Daniel Konings and Blair Dixon for their continued support, coffee and lunch dates and stress-relieving ranting sessions that helped me overcome the built-up anxiety and frustration whenever I encountered hurdles.

Personally, I would love to thank my mum for her unwavering love, support, and encouragement throughout this PhD and for patiently dealing with my dissertation exasperation. Thank you to the many friends who supported me and provided some normalcy for me to escape to.

ABSTRACT

Additive Manufacturing (AM) technologies have the potential to create complex geometric parts that can be used in high-end product industries, aerospace, automotive, medical etc. However, the surface finish, part-to-part reliability, and machine-to-machine reliability has made it difficult to qualify the process for load dependent structures. The improvement of surface finish on metal printed parts, is a widely sought solution by these high-end industries and non-destructively characterizing the mechanical aptitude of metal printed parts, would pave the way for quality assessment strategies used to certify additively manufactured parts. This thesis examines the capability of laser polishing and non-destructive testing technologies and methods to address these difficulties.

This research study presents an investigation into quality management strategies for Direct Metal Printing (DMP) with powdered Stainless Steel 17-4 PH. The research aim is split into two key categories: to improve the surface finish of metal additive manufactured parts and to non-destructively characterize the impact of defects (metallurgical anomalies) on the mechanical properties of the printed part. To improve surface finish of a printed part, a novel methodology was tested to laser polish the Laser-Powder Bed Fusion (L-PBF) parts during print with the built-in laser. Numerous technologies for non-destructive testing techniques already exist, and in the duration of this doctoral study various technologies were explored. However, the final solution focuses on layer-wise capture with a versatile low-cost imaging system, retrofitted within the DMP machine, to capture each layer following the lasering process. In addition, the study also focuses on progressing the characterization of data (images), using a combination of image processing, 3D modelling and Finite-Element-Analysis to create a novel strategy for replicating the as-built specimen as a computer-aided design model and performing simulated fatigue failure analysis on the part.

This thesis begins with a broadened justification of the research need for the solutions described, followed by a review of literature defining existing techniques and methods pertaining to the solutions, with validation of the research gap identified to provide novel contribution to the metal additive manufacturing space. This is followed by the methodologies developed, to firstly, control the laser parameters within the DMP and examine the influence of these parameters using surface profilometry, scanning electron microscopy and mechanical hardness testing. The control variables in this methodology combines laser parameters (laser power, scan speed and polishing iterations) and print orientation (polished surface angled at 0º, 20º, 40º, 60º, 80º and 90º degree increments from the laser), using several Taguchi designs of experiments and statistical analysis to characterize the experimental results.

The second methodology describes the retrofitted imaging system, image processing techniques and analysis methods used to reconstruct the 3D model of a standard square shaped part and one with synthesized defects. The method explores various 2D to 3D extrusion-based techniques using a combination of code-based image processing (Python 3, OpenCV and MATLAB image processing toolbox) and ready-made software tools (Solidworks, InkTrace, ImageJ and more).

Finally, the new research findings are presented, including the results of the laser polishing study demonstrating the successful improvement of surface finish. The discussion surrounding these results, highlights the most effective part orientation for laser polishing the outline of an AM part and the most effective laser parameter combination resulting in the most significant improvement to surface finish (roughness and profile height variation). Summarily, the best improvement in surface roughness was achieved with the ∠80 angled surface with the laser speed, laser power and polishing iterations set to 500mm/s, 30W, 3 respectively. The sample set total average measured a 16.7% decrease in Ra. NDT digital imaging, thermal imaging and acoustic technologies were considered for defect capture in metal AM parts. The solution presented is primarily focused on the expansion of research to process digital images of each part layer and examine strategies to move the research from a data capture stage to a data processing strategy with quantitative measurement (FEA analysis) of the printed part's mechanical properties. In addition, the results discuss a method to create feedback to the DMP to selectively melt problematic areas, by re-creating the sliced part layers but removing the well-melted areas from the laser scanning pattern.

The methods and technological solutions developed in this research study, have presented novel data to further research these methods in the pursuit of quality assurance for AM parts. The work done has paved the way for more the research opportunities and alternative methods to be explored that complement the methods detailed here. For example, using a combination of in-situ laser polishing, followed by post-processing the AM specimens in an acid-based chemical bath. Alternatively, further exploring acoustic NDT techniques to create an in-built acoustic-based imaging device within the AM machine. Finally, this thesis cross-examines the work done to answer the research questions established at the start of the thesis and verify the hypotheses stated in the methods chapter.

TABLE OF CONTENTS

PREFACE ..... **I**

ACKNOWLEDGEMENTS ..... **II**

ABSTRACT ..... **III**

TABLE OF CONTENTS ..... **V**

LIST OF FIGURES ..... **VIII**

LIST OF TABLES ..... **XI**

LIST OF TERMS AND DEFINITIONS ..... **XIII**

LIST OF PUBLICATIONS ..... **XV**

1 INTRODUCTION **1**

1.1 Background and Motivation 1

1.1.1 Summary of research focus on quality strategies to improve the surface finish of Metal AM parts *2*

1.1.2 Summary of research focus on quality strategies to investigate defects in Metal AM parts *3*

1.1.3 Personal Motivations *5*

1.2 Thesis Objectives and Research Questions 5

1.3 Thesis Structure 6

1.4 Additive Manufacturing 8

1.4.1 Manufacturing Regions *9*

1.4.2 Economic Strategies *11*

1.4.3 Quality Assurance and Quality Control for AM *13*

1.4.4 Industry Surveying *16*

CHAPTER 2 ..... **17**

2 STATE OF ART **17**

2.1.1 Metal Additive Manufacturing *17*

2.2 Laser Powder Bed Fusion 19

2.2.1 Process Parameters *20*

2.2.2 Surface Finish in AM *23*

2.2.3 State of Art for Surface Finish improvement techniques *25*

2.3 Non-Destructive Testing in AM 29

2.3.1 Defects in LPBF parts and Defect Formation Mechanism 29
2.3.2 State of art for NDT testing in Metal AM 35
2.4 In-situ Optical Imaging Technologies and Processing for Defect Capture and Identification 38
CHAPTER 3 43
3 METHODOLOGY 43
3.1 Direct Metal Printing 44
3.1.1 Optimization of setup, printing, and post processing for the DMP printer 45
3.1.2 Results of calibration tests for best scan settings 46
3.2 Stainless Steel 17-4 PH 47
3.2.1 Chemical Composition 48
3.2.2 Mechanical Properties for parts built in a DMP ProX 100 48
3.3 Case study 1: Characterization of in-situ Laser polished DMP SS 17-4 PH surfaces 49
3.3.1 Methodology 50
3.3.2 Surface Profilometry Data Representation 57
3.3.3 Optical Topographic Analysis 58
3.3.4 Hardness testing 59
3.3.5 RPD DOE Analysis Methodology 59
3.4 Case study 2: Quality Monitoring Strategies using Non-Destructive Testing Systems 61
3.4.1 Methodology 64
3.5 summary 77
CHAPTER 4 78
4 CHARACTERIZATION OF IN-SITU LASER-POLISHED DMP SS 17-4 PH SURFACES 78
4.1 SS 17-4PH Direct Metal Printed Test Specimens 80
4.2 Statistical RPD Analysis of – T samples 81
4.3 Statistical Analysis of RPD L9 experiments after laser polishing the outline of the external ANgled walls for the SS 17-4 PH test specimens 84
4.3.1 ANOVA for Ra 87
4.3.2 Regression Analysis for each L9 RPD 92
4.3.3 SEM Surface Defects and Layer Thickness Analysis 93
4.4 Discussion 95
CHAPTER 5 100
5 QUALITY MONITORING STRATEGIES USING NON-DESTRUCTIVE TESTING SYSTEMS 100
5.1 Practical developments with NDT Testing methods 101
5.1.1 Digital and Thermal In-Situ Monitoring System 101

5.2 SOFTWARE DEVELOPMENT FOR NDT STRATEGIES 106
5.2.1 Detection of Parts and Defect with metric Sizing 106
5.2.2 2D to 3D layer Extrusion 109
5.2.3 Layer Surface Profile Mapping 111
5.3 NDT CALIBRATION AID FOR DMP PROX 100 112
5.4 ALTERNATIVE NDT METHODS 113
5.5 DISCUSSION 116

CHAPTER 6 121

6 FUTURE WORK AND RECOMMENDATIONS 121

CHAPTER 7 124

7 SUMMARY OF RESEARCH OUTPUTS 124

8 CONCLUSION 128

REFERENCES 130

APPENDIX 136

APPENDIX A – CHAPTER 3 PARTS IN IN-SITU MONITORING SYSTEM 136

8.1.1 Final Design Hardware 136

APPENDIX B – CHAPTER 4 – LASER POLISHING RESULTS 139

APPENDIX C – CHAPTER 3 – CODE DEVELOPED FOR IN-SITU MONITORING GUIS AND IMAGE PROCESSING 145

APPENDIX D – CHAPTER 5 – PART SIZING EXAMPLES 159

APPENDIX E – CHAPTER 3 – 3D TEXTURE APPLICATION EXAMPLE 163

APPENDIX F – CHAPTER 5 – DEFECT DETECTION ATTEMPTS 163

APPENDIX G – CHAPTER 1 – INDUSTRY SURVEYING 164

APPENDIX H – STATEMENT OF CONTRIBUTION FOR PUBLICATIONS 166

LIST OF FIGURES

FIGURE 1-1. SUMMARY OF AM TECHNOLOGIES AND CHARACTERIZATION; SLA: STEREOLITHOGRAPHY, DLP: DIGITAL LIGHT PROCESSING, CDLP: CONTINUOUS DIGITAL LIGHT PROCESSING, BJ: BINDER JETTING, MJF: MULTI JET FUSION, LENS: LASER ENGINEERING NET SHAPE, EBM: ELECTRON BEAM MELTING, LM: LASER MELTING, MJ: MATERIAL JETTING, FDM: FUSED DEPOSITION MODELLING, LS: LASER SINTERING, LOM: LAMINATED OBJECT MANUFACTURING AND DOD: DEEP-ON DEMAND. 8

FIGURE 1-2 TITANIUM METAL AM ACETABULAR CUP 9

FIGURE 1-3 STEREOLITHOGRAPHY AM MOULD FOR HEARING AIDS 9

FIGURE 1-4 POWDER-BED-FUSION, LASER-SINTERING AM PRINTED MOBILE PHONE CASES 9

FIGURE 1-5 AM VS TM MANUFACTURING FEASIBILITY WITH REFERENCE TO VOLUME, COMPLEXITY AND CUSTOMIZATION .. 11

FIGURE 2-1 POWDER BED FUSION PROCESS 18

FIGURE 2-2 DIRECTED ENERGY DEPOSITION PROCESS 18

FIGURE 2-3 SHEET LAMINATION PROCESS 18

FIGURE 2-4 BINDER JETTING PROCESS 18

FIGURE 2-5 CAD MODEL OF A LASER-POWDER-BED-FUSION ADDITIVE MANUFACTURING SYSTEM (MODELLED AFTER THE DMP PROX100 PRINTER USED IN THIS STUDY) 19

FIGURE 2-6 SURFACE PROFILE CHARACTERISTICS; TOTAL PROFILE, WAVINESS PROFILE, ROUGHNESS PROFILE AND LAY 24

FIGURE 2-7 EXAMPLE OF A METAL AM LASER-POLISHED SURFACE 27

FIGURE 2-8 SURFACE LASER POLISHING 27

FIGURE 2-9 EXAMPLE OF SHRINKAGE AND EXTREME SURFACE DEFECTS IN DMP PRINTED SS 17-4 PH CALIBRATION TENSILE DOG BONES 33

FIGURE 2-10 APPLICABILITY OF VARIOUS NDT METHODS TO THE PRIMARY QUALITY CONCERNS IN ADDITIVE MANUFACTURING. N – NOT APPLICABLE, S - SURFACE SENSITIVE, I - INTERNAL OR THROUGH-THICKNESS, Y - APPLICABLE, * 36

FIGURE 2-11 THERMAL IMAGE OF METAL PRINTED CUBES USING A LOW-COST COMMERCIAL THERMAL CAMERA 40

FIGURE 3-1 DMP PROX 100 ORIGINAL BUILD CHAMBER 44

FIGURE 3-2 HEXAGONAL PRINTING PATTERN FOR ONE SLICE OF A DMP PRINTED ASTM E8 TENSILE DOG BONE 44

FIGURE 3-3 DMP PRINTING PROCESS: PRE-PROCESSING, PRINT AND POST-PROCESSING STEPS 45

FIGURE 3-4 CLOSE UP OF VOIDS ON THE TOP SURFACE OF ONE CALIBRATION PRINT 45

FIGURE 3-5 CAPTURE OF CALIBRATION PLATES WITH TABLE 1-1 LASER PARAMETERS 46

FIGURE 3-6 CALIBRATION FULL PLATE TEST WITH TESTS (A) 90% LP -2MM LASER DEFOCUS, (B) 90% LP 2MM LASER DEFOCUS, (C) 98% LP 2MM LASER DEFOCUS, AND (D) 98% LP -2MM LASER DEFOCUS 47

FIGURE 3-7 SELECTED IMAGES FROM SPECTRUM ANALYSIS OF RECYCLED SS 17-4 PH POWDER 48

FIGURE 3-8 SURFACE REFERENCES: (A) TOP SURFACE, (B) ANGLED WALL/SURFACE, (C) VERTICAL WALL/SURFACE, (D) INNER WALL/SURFACE/CHANNEL. 51

FIGURE 3-9 FRONT AND SIDE VIEW OF ANGLED SURFACE ORIENTATION FOR 20º, 40º, 60º, 80º AND 90º. *PART ORIENTATION (PO) AND LASER ANGLE (LA). **SIDE VIEW (SV) AND FRONT VIEW (FV) 52

FIGURE 3-10 DMP PROX MANUFACTURING SOFTWARE INTERFACE 53
FIGURE 3-11 LASER SPEED 100 MM/S WITH APPROPRIATE COMPENSATIONS 53
FIGURE 3-12 LASER SPEED 500 MM/S WITH APPROPRIATE COMPENSATIONS 53
FIGURE 3-13 LASER SPEED 1000 MM/S WITH APPROPRIATE COMPENSATIONS 53
FIGURE 3-14 CREATING ZONE LAYERS TO POLISH 1X 53
FIGURE 3-15 CREATING ZONE LAYERS TO POLISH 3X 53
FIGURE 3-16 CREATING ZONE LAYERS TO POLISH 5X 53
FIGURE 3-17 HEXAGON (LEFT) VS OUTLINE STYLE (RIGHT) 54
FIGURE 3-18 SURFACE ROUGHNESS DATA INTERPRETATION AND REFERENCE 57
FIGURE 3-19 SCANNING DIRECTIONS FOR SURFACE PROFILOMETRY TESTING OF SS 17-4 PH PRINTED SAMPLES 58
FIGURE 3-20 (A) SEM IMAGE OF SS 17-4 PH REPOLISHED SAMPLE WITH LAYER THICKNESS MEASUREMENT AND INCLUSION MEASUREMENT (B) OPTICAL MICROSCOPE STAGE AND IMAGE CAPTURE 58
FIGURE 3-21 IMAGEJ MECHANICAL HARDNESS ACQUISITION FOR THE SS 17-4 PH SAMPLES 59
FIGURE 3-22 DMP PROX 100 PRINTING CHAMBER DIMENSIONS 65
FIGURE 3-23 DMP PROX 100 PRINTING CHAMBER BACK PLATE DIMENSIONS 65
FIGURE 3-24 ORIGINAL DMP PROX 100 BUILD CHAMBER 66
FIGURE 3-25 DMP PROX 100 PRINTING CHAMBER WITH RETROFITTED IMAGING SYSTEM 66
FIGURE 3-26 FRONT VIEW OF THE DMP PROX 100 PRINTING CHAMBER WITH RETROFITTED IMAGING SYSTEM 66
FIGURE 3-27 DIGITAL CAMERA GUI 67
FIGURE 3-28 DIGITAL CAMERA CHECKERBOARD CALIBRATION 67
FIGURE 3-29 THERMAL CAMERA GUI VIDEO CAPTURE 67
FIGURE 3-30 THERMAL CAMERA VIDEO POST PROCESSING FOR IMAGE CAPTURE 67
FIGURE 3-31 (A) MODEL OF SQUARE TEST SPECIMEN REPRESENTING THE TRUE SAMPLE SPECIMEN (DIMENSIONS IN MM). (B) SQUARE SPECIMEN WITH SYNTHESIZED DEFECTS IN MM (WIDTHS: 0.01, 0.02, 0.03, 0.04, 0.05 AND LENGTH: 10MM) 68
FIGURE 3-32 TYPICAL PROCESS STEPS TO EXTRACT KEY DATA POINTS SUCH AS EDGES, COLOUR GRADIENTS AND MORE 68
FIGURE 3-33 ORIGINAL STANDARD LAYER IMAGE WITH NO PROCESSING 69
FIGURE 3-34 ORIGINAL DEFECTIVE LAYER IMAGE WITH NO PROCESSING 69
FIGURE 3-35 GRAYSCALE STANDARD LAYER IMAGE (MATLAB) 69
FIGURE 3-36 GRAYSCALE DEFECTIVE LAYER IMAGE (MATLAB) 69
FIGURE 3-37 3D TEXTURE EXTRUSION METHOD 74
FIGURE 3-38 BITMAP TRACE AND DXF CONTOUR EXTRUSION 74
FIGURE 3-39 EXTRUSION METHOD USING *SVG FILE AND BLENDER EXTRUSION TO CREATE STL 75
FIGURE 4-1 VERTICAL SAMPLES ARRANGED WITH THE AFFECTED SURFACE PERPENDICULAR TO MEASURING TOOL 80
FIGURE 4-2 ∠20, ∠40, ∠60, ∠80 SAMPLES ARRANGED WITH THE AFFECTED SURFACE PERPENDICULAR TO MEASURING TOOL 80
FIGURE 4-3 HORIZONTAL SAMPLES AS BUILT BEFORE REMOVAL FROM THE BUILD PLATE 81
FIGURE 4-4 - T SAMPLES MEAN OF MEANS FOR RA (SURFACE ROUGHNESS) 82

FIGURE 4-5 - T SAMPLES MEAN OF SN RATIOS FOR RA (SURFACE ROUGHNESS) 82
FIGURE 4-6 GRAPHICAL REPRESENTATION OF MEASURED RA VALUES FOR ALL L9 RPD EXPERIMENTS 85
FIGURE 4-7 GRAPHICAL REPRESENTATION OF MEASURED RZ VALUES FOR ALL L9 RPD EXPERIMENTS 85
FIGURE 4-8 INTERACTION PLOT FOR ∠80º SURFACE ROUGHNESS (RA) 89
FIGURE 4-9 INTERACTION PLOT FOR ∠80º SURFACE ROUGHNESS (RZ) 89
FIGURE 4-10 CONTOUR PLOT OF SURFACE ROUGHNESS (RA) VS *P* AND *V* FOR THE (A) -SV OUTLINE TEST 91
FIGURE 4-11 CONTOUR PLOT OF SURFACE ROUGHNESS (RA) VS *P* AND *V* FOR THE ∠A80 OUTLINE TEST 92
FIGURE 5-1 FINAL MANUFACTURED IN-LINE MONITORING SYSTEM INSTALLED INSIDE THE DMP PROX 100 CHAMBER 102
FIGURE 5-2: PART SIZING ALGORITHM APPLIED TO A PRINT WITH NINE 15MM X 15MM SQUARES 107
FIGURE 5-3 (A) CORRECT EXTRUSION OF BITMAP CONTOUR PROFILE OF THE PART (B) MISSING BITMAP CONTOUR PROFILE, INVERTED BOTTOM PART WHEN IMPORTED INTO BLENDER 109
FIGURE 5-4 EXTRUDED LAYERS WITH THE BRIGHTER PIXEL INTENSITIES VISIBLE ON TOP 110
FIGURE 5-5 MATLAB SURFACE PLOTS (WITH CONTOUR MAPPING) FOR 4 DIFFERENT LAYERS CAPTURED IN THIS CASE STUDY 111
FIGURE 5-6 CAPTURE OF THE CALIBRATION PRINT LAYERS 112
FIGURE 5-7 (A) STRESS DISTRIBUTION ON CAD MODEL OF E8 SUBSIZE TENSILE TESTING SPECIMEN (B) DISPLACEMENT OF LASER SCANNED PRINTED SAMPLE WITH RESPECT TO THE ORIGINAL CAD SPECIMEN (C) SURFACE MAPPING WITH LASER SCANNER TO DEMONSTRATE SURFACE TEXTURE 113
FIGURE 5-8 EACH EXAMPLE CONSISTS OF 2 PHOTOS OF TENSILE FAILURE, THE CAD MODEL OF THE TENSILE SAMPLE AND THE PLACEMENT OF THE VOID IN THE SAMPLE (A) LEFT TENSILE SPECIMEN SHOWS BREAKING ALONG THE PLACED VOID AND THE RIGHT SHOWS BREAKING VEERING TOWARD THE PLACED VOID. (B) BOTH SPECIMENS CRACKED ALONG THE VOID. (C) THE CRACKS OCCURRED THROUGH THE VOID BUT AT DIFFERENT ANGLES 117

LIST OF TABLES

TABLE 2-1 MATERIAL (POWDER) PARAMETERS AFFECTED BY LASER SCANNING PARAMETERS 22

TABLE 2-2 SUMMARY OF SURFACE FINISH IMPROVEMENT TECHNIQUES, AND THE ROUGHNESS VALUE ACHIEVED 25

TABLE 2-3 COMPARISON OF LASER POLISHING VS ELECTROPOLISHING FOR SURFACE ROUGHNESS IMPROVEMENT OF INTERNAL WALLS OF LPBF PARTS 26

TABLE 2-4 LASER POLISHING PARAMETERS AND DEFINITION 28

TABLE 2-5 LPBF INTERNAL LAYER DEFECTS 30

TABLE 2-6 ENERGY DENSITY PARAMETERS FOR THE DMP PROX 100 LASER SETTINGS AT 98% POWER 32

TABLE 2-7 X-RAY DIFFRACTION TECHNIQUE AND EXPERIMENTAL VARIABLES FOR SS 17-4 PH 34

TABLE 2-8 CONTACT AND NON-CONTACT NDT TECHNIQUES 35

TABLE 2-9 POST PRINT NDT TECHNIQUES VS IN-SITU SHM SENSORS 35

TABLE 2-10 OPTICAL IMAGING TECHNIQUES FOR LAYER-WISE CAPTURE 39

TABLE 2-11 THERMOGRAPHY CLASSIFICATIONS 41

TABLE 3-1 CALIBRATION EXPERIMENTAL SET-UP FOR DMP PROX 100 SCAN PARAMETERS 46

TABLE 3-2 CHEMICAL COMPOSITION OF SS 17-4 PH POWDER COMPARING THE DATA SHEET SPECIFICATION VS THE RECYCLED STATE OF THE POWDER 48

TABLE 3-3 SUMMARY OF MECHANICAL PROPERTIES FROM THE DMP PROX 100 DATASHEET 48

TABLE 3-4 CASE STUDY 1 TESTING SPECIMEN DIMENSIONS 52

TABLE 3-5 TESTING INPUT PARAMETERS FOR DESIGN OF EXPERIMENTS IN CASE STUDY 1 52

TABLE 3-6 DOE FOR TOP SURFACE IN-SITU LASER POLISHING OF DMP PROX 100 PRINTED SS 17-4 PH SAMPLES 54

TABLE 3-7 DOE FOR OUTLINE SURFACES INCLUDING THE VERTICAL, ANGLED AND INNER CHANNEL SURFACES FOR IN-SITU LASER POLISHING OF DMP PROX 100 PRINTED SS 17-4 PH SAMPLES. 55

TABLE 3-8 CHARACTERIZATION TESTING METHODS, EQUIPMENT, AND STANDARDS FOR ANALYSING THE TEST SPECIMENS IN CASE STUDY 1 RESULTS 56

TABLE 3-9 S/N RATIO FORMULAS FOR TESTING STRATEGIES 60

TABLE 3-10 EDGE DETECTION ALGORITHMS APPLIED TO THE GRAYSCALE IMAGES FOR THE STANDARD AND DEFECTIVE PART LAYER 70

TABLE 3-11 - IMAGE ANALYSIS TO PROCESS DIGITAL IMAGES 73

TABLE 4-1 TEST SPECIMEN ABBREVIATION REFERENCES 80

TABLE 4-2 RPD L16(8^1 2^2) EXPERIMENTAL DESIGN FOR HORIZONTALLY PRINTED SAMPLES (- T), ... 83

TABLE 4-3 INPUT VARIABLE RANKING FOR THE DELTA VALUE BASED ON SN RATIO 86

TABLE 4-4 INPUT VARIABLE RANKING FOR THE DELTA VALUE BASED ON MEANS 86

TABLE 4-5 DEGREES OF FREEDOM FOR EACH RPD STUDY 87

TABLE 4-6 SUMMARY OF %CONTRIBUTION OF INDEPENDENT CONTROL VARIABLES ON THE VARIATION IN RA FOR EACH RPD. 88

TABLE 4-7 INTERACTION PLOTS FOR THE -SV, REPRESENTING THE CORRELATION BETWEEN *V*, *P* AND *N* ON THE OUTPUT ROUGHNESS PROFILE FOR THE RA AND RZ MEASUREMENTS 90
TABLE 4-8 SEM IMAGES EXEMPLIFYING THE SURFACE MORPHOLOGY IN THE ORIGINAL, BEST (RA) AND WORST (RA) WITH RESPECT TO EACH ANGLED PRINT ORIENTATION. 94
TABLE 5-1 COST ANALYSIS OF HARDWARE USED IN IN-SITU MONITORING SYSTEM 118

LIST OF TERMS AND DEFINITIONS

Term	Abbreviation	Definition
Additive Manufacturing	AM	Technologies that manufacture a part layer-by-layer to create a 3D object
Laser Polishing	LP	When a target is exposed to highly focused pulsed laser light, and a small volume of material is instantly evaporated.
Laser-Powder Bed Fusion	L-PBF	AM process that uses a laser to sinter/melt a powdered material to its molten state and bond it to the particles surrounding it in a predetermined scanning pattern.
Direct Metal Printing	DMP	Metal L-PBF process using laser melting to additively manufacture a part.
Build Plate		The substrate upon which an AM part is manufactured.
Part Orientation		The angle which a part is built relative to the z-axis (vertical).
Melt-pool		Zone of molten material directly under the path of the laser.
Non-Destructive Testing	NDT	Testing strategies used to evaluate material, structural, component or system properties for characteristic differences without causing damage to the original part.
Computer Aided Design	CAD	A computerized creation of a model, analysis, or optimization of a design.
Finite Element Analysis	FEA	Simulation of any given physical phenomenon (structural or fluid behaviour) using the numerical technique Finite Element Method.
Defect		Any physical anomaly within an AM printed part that negatively impacts a part mechanical aptitude.
Assist gas	-	Inert gas used within a printing chamber to reduce the effect of oxidation introduction into the melted metal material.
Pre-processing	-	Any process or action taken before the AM layer-wise manufacturing begins

Post-processing	-	Any process applied to the manufactured AM part after removal from the AM machine
In-situ	-	Within the chamber of the AM machine.
Outline profile	-	The outline edge of each layer.

LIST OF PUBLICATIONS

Pereira, T.; Potgieter, J.; Kennedy, J.V. 2017. A fundamental study of 3D printing testing methods for the development of new quality management strategies. paper 510 In: Proceedings of Mechatronics and Machine Vision in Practice, Massey University, Auckland, New Zealand, 21-23rd November 2017. Auckland, N.Z.: University of Auckland

Pereira, T.M.; Kennedy, J.V.; Potgieter, J. 2019. Development of quality management strategies for 3D printing testing methods – A Review. doi: 10.1109/APWConCSE.2017.00047. Proceedings of the 4th Asia-Pacific World Congress on Computer Science and Engineering (APWC on CSE), Mana Island, Fiji, 11-13th December 2017.

Pereira, T.M.; Kennedy, J.V.; Potgieter, J. 2019. A comparison of traditional manufacturing vs additive manufacturing, the best method for the job. p. 11-18; doi: 10.1016/j.promfg.2019.02.034 In: Yarlagadda, P.K.D.V.; Xavior, A.M.; Gibson, I.; Zhu, Y. (eds) Digital manufacturing transforming industry towards sustainable growth. Amsterdam: Elsevier. Procedia Manufacturing 30. Proceedings of the 14th Global Congress on Manufacturing & Management (GCMM 2018) – Brisbane, Australia

Pereira, T.; Potgieter, J.; Kennedy, J.V.; Mukhtar, A.; Fry, M. 2018. The effect of reheating layers in metal additive manufacturing on the external surface finish of a printed part. doi: 10.1109/M2VIP.2018.8600902 In: Veri, A.; Xu, P.; Csiszar, A. (eds.) The proceedings of the 2018 25th International Conference on Mechatronics and Machine Vision in Practice (M2VIP). IEEE.

Pereira, T.; Potgieter, J.; Kennedy 2021. In-Situ low-power-laser-polishing of Direct-Metal-Printed specimens for an improved surface finish. Proceedings of the 2021 Manufacturing, Design and Entrepreneurship (MaDE) - Auckland, New Zealand

Statement of contribution for each publication can be found in Appendix H.

1 INTRODUCTION

1.1 BACKGROUND AND MOTIVATION

The increased interest in '3D printing', more formally known as Additive Manufacturing (AM), has created numerous research opportunities for engineers, scientists, and software developers. 3D printers have become commonplace in research institutes, industrial businesses, and even at home for hobbyist 3D-printing enthusiasts. The development of AM technologies over the last 50 years has focused on creating new technologies, characterizing machine settings and material properties [1]. Recent interest has moved into creating quality strategies to progress AM in the industrial setting and provide feedback for certification of AM parts. Most AM enthusiasts highlight the capability to manufacture complex geometries as one of AM's advantages. However, many AM users have noted the absence of methods to either polish the surface of these complex geometries or guarantee the reliability of the objects mechanical and structural properties [2]. This thesis addresses these issues in detail, expanding on the research objectives, solutions considered, results achieved, and conclusions drawn to develop novel contributions to the academic community.

AM technologies are in direct competition with established, reverse-engineered, Subtractive-Manufacturing (SM), Formative-Manufacturing (FM) and joining-process techniques, otherwise referred to as Traditional Manufacturing (TM). Reviews of AM's capability to penetrate the end-user product market, often compares its ability to fit into established manufacturing regions [3]. To summarize, economically AM dominates TM methods only where the product has increased complexity and customizability, due to its high capital, material procurement, and running costs. For this reason, high impact industries such as aerospace, medical, food, automotive, engineering etc, who focus on high-value low-volume production and seek to create end-user products with Additive technologies. For example, commonly referred to in the AM field, General Electric (GE) Aviation, in 2017 predicted a new line of over 100,000 additive parts by 2021 [4]. The National Space Agency of America (NASA) have also proposed a range of engine components (valves and injectors) utilizing AM. These companies and more share a desire to discover better quality assurance strategies to validate and certify their AM processes (per machine), particularly for metal AM parts.

An early review in this research study and surveying of key AM businesses in New Zealand, revealed two significant areas of research growth related to the development of quality

assurance strategies. The first being the rough surface finish of metal AM parts, and secondly, non-destructively investigating and characterizing internal flaws within each layer of the part.

1.1.1 SUMMARY OF RESEARCH FOCUS ON QUALITY STRATEGIES TO IMPROVE THE SURFACE FINISH OF METAL AM PARTS

The surface finish of metal AM parts (as built) is a key issue, where more time and money are spent in post-processing rather than manufacturing the printed part. To date, manufacturers have concentrated on using AM technologies to reduce material by topology optimization, but this is a limited research area and well-studied. The heightening cost of AM machines require new and novel applications to satisfy economic and creative demand. To exploit AM technologies to its fullest potential, it is necessary for AM industries to manufacture products designed with complex geometries, which can be polished to a desirable surface finish and texture. However, existing finishing methods using subtractive tooling and polishing methods are not entirely reliable to access hidden channels in curved geometric parts. A technique to target this issue would be highly desirable in all applications of AM, more so in fluid/soft texture channels seen in the petroleum, food, automotive and many other manufacturing industries.

This research explored various methods to solve this issue, including existing surface improvement strategies such as subtractive machinery, electro-polishing, media-polishing, laser-polishing and more noted in Chapter 2. Subtractive-tooling and media-polishing have been the most popular post-processing techniques to improve the surface finish and polish metal AM parts. While these two techniques are notably the fastest and most accurate methods for polishing, there are drawbacks that prevent industries from manufacturing complex geometries. The biggest drawback is the inability to adapt the standard techniques to access internal chambers within a part (e.g., multi-channel manifolds). Two methods were of immediate interest, for their ability to access hard to reach areas (curved/hidden geometries); electro-polishing and laser-polishing. Electro-polishing was considered briefly but eliminated due to the work published already by the University of Louisville demonstrating this method as a surface roughness improvement technique, with other studies noting a worsening effect of the surface finish. This directed the focus to laser-polishing (LP) and the discovery of a technique to improve the surface profile and texture of metal AM parts.

This research examines the effect of LP on Laser-Power Bed Fusion (L-PBF) parts. L-PBF is one of the most popular metal AM processes, seen as advantageous for the small layer size and accuracy that can be achieved. Typically, laser-polishing is performed as a post-processing technique with a high-powered laser that re-melts the surface to smoothen the abrasive texture. However, it was determined the best time (most access to internal areas) and most novel approach,

was to try laser-polishing the part within the printer as the part builds layer-by-layer. L-PBF metal printers are equipped with low-to-high powered lasers (50W-20kW power used to sinter/melt the powdered material), with varying build characteristics; material, powder size, build volume, laser settings and more. The L-PBF machine used in the research experiments conducted is a Direct Metal Printer (DMP) ProX100, a research-grade machine with variable and accessible laser and machine settings. Initial experimentation performed focused on calibrating the DMP laser settings and optimizing pre-processing and post-processing methods for preparing the printer, powdered material, build plates and part removal. Following this, the first experimental study involved experimentation to characterize the surface finish of each side of a 3D-printed part. The lack of existing reference data prompted this study to create a comparative basis to recognise improvement or detrimental changes in the surface profile during the LP experiments. Each side (top, bottom, vertical side, and angled surfaces) exhibited different surface profiles, textures, and roughness. The first case study (defined in Chapter 3) took this into consideration, while determining the effect of LP on the DMP printed specimens. Various Taguchi design of experiments were used to create the experiments and analyse the effect. The analysis was based on results taken from visual inspection and mechanical testing performed to study changes in the surface topology and specimen properties.

1.1.2 SUMMARY OF RESEARCH FOCUS ON QUALITY STRATEGIES TO INVESTIGATE DEFECTS IN METAL AM PARTS

This research equally focused on the adaptation of non-destructive testing (NDT) technologies to examine flaws within L-PBF parts. To begin with, some companies believed established mechanical testing standards could be applied to AM products too, but not only is the process unreliable, the economic model proved otherwise; AM is an expensive process and wasting parts in a destructive test is not financially feasible [5]. AM parts can vary in repeatability and consistency along different areas of the print bed for a single machine and machine-to-machine, which is the leading reason traditional ‘batch’ testing cannot be recommended; batch testing is commonly used to certify the mechanical properties of a part, using established mechanical tests (destructive: tensile testing, fatigue testing, hardness testing etc).

In metal AM alone, each different manufacturing method have many quality considerations to regularly assess, from the feedstock to machine repeatability, power source, feed-rate and spread ability of feedstock, alignment of the build plate and other varying factors discussed further in this thesis.

The introduction of non-destructive testing (NDT) in AM, has seen research and development focused on applying established testing strategies, such as X-Ray, Computed Tomography, Eddy Current Testing, Digital and Thermal cameras etc. This is still a very underdeveloped area of research with companies and AM consumers eagerly awaiting testing standards for NDT characterization. The vast difference in each AM process and its material properties, has opened major research gaps; to characterize the nature of defects in each process, monitor them, assess their impact, and provide some feedback control. Since the start of this research study, several companies have now integrated NDT monitoring systems within AM machine to in-situ capture digital and thermal data primarily. However, the commercially available systems are expensive, can require a supercomputer for data processing and an extreme amount of storage capacity for the data collected. At present the data captured can only be interpreted by a trained professional, and with the vast amount of data captured per print, it is a time consuming and expensive process to analyse manually. A few companies and academic research groups are currently creating deep learning models and trained artificial intelligence systems to sort through the data. Each system is adapted to work with a singular AM process and brand. The scope of this study was narrowed to the development of quality strategies for the L-PBF process, particularly using the DMP ProX 100 printer.

The second case study, focused on the NDT research gap, sought to develop an in-situ digital and thermal capture system to perform layer-wise capture. The purpose of this experimental study was to develop an adaptable system that could be retrofit into various fully enclosed AM machines. The aim of this experiment was to capture and isolate the melted part from the unfused powder to re-build the images as slices in a 3D model that would provide a comparative CAD model for FEA analysis. Secondly, to determine if micro-defects could be identified using a machine learning approach to identify key layers of concern. This quality strategy was developed to discard unnecessary data and eliminate the need for a trained technician to review every layer. The third quality strategy used by this approach sought to provide file verification (the model file sent to the printer is same as the model being printed) by matching the sliced layers captured to the generated software layer-slices.

A thermal camera was implemented to capture the thermal profile of each layer, to classify specific thermal signatures that can be related to micro-defects. Thermal sensors have been widely used to study the melt-pool, heat zones, and heat dissipation of a sintered/melted layer. Most solutions used thermal cameras mounted externally, or single-signal based thermocouples. Scarce literature exists that documents thermal profiles of defects in metal AM parts. Previous studies have used expensive thermal capture systems for NDT monitoring of AM, this study focuses on the minimum sized defect you can detect with a low-resolution development thermal imager. The quality approach created can be implemented into other forms of Additive

Manufacturing that have a layer-wise, low temperature chamber printing method (laser-powder-bed-fusion printers or even bio-printers).

The purpose of this Ph.D. research is to further technological progress in NDT solutions for Metal Additive Manufacturing, address the need for better surface finish in printed parts and to contribute new data for the characterization of defects using digital and thermal technologies. The solutions presented within this thesis serve this purpose and the personal motivations listed in the sub-section below. Results from the experiments conducted have been analysed and justified for significance and their novel contributions to the academic and industrial AM space.

1.1.3 PERSONAL MOTIVATIONS

This Ph.D. research was funded externally, by NZProduct Accelerator, whose primary focus is to connect industry and researchers focusing on Materials and Additive Manufacturing research. Their unique approach to research, drives funded researchers to focus on the commercial value of their research, by first discovering a business opportunity. Following this a literature review is performed to discover the research gaps, problem space and solution space. As such, the research objectives documented in this work addresses a need, unanimously suggested by industry, for better part surface finish and non-destructive defect characterization.

The author's background in mechatronic engineering and prior experience with sensors and a passion for manufacturing solutions, sparked interest in NDT solutions for AM. This research allowed the author to develop skills in practical engineering: various machine operation (AM and subtractive), testing technologies, design, and development of custom jigs, software development and more. Additionally, to attain research-based skills, in reviewing literature, upskilling, personal leadership, design of experiments, critical and statistical analysis of results. This thesis exemplifies the skills stated and the knowledge garnered throughout this doctoral study.

1.2 THESIS OBJECTIVES AND RESEARCH QUESTIONS

The main objective of this thesis is to develop quality strategies to characterize the nature of defects and surface treatment in Direct-Metal-Printing (DMP) specimens through an Engineered solution. The main objective is deconstructed into the following aims:

1. Develop a quality strategy to improve the external surface finish (texture, roughness etc) of a L-PBF part.

2. Develop a machine learning strategy to identify micrometre defects within each layer of a L-PBF part.
3. Identify signature thermal characteristics associated with micrometre defects within each layer of a L-PBF part.

The following research questions arose from the objectives listed above:

What is the effect of laser polishing the external surface of metal AM parts using the in-built laser during print? What key printer parameters have the most positive effect on the part's surface texture and mechanical aptitude?

How can you detect, characterize, and quantify critical defects in Metal Additive Manufactured parts using in-situ monitoring Non-destructive technologies?

Which NDT technique(s) can be used to quantify the effect of defects with comparison to mechanical testing strategies?

1.3 THESIS STRUCTURE

This doctoral thesis is organized into seven main chapters, beginning with the current introductory chapter (**Chapter 1**). This chapter provides a holistic overview for the topics surrounding the thesis objectives, including the motivating factors that led to the study of NDT and surface finish improvement strategies for L-PBF AM manufacturing.

Chapter 2 exemplifies the state of art surrounding AM technologies, focusing on metal Additive Manufacturing (particularly Laser-Powder-Bed-Fusion) to detail the research opportunity identified. The chapter justifies the need for new quality strategies for metal AM, based on a review of literature and industry surveying, with a detailed analysis of different solutions considered. The section explains in detail the processes, jargon, and associated technologies considered in the research study.

Chapter 3 presents the research methodology, which introduces the research aim and hypotheses, followed by the research experiments and methods carried out in this study. Detailed description of the equipment used in the creation of test specimens and for experimental analysis is described to aid the reader's understanding of the results presented in the following chapters. The chapter is split into two case overarching research studies. The first is in relation to surface finish improvement for metal AM parts. The second explores NDT methodologies to be used in defect detection of metal AM parts

Chapter 4 presents the results and discussion from the first AM quality assurance study to improve the surface finish of Stainless-Steel 17-4PH parts created in a Direct-Metal-Printer. The results exemplify the evolved properties of the test specimens re-melted with the hope of improving the surface texture and topography. The properties of the altered parts are studied using several testing techniques as detailed in the methodology including surface profiling, optical imaging, and mechanical testing.

Chapter 5 reports resolutions developed to address defect identification, file security, 3D model reconstruction for a simulated finite element analysis.

Chapter 6 discusses the future and expanding work that has resulted from this research to progress the laser polishing method presented for surface finish improvement and further explore NDT quality technologies and strategies for metal AM.

Chapter 7 concludes the research study with a final overview of the work performed within the thesis, highlighting the novel contributions this research study has made. In addition, this chapter provides a summary of work done to answer the research questions presented within this first chapter and verify the hypothesis presented in chapter 3 against the results presented in chapters 4 and 5.

1.4 ADDITIVE MANUFACTURING

The ASTM F2792-12a standard, defines Additive Manufacturing (AM) as “a process of joining materials to make objects from 3D model data, usually layer upon layer, as opposed to subtractive manufacturing methodologies” [4]. With rapid progression, AM technologies now integrate several manufacturing techniques; powder-bed-fusion, directed-energy-deposition, material-extrusion, binder-jetting, curing, lamination. Several comprehensive AM technology reviews have been documented in previous works for further explanation. Current AM processes with relation to AM materials is characterized in Figure 1-1. [6] below. The extensive range of technologies has created numerous research gaps; for innovative complex design, material topology optimisation, economic strategies, environmental impact, certification strategies and hybrid solutions, to name a few.

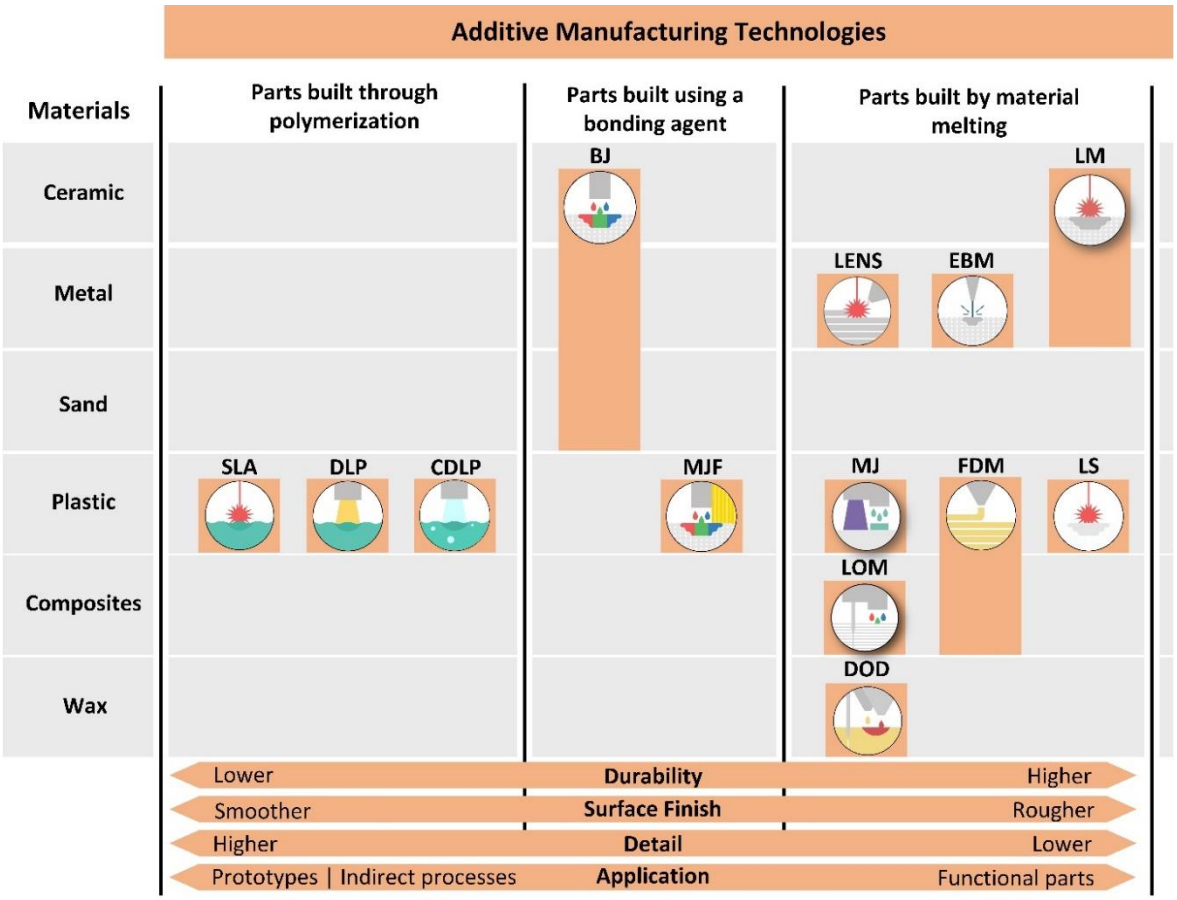

Figure 1-1. Summary of AM technologies and characterization; SLA: Stereolithography, DLP: Digital Light Processing, CDLP: Continuous Digital Light Processing, BJ: Binder Jetting, MJF: Multi Jet Fusion, LENS: Laser Engineering Net Shape, EBM: Electron Beam Melting, LM: Laser Melting, MJ: Material Jetting, FDM: Fused Deposition Modelling, LS: Laser Sintering, LOM: Laminated Object Manufacturing and DOD: Deep-On Demand.

The focus on AM's industrial progression at the start of this research required an in-depth review to understand what the research gaps in this field were. One publication outputted early in this research compares AM's introduction into industry, compared to established traditional Subtractive, Formative and Joining Manufacturing processes. Key topics of interest pulled from this publication are described below focusing on Manufacturing Regions, Economic Strategies (the financial overview and societal impact) and Quality Assurance and Quality Control for AM.

1.4.1 MANUFACTURING REGIONS

Manufacturing regions can be classified and defined by three key attributes: complexity advantage, customization, and volume. Complexity advantage is the final geometric complexity and feature location a manufacturing method can achieve. Customization is focused on the ease of feature and individualistic variability the manufacturing technology offers that makes a similar product unique to each other with a customizable feature [7]. Volume refers to the production quantity of parts in an order or batch, whereby the production volume can range from singular to multiple parts. Following its rapid advancement, the focus of AM has moved from rapid prototyping to rapid tooling and manufacturing. Several factors contribute to the selection of a manufacturing method: cost, part complexity, material usage and material property requirements, time, energy consumption, sustainability and so on. The Wohler's 2013 Report provides an extensive overview of AM's integration into the industrial market [8].

High-Production-Volume Manufacturing

Low-cost high-volume production has been the primary focus of traditional manufacturing industries; dominated by injection moulding. This is especially true for Mass Manufacturing; parts characterized by their simplicity and lack of customizability [9]. The high capital investment required to create assembly and production lines using AM, prevents its penetration into industry as a competitive mass manufacturing technique. However, the complexity advantage offered by AM, has provided the opportunity to essentially 'hit two birds with one stone'; with the ability to eliminate forging and joining processes by printing complete parts in one print. An example of this is the metal acetabular cup [10] (Figure 1-2) used in hip replacement surgeries, where nearly 440,000 hip replacement surgeries are performed in the U.S alone [11]. The cup is one part of the implant inserted into the hip, previously manufactured using numerous SM and formative manufacturing methods (forging, machining, coating etc.)

Figure 1-2 Titanium Metal AM Acetabular cup

Figure 1-3 Stereolithography AM mould for hearing aids

Figure 1-4 Powder-bed-fusion, laser-sintering AM printed mobile phone cases

An AM powder-bed-fusion metal printer, can build the acetabular cup, adding the porous surface into the surface layers in a single print. Production of this product falls within the Mass Complexity and Customization region, where the part exhibits complex geometries with customizable porosity, size, and shape levels.

The medical industry has capitalized on this manufacturing region for implants and protheses through the replication of translated scans (Computed Tomography X-RAY and MRI) [12]. The third high-volume-based manufacturing region is Mass Customization, defined by its ability to provide individually designed products and services to every customer, through high process agility, flexibility, and integration [13-15]. An agile and quick approach to change is a key characteristic company's desire, to stay ahead of the market with innovation and competition [7]. The absence of lead time and quick design adaptation in AM, with unique characterization provided by 3D scanning, sets AM ahead of conventional manufacturing methods for this region. Popularly known products now produced through a mass customization manufacturing model include, Invisalign brace molds (clear braces) by Align Technologies using AM Stereolithography printers [16], with nearly 17.2 million braces created in 2012 alone. Reeves et al [17], documents other instances of mass customization of AM and details the associated financial model [18] for hearing aids (Figure 1-3), phone cases (Figure 1-4), computers etc.

Low-Production-Volume Manufacturing

This region refers to low-volume (numerically unique for each product type) production of products. The product manufactured by conventional methods have limited complexity and customization (the manufacturer might offer minor variations for customer preference), however with AM manufacturers can achieve a high degree of complexity for the same cost. Low volume is defined specific to the industry, product, and sale capacity [18]. The introduction of AM into the manufacturing sector began with low-volume production for rapid prototyping, with Stereolithography. Functional-assembly manufacturing is still the primary use of AM according to the Wohler's report [8]. However, investors are now interested in direct-part manufacturing, particularly aerospace, automotive and rapid-tooling industries.

Hopkinson and Dickens et al [19], provide a successful cost model to illustrate the breakeven point of AM vs SM for volume. The study examined the cost of fabricating a small-plastic lever using AM powder bed fusion vs conventional-injection-molding manufacturing. the

study concluded for a production volume smaller than 10,000, AM had a reduced unit cost compared to injection molding [20]. While SM dominates the Mass Manufacturing region financially, AM is better suited to fabricate tooling and fixtures required for conventional Mass Manufacturing molds. AM offers a reduced lead time and cost to capitalize on high value, low production of parts such as those used in ships, automation, aviation, satellites etc. This concept is known as Rapid Tooling, referring to tools able to form several thousand or even millions of parts before wearing out. Levy et al [21] provides a summary of direct and indirect AM technologies used for rapid tooling.

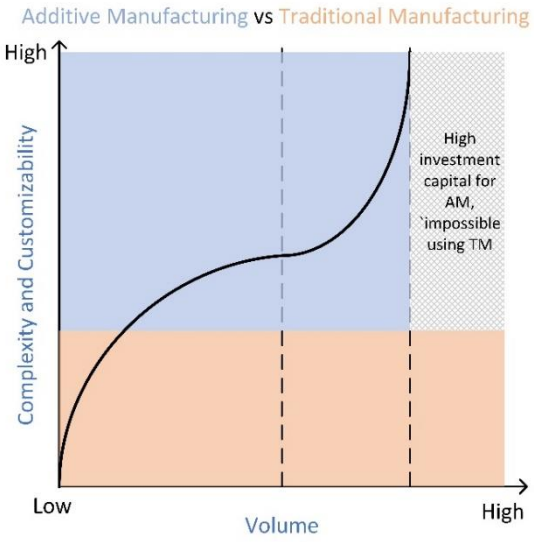

Figure 1-5 AM vs TM manufacturing feasibility with reference to Volume, Complexity and Customization

1.4.2 ECONOMIC STRATEGIES

The economic impact a manufacturing strategy has financially and societally, can determine the areas of success or advancement for businesses to pursue. This is particularly true for those countries seeking to further their manufacturing specialty and accomplish the major success low-impact countries have had with mass manufacturing. Studies conclude that AM would best dominate the low production manufacturing sector for its customizability, short lead time and complex geometric capability. Petrick et al [22] studies the disruption in manufacturing caused by the new manufacturing and design opportunities offered by AM. The paper examines the economic status quo surrounding AM, including the established and reformed finance/economic models that support different AM technologies currently. Figure 1-5 provides a collaborative summary of economic models concluded by previous works, tied in with the manufacturing regions (Section 1-1-1). The model surmises the higher the customizability and complexity, AM process would be better suited than TM. Furthermore, it highlights a major field for new innovative designs that were previously impossible to produce by TM methods. The curved line represents the increase in price to produce parts with the relative volume, complexity, and customizability for AM only, it is the opposite for TM.

Previously, companies have monopolized on the successful method of reducing variability in design, to maximize on the repetitive production of interchangeable parts, following the Design for Manufacturing (DFM) advantage offered by traditional manufacturing methods dating back to the 1990s [23, 24]. DFM set designers and manufacturers to follow a set of rules,

limiting creative expression and instead encouraged cost-effective production. This created the 'design-build-deliver' model, from which companies have attained high-quality products at a reduced price, with higher success. The rapid improvement in transportation caused by the introduction and advancement of digital technologies, brought low-wage countries, such as China, onto the world stage of competitive manufacturing.

Alternatively, AM offers flexibility which enables manufacturers to create an optimal design for lean production [25]. AM has created the opportunity for supply chain simplification and has successfully been implemented for 'single unit and very low-volume production' in several sectors. These sectors range from the highest implementer of metallic AM Aerospace [26] products to plastic-FDM-printed AM prosthetics [27], customized for the individual hearing aids [22], medical implants [12], and brace molds [18], unique-complex-patterned art and fashion.

AM machines offer production flexibility; the machines do not require expensive set-up arrangements, making the technology economical for smaller batch production [28]. However, AM is still a considerably expensive investment compared to traditional manufacturing machines [29]. Entry level printers begin at around US$150; these are rudimentary small-bed-FDM-prototyping personal-use printers [30]. Although, production level printers can range from US$5,000 to near US$1,000,000 [31]. Machine purchase aside, material cost varies for polymers, elastomers, and even metallic feedstock (powder, resin, wire, sheets). Additionally, running costs for the machine, and gas used for AM machines requiring an inert environment, and several other contributing costs, add to the high expense of the process.

DMRC [1] identifies 3 main industries to lead AM's future: aerospace (morphing and multifunctional structures), automotive (handling of fluids and optimized tooling), and electronics (functionally integrated parts and testing systems). However, these areas specified are still active research areas with issues in the process stability, surface roughness and building scalability vs laser resolution. Furthermore, it is clear the medical sector has a distinctive lead with several current AM achievements and many future AM product research and deliverability aims [12].

AM processes typically utilize a binder, laser, or electron beam to bond material as it is directed along the build path or through a scan over a layer of material. Polymers, metals, and ceramics have been used successfully with these AM strategies [22]. Where polymers have shown to produce functional, finished parts with minimal additional finishing required; metallic parts tend to require SM techniques such as grinding and polishing to achieve the desired surface finish tolerance (Figure 1-1).

However, the capabilities of higher AM printer/machines continue to improve. The rapid rate of improvement is causing an extensive rise in cost for minor advantages offered by each machine with every upgrade. Industries have attempted to continually decrease the average AM

machine price to adjust for inflation, where between 2001 and 2011 the average price decreased 51%. The National Institute of Standards and Technology (NIST), U.S. Department of Commerce, present a comprehensive summary of cost analysis and cost effectiveness in AM technologies [32].

To summarize, the review states AM is cost effective for low volume/small batch manufacturing with continued centralized manufacturing rather than distributed manufacturing. Currently, research models conclude that while there is an expensive initial investment for machine and personal costs, distributed production (proximity to the site of use), is not a viable option for AM. However, should AM develop into a widely adopted process with increased automation and reduced machine costs, distributed production may become more feasible.

1.4.3 QUALITY ASSURANCE AND QUALITY CONTROL FOR AM

Precision manufacturing and standardization of products are dependent on Quality Assurance (QA) and Quality Control (QC) standards and procedures [33]. The complex geometry, internal lattice structure, surface finish, layer orientation and topology optimization, all contribute to the mechanical aptitude of an AM part. In cases where powdered material is inserted into parts, careful design optimization is required to determine how it can be extracted. Loose powder within the part could not only be considered a health and safety concern but also impact the mechanical and structural integrity [34].

The vast capability of AM, referring to material variety and manufacturing process differentiation, has resulted in multifaceted quality requirements and standards. For this reason, SM continues to dominate AM in quality, precision, and reliability [35]. In turn, the inconsistency and complexity of each AM system has made it a challenge to develop a standard set of rules, causing a slow development of Quality Assurance (QA) strategies. Quality is quantified and qualified differently depending on the part produced. The degree of quality required is often dependent on the risk related to health-and-safety assurances required. For instance, a model toy plane would have an extremely low risk in comparison to a hinge printed for a commercial aircraft. Furthermore, each AM printer requires calibration and customization of the printer parameters, sometimes specific to certain types of builds.

The size, orientation, sharpness, and location (within joints, exterior surfaces, or critical sections of the structure) of defects within an AM part can impact the mechanical properties negatively [36]. This is no different for SM manufacturing, in fact the type of defects is almost similar; porosity, cracks, inclusions, voids, balling, rough surface finish [37-40]. However, in AM, aside from geometric imperfections, volume mismatch, layer removal and undesirable internal surface finish are issues that cannot be detected through typical mechanical tests. In SM,

batch testing is the most used QA/QC technique, where one test piece within a batch can be mechanically tested (i.e., tensile, compression and fatigue tested), as a reflection of the mechanical strength reference for the remaining parts within that batch.

While some AM manufacturers attempt to use a similar method for each print (can have multiple parts in one print in a big enough bed size), there have been concerns surrounding the impact of layer orientation, heat affected zones and inconsistent defect introduction that indicate batch testing cannot be applied to AM. Certification is usually achieved through repeatability and reliability of a manufacturing technology. An AM system has more dependent variables than SM. However, despite the lack of AM standards, traditional standards commonly used in other manufacturing processes or materials have been applied to select AM printers/products by conforming to set parameters for individual machines (i.e., laser power, scan speed, powder spread etc.).

Ensuring the use of quality-tested powder/wire feedstock is important, inconsistencies in the particle size, wire/filament diameter and sheet thickness can impact the structural integrity, with the wrong machine parameters. Lloyds Register and TWI Ltd have developed a document detailing the process for AM certification [40]. The guidelines were developed following traditional certification process standards, with the allowance of independent testing to be done by the industry/company specific to certain test cases. This approach is not always suitable, nor efficient, for AM technologies [41]. The reason for this, is the intricate system that makes up an AM machine; unlike traditional calibrated machinery, AM does not always ensure the repeatability or reliability required for precision manufacturing.

The four main contributing factors of concern in AM quality are the feedstock characteristics, the build environment, melt pool monitoring and build characteristics [37]. The need for new standards has been acknowledged by industry, research centres and academia, dating back several years with numerous surveys having been carried out. Gausemeier et al [1] states certification processes customized to suit AM are a key success factor for the future of the AM industry. In 2009, the ASTM Committee F42 was formed for Additive Manufacturing Technologies, consisting of approximately one hundred members (experts predominantly from USA and Europe). Following this, in 2011, the ISO Committee TC 261 for Additive Manufacturing was established. The AM board has developed strategies [42] for quality inspecting individual aspects of an AM process using the following test methods; Chemical analysis, Mechanical Testing, Performance Evaluation, Metallurgical Analysis, Powders Evaluation and Non-Destructive Testing (NDT) [43]. NDT testing is currently a major R&D area, with companies such as EOS and ARCAM developing in-situ monitoring system for NDT quality assurance [44]. While several companies are now incorporating cameras and sensors into their

machines, specialized NDT technicians are required to interrupt the data. The vast amount of data produced from a single print, would require a huge storage device, and take the technician considerable time to review it. Additionally, there is still a great deal of work to be done to achieve a lifetime Structural-Health-Monitoring (SHM) [45] system for AM machines. Sharratt et al [37], details a comprehensive review of NDT techniques for the qualification of AM parts and processes, required to develop an SHM system and the importance/need for it. Namely that the four contributing factors (feedstock characteristics, build environment etc.) to AM quality mentioned previously, require further research to certify each AM process. This is especially significant for those products with a higher risk, dependent on a fatigue load or fracture resistance.

Another rapidly developing research area, is the advancement of computational software for modelling and simulation; to determine mechanical stresses in an AM part based on parameter selection. Engineers are interested in using a computational approach, for AM build-planning, to solve the Multiphysics process [46] (considering build orientation, layer thickness, support material etc.) of AM. To produce a complete representative simulation; however, including a wide range of time and length scales; researchers claim that more than 130 variables need to be considered. The complexity of such a system, means most computational models would be run-in high-performance computing facilities only. Simplified computational software exists, but the investment cost is too high for most small businesses to consider using. Presently, more sophisticated models of AM processes can be found at the US National Laboratories, a company possessing immense computing capabilities [47].

Key requirements for the penetration of AM in the future into the wider commercial market, include high process stability, a database containing properties of AM materials, On-line, quality-control processes, continuous certification, and provision of design rules [1]. Furthermore, material heterogeneity and structural reliability are also essential factors to consider. It is clear, depending on impact of risk mitigation, that a product's quality assurance has a huge influence on the level of QA required. To ensure manufacturers neither underprepare or over-invest in QA technologies, it is important to evaluate the level of QA required for each part printed utilizing AM technologies [46].

1.4.3.1 SUMMARY OF ISSUES DISCOVERED FROM LITERATURE

The above review highlighted several areas of interest to progress AM research, namely:

- A focus of low-volume manufacturing industries, where critical QA is required and financially feasible.
- An improvement of QA strategies to achieve a Structural-Health-Monitoring (SHM) system.
- Furthering non-destructive testing research for achieving a SHM system.

1.4.4 INDUSTRY SURVEYING

This section presents a summary of AM company surveying for a validation of conclusions made from a review of literature and to discover the current issues commercial AM companies are seeking to improve to progress their product line. Four leading AM companies in New Zealand were approached and Appendix E details a summary of these companies and key points taken away from the interviews.

1.4.4.1 SUMMARY OF ISSUES DISCOVERED FROM INDUSTRY INTERVIEWING

Every industrial company approached claimed surface finish to be a major issue. The lack of techniques suited for testing AM parts is lacking, they doubt the reliability of traditional tests to validate critical parts should they begin manufacturing them. In any case, due to the rigorous testing required, each AM machine can only be certified for one purpose, to print one part with specific calibration parameters. The three major issues identified are listed below and they closely match issues found in the early literature review above.

The three key quality assurance issues identified were:

1. Surface Finish
2. Residual Stress
3. Defects within internal layers

CHAPTER 2

2 STATE OF ART

This chapter examines the state of art for resolutions pertaining to surface finish, residual stress, and defects in AM parts, as stated in Chapter 1. The chapter begins with a review of metal AM technologies and process characterization. The chapter then delves into the current state of art for quality strategies regarding surface finish improvement techniques and non-destructive characterization of defects in metal AM.

2.1.1 METAL ADDITIVE MANUFACTURING

The scope of this PhD was narrowed to only consider metal AM for the following reasons.

1) Metal AM research and development is highly desired in high-impact low-manufacturing-volume industries.
2) The advantageous characteristics of metal AM (strength, durability, longevity, weight etc) make it better suited for an extensive range of applications, aerospace, medical automotive and automation lines etc.
3) Critical parts, which need rigorous QA strategies are primarily constructed with metal.
4) Numerous opportunities for novel contribution, through work pertaining to the development of fundamental design guidelines, materials characterization, and quality management strategies etc.

This sub-section describes the manufacturing methods used by commercially available metal AM processes and their popularity in the commercial space. Each metal AM process and machine varies in build-environment, material-state, and melting-technique. For this reason, novel testing techniques are required to accommodate the differences. The process of interest in this research study is Powder-Bed-Fusion (PBF), particularly Laser (L-PBF) based methods. This is the most commercially utilized method here in NZ and internationally due to its high development and interest. The four most common Metal AM processes are detailed below.

Powder Bed Fusion (PBF)

PBF (Figure 2-1) a laser or electron beam to fuse powder that has been spread from the feed system to the build platform as shown in the corresponding illustration [48, 49]. This is the most popular method of AM used commercially in NZ, with some companies focusing on EBM for its reduced residual stress and others focusing on Laser based systems. EBM systems have a

heated chamber and laser systems have an inert chamber. Laser-Powder-Bed-Fusion (L-PBF) is the main system of interest in this study due to its popularity in NZ and international companies. Laser systems are currently dominating the commercial space with sintering and melting techniques.

Directed Energy Deposition (DED)

DED (Figure 2-2) involves the deposition of either a wire or powder feedstock, by a guide, bonded using a laser or electron beam. NASA has developed a range of these machines and continues to work on improved revisions of their EBF machines [4]. These machines are particularly useful for repairing complex parts, depending on the systems degrees of freedom (some have up to 6).

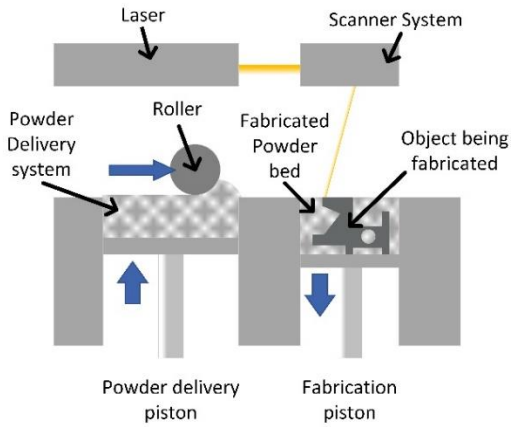

Figure 2-1 Powder Bed Fusion process

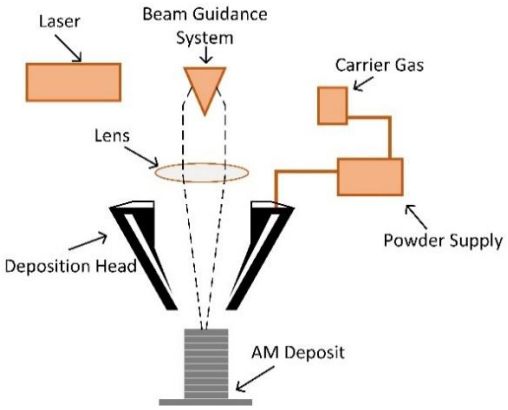

Figure 2-2 Directed Energy Deposition process

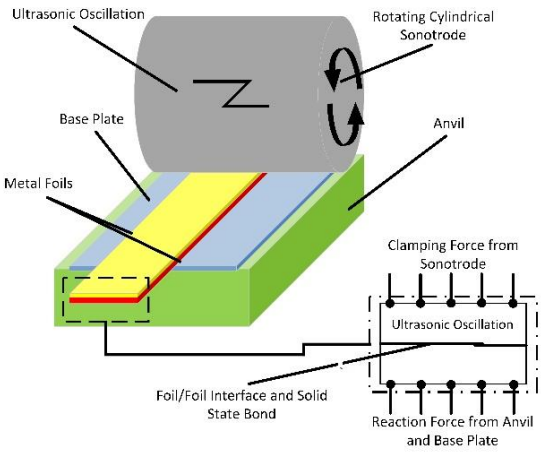

Figure 2-3 Sheet Lamination Process

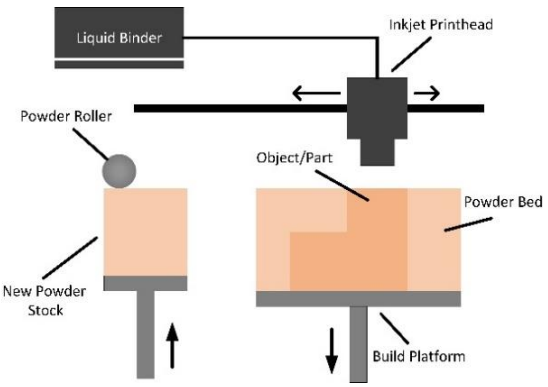

Figure 2-4 Binder Jetting Process

Sheet Lamination

Sheet Lamination (Figure 2-3) combines Additive and Subtractive technologies to bond metal sheets (foils) together [50]. Utilizing a thermal bonding or ultrasonic technique to bond the sheets together, the finished block is then CNC machined to achieve the desire geometry. Though an interesting concept this method ranks low in popularity for commercial metal AM application or utilization.

Binder Jetting (BJ)

BJ (Figure 2-4) shares a similar application to the PBF method in material deposition [28]. However, a liquid binder is used to bond the material and post processing is required to achieve the desired shape. While the AM processes for BJ is uncomplicated, it is the least popular method in the commercial space due to the complexity and time-consuming nature of the post-processing required.

2.2 LASER POWDER BED FUSION

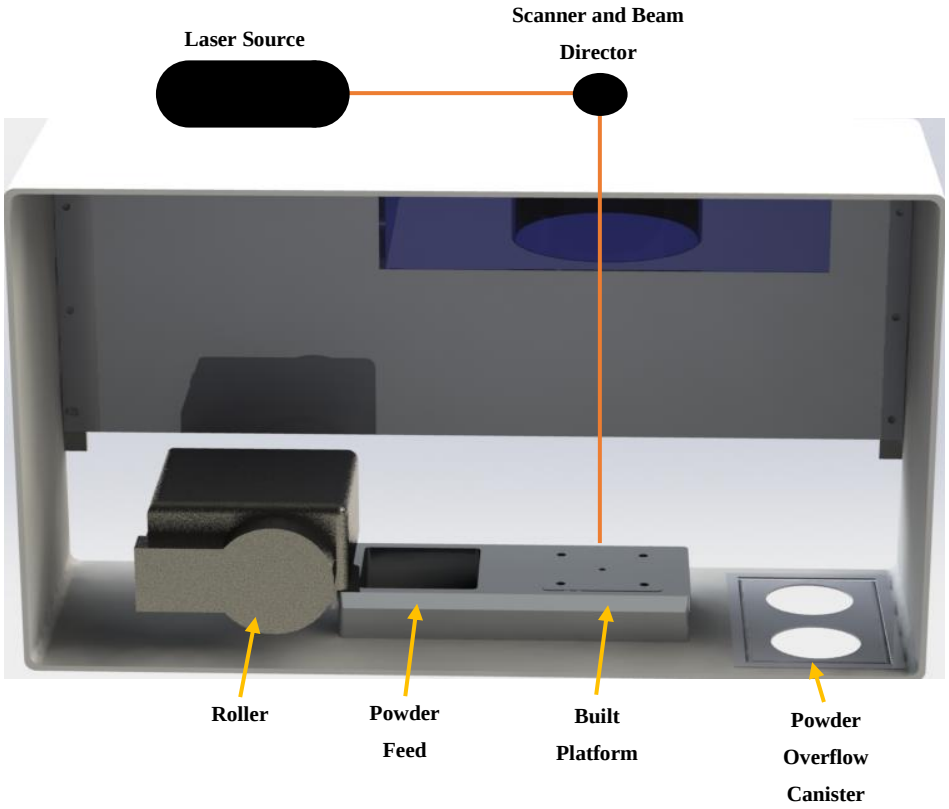

Figure 2-5 CAD model of a Laser-Powder-Bed-Fusion Additive Manufacturing system (modelled after the DMP ProX100 printer used in this study)

Laser-Powder-Bed-Fusion (L-PBF) systems as shown in Figure 2-5, typically use a spreader (roller/blade) to evenly distribute a layer of powder from the powder feed onto the build platform [51]. A laser then sinters/melts the powder according to the provided scanning parameters. The build platform lowers the part to the specified layer thickness after lasering, to repeat the process for each subsequent layer.

Excess/un-sintered powder falls into the powder overflow canisters, is then removed when full and recycled after sifting the powder. The sifting process ensures any solidified and large powder particulates are removed, to keep the powder particle size consistent with the standard specification. L-PBF systems typically use an inert gas environment or gas shielding technique to prevent excessive oxidation.

2.2.1 PROCESS PARAMETERS

Laser Characteristics

A laser heat source provides monochromatic coherent light, that works with both conductive and non-conductive materials unlike an electron beam [52]. Typically CO_2 or Nd:YAG laser sources ranging 50-500W in power are used in metal AM, with ultra-short pulse timing (typically Q switching), with instances of higher powered CO_2 lasers (18kW) used in some applications. Nd:YAG lasers have a shorter wavelength ($\lambda = 1064\ nm$), exhibiting a higher energy absorption in metallic materials, with a tighter focusing capability, though not as small as an electron beam spot size.

Compared to a continuous-wave laser, the pulsed-wave mode used delivers energy promptly in short millisecond(s) intervals for both sintering and melting applications resulting in a shorter interaction time [53]. Sintering refers to LBPF processes where-in the material is fused through a combination of heating and applied pressure without liquifying the material. Melting occurs when two metal particles are joined when liquified [54]. While the two methods are similar, and often mistakenly referred to as laser sintering, it is important to note the difference between Direct-Metal-Laser-Sintering and Direct-Metal-Laser-Melting.

Laser Scanning Characteristics

Scanning characteristics refer to the laser scanning speed (mm/s), spot size and scanning pattern of the laser spot. Glardon et al [55] defined the energy density (E) of the laser source to be:

$$E = \frac{P}{v_b . d} \tag{2-1}$$

where P represents the average laser power (average rate of energy flow over one full period), v_b is the scan velocity, and d is the beam diameter. Sears and Collins characterized that acceptable material properties exist above a certain minimum energy density. Where in, Equation (2-1) represents a proportionality; dependent on the fluctuating shape of the laser-powder melt pool. E is directly proportional to the average laser power and inversely proportional to the laser scanning speed. Several material and process characterization studies [35, 52, 56] of existing and newly developed machines aim to discover a balance in these parameters; to determine the limited operational range wherein desired part characteristics can be accomplished. Desired characteristics include an optimal scan velocity correlating with an ideal cooling rate (material thermal gradient), material microstructure, texture, compositional homogeneity and most significantly the production rate of the machine.

Typical L-PBF machines have a single laser beam, but advanced machines have been equipped with multiple laser beams. It follows, in these multi-beam systems, new process variables must be considered (beam overlap, power and frequency variations and more). This study focuses solely on single beam lasering systems. During the L-PBF process, the laser follows a predetermined scanning pattern; single-beam lasers classically use sequential scanning vectors. The scanning pattern impacts the thermal profile on the material and part, just as much as the scanning characteristics [57].

Studies have found increased thermal and unwanted residual stresses (often tensile and failure inducing in nature) can build up within the part if an area if the laser concentrated there for too long. To combat this, manufacturers often recommend the use of hexagonal patches, chessboard (zigzag), or parallel scanning patterns combined with rotating scanning directions [56].

Powder

Several powders have been standardised by ASTM, for LPBF processes, including grades of Stainless Steel, Titanium, Inconel (Nickel-based alloy), Aluminium and Cobalt Chromium [44]. AM material characterization is an ever expanding and highly desired area of research. Titanium is the most documented and researched metal [48, 58-60], with defined material characterisation and classifications, popular in aerospace and medical applications. Stainless Steel, Inconel, and Aluminium follow closely, due to their abundance and relative applications, where Cobalt Chromium is reserved for high-end niche applications [1, 61].

This study explores quality assessment strategies for L-BPF of Stainless Steel, as it holds a higher interest for its application in the major NZ industries, including the food processing, geothermal, petroleum industries etc [53, 62]. Understanding the effect of L-PBF machine

parameters, is made easy by previous works studying the material properties (particle size ratio), laser properties (melt-pool analysis), and build orientation of a part. Gibson et al [49] provides a well-document summary of this information for the Laser-sintering process. Table 2-1 notes significant material parameters and their relevant mathematical definition, which are affected by the laser scanning settings.

Table 2-1 Material (Powder) Parameters affected by laser scanning parameters

Powder Parameters	Definition	Relevant Equation	Equation definition
Absorptivity	Ratio of absorbed radiation to the incident radiation, based on the material and wavelength of the incident radiation.	-	-
Surface Tension (Wettability)	The tension of the surface film of a liquid caused by the attraction of the particles in the surface layer by the bulk of liquid.	$\cos\theta = \frac{\gamma_{sv} - \gamma_{sl}}{\gamma_{lv}}$ (2-2)	$\cos\theta \rightarrow 1$, liquid completely wets the solid γ_{sv} = solid-vapour interface tension γ_{sl} = solid-liquid interface tension γ_{lv} = liquid-vapour interface tension
Viscosity (μ)	Magnitude of internal friction in a fluid. (2-3) viscosity of molten pool (solid liquid mixture). (2-4) dynamic viscosity during completed liquid formation.	$\mu = \mu_0(1 - \frac{1-\varphi_l}{\varphi_m})^{-2}$ (2-3)	μ_0 = base viscosity φ_l = volume fraction (liquid phase) φ_m = volume fraction (solids)
		$\mu_0 = \frac{16}{15}\sqrt{\frac{m}{kT}\gamma}$ (2-4)	$m =$ atomic mass $k =$ Boltzmann constant $T =$ temperature $\gamma =$ surface tension of the liquid
Thermal Conductivity – packed powder (K_p)	Rate of heat transfer by conduction through a unit cross-section area of a material when a temperature gradient exits perpendicular to the area.	$K_p \cong (1 - \omega)K$ (2-5)	$\omega =$ packing density of powder bed $K =$ conductivity of the dense material.

The absorptivity of metal represents the energy balance of the process and affects the critical (minimum) energy density. Tolochlko et al [63] and the CRC Handbook [64] note the absorptivity (powder and dense form) of common materials used in additive manufacturing corresponding to the Nd:YAG and CO_2 lasers, excluding Stainless Steel. The surface tension (Equation (2-2) varies according to the spatial variation of temperature within the melt pool and drives the melt pool to move from lower to higher surface tension regions (Marangoni convention) [65]. The viscosity (wettability) (Equations (2-3 & (2-4) of the liquid metal enables the melt pool to span across the previously deposited layer [66]. The thermal conductivity (Equation (2-5) and corresponding thermal characteristics of the material, substrate and environmental processing conditions affect the cooling and solidification rates; influencing the resulting part microstructure [66].

The physical powder measurements can impact the in-process and final part characteristics including its minimum layer thickness, laser settings, spread ability, minimum inclusion size, shield gas reactivity (chemical reaction) and more [67]. These properties are impacted by the powder particle size, shape, elemental composition, and particle size distribution.

Substrate and support structures

LPBF parts are often manufactured upon a base plate or substrate, to which the part is melted/sintered onto. Therefore, it is important the substrate exhibits necessary thermal characteristics to provide adequate cooling and support during the layering process. Often the substrate is removed and recycled for reuse using some form of machining or cutting tool, and in rare cases incorporated into the final part design. L-PBF parts require support material between the substrate and the part (often the thickness of the tool used in the part removal), and to support certain extending/hollow areas of the part. The support material often penetrates the part layers and leaves an area of the roughest surface texture on the face of the part. For this reason, careful consideration is given to the build orientation of the part to reduce the required area of support structure [61, 68, 69].

2.2.2 SURFACE FINISH IN AM

There are several post-processing techniques required to extract the part from the build platform, ensure the surface finish is of a commercially accepted standard and heat treat the part to reduce stresses build up in the part during the build. For the LPBF methods, the part is fabricated on a build platform with support layers. The surface finish on metal parts as removed from the machine is often rough and inconsistent (exhibits a staircase like effect) due to the layering nature of the process. Current techniques used to improve surface finish include; milling, sanding, grinding, bead blasting, abrasive or polishing [70, 71]. L-PBF parts often have built up

residual stresses within the part, as such ASTM standards (for Titanium and Nickel Alloys) have been developed to use post heat treatment to solve this [37, 57].

Surface finish, alternatively known as surface texture or the surface topography, is the nature of a surface as defined by its characteristics (lay, surface roughness and waviness) [72]. Manufacturers often desire a specific surface finish for 1 of these 3 reasons; to visually improve its appearance or texture, remove perturbations to better fit between/into another part, and to control the process that results in the surface required. The key categories into which surface texture is often categorized are roughness, waviness, spacing and hybrid. Surface finish is popularly categorized by its surface roughness value (Ra), used to determine friction, wear, surface contact, lubrication, fatigue strength and tightness of joints [73]. Industry's requirement for specific roughness values is gradually becoming more stringent. Figure 2-6 [72] depicts the surface characteristics described (roughness, waviness, lay and surface profile). The waviness and roughness profiles can be used to numerically define the surface profile.

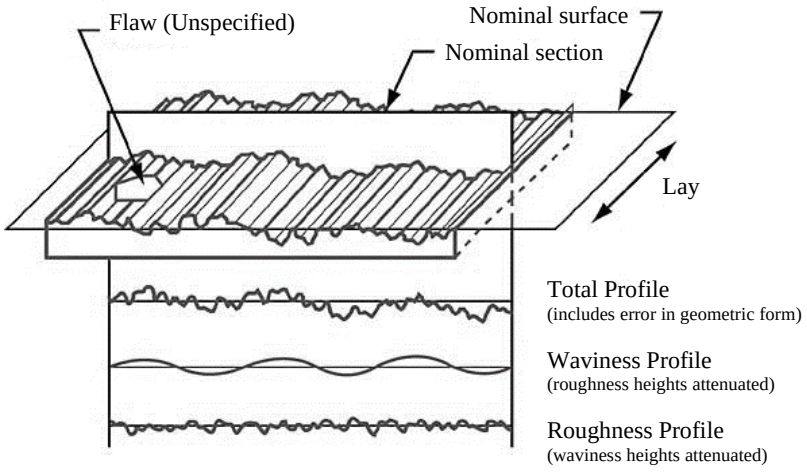

Figure 2-6 Surface profile characteristics; total profile, waviness profile, roughness profile and lay

The surface quality of L-PBF AM parts, is an established issue, with the staircase like effect created on the surface from the layered nature of the process [37]. The rough texture leaves an undesirable finish that is not only visually unappealing but can cause geometric inaccuracies and serve as defect initiation (cracks etc.) sites. Surface finish in L-PBF AM as-built parts exhibit considerable surface roughness, ranging from 5µm to 25µm. Additionally, different faces of a L-PBF part exhibits different surface textures/roughness; (a) the top face always has the best surface finish, (b) faces that have support material are the roughest, (c) the sides of a part, effected also by its angle of lean, have a varying surface roughness dependent on the staircase effect caused by the layering build procedure.

Previous studies have been performed to improve the as-built finish, but only slight improvement is shown with tightly controlling the processing parameters [70, 71, 74]. The as-built roughness range is comparable to sand cast parts (Ra 12.5 - 25µm), but post processing is often required to achieve values comparable to other cast or machined surfaces (Ra 0.4 – 6.3 µm) [37]. Controllable parameters within LPBF printers have been previously explored including, laser power, scan speed, hatch spacing, particle size distribution and layer thickness. Each of these parameters affect the final finish of the printed part, and every machine must be calibrated to achieve the best finish prior to printing.

The relevance of surface roughness in this study is two-fold. Firstly, to discover a method to reduce the post-processing required to improve surface roughness. Secondly, to determine methods of improving surface roughness within an internal chamber of a part that cannot be accessed by traditional roughness reducing processing methods.

2.2.3 STATE OF ART FOR SURFACE FINISH IMPROVEMENT TECHNIQUES

Literature documents several research methods employed post-print to improve the external-surface-finish of a part, however, next to no study has been done on internal surface finish improvement. This section reviews the different techniques considered, early in this research study, to improve the internal surface finish. Table 2-2 provides a summary of surface roughness achieved by traditional finishing tools [71].

Table 2-2 Summary of surface finish improvement techniques, and the roughness value achieved

Process	Roughness Range Achieved, Ra (µm)
Polishing	0.1-0.4
Grinding	0.1-1.6
Laser Cutting	0.8-6.3
Die Casting	0.8-1.6
Extrusion	0.8-3.2
Drilling	1.6-6.3
Sawing	1.6-25
Note* Industrial applications reliant on a good surface finish seek roughness values around the (Ra) 0.8µm mark.	

There have been several documented works to understand the variety of methods (laser polishing, shot peening, etc) and parameters (power, speed, hatch distance etc) that may be applied to this study [58, 75]. Dadbakhsh et al [76], has created a reference for laser-polishing parameters for laser-metal-deposition parts. Luong et al [77] studies the combined effect of laser-peening and shot-peeing on Aluminium AM specimens to determine the effect on the fatigue life

of a part following surface improvement. AlMangour et al [75] applied shot peening to Stainless Steel 17-4, concluding effective enhancement of roughness, hardness, compressive yield strength and wear resistance. Jamal et al [78] provides a comprehensive review of mass manufacturing surface improvement techniques, with a focus on drag finishing and concluded all methods stated in the study can achieve the desired surface finish (0.8μm).

Four surface-roughness improvement techniques were reviewed, with relation to metal AM: laser-micro machining, vibratory-bowl-abrasion, optical polishing, and chemical post-processing. Of the four, optical polishing and chemical post-processing could access the internal channels/chambers and walls of a complex AM part. The optical polishing method was chosen, considering the L-PBF process uses a laser with variable settings. Electropolishing was considered as a chemical post-processing method [70]. Both methods are reviewed in Table 2-3.

Based on the assessment of novelty, the authors background in Mechatronic systems vs chemical processes, and the additional benefit of in-situ surface finish improvement to reduce post-processing, laser polishing was chosen as the option to investigate for the research study presented within this thesis.

Table 2-3 Comparison of laser polishing vs electropolishing for surface roughness improvement of internal walls of LPBF parts

Technique	Description	Accessing the internal walls/valves/chambers	Research Contribution
Laser polishing	The laser within the LPBF printer can be set to apply different laser parameters (Speed, power etc.) The laser is used to re-melt a metal surface to even out particulates, and increase the bonds between horizontal layers; all contributing to a smoother surface	Needs to be done in-situ (during print)	Laser polishing has been previously studied post print for improvement in the external surface of the part. However, it has never been applied in-situ as a part is printing.
Electropolishing	Electropolishing is the application of Faraday's Law, whereby the metal surface is submerged in an electrolyte solution, and the treated section is connected to the anode (reverse of electroplating).	Can be accessed post print	This is a concept successfully being explored by the University of Louisville, who have already published a document to demonstrate the proof of concept. [79]

Laser polishing

Laser polishing (LP) is a finishing process, that can be used to smoothen a workpiece, enhance properties such as surface wear, remove oxidation, respect tolerances, create a reflective surface or prevent corrosion [80]. The process uses focused radiation of a laser beam to melt a microscopic layer of surface material (Figure 2-8).

Compared to the traditional methods mentioned previously (drilling, grinding etc.), LP guarantees no tool wear, less pollution (no abrasive or liquids), no debris, less machining time and proven to work with 3D complex workpieces. Studies have proven LP to be an effective method for surface finish in Metal AM parts, particularly in dies and molds (Figure 2-7) [58, 76, 80].

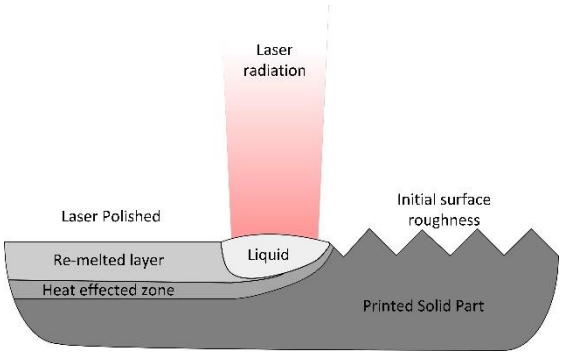

Figure 2-8 Surface laser polishing

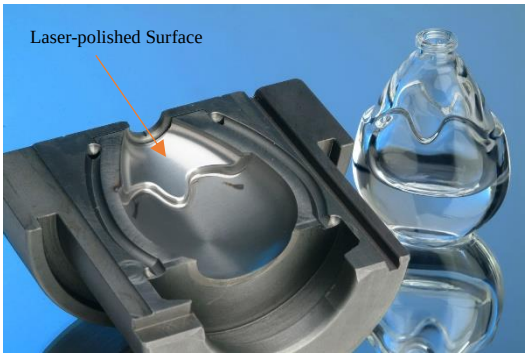

Figure 2-7 Example of a Metal AM laser-polished surface

The process is often performed with an assist gas, to reduce oxidation on a surface usually caused by molten droplets that can spray when the laser hits the part surface. This phenomenon is common in power-printed parts. Giorleo et al [58] noted, the surface roughness was improved further without the assist gas, but the oxygen phenomenon was detrimental to the part's quality. LP is achieved through 3 main levels; (a) polishing by large area ablation (i.e., large surfaces are polished), (b) polishing through localized ablation, to control power density where only rough surfaces are melted to reach a surface level, (c) polishing by re-melting.

This study focuses on laser re-melting, to perform the LP within the printer, so that internal walls can be accessed. These walls cannot be accessed using traditional post-processing laser-polishing methods. Re-melting in L-PBF occurs by re-sintering the lasered powder at varied laser settings to achieve the smoother surface. No literature exists to show this method has been previously employed to laser polish the surface.

Laser Polishing parameters

Key parameters documented in literature, for established LP strategies, primarily focus on laser power, laser scan speed, laser overlap, laser scan pattern, laser spot size and the laser energy density [80]. Table 2-4 defines each relevant parameter.

Table 2-4 Laser Polishing Parameters and definition

Laser Polishing Parameter	Definition
Laser Power (W)	Laser Power is a measure of energy supplied at a set wavelength, controlled by machine settings.
Laser Scan Speed (mm/s)	Laser Scan Speed refers to the passing velocity of the laser, with respect to the laser path during polishing. This parameter is also controlled by machine settings.
Laser Overlap (µm)	Laser Overlap is the distance from the centre of the parallel laser line to the next.
Laser Spot size (µm)	The size of the laser focus after it has travelled through the directional mirroring system and focusing lens onto the build area.
Laser energy density	The laser energy density is a combinative measure of the relationship between laser power, feed rate and the spot diameter.
Assist Gas	The gas used to inert the process chamber to help prevent oxidation

Laser Power and laser speed are the most varied parameters in determining the best methodology to improve surface roughness using LP. Most other studies review the effect of different assist gases (Argon and Nitrogen), laser overlap (hatch spacing), laser spot sizing and number of passes [61, 71, 76, 78]. These studies measure the improvement of surface texture through a study of surface and material characterization techniques; surface profilometry, SEM, X-Ray diffraction, electron back-scatter diffractometry, white light interferometry, hardness testing through micro/nano indentation, glow discharge emission spectroscopy and several other methods. Techniques used in this study are listed with further definition, for the readers understanding, in the methodology (Chapter 3).

2.3 NON-DESTRUCTIVE TESTING IN AM

2.3.1 DEFECTS IN LPBF PARTS AND DEFECT FORMATION MECHANISM

Defects exist in all metals. The size of the artifact can range from faults on an atomic scale that are inherent to crystallographic structures, or larger flaws that are introduced during fabrication and processing. Not all defects cause failure, but it is important to observe the flaws, rectify them where possible, or discard faulty components. Defect is a generalized term to describe microstructural anomalies for any of these cases and not always related to mechanical or cyclic failure [81]. Defects can be characterized by several factors including their origin and shape.

The microstructural features in AM components (i.e., powder particle size, surface and layer texture, solute distribution etc.) are influenced by variations in process parameters and material characteristics. The variation of these parameters may induce defects within the layers of the printed part. Table 2-5 presents the defects found in LBPF AM parts, taken from a summary provided by Everton et al [36]. The following sub-sections provide further detail on the defect description and defect formation mechanism. Numerous studies [82-84] (e.g., Rombouts et al and Slotwinski and Garboczi) document the effect of laser power, scanning parameters, layer thickness, hatch spacing, powder feed rate, powder size distribution and surface chemistry on the final microstructural characteristics and quality of the deposited material. To date, the combined influence and correlation between all related parameters, is yet to be understood, requiring more robust process models and critical experimentation.

Microstructural Anomalies

Defects within Metal AM parts resemble those commonly found in the casting process [38, 85]. Structural and mechanical flaws can form during the fabrication process and in the post-processing treatments. Anomalies in casting, exhibited in AM parts as well, include segregation, holes, and porosity, trapped gas pores, shrinkage and piping, inclusions, shrinkage, and piping [38, 39, 86, 87]. Misapplication of post-process manufacturing can lead to cracking, surface defects, release of shield gas pores within the part, residual stresses, and embrittlement effects within the AM part.

Table 2-5 LPBF internal layer defects

Material Discontinuities	Photo	Description	Typical sizes
(Gas) Pores	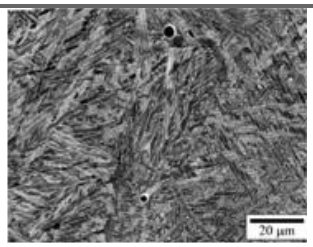	Entrapped gas pores within the bulk of the material. Material dependent.	~9.9 µm (electron beam-PBF) 5–20 µm (laser-PBF)
(Elongated) Pores	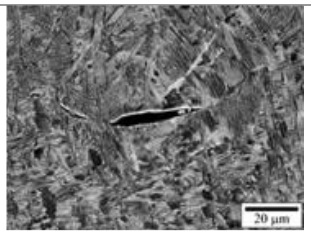	Lack of fusion pores in between layers of the AM process.	50–500 µm
Balling	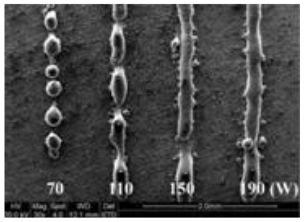	Molten material is not a flat layer, but instead creates large spherically shaped particles on the surface.	Part dependent — theoretically up to the length of the part.
Unfused Powder	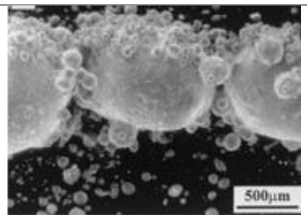	The melt pool varies in size and unfused powder is present.	Satellite powder clumps: 100–150 µm.
Cracking	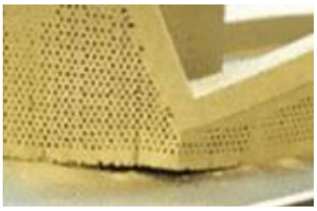	Cracks can be within the component or more commonly, a disconnection of the part from the baseplate is seen.	Parts on bed: residual stress in the range of materials yield strength. Parts removed from bed: deformation may occur without heat treatment or further processing.

Porosity

There are two types of porosity in LPBF parts: gas porosity and lack of fusion (LOF)/ elongated porosity (Table 2-5). Adjusting the build parameters can critically affect the level of porosity in LPBF parts [88]. Sintering and fusion laser-based methods exhibit porosity that is primarily micro-sized but can also be macro-sized (elongated pores) too. Entrapped shield gas (nitrogen/argon) can escape through some post-processing techniques but may lead to the formation of residual stresses (noted below). Some AM industries (e.g. medical hip implants) integrate porosity into their designs through the build file and build parameters [10]. Gas porosity, *P*, can be theoretically calculated as a percentage, based on the materials theoretical and measured density ((2-6) [88-90].

$$P = \left(1 - \frac{\rho_{measured}}{\rho_{theoretical}}\right)100 \tag{2-6}$$

Wu et al and Hann et al [91], derived that (2-7 can be used as a porosity percentage indicator for laser AM parts and that the formation of pores can be connected to the specific energy *E* applied per unit volume Equation (2-1 .

$$\frac{\Delta H}{h_s} = \frac{\eta P}{\rho h_s \sqrt{\pi \alpha \sigma^3 v}} \tag{2-7 }$$

ΔH is the specific energy (J/kg), h_s is the enthalpy at melting (J/kg), η is the surface absorptivity, P is the power (J/s), ρ is the density at melting (kg/m3), α is the thermal diffusivity (m2/sec), σ is the half width of beam spot (m) and *v* is the speed *(msec)*. Higher energy densities have been proven to eliminate gas pores but can result in rougher surface textures and create other microstructural anomalies. Consecutive layers deposited over a rough layer will continue to build ineffectively.

Hot isostatic pressing (HIP) is used to eliminate porosity and change the microstructure in AM parts [92-94]. This is a proven method to tackle internal porosity within an AM part, with improvement in ductility and fatigue resistance. However, the HIP does not affect surface anomalies, and the part still needs other post-processing measures to achieve the desired surface finish. Machining the part after the HIP treatment, can cause some internal pores to return with the release of trapped shield gas bubbles.

The following table (Table 2-6) contains the values (obtained from either literature, the machine datasheet, material datasheet or calculated), used to theoretically solve for the expected porosity percentage based on the varying laser power and speed (which affects the enthalpy at melting).

Table 2-6 Energy density parameters for the DMP ProX 100 laser settings at 98% Power

Porosity % parameters $\frac{\Delta H}{h_s} = \frac{\eta P}{\rho h_s \sqrt{\pi \alpha \sigma^3 v}}$	**η – surface absorptivity**	**P – Power (J/s)**	**ρ – density at melting (kg/m3)**	**h_s – enthalpy at melting**	**α – thermal diffusivity (m2/sec)**	**σ – is the half width beam spot (m)**	***v* – speed (msec)**
	0.07	49	660000	30	0.00058	0.00004	0.14

Lack-of-Fusion defects

Lack-of-fusion (LOF) defects (e.g., illustration of elongated pores in Table 2-5) can occur in sections where the energy density of the laser beam fails to melt the metal powder completely, so that the new layer is deposited with sufficient overlap. In the L-BPF process, the laser melts the powder according to predetermined scan strategy (size of points, lines, layers), to complete a whole layer [90]. If the laser energy drops during the melting phase, the width of the molten pool shrinks, resulting in minimal overlap between the scan tracks. LOF defects form regions of un-melted powder that cannot be completely melted once the successive layer is deposited. The surface upon these regions exhibits a rougher texture "which contributes to the flow of the molten metal to form interlayer defects". LOF defects are also referred to as pores and affect the overall porosity within the part.

Surface defects

As previously noted, the stair-case effect in AM processes caused by the slicing of part into layers, can lead to dimensional inaccuracies [95]. The melt pool dynamic influences the sidewall dimensions and overall topography of the parts surface. Dimensional inaccuracies causing surface defects (Figure 2-9) can be attributed to other defects formed within the part during print (porosity, cracking, LOF etc.). Which may result in problematic stress concentrations weakening the parts fatigue load, and undesirable for components that require accurate dimensional control. The material and build parameters affect the risk of shrinkage, curling, waviness, and surface roughness, which is why calibration tests should be performed to find the optimal printing conditions for the type of part to be printed and the best orientation.

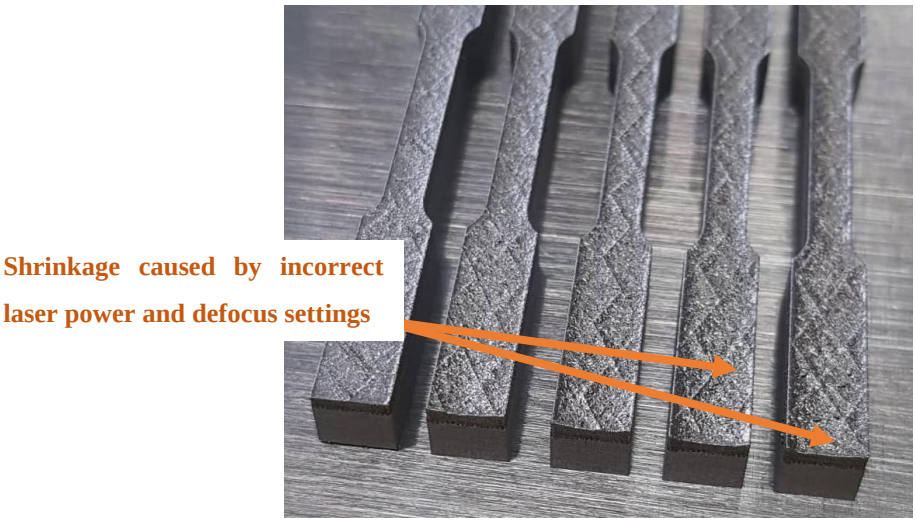

Figure 2-9 Example of shrinkage and extreme surface defects in DMP printed SS 17-4 PH calibration tensile dog bones

Residual Stress

Residual stress in a component can be attributed to several phenomena, including non-uniform plastic deformation during mechanical processing, phase transformations (cooling from a high temperature), heterogeneity of chemical or crystallographic order and some surface treatments [54, 57, 96, 97].

The rapid heating-cooling thermal process for AM part fabrication, can lead to the build-up of residual stresses within the part (like the welding process). During the melting process for direct-laser-melting, the laser source with high energy intensity rapidly heats the metal powder, causing thermal expansion (a compressive stress state) which is restrained at the targeted area by the surrounding powder. This is known as the temperature gradient mechanism (TGM) documented by Mercelis et al [54]. This mechanism is followed by a cool-down phase model, where the heat is removed, and the heat affected area begins to cool down and the material in the affected zone shrinks restrained by plastic strain formed during the heating stage. A tensile residual stress is formed in the heated zone, balanced by a compressive zone. C.Li et al [96] proposes a different graphical model should be used to compensate for the complicated nature of the AM process; the varying number of layers, lasering pattern and energy density. The author notes, residual stresses can be destructive as the layers are added onto each other and cause parts to pull away from the support structure. In extreme cases the stresses can exceed the mechanical aptitude of the part and cause catastrophic failure. Differentiated by their length scale there are 3 different classifications for residual stress: type I, type II, type III [45, 64, 81]. Type I refers to macro sized defects, the most failure inducing type of residual stress. Type II residual stresses are micro sized and type III are on the nanoscale, these two types have a limited effect on a structural integrity and mechanical performance of a metal AM part. Wu et al, demonstrates residual stresses

tend to be compressive internally and tensile in nature near the external surface for melted metal AM parts.

The effect of residual stresses within a part can be beneficial or detrimental, determined by the combination and type of stresses (tensile or compressive) within a part. Residual stresses that are tensile, when large enough, can cause a component to distort or crack. The presence of tensile stresses can cause fatigue failure and stress corrosion cracking. Residual stresses are numerically summed from the applied stress, and surface residual tensile stresses added to an applied tensile stress can reduce the reliability of components. On the other hand, compressive residual stress on the surface of a part will reduce the effects of applied tensile stress and most likely improve fatigue strength and resistance to stress-corrosion cracking [98]. Typically, hole drilling is used to measure residual stresses, because it is a relatively inexpensive process with an accuracy of ±50 MPa and resolution of 50-100 μm depth [99, 100]. The most accurate method and non-destructive testing (NDT) technique is X-ray diffraction with an accuracy of ±20 MPa and a 20 μm depth resolution [69, 92, 101, 102]. Curvature analysis and Neutron diffraction are two other residual stress measurement techniques but rank lower than hole drilling and X-ray diffraction [97].

The recommended X-Ray diffraction technique and experimental variables for Stainless Steel 17-4 PH is noted in Table 2-7.

Table 2-7 X-Ray diffraction technique and experimental variables for SS 17-4 PH

Radiation	**Lattice plane, (hkl)**	**Angle (2θ), degrees**	**Elastic constants(a)(E/1 =v) GPa (10^6 psi)**		**Bulk Error %**	**K_{45}(b)**			**Linear Absorption Coefficient (μ) $in.^{-1}$**
			(hkl)	Bulk		MPa	Ksi	cm^{-1}	
Cr Kα	(211)	155.0	180.0±0.7 (26.1±0.1)	158.9(23.0)	-11.9	696	101 .0	888	2254

Residual stress in metal AM parts can be relived with heat treatment. Cheruvathur [103] studied the post treatment of Stainless Steel (SS) 17-4 PH to achieve a reproducible microstructure with an improved Vickers micro-hardness. His research compared standardized methods for heat treating SS 17-4 PH to retain a certain percentage of austenite (FCC) to martensite (BCC) ratio (achieving a 1:9 [FCC: BCC] ratio respectively). Laser-based PBF methods can require post heat treatment because the build chamber is rarely heated, unlike the EBM-based PBF processes. Literature examines methods for monitoring thermal gradients, residual stresses and the heat affected zone during an AM print, used to characterize the effect of scan and build parameters on the AM part's mechanical properties, finish, and performance.

2.3.2 STATE OF ART FOR NDT TESTING IN METAL AM

The initial expectation of this research study was to focus on NDT monitoring of layer wise defects in AM machines. Reviewing the current state of art, for NDT testing for AM technologies, it was evident existing NDT technologies were being retrofitted to examine AM parts too. These technologies, as summarized in Table 2-8, are split into two categories: contact and non-contact. Further reading to define these methods can be found in these references [37, 104, 105].

Table 2-8 Contact and Non-Contact NDT techniques

Contact Methods	**Non-Contact Methods**
Eddy Current Testing	Through transmission Ultrasonic
Traditional ultrasonic Testing	Radiographic testing
Magnetic Testing	Thermography
Electromagnetic Testing	Infrared Testing
Penetrant Testing	Holography
Liquid Penetrant	Shearography
	Visual Inspection

Table 2-9 Post print NDT techniques vs In-situ SHM sensors

Passive and Active Sensors	**In-situ Sensor Array (Continuous SHM)**
Ultrasonic probing	Vibration Monitoring
Eddy Current	Strain Monitoring (electrical and fibre optics)
Liquid Penetrant	Peak-Strain indicators
Thermography and Vibro-thermography	Acoustic emission
Magnetic Particles and Magnaflux	Dielectric response
Computer thermography	Elastic wave emitter – detector pairs
Laser Ultrasound	Electro-mechanical impedance
Low power impulse radar	

NDT testing of AM parts can be further classified by whether the inspection was performed post-print or in-situ (Table 2-9) [106]. Computed Tomography (CT) has been established as the best method for post-print NDT inspection, and of the defects listed in Table 2-5 [37]. The NDT technology can successfully inspect porosity, structure, delamination, shape, cracks, and damage. But it cannot detect residual stresses, and the finer the micro-defect the longer

the processing time (hours). Furthermore, it is challenging to link the required detectability threshold to the capabilities of the diverse range of commercially available systems. Some microcracks may not have an empty volume and it is questioned if CT is an effective technique for detection in this case. CT is sensitive to orientation, cracks that are perpendicular to the x-ray beam may not be detected. Due the depth of research performed on CT; it was considered as an NDT technique of interest in defect monitoring. Extensive work has been performed to validate this method, but researchers highlight the need to examine more inexpensive and less time-consuming methods. Particularly methods that can be linked to feedback control, to "correct" defects within a part during the building stage [107].

Methods	*μStructure*	*Cracks, Porosity, Voids*	*Mechanical Properties*	*Geometric Accuracy*	*Surface Roughness*	*Residual Stress*
Visual	N	S	N	S	S	Y
Ultrasonic	Y	S, I	Y	Y*	N	Y*
Eddy Current	Y*	S*	N	N	N	N
Radiographic	Y	S, I	N	S, I	S, I	N
Magnetic Methods	Y	S*	N	N	N	Y*
Liquid Penetrant Test	N	S*	N	N	S*	N
Shearography	N	S, I*	N	N	N	Y*
Acoustic	Y	Y*	Y	Y*	Y*	Y*
Thermography	N	Y*	N	N	N	N

Figure 2-10 Applicability of various NDT methods to the primary quality concerns in additive manufacturing. N – not applicable, S - surface sensitive, I - internal or through-thickness, Y - applicable, *

From the summary of detection methods presented in Figure 2-10 [37], Acoustic NDT methods were considered one of the more versatile but under-explored options to consider. The presence of changes of in microstructure, surface and internal defects, geometric anomalies and changes, variations in surface roughness and residual stress (due to corresponding changes in the microstructure) all affect the signature of sound moving through the part. The challenge in using this technique realistically and practically, would likely result in a qualitative not quantitative NDT technique, where the sound signature (tap or other impact), could be compared to an expected signature [108]. A depth of knowledge in acoustic waveforms, harmonics and signal processing would be required to progress this technology into a quantitative research strategy. Before this research study matured, Acoustic Emission (AE) had not been widely applied in AM for this reason. However, since then several studies have now examined and highlighted the

difficulty in isolating signature signals indicative of defects (particularly crack initiation). One study found by Strantza et al [109], documents the use of AE for crack detection post print using elastic waves that are emitted in a medium due to crack nucleation or propagation. It was surmised research into acoustic ultrasound and resonance testing should be explored to see the effect of trapped powder within the part on the reading of transmitted and received signals on an oscilloscope. However, this research, though prominent for novel contribution, was only briefly explored (Chapter 5 discussion) due to the time restriction and focus on other quality strategies tied to feedback control.

The defective mechanisms that occur in metal AM parts as described above, can primarily be related to un-fused powder or trapped gases. Research documents various NDT technologies and sensors that examine the melt pool, each layer individually or multiple layers together, the feedstock feed rate, heat-affected zone, thermal profiles, signature acoustic sound waves etc. Most techniques singularly focus on one issue, which has resulted in commercial entities releasing machines with many sensors. The vast amount of data, collected by these sensors and NDT health monitoring systems, require supercomputers to store and process the data. In the last 2 years focus on NDT research for AM process certification has evolved from adapting existing NDT technologies to fit into AM production lines, to using image processing and object identification methods to move toward a machine learning and deep learning solution. However, these systems are expensive and singularly focused on AM machines made by the same manufacturer. Limited information is publicly available for commercial NDT AM systems, i.e., for other researchers and companies to improve on the solution. This research exposed an opportunity to create an open source, adaptable solution that could work in multiple research environments. Consequently, this study explored in-situ thermography and digital layer-wise capture with a low-cost solution, and subsequently developed a quality strategy linked to feedback control, defect identification and minimization. The following sections detail the background literature and explore solutions to discover an appropriate low-cost NDT quality management strategy and build set-up.

2.4 IN-SITU OPTICAL IMAGING TECHNOLOGIES AND PROCESSING FOR DEFECT CAPTURE AND IDENTIFICATION

An optimal digital photography/videography quality monitoring system for metal AM systems will work toward creating a machine learning or deep learning solution [110-113]. This would create an online health monitoring NDT system to verify the quality and precision of a printed part. Previously discussed, are the process differences that exist in each metal AM machine. Therefore, while a universal monitoring solution may exist, for several AM machines, the data input and process monitoring would be different.

The previous sub-section already details the data investigated (i.e., defects). The build area and workable camera focal distance within the printer limited the best digital solution for the job. Various solutions were considered for an appropriate optical imaging technology including high speed cameras, high resolution cameras, time-of-flight, thermal cameras and more [73, 114-117]. Due the size of the artifact needing to be detected (10µm to 500 µm), a high-resolution solution was required. Reflectometry, interferometry, and spectrometry were light-based optical detection methods considered to map the profile of each layer [118].

Michaelson's interferometry captures the difference in amplitudes between a light profile passing through a beam splitter and mirrors with the original beam. The superimposed combination of these two profiles is studied to capture the part's surface profile. MIT has created a custom enclosed printer with a Michaelson's interferometer built-in to capture microprinted parts [119]. While this would be an excellent solution for imaging micro-defects the capture area is small, setting up the system in existing systems would be difficult, expensive and require regular re-calibration. Spectroscopy was ruled out for similar reasons, including its suitability to nano-scale artifacts rather than micro. Table 2-1 describes 3 other methods that were seriously considered including spectral reflectometry, laser-scanning, and laser speckle. Laser scanning has already been incorporated into new model printers and is a high-cost solution. While laser speckle was considered a good solution, it was not explored in the duration of this study but included in the future work section. Spectral reflectometry was further explored due the set-up simplicity, effectiveness, and low-cost nature.

Table 2-10 Optical imaging techniques for layer-wise capture

Detection Category	Technology	Description	Typical Experimental Setup
Optical	Spectral Reflectometry	This is a non-contact optical that utilises the lasers wavelength, a light source, and a camera to capture the superimposed image of the interaction between the laser and light colour.	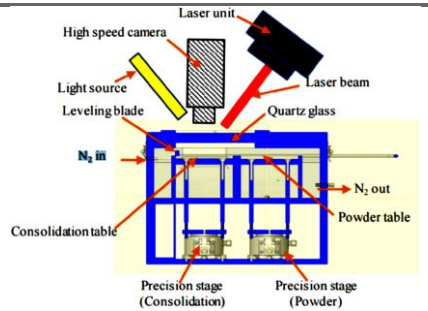
	Laser Scanning - Electronic Distance Measurement	Surface roughness can be determined by averaging the height of the surface profile at set incremental points. Laser scanning technologies employ an Electronic Distance Measurement system to determine the height between the scanner and surface and create a 3D image of the surface.	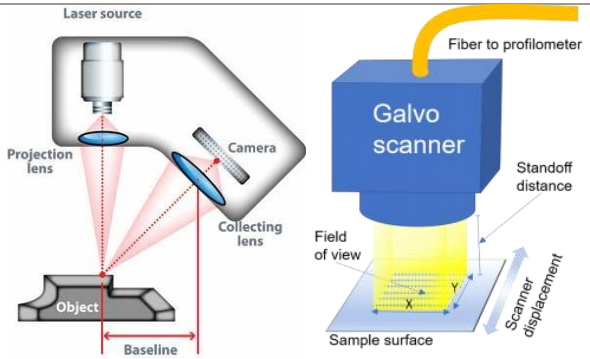
	Laser Speckle – with Digital Image Correlation	Laser speckle interferometry uses the intensity distribution pattern formed from space interference which is illuminated by coherent light cast upon the rough surface. Digital image correlation uses the speckle image to measure the light intensity before and after deformation and uses the peak cross correlation function to derive the displacement of the object.	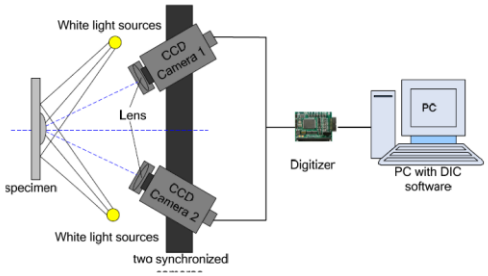

While the digital high-resolution camera solution could perform layer-wise capture of each layer, there was no information linked to the thermal stresses. Therefore, the considered solution was evolved to include a thermal camera too. While high-resolution digital cameras are respectfully affordable, high-resolution thermal cameras are not. Low-cost thermal cameras overlay a digital camera image with a thermal grid sensor to create clearer images (Figure 2-11). Chapter 3 describes the custom high-resolution digital camera and low-resolution thermal camera fusion that was used in this study. Spectral reflectometry works well for both digital and thermal cameras, to provide excitation on the surface of the printer part.

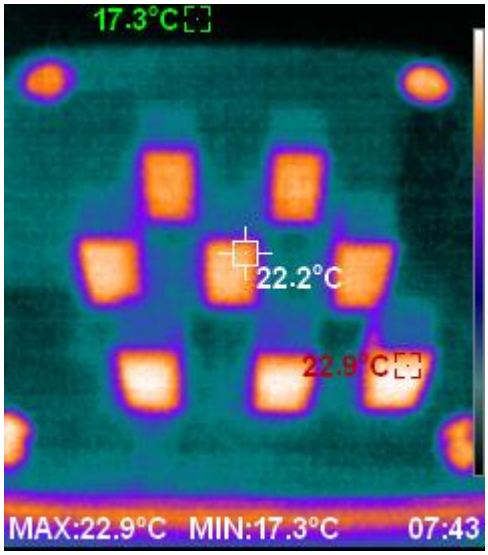

Figure 2-11 Thermal image of metal printed cubes using a low-cost commercial thermal camera

Thermography

Infrared thermography is the measurement of radiation being emitted from an object, using a thermal sensor [120-123]. Thermal Imaging is an established non-destructive characterization technique, and practical implementation within the field requires a compact and mobile system. The use of thermography in AM will enable technicians to measure the temperature profile of the printed part and study the active area for temperature cycling on the part. Observation of the thermal profile may prove fruitful in the discovery and characterization of defects within a metal printed part.

Thermal imaging techniques are often classified by Passive thermography and Active Thermography [123]. Passive thermography involves observing the sample/specimen with just the thermal camera recording its ‘passive’ temperatures and heat signatures. In some cases, the specimens need to be excited to observe a better thermal image; in this case active thermography is required. Active thermography has many sub-classifications and techniques that determine the experimental set-up and type of data that is collected from thermal imaging a specimen. Active thermography is split by internal excitation which uses a lock-in thermography experimental assembly and secondly external excitation that can be done using a pulse phase thermography set-up or the lock-in/modulated thermography experimental set-up. Table 2-11 below defines the relative thermography techniques/classifications.

Table 2-11 Thermography Classifications

Technique/Classification	Definition
Passive Thermography	Monitoring a heat signature on a specimen using a thermal camera
Active Thermography	Inducing a heat flow by an energetic excitation of a test object through Electrical, Ultrasound, Induction, Optical or thermal means, and observing the test specimen using a thermal camera
Internal Excitation	Internal Excitation (Electrical, Ultrasound, Optical and Induction), has a set energy source that excites the test specimen constantly and the IR radiation emitted from the part is then measured by a thermal camera.
External Excitation	External Excitation (thermal/optical/water/air) is a triggered energy source that is pulsed or locked in for a period, the effect is observed by the thermal camera.
Pulsed Phase Thermography	A pulse of energy is supplied to the test specimen, which launches a thermal front that propagates under the surface of the part by diffusion. The duration of the pulse is variable depending on the thickness of the material.
Lock-in/Modulated Thermography	The lock-in thermography principle applies a periodic input energy (Excitation) to the surface of an object being examined and analysing the resulting local temperatures on the surface of the object.

Active Thermography

A heat flow is induced by an energetic excitation of the test object, which can be done in a transmissive or reflective setup. The resulting heat flow is influenced by interior material layers and defects. A transmissive (source under the part) set-up is ideal for penetrating larger samples, whereas a reflective set-up (source pointing toward the surface of the part) can penetrate a small depth of the sample. Many researchers prefer the reflective set-up in applications because very seldom they have access to both sides.

In metal AM, only the top surface of the part is accessible, therefore a reflective set-up using lock-in thermography was considered to reduce the required excitation power and the data acquisition requires one lamp like the spectral reflectometry set-up.

Lock-in Thermography (LT)

LT was derived from a technique in which a miniscule surface area is periodically illuminated by a modulated laser beam to inject thermal waves into the specimen [122]. The thermal response is recorded simultaneously through an infrared detector and decomposed by a lock-in amplifier to extract the amplitude and phase of the modulation. This phenomenon is also known as photothermal radiometry. LT can consist of a simplified set-up using a halogen heat

source for example. Halogen lamps are a low-cost solution compared to flash lamps and other heating sources. The second requirement is the infrared detector (with the camera as previously described, 320 x 256 or 640 x 512) and the third hardware with LT software to mathematically extract the amplitude and phase of the response. The relevant theory is further discussed in Chapter 3 with relation to the application. Ibarra-Castanedo et al documents a comparison of different active thermography techniques to detect defects in honeycomb structures. The review concluded LT and pulsed phase thermography to output clearer raw thermal images (more visible defects), however the defects were quite large (< 1 inch). The leading research for thermography in AM, Krauss [120, 124] documents several thermal, digital and pyrometric device set-ups to monitor the build external to the printer through the germanium viewing glass to detect defects within the 40µm to 500 µm range. The observed flaws were induced artificially into the print and exhibited a decelerated cooling characteristic due to the lower heat conductibility. The use of a bolometer in the study eliminated the need for an active excitation source. The methodology detailed in the subsequent chapter takes inspiration from both experimental designs.

CHAPTER 3

3 METHODOLOGY

This section examines the research methods developed around the investigative questions and problem statement presented in the introductory chapter and provides a technological review to aid the readers understanding of the next two results-based chapters. The chapter begins with an overview of Direct-Metal-Printing (DMP) the metal AM process used to generate test specimens and around which the solutions of this thesis have been adapted to. During this research study, the printer required several optimization tests and post-print operation strategies to be amended to create a more efficient workflow process and ensure the quality of the test specimens. Further detail on the optimization process follows below. The chapter is then divided into two case studies that focus on the key issues surmised in the literature review: surface finish improvement and NDT testing. Case study 1 was developed around in-situ laser polishing the surface of the DMP SS 17-4 PH printed parts and took a considerable amount of time out of this doctoral study period. The research aim, hypothesis and experimental methodology was obvious and developed efficiently to maximize the number of trials (sample size and iterations) that could be done to ensure enough time remained for post-processing the printed samples, and data gathering.

Case Study 2 was developed in parallel to focus on the studying NDT methods to create novel quality strategies catering to the unique nature of the LPBF metal AM machine used in this study. However, a significant amount of time was spent exploring different NDT methods to understand the technologies (visual inspection, thermal and acoustic methods) and determine the best experimental set-up that would work within the research scope (time restrictions) and provide fruitful research to the quality inspection techniques designed for the metal AM research space. The digital and thermal camera actuation system described further in this chapter was the first practical modification made to the DMP ProX 100 to explore in-situ NDT testing. Digital and thermal NDT data capture strategies are not novel, which is why a considerable amount of time was spent exploring acoustic solutions. But it was deemed un-feasible to develop a novel methodology, interpretation of the results and complete the testing the results within the doctoral research period alongside the other case studies (i.e., it needed to be the sole focus from the start of the research). The conceptual research, considerations and work done to explore acoustic NDT methods is described further in the Chapter 5 discussion. The exploration of digital and thermal imaging focused on exploring machine vision techniques complemented by spectral reflectometry with a white light for quality assurance applications (file security, part/defect detection and sizing, 3D reconstruction of surface topography for a realistic representation and simulated analysis).

3.1 DIRECT METAL PRINTING

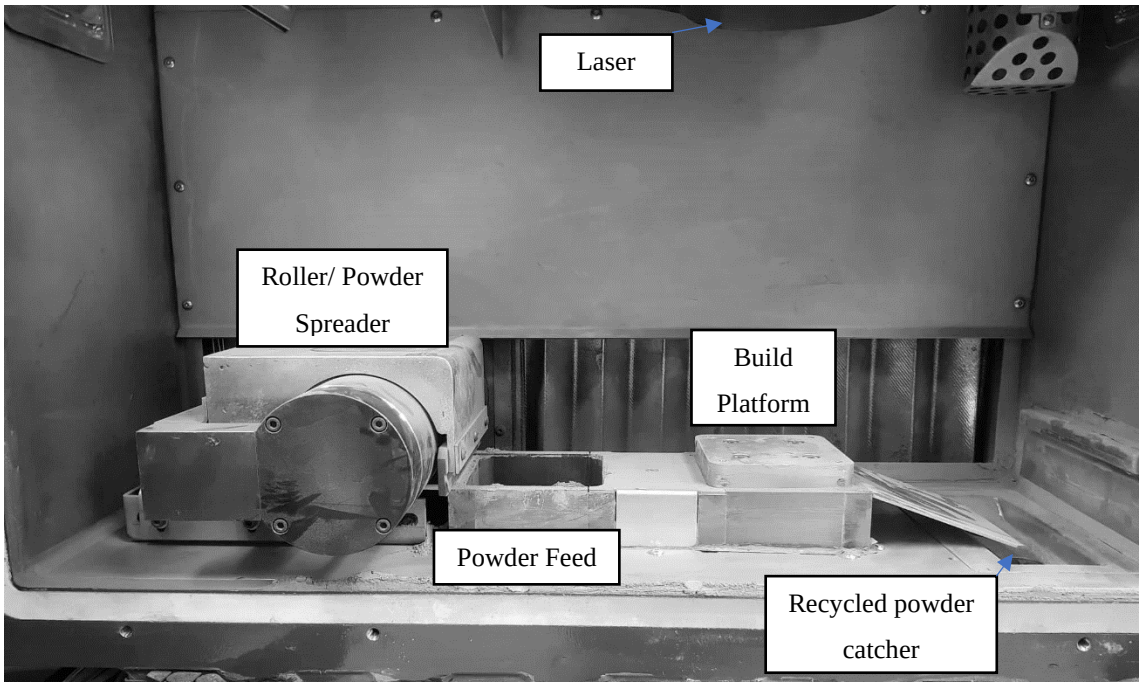

Figure 3-1 DMP ProX 100 original build chamber

Direct-Metal-Printing (DMP) a form of L-PBF, is the AM method at the center of this study, used to fabricate all test specimens documented in this thesis [125]. The DMP ProX 100 used in these experiments is an ideal research machine that gives the user access to change its build settings, laser settings and assist gas settings. The DMP ProX 100, is equipped with a 50W Fiber laser, with 1070 nm wavelength and a build envelope capacity (X x Y x Z) of 100mm x 100mm x 100mm. The chamber of the DMP is inerted with a Nitrogen assist gas, and during print maintains on average 1000 ppm (parts per million) oxygen within the chamber. CAD files are imported and sliced within the DMP's own 'DMP Manufacturing' software. This software allows the user to add support layers, configure laser settings, control powder feed-rate, and place the part in the desired build orientation. The DMP prints in a hexagonal lasering pattern (Figure 3-2), which was made to reduce residual stresses from forming within the part. The laser will target different hexagons in the part slice to reduce heat build-up through continuous printing.

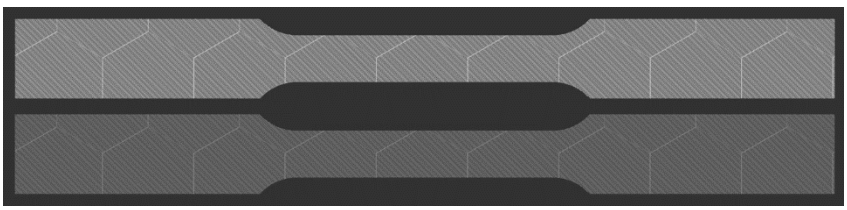

Figure 3-2 Hexagonal printing pattern for one slice of a DMP printed ASTM E8 Tensile Dog bone

3.1.1 OPTIMIZATION OF SETUP, PRINTING, AND POST PROCESSING FOR THE DMP PRINTER

Figure 3-3 DMP printing process: pre-processing, print and post-processing steps

Figure 3-3 illustrates the DMP manufacturing pre-processing, printing, and post-processing steps. The pre-processing stage involves the steps from preparing the build plate to setting up the printer. The 100mm x 100mm Stainless Steel build plates are re-used to minimize material wastage: the accurate levelling and tooling allowed in the CNC, allows for micrometre removal of the used surface. The print surface of the build plate is then roughened by running sandpaper in one direction only. The roughened lines are placed perpendicular to the powder spread, to prevent the powder from sliding off as the roller spreads the first layer of powder onto the build plate. Previously, a linisher was used to create the rough texture on the build plates, but it was found to leave a detrimental imbalance on the surface, which caused several prints to fail. It was determined, medium hand-sanding proved to be a more efficient and accurate method for every print.

The prepared build plates are then loaded into the machine to start the AM process. New powder was purchased for the experimental research documented in this thesis. The powder was recycled no more than 3 times, though the sifter ensures powder particulates of the standardized size remains whilst the rest is discarded. The recycled powder was examined in an SEM using EDX analysis to determine whether its chemical composition complied with the datasheet specified ratio.

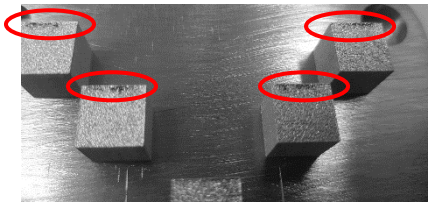

Figure 3-4 Close up of voids on the top surface of one calibration print

The composition is detailed below in section 1.3.1. The printer is inerted with nitrogen gas, provided from reusable and replaceable canisters. The DMP requires regular re-calibration to determine the best laser sintering settings. The calibration test (Table 3-1) studies the effect of laser power vs the laser defocus (in mm how high or low the print bed must move during the lasering stage). The laser power ranges from 80% to 98% and the defocus from -4mm to +4mm. The following table and illustrations (Figure 3-5) detail one of 3 calibration tests performed to ensure the ‘best’ laser settings were chosen for the experimental specimens detailed in the following sections.

Table 3-1 Calibration experimental set-up for DMP ProX 100 scan parameters

Cube (as labelled in Figure 3-5)	Laser Power (%)	Laser Power (W)	Laser Defocus (mm)
1	98	49	-4
2	98	49	-3
3	98	49	-2
4	98	49	-1
5	98	49	0
6	98	49	1
7	98	49	2
8	98	49	3
9	90	45	0
10	85	42.5	0

3.1.2 RESULTS OF CALIBRATION TESTS FOR BEST SCAN SETTINGS

During the calibration test key checks to assess which setting work best includes the sparks flying as the laser melts the powder, and voids (Figure 3-4) or inclusions (roller will not move over the part), discoloration (burning the powder), and finally any areas of shrinkage when the part is completed. The test specimens printed at - 2mm and + 2mm laser defocus showed good sparking (lots of sparks), and coloration on the surface throughout till the final print layer. The next test examined the effect of two different laser powers (90% and 98%) with these two defocuses with test cubes printed across the build platform. Figure 3-6 illustrates four of the build plates from the test. The + 2mm defocus and 98% laser power was chosen as the scan parameters based on even performance across the build plate (no shrinkage, no burnt layers, micro-voids etc). These settings were then applied to tensile specimens to determine if the tensile strength of the printed part matched the datasheet specifications of 1100 MPa ± 50. Confirming this, 98% laser power and + 2mm defocus was used for all experiments across the case studies presented in this thesis.

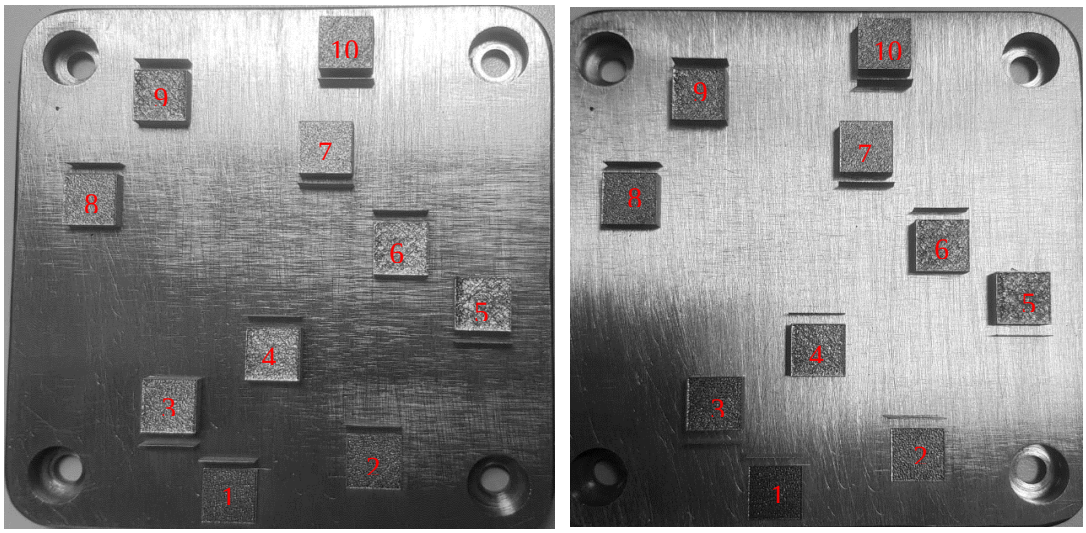

Figure 3-5 Capture of calibration plates with Table 1-1 laser parameters

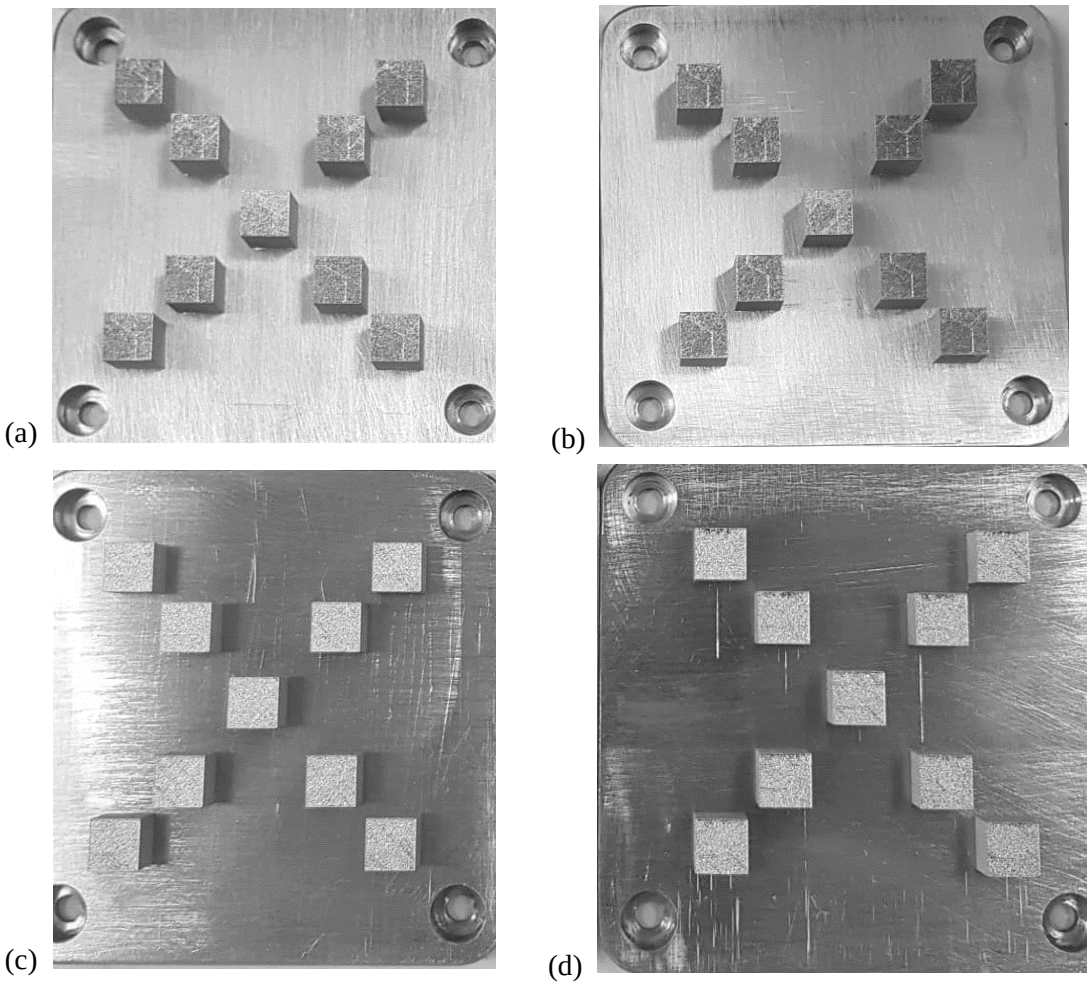

Figure 3-6 Calibration full plate test with tests (a) 90% LP -2mm laser defocus, (b) 90% LP 2mm laser defocus, (c) 98% LP 2mm laser defocus, and (d) 98% LP -2mm laser defocus

3.2 STAINLESS STEEL 17-4 PH

Stainless Steel (SS) 17-4 PH (precipitation-hardened) is widely used as a structural material in applications that require a corrosion resistance, high tensile/impact strength, fracture toughness and with a service temperature below 300ºC [75]. Application includes aerospace, petrochemical, power plants and marine environments. The specifications noted below in Table 3-2, are the elemental make-up for the martensitic stainless steel, strengthened by precipitation copper (Cu) rich spherical particles in the martensite (α) matrix (bcc, a = 2.86 Å). There are different grades of SS 17-4 PH, where the powder particle size can range from 6-45 µm. The build environment is typically inerted with a shielding gas of either Argon (Ar) or Nitrogen (N). For all experiments documented in this thesis, the powder used is LaserForm®17-4PH (B) (PS4542A: Stainless steel 17-4 PH) provided by 3D systems, and a Nitrogen shielding gas.

3.2.1 CHEMICAL COMPOSITION

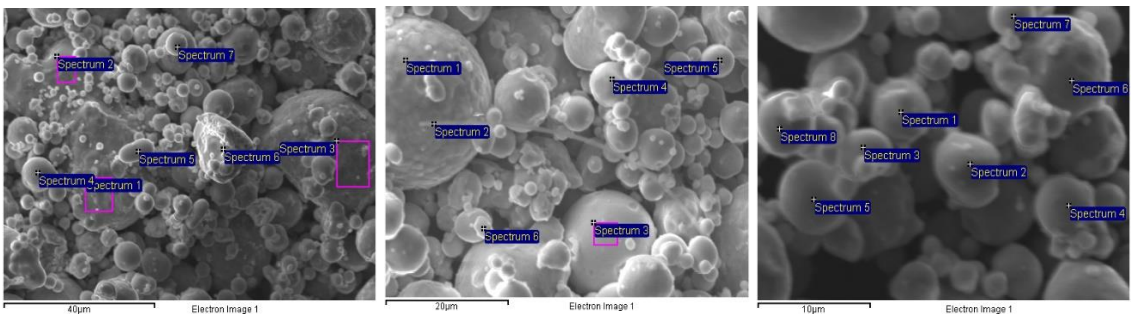

Figure 3-7 Selected images from spectrum analysis of recycled SS 17-4 PH powder

The images in Figure 3-7 illustrate the state of SS 17-4 PH after being recycled and reused following several prints. The images were taken in a Zeiss EVO MA25 scanning electron microscope (SEM) equipped with an energy dispersive X-ray spectrum analyser (EDX, Oxford Instruments). Several images were taken with eight measurements of detected elements and their ratio. The average is presented in Table 3-2.

Table 3-2 Chemical composition of SS 17-4 PH powder comparing the data sheet specification vs the recycled state of the powder

Data sheet specification (%)						
Si	Cr	Mn	Fe	Ni	Cu	Nb
<1.0	15.0-17.0	<1.0	Balance	3.0-5.0	3.0-5.0	0.15-0.45
EDX analysis of recycled powder (%)						
Si	Cr	Mn	Fe	Ni	Cu	Nb
0.83	17.38	0.85	71.76	4.7	4.22	0.27

3.2.2 MECHANICAL PROPERTIES FOR PARTS BUILT IN A DMP PRO X 100

The table below provides a summary of reference mechanical properties taken from the DMP ProX 100 datasheet.

Table 3-3 Summary of Mechanical Properties from the DMP ProX 100 datasheet

Mechanical Property	As built	After post heat treatment
Ultimate Tensile Strength (ASTM E8)	1100 MPa ± 50	1300 MPa ± 50
Yield Strength (ASTM E8)	620 MPa ± 50	110 MPa ± 50
Elongation at Break (ASTM E8)	16% ± 2.0	10 % ± 2.0
Hardness	300 ± 20 HV5	400 ± 20 HV5

3.3 CASE STUDY 1: CHARACTERIZATION OF IN-SITU LASER POLISHED DMP SS 17-4 PH SURFACES

The need for specialized surface improvement techniques to create a novel solution that addresses the impossibility of subtractive machinability for inaccessible areas, in a metal AM part, was identified as a major research gap. The purpose of this case study was to observe and characterize the textural and mechanical aptitude on the surface of metal 3D printed parts, with respect to changing printing parameters. This section details the test specimens, design of experiment (DOE), characterization tools and analysis techniques used to achieve the study's aim. Initial testing for this study examined the effect of using the optimized print settings (laser power, speed, hatch spacing etc.), re-lasering the surface with varying polishing runs, whilst alternating the laser scan pattern. This study was published in an IEEE conference proceeding "*The effect of reheating layers in Metal Additive Manufacturing on the external surface finish of a printed part"*. The test specimens were square and circular in shape, however only the final flat ($\angle 90^{o}$ to the laser) surface was re-polished. This study concluded the repolishing with the single laser beam does topographically alter the surface of the printed art, and while it improved the lustre of the surface texture, the surface roughness (Ra) worsened. The effect on the part prompted the next series of tests conducted within this case study, to examine the effect of varying the laser speed, laser power, hatch spacing (where relevant) and number of repolishing coats.

This case study focuses primarily on improving the Ra value of different 'faces' on a metal printed part, consequently observing the effect on the mechanical and topographical variations.

Aim

To use single-beam laser re-polishing to improve the surface finish (roughness, textural features and reduce surface defects) without compromising the mechanical hardness and strength of the sample. Consequently, to determine if this strategy can be used for in-situ improvement of complex angles and hard-to-access (by post-processing machinery) surface topography.

Hypothesis

What is the effect of laser polishing the external surface of metal AM parts using the in-built laser during print? What key input parameters have the most positive effect on the part's surface texture and mechanical aptitude?

The following hypothesis was developed in response to the above research questions. Laser polishing is an established technique proven to improve the surface finish of metals parts including their texture, surface profile, lustre, reduce sub-surface defects and improve surface hardness. Laser polishing is typically performed as a post-processing technique that scans the surface of a part in a multiple axis system. The DMP ProX laser melting machine used in this study has a fixed laser angle of 90 degrees and a fixed base. Parts can be printed at different orientations as shown in

Figure 3-8. Therefore, it was theorized by rotating the part build-orientation at different angles could provide the rotational component typically found in laser polishing systems. Figure 3-9 illustrates the part orientation from the front and side, with the angle of lean respective to the laser. **It is hypothesized that varying laser parameters (laser speed, laser power, and pattern repetition) with respect to the wall/surface orientation, to polish the surface during print will produce varying layer thickness that will alter the surface topography. Moreover, it will affect the mechanical hardness, surface profile (change in R_a, R_{sm} and R_z values) and the chemical composition of the surface elements (increased oxidation). Characterizing this variation should provide critical and novel data to create a quality improvement strategy that recommends the best part-orientation combined with LP settings, for improved mechanical and structural topographical features that will subsequently reduce the post-processing time required to polish the part.** Previous laser polishing studies [58, 76, 80] prove hatch spacing to be a key parameter in improving the surface finish of a part. The only orientation that will work to study the effect of varying the hatch spacing is the top surface, subsequently one drawback of this study this parameter cannot be tested on the angled surfaces.

3.3.1 METHODOLOGY

Test Specimens

Test specimens are created according to the corresponding testing standard criteria required. The analysis performed on the samples, in this case study, primarily quantifies and maps the surface profile of the part. Therefore, following the ISO4288: ’96 standard for measuring the R-parameter for the Ra (µm), Rz (µm) and RSm (mm), a sampling length of 2.5mm (ℓ x r) and total evaluation length of 12.5mm (ℓ x r x 5 = 2.5mm x 5). To give the roughness gauge room to measure this length the sample surface area (L x W) was set to 15mm x 15mm. The specimens created with the circular cut in the center of the sample were set with a diameter of 8mm (minimum size to allow the profilometer probe to fit and actuate smoothly along the surface). Since the other inspection techniques were optical based with no standard size required, they did not influence the size or shape of the test specimens.

Figure 3-8 references the five types of testing specimens created in this experiment to analyse the effect of angle of lean on the layer thickness as the surface edges are remelted. This include laser-polishing the top surface at ∠ 0º, ∠ 20º, ∠ 40º, ∠ 60º, ∠ 80º and ∠ 90º degree angles (relative to the laser). The build plate in Figure 3-8 (c), exhibits the different laser polishing settings applied in the DMP ProX manufacturing software, the different colours represent different machine setting profiles.

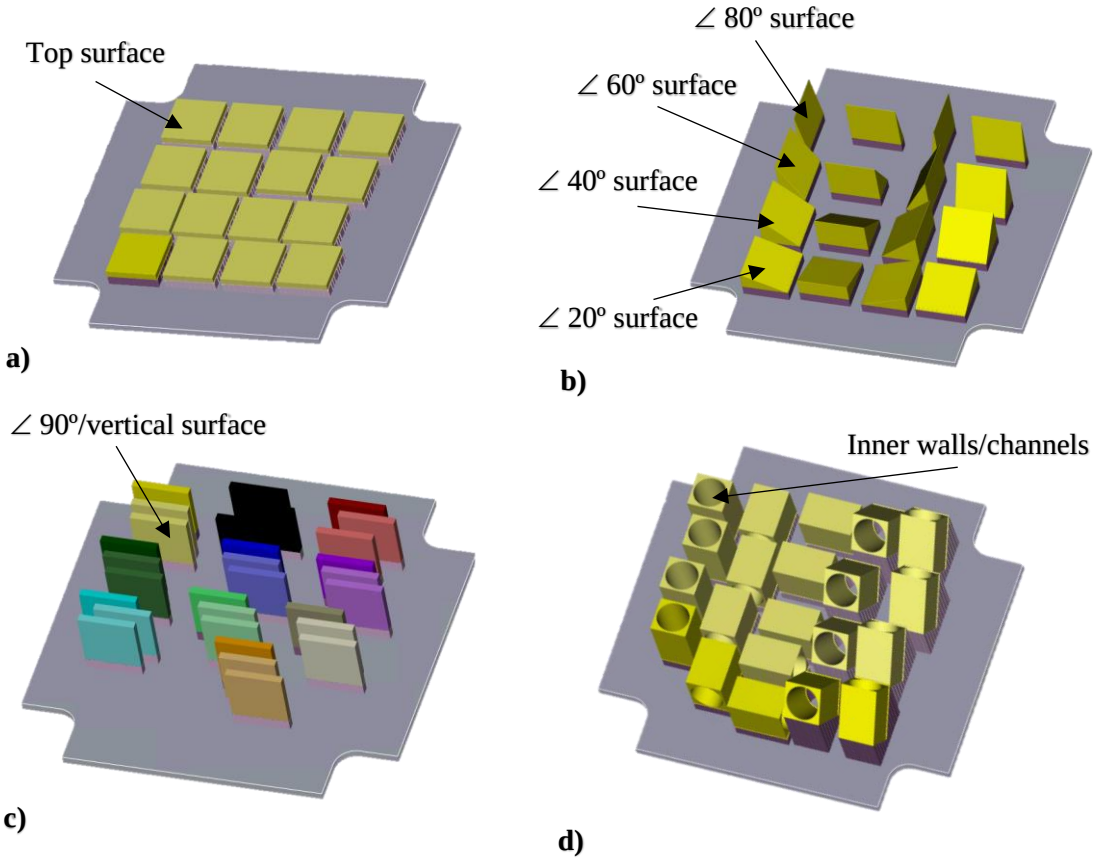

Figure 3-8 Surface references: (a) Top surface, (b) angled wall/surface, (c) vertical wall/surface, (d) inner wall/surface/channel.

Table 3-4 specifies the dimensions of each testing specimen used in this experiment. While Figure 3-8 (d) illustrates the inner-wall circular samples printed in the vertical, horizontal and a 45 º angle of lean, only the vertical samples manufactured successfully (keeping the printer parameters consistent with the other samples) and tested for this case study. Several attempts were made to manufacture the inner-wall samples horizontally or at an angle, but after continuous failure, the decision was made to exclude these from the study and pursue it later if there was significant improvement in the surface texture characteristics.

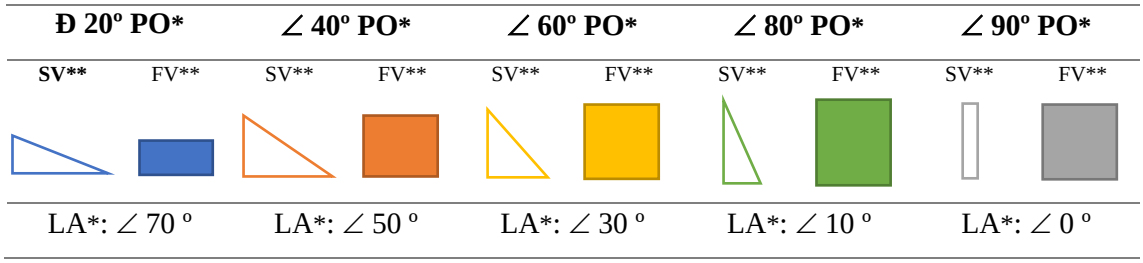

Figure 3-9 Front and side view of angled surface orientation for 20º, 40º, 60º, 80º and 90º. *Part Orientation (PO) and Laser Angle (LA). **Side View (SV) and Front View (FV)

Table 3-4 Case Study 1 testing specimen dimensions

Sample type	Testing Area	Sample testing area size	Height
Top Surface sample	External	15mm x 15mm	2 mm
Vertical surface	External	15mm x 15mm	15 mm
20º surface	External	15mm x 15mm	4.09mm
40º surface	External	15mm x 15mm	7.74 mm
60º surface	External	15mm x 15mm	10.41 mm
80 º surface	External	15mm x 15mm	11.55 mm
Inner-Wall Circular Samples	Internal	15mm (only height is applicable)	15mm

Testing Input Parameters and Manufacturing Settings

The samples were all printed in the DMP ProX 100 machine with Stainless Steel 17-4 PH powder on a 100mm x100mm build plate as previously specified. The samples were all printed at 98% laser power (LP) and +2mm laser defocus (LD). Using the DMP ProX Manufacturing software, the parameters to polish the external surface (top, angled, inner) were set to the specifications shown in Table 3-5.

Table 3-5 Testing Input Parameters for Design of Experiments in Case Study 1

Sample type(s)	Testing Parameter	Parameter range	Design of Experiment	Number of Trials
Top Surface samples	Laser Power	10% to 80% (increments of 10%)	Taguchi L16 (8^1 2^2)	4
	Laser Spacing	50um, 100um		
	Polishing Runs	1-2		
Outline samples (Vertical surface, 20º surface, 40º surface, 60º surface, 80 º surface, Inner-Circular Samples)	Laser Power	60%, 70%, 80%	Taguchi L9(3^3)	4
	Laser Speed	100mm/s, 500mm/s, 1000mm/s		
	Polishing Runs	1x, 3x, 5x		

DMP ProX Manufacturing Software

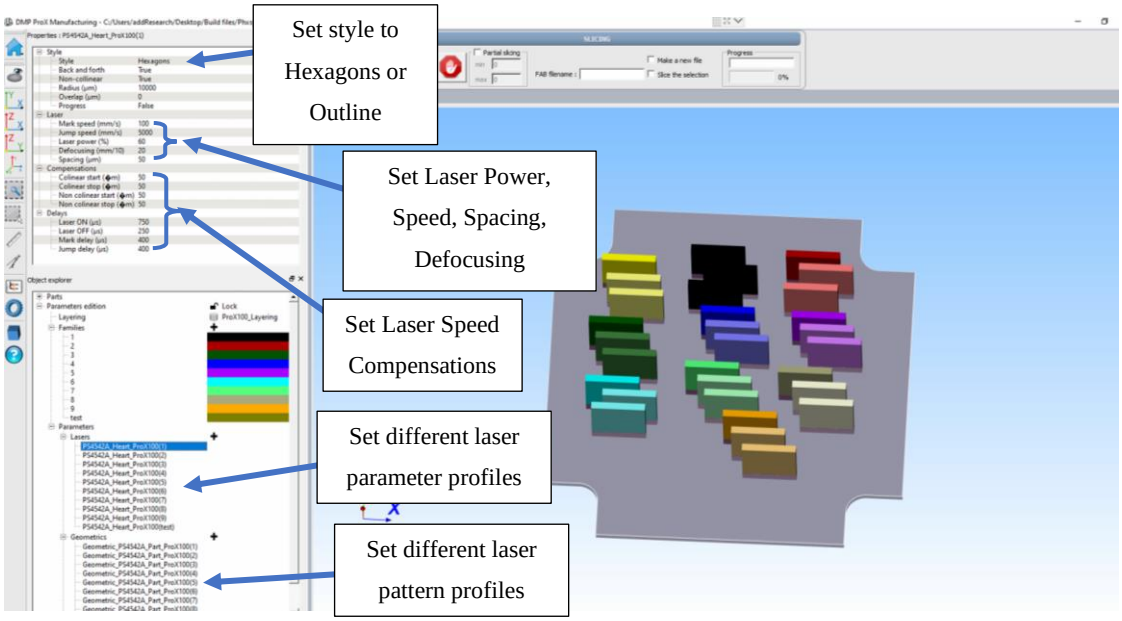

Figure 3-10 DMP ProX Manufacturing Software Interface

Style	
Style	Outline
Start policy (open)	None
Start policy (closed)	None
Laser	
Mark speed (mm/s)	100
Jump speed (mm/s)	5000
Laser power (%)	60
Defocusing (mm/10)	20
Spacing (µm)	50
Compensations	
Colinear start (µm)	50
Colinear stop (µm)	50
Non colinear start (µm)	50
Non colinear stop (µm)	50
Delays	
Laser ON (µs)	750
Laser OFF (µs)	250
Mark delay (µs)	400
Jump delay (µs)	400

Figure 3-11 Laser Speed 100 mm/s with appropriate compensations

Style	
Style	Outline
Start policy (open)	None
Start policy (closed)	None
Laser	
Mark speed (mm/s)	500
Jump speed (mm/s)	5000
Laser power (%)	60
Defocusing (mm/10)	20
Spacing (µm)	50
Compensations	
Colinear start (µm)	150
Colinear stop (µm)	140
Non colinear start (µm)	150
Non colinear stop (µm)	140
Delays	
Laser ON (µs)	747
Laser OFF (µs)	250
Mark delay (µs)	400
Jump delay (µs)	400

Figure 3-12 Laser Speed 500 mm/s with appropriate compensations

Style	
Style	Outline
Start policy (open)	None
Start policy (closed)	None
Laser	
Mark speed (mm/s)	1000
Jump speed (mm/s)	5000
Laser power (%)	60
Defocusing (mm/10)	20
Spacing (µm)	50
Compensations	
Colinear start (µm)	320
Colinear stop (µm)	220
Non colinear start (µm)	320
Non colinear stop (µm)	220
Delays	
Laser ON (µs)	750
Laser OFF (µs)	250
Mark delay (µs)	400
Jump delay (µs)	400

Figure 3-13 Laser Speed 1000 mm/s with appropriate compensations

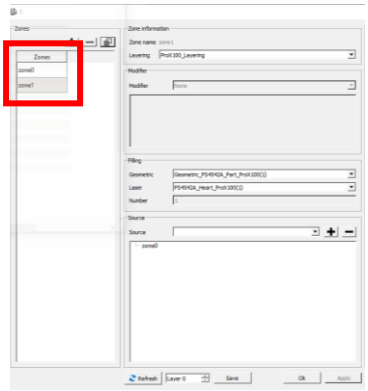

Figure 3-14 Creating zone layers to polish 1x

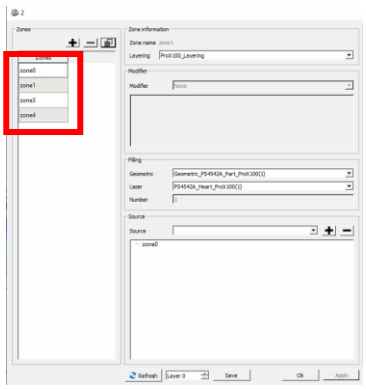

Figure 3-15 Creating zone layers to polish 3x

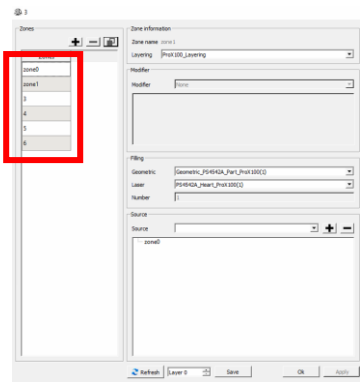

Figure 3-16 Creating zone layers to polish 5x

To polish the top surface, the different laser parameter profiles were set as shown in Figure 3-10. For these experiments the last layer was manually re-run on the printer for the 2x polishing run tests. 'Hexagons' in the style section refer to the entire part in the layer with the design as shown in Figure 3-2, and in the left image of Figure 3-17. The outline refers to the edge that surrounds the part as shown in the right image for Figure 3-17. All specimens except the top surface required the outline to polish the vertical/angled walls of the part. For this reason, the study distinguishes between the two types of tests as the top surface and the outline surfaces Table 3-5. To set the laser speed to 100 mm/s, 500 mm/s and 1000mm/s for the outline surface experiments, the laser compensations and delays need to be adjusted to ensure the laser does not overshoot the point it is meant to hit. The compensations and delays are shown in Figure 3-11, Figure 3-12 & Figure 3-13 for each respective laser speed. The polishing runs were set by creating zone profiles, where zone 0 is the normal printing settings for the entire part, and the subsequent zones represent each polishing run for the outline of the part (Figure 3-14, Figure 3-15 & Figure 3-16).

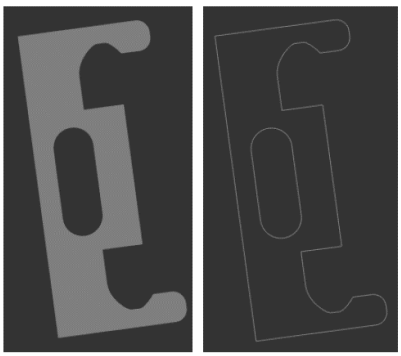

Figure 3-17 Hexagon (left) vs Outline Style (right)

Design of Experiments

The experiments in this case study are split into 2 primary groups of testing: the top surface profile, and the outline polishing profiles. The design of experiments (DOE) in this methodology follows a Robust Parameter Design (RPD), commonly known as a Taguchi design, due to the time consuming and high-cost nature of metal printing. Following the initial experiments performed to test the proof of concept for in-situ laser polishing to improve the surface finish of SS 17-4PH parts in the DMP ProX 100, the experimentation moved focus to the top surface and studying the effect of different laser powers primarily, before characterizing the reactions between other parameters.

The RPD L16 DOE in Table 3-6 was created accordingly for in-situ polishing the top surface. The DOE was run for 4 trials.

Table 3-6 DOE for top surface in-situ laser polishing of DMP ProX 100 printed SS 17-4 PH samples

Input Parameters			**Output Parameters**		
Laser Power (%)	Spacing (um)	Laser Polishing Runs	Surface Profiling (Ra,Rz,RSm)	Mechanical Hardness	Weld line thickness
10	50	1	-	-	-
10	100	2	-	-	-
20	50	1	-	-	-
20	100	2	-	-	-

30	50	1	-	-	-
30	100	2	-	-	-
40	50	1	-	-	-
40	100	2	-	-	-
50	50	2	-	-	-
50	100	1	-	-	-
60	50	2	-	-	-
60	100	1	-	-	-
70	50	2	-	-	-
70	100	1	-	-	-
80	50	2	-	-	-
80	100	1	-	-	-

Once the results for the top surface DOE was analysed (results in Chapter 4), the subsequent studies focused on the interaction between laser power, laser speed and laser polishing runs The RPD L9 DOE in Table 3-7 was created for each outline surface mentioned in Table 3-5. Each DOE (total of 6) was run for 4 trials.

Table 3-7 DOE for outline surfaces including the vertical, angled and inner channel surfaces for in-situ laser polishing of DMP ProX 100 printed SS 17-4 PH samples.

Input Parameters			**Output Parameters**		
Laser Power (%)	Laser Speed (mm/s)	Laser Polishing Runs	Surface Profiling (Ra,Rz,RSm)	Mechanical Hardness	Layer thickness
60	100	1	-	-	-
60	**500**	**3**	-	-	-
60	1000	5	-	-	-
70	**100**	**3**	-	-	-
70	500	5	-	-	-
70	**1000**	**1**	-	-	-
80	100	5	-	-	-
80	**500**	**1**	-	-	-
80	1000	3	-	-	-

Testing Analysis to Characterize the Polished Specimens

Topographical characterization of surfaces can be performed using quantitative testing such as surface profilometry or mechanical hardness testing. Alternatively, high resolution imaging solutions such as an optical microscope or scanning electron microscopy (SEM) can be used to observe and measure flaws or surface abrasions in the micro or nano scale. A combination of these techniques and their relevant testing standards have been used to analyse the test specimens from the above DOE experiments (Table 3-8).

Table 3-8 Characterization testing methods, equipment, and standards for analysing the test specimens in Case Study 1 results

Testing Method	Equipment name	Abbreviation	Equipment Model	Testing Standard	Output parameter(s)
Surface Profilometry	Roughness tester	RT	STARR Instruments Surface Roughness Gauge: RTD-210	ISO4288: '96	Ra (µm), Rz (µm), Rsm (mm), graphical representation of surface profile.
	Atomic Force microscopy	AFM	-	-	Graphical representation of surface profile in the nanoscale.
Optical Topographic Analysis	Digital Optical Microscope	DOM	-	-	Digital high-resolution images of the surface topography, can measure layer/weld line thickness (µm) and flaw sizes (µm).
	Scanning Electron Microscope	SEM	Ziess EVO MA25 and Hiatchi TM3030Plus	-	
	Energy Dispersive X-Ray Analysis	EDX/EDS	Ziess EVO MA25 and Hiatchi TM3030Plus	-	Elemental analysis of a section of the surface. Quantified chemical composition (%)
Mechanical Testing	Tensile Testing	TT	Instron Universal Testing machine	ASTM E8 subsize	Ultimate Tensile Strength (MPa), Young's Modulus (MPa).
	Vickers Micro Hardness Testing	HT	Vickers Micro Hardness Tester	ASTM E92 – 17	Hardness measurement (HV)

3.3.2 SURFACE PROFILOMETRY DATA REPRESENTATION

Figure 3-18 illustrates the DataView V1.1 software used to capture and store the surface profile data from each roughness measurement. The key data values (Ra, Rz and Rsm) and graphs (roughness and profile curves) have been encircled with a red outline in Figure 3-2. For these tests, 5 readings were taken from each sample and averaged. When measuring the peaks and valleys in the surface profile of a sample the Ra value and Rz value are commonly compared to each other. The Ra value is representative of the average peaks and valleys of the surface profile, neutralizing any outlying points that may be extreme points with no significant impact on the result. The Rz values averages the five highest peaks and the five deepest valleys including the most extreme outline points. Therefore, there can be a significant difference in between these two averages, typically a ratio range for Rz-to-Ra = 4:1 or 7:1 for a safe conversion is dependent on the manufacturer's specification and the customer requirement, and whether it is the Ra or Rz parameter that is accepted.

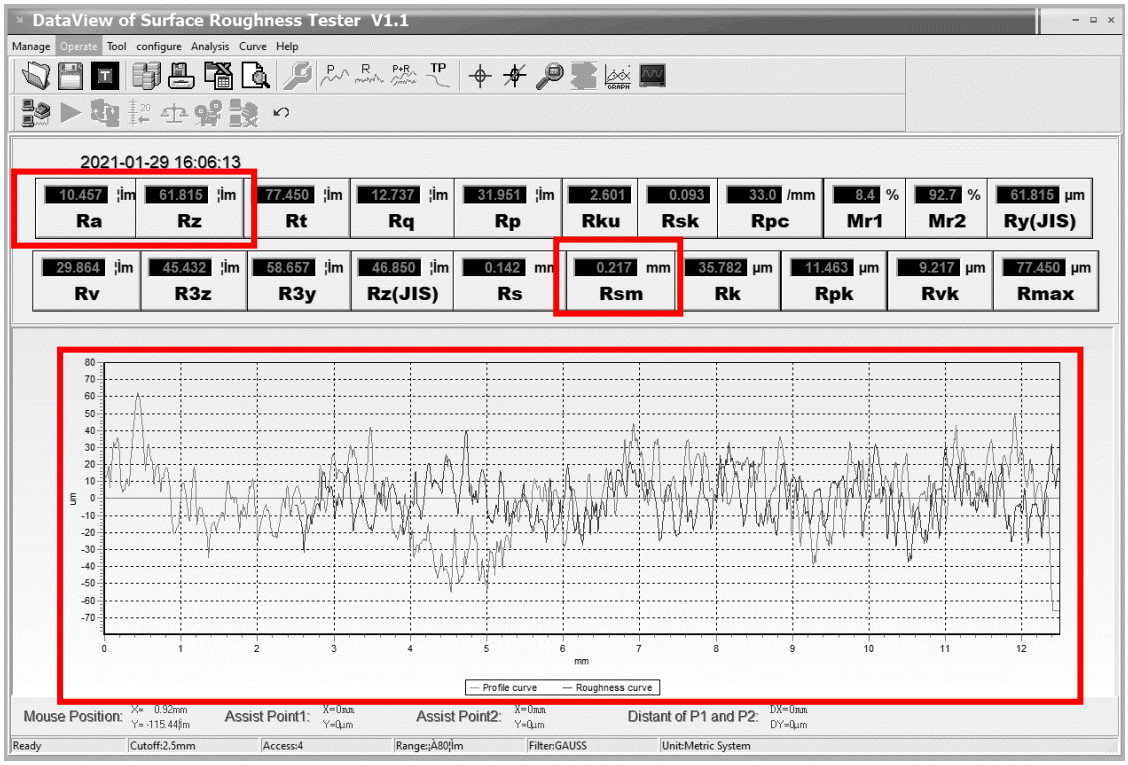

Figure 3-18 Surface Roughness Data Interpretation and Reference

Figure 3-19 below, illustrates the different profilometer scanning directions used when measuring the surface profile of each sample. The top surface used a combination of all these scanning vectors, due to the change in orientation of the laser scanning pattern (Figure 3-2). The vertical and angled surfaces were scanned vertically or horizontally, to scan against the build orientation.

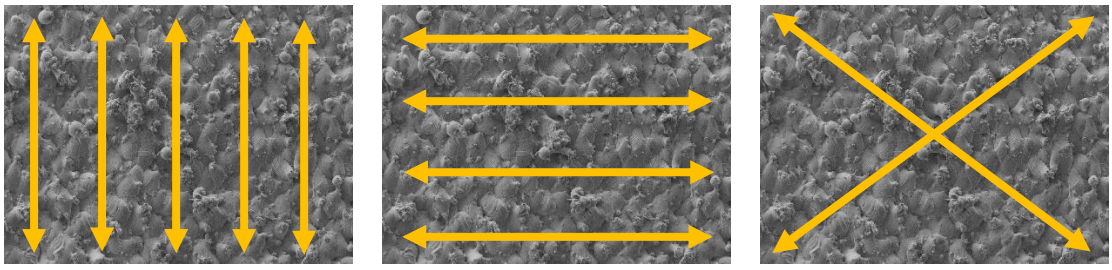

Vertical Scanning Horizontal Scanning Diagonal Scanning

Figure 3-19 Scanning directions for surface profilometry testing of SS 17-4 PH printed samples

3.3.3 OPTICAL TOPOGRAPHIC ANALYSIS

All samples were examined at a micro level, using either the Optical Microscope or SEM. These instruments are excellent visual inspection tools to examine the topographical and cross-sectional surfaces of test specimens. The surface of each sample was examined for surface defects (pores, loosely bonded powder, inclusions, discolouration etc…) and change in layer thickness. Using the in-built measuring tool, 5 reading for the layer thickness for all samples were taken and averaged.

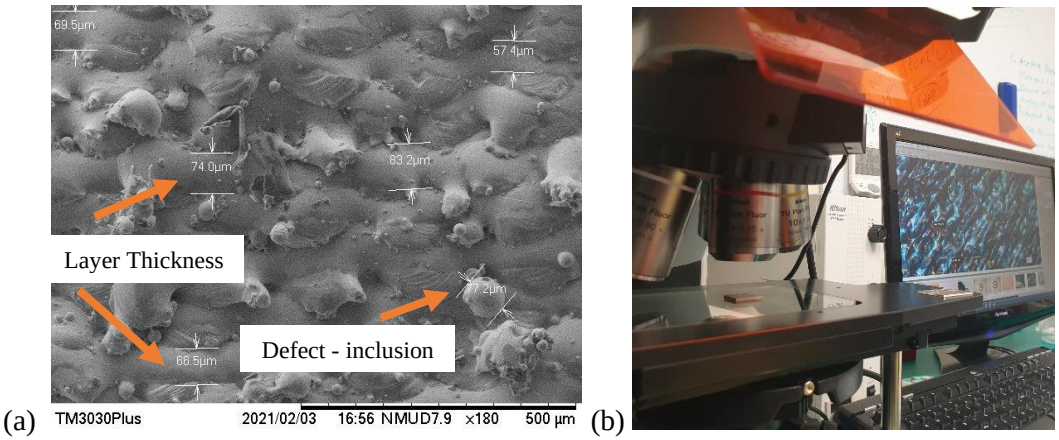

(a) (b)

Figure 3-20 (a) SEM image of SS 17-4 PH repolished sample with layer thickness measurement and inclusion measurement (b) Optical Microscope stage and image capture

The in-built Energy Dispersive X-Ray Spectrum analyser (EDX/EDS) was used to study the chemical composition for various areas of the surface of the samples. This analysis was performed to observe any fluctuations in the elemental ratios that make up the SS 17-4 PH powder.

3.3.4 HARDNESS TESTING

Five measurements of mechanical hardness were taken from each specimen and averaged, using a Vickers Micro Hardness tester. ImageJ was used to measure the corner points of each indent, calibrated to the magnification of the hardness testing equipment image capture (Figure 3-21). Several readings were taken from the hardness tester manually for comparison to ensure continuity and the reliability of the results from the digital data acquisition method instead.

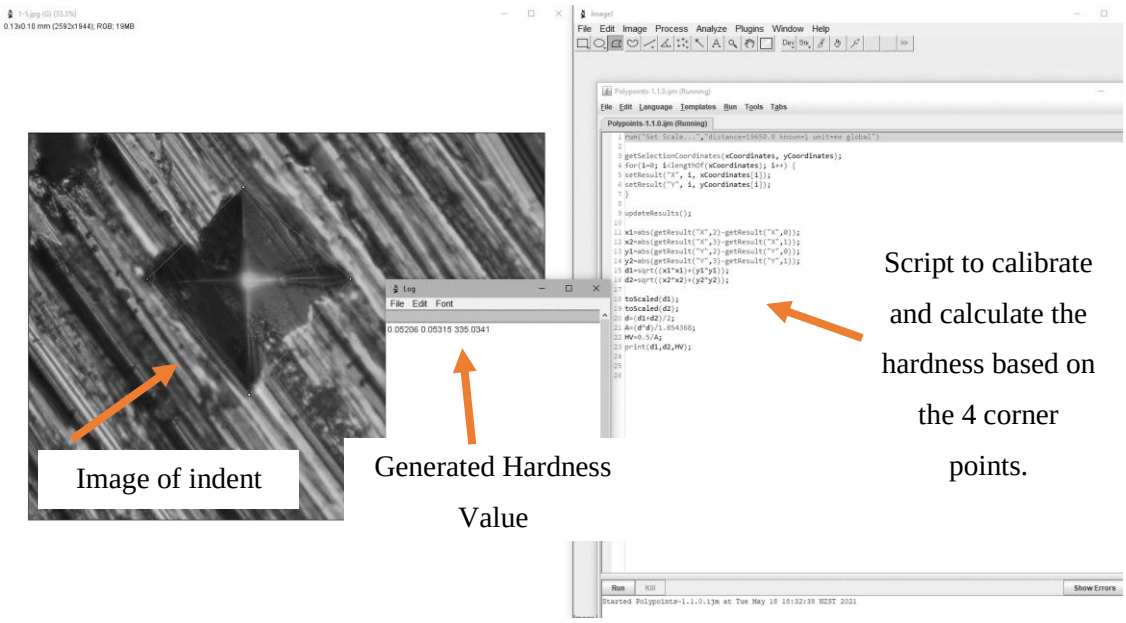

Figure 3-21 ImageJ mechanical hardness acquisition for the SS 17-4 PH samples

3.3.5 RPD DOE ANALYSIS METHODOLOGY

Minitab 19 was used to create the Taguchi experimental DOEs (which enables researchers to quantify an otherwise qualitative study, to create a robust design for parameter and tolerance influence) and analyse the statistical results. Different Orthogonal arrays (OA) were created to work for different experimental set-ups. In the case of this study, the L16 OA was used to test more variables for the LP parameter, and the L9 OA was used for all other experimentation (build orientations and affected surface angle) to meet the minimum parameters settings for a robust DOE and a significant analysis. The analysis in the Taguchi DOE is based on the S/N (signal-to-noise) ratio, where 3 logarithmic functions define the inverse of variance in the sampling data. The corresponding testing strategy for the results documented in Chapter 4, is detailed in the final column of Table 3-9 to match the data expectation (i.e., a lower surface roughness (Ra, Rz or RSM) value is better, so the ‘smaller is better’ data expectation is used).

Table 3-9 S/N Ratio Formulas for Testing Strategies

Data Expectation	S/N ratio Formulas	Goal of experiment	Testing Strategy
Smaller is better	$\frac{S}{N} = -10 \log [\frac{1}{n}\sum_{i=1}^{n} y_i^2]$	Minimize the response	**Surface Roughness (Ra, RSm, Rz)**
Nominal is better	$\frac{S}{N} = 10 \log \frac{\mu^2}{\sigma^2}$	Target the response and base the S/N ratio on the means and standard deviations	**Layer Thickness**
Larger is better	$\frac{S}{N} = -10 \log [\frac{1}{n}\sum_{i=1}^{n} \frac{1}{y_i^2}]$	Maximise the response	**Mechanical Hardness**

Statistical analysis involved observing the *F* and *P* values for each result type and the impact of the input variables (Laser Power, Laser Speed and Polishing repetition). These values are important indicators to determine if a factor is significant (a *p*-value less than 0.05 is required) or not. The impact of each input variable was also ranked based on its Delta value for its S/N ratio and Means. The top two most impactful factors, for each L9 OA (the outline-polishing tests), were selected as the input variables for contour plots, to demonstrate the correlation between the input variables and the main output surface roughness (Ra). ANOVA (analysis of variance) was applied to calculate the statistical confidence for the determinations made from the Taguchi results analysis. Finally, the regression models for each Taguchi Study were obtained.

3.4 CASE STUDY 2: QUALITY MONITORING STRATEGIES USING NON-DESTRUCTIVE TESTING SYSTEMS

This doctoral study began with an investigation into NDT techniques for quality assurance in AM. After assessing the key issues affiliated with AM technologies, particularly metal AM, the research scope was narrowed to investigate defect detection, residual stress detection and surface finish improvement methods. Exterior surface finish improvement was addressed in CS 1, however, there was potential to use microscopic imaging and machine vision to detect internal surface impurities/permeations and create a quality maintenance strategy to use the detected data and create a feedback control strategy. The feedback control being a strategy to laser melt any partially fused areas, smoothen rough peaks, and analyse its impact on the part's topographic characteristics, thermal stresses, and mechanical aptitude.

The literature review in Chapter 1 revealed an opportunity to explore novel testing strategies by implementing existing NDT methods and characterizing the process to suit the unique nature of a particular AM build process. However, many existing studies use camera vision technologies for quality inspection of parts. Retro-fitting the visual inspection system described further in this chapter is a practical engineered output of this doctoral study but the use of spectral reflectometry is not a novel concept. While this part of the research did not yield any novel technologies (aside from the in-situ camera vision system being designed specifically for the DMP ProX 100 machine), the comparison of 2D image to 3D model conversion techniques has yet to be documented. Furthermore, it proved an excellent starting point in the pursuit of novel quality control strategies for defect detection and opened an avenue to begin exploring the use of real-time layer analysis used to create scanning patterns for the AM machine to target defective areas on a part layer.

Creating an online in-situ digital surface profilometry technique that can be used in layer-wise re-melting/polishing was one advantage of this research. However, the second justification for pursuing NDT technologies for QA in AM, was to create a method to eliminate the material wastage caused by traditional mechanical testing techniques. The aim of this strategy was to progress the digital analysis techniques from just visual inspection to reconstructing the manufactured part as a digital 3D model with dimensions. Then use the 3D model in a simulated analysis to generate a mechanical, thermal, or flow analysis and provide the manufacturer with a visual and quantitative representation of the part's mechanical characteristics (i.e., life-cycle analysis, thermal stresses and more).

The methodology for CS2 highlights the practical work done to develop the in-situ imaging system, capture the 2D layers with varying light intensity and use image processing algorithms (python with OpenCV) and Solidworks modelling and simulation. Chapter 5 goes on to examine the output of the work done and present a discussion surrounding the experimental study chosen and other solutions considered with the brief experimentation performed with thermal and acoustic NDT methods.

This case study is categorized into 2 key quality assurance goals that were the driving need for this study: defect analysis and feedback control.

Aim

To use Machine Vision (MV) to extract the surface profile characteristics from 2D images of each layer of a DMP ProX 100 part. Then compare image processing techniques to replicate the surface characteristics as a 3D model to be used in a FEA analysis. This is to create an NDT instrumentation that can be adapted into other L-PBF printers as a low-cost research tool. The aim of this study was to provide the groundwork required to progress NDT research past layer capture and defect identification by focusing on the following research goals:

1. Characterizing surface defects with 2D layer wise DMP ProX SS 17-4PH part capture and using feature detection algorithms to differentiate between the correctly melted areas and the defective areas.
2. Compare 3D extrusion methods to recreate the 2D images as a 3D layer (depth matching the layer thickness of the AM machine) and then model the stacked layers as a 3D replication of the printed part and perform FEA analysis on it.

Hypothesis

How can porosity in a metal AM part be characterized using an NDT quality strategy? How can an NDT strategy be developed to detect the impact of crack size in a metal AM part on its the fatigue strength and failure? How can you guarantee file security in AM parts?

Chapter 2 highlights the key defects found in L-PBF parts, including pores (gaseous, unfused powder, and elongated micro-cracks), residual stresses and surface defects. The highest percentage of defects residing within a Metal AM part can be linked some form of porosity within the part. Porosity in this study is an over-arching reference to surface texture (profile/defects) in AM parts. The laser melting nature of the L-PBF process induces a level of porosity (defined in Chapter 2), and Metal AM designers and fabricators will often adjust the printing parameters to mitigate or manipulate the porosity. Typically, theoretical porosity prediction algorithms are used

to advise the manufacturer of the degree of porosity to expect in an AM part based on its machine settings. In applications, where parts experience some form of loading or stress, it is important to understand the impact of the percentage of porosity regarding crack initiation, surface texture requirements and the overall lifespan of the part before failure.

Case Study 2 begins with an experimental methodology to digitally capture the level of porosity in 2D images and recreate the surface texture on corresponding layer for the original CAD file the part is manufactured from. Assessing the porosity in 2D and 3D images using image processing has been seen commonly in geological, biological and AM applications. The methodology in this case study draws influence from these studies.

Aside from defect analysis in parts, AM manufactures often take advantage of the online plug-and-play nature of AM machines. Manufacturing the wrong part can be time-costing, cause material wastage and failure if the wrong settings are selected for the part. Therefore, it is important for the manufacturer to ensure the CAD file and sliced print file match. Other documented works explore strategies for file security by preventing corruption or modification to files through a software-based security algorithm. Some works encourage a machine learning approach and commercial AM machine manufacturers are popularly attempting to integrate deep learning system to monitor several aspects of the AM process (laser beam, print bed, heating chamber, powder feed etc…) resulting in the need for expensive processing hardware and custom software made to work only within their brand of printers. This work attempts to realize a low-cost solution with a universal solution that works with the sliced design file (all components being printed simultaneously) and the 2D layer images of the printed parts covering the entire print area.

To investigate the research questions above, the experimental methodology focused on the following key elements:

- Type of defect
- Size of defect
- 3D model extrusion methods
- FEA Analysis

The hypothesis of this study was developed around characterizing the detectability of defects (synthesized or real) under the variation of the elements listed above. The rapid development of simulation software to work with complex geometries is being constantly optimized to become more accessible (workable on commonplace machine hardware). A concern in pursuing digital analysis of 3D modelled CAD files for AM parts is the large number of data points that could affect the complexity of the mesh generated which is required in finite element analysis. Spectral reflectometry illuminates the surface of a captured part to create areas of

brightness and darkness. Studying the degree of illumination (represented by a number between 0 to 255 on the grayscale spectrum) through image processing aids the creation of a 3D surface map. There were 3 methods considered to achieve a 3D replication of the print file; 3D texture in Solidworks, DXF file creation from the 2D image with Inkscape, and a basic surface plot in MATLAB generated into an STL file (these methods are described in further detail later**). It is hypothesized that each method will be advantageous in either more accurately representing the curvature of the surface profile for modelling and simulation or be a more efficient method for creating the 2D scanning patterns required for feedback to the AM machine to test the impact of laser polishing to improve defective areas within the part and improve the overall surface finish.** Because the aim of this study is twofold, the end-result will be to measure each solution against its ability to satisfy this hypothesis.

3.4.1 METHODOLOGY

Retro-fitment of image capture system within the DMP ProX 100 for NDT quality strategy development studies

This section details the testing rig developed for the NDT quality strategy in tandem to the surface profile characterization study. To implement a digital and thermal camera system within the DMP ProX 100, several modifications and considerations were required. These modifications included electronic wiring access to run power cables to the image capture system and the replacing the removable back plate with a custom made one designed to mount the actuation system described further ahead. The aim of the design was to focus on a low cost, versatile design that could be used in other applications/printers. The system catered to layer-wise capture, rather than videoing the melting process (focusing on the melt-pool or laser energy-density). The restrictions and design specifications are as follows.

Design Specifications

Working within the fully enclosed and inerted DMP ProX 100 printer, required many considerations to accommodate the design restrictions. The only restrictions on the cameras used in the subsequent studies, was to be compact and remain out of range of the laser (when melting) and the roller (when spreading the powder). The main consideration whilst retrofitting the imaging system was to ensure, if the system were removed the printer could be restored back to its original state. Determining an access point for any cables running into the printer and ensuring any foreign objects introduced into the printing chamber were enclosed in stainless steel was challenging. Considering these restrictions, the key design specifications are listed below.

Size of the Printer Chamber

Figure 3-22 illustrates the shape and size of the DMP ProX 100 printing chamber. To retrofit the imaging system described ahead and ensure the printer could be returned to its original state, the back plate was replicated and modified for mounting the components to. As every component was enclosed in Stainless Steel, there was considerable weight to support and the back plate screwed in with the many holes shown in Figure 3-23, held the plate securely to the printer. Additionally, it provided a stable, removable, and adaptable surface to mount the components against with nuts and bolts.

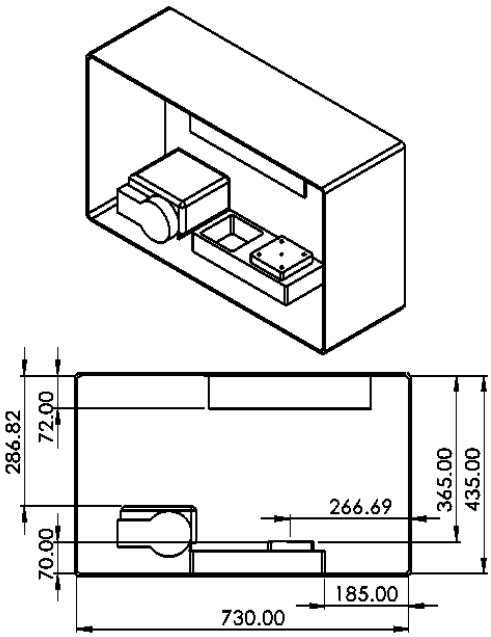

Figure 3-22 DMP ProX 100 printing chamber dimensions

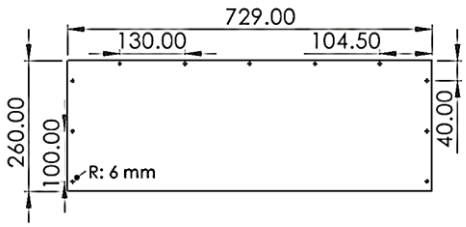

Figure 3-23 DMP ProX 100 printing chamber back plate dimensions

Electronic Equipment Power Source and Access

No cables run into the printing chamber which is completed sealed with Stainless steel. The only access in was to drill a hole into an entry point on the printer (steel back plate or exhaust tubing taking the air out of the printer). For the most non-evasive solution the exhaust tubing was select. The tubing was cut, and an extended hollow steel cylinder was inserted and clamped to ensure no air could escape. A hole was drilled into the steel sleeve and the power cables for the electronic equipment was inserted, then closed and made airtight with a setting gel sealant.

Stainless Steel Chamber

All components (actuators, nuts, bolts, electronics, mounting brackets etc..) were either made or enclosed in Stainless Steel to stop the loose powder circulating in the chamber from being contaminated or reacting with a foreign material. While the enclosure was not heated, there was a heating element on the right side of the laser that could get as warm as 40°C (measured with a thermal camera), creating an area to avoid for any plastic cables running along the steel back plate.

Digital and Thermal Camera Imaging System Retrofitted into the DMP Pro X 100 Metal AM machine

The original chamber without any modification is displayed in Figure 3-24. Figure 3-25 and Figure 3-26 illustrate the retrofitted back plate, actuation system, electronic control box, digital and thermal cameras. The back plate was waterjet cut to match the original plate with the addition of mounting holes and a measurement grid to align the cameras directly above the center of the build plate with a set focal distance. A Raspberry Pi 4B+ was chosen as the control board within the printer, due to its hardware capabilities, desktop environment and WIFI module that enabled VNC viewing and remote control of the system. The actuator was chosen to travel specifically 100 mm (the distance from the center of the build plate to minimum distance out of laser range). Additionally, it had to hold the weight of the two cameras, lens, and the mounting bracket of considerable weight. The product specifications for every component chosen in this system is detailed in Appendix A. Relays were used to control the halogen lamp (extra light and heat for thermal tests) and actuator. Initial designs attempted to power the electronics using a battery, but the battery was too large for the chamber and needed appropriate shielding and recharging. Without the battery, the printer was not opened for maintenance until the usual cleaning time for the entire printer and system, reducing the wastage of nitrogen gas. A custom PCB was created to transfer power from a single source to each component.

Figure 3-24 Original DMP ProX 100 build chamber

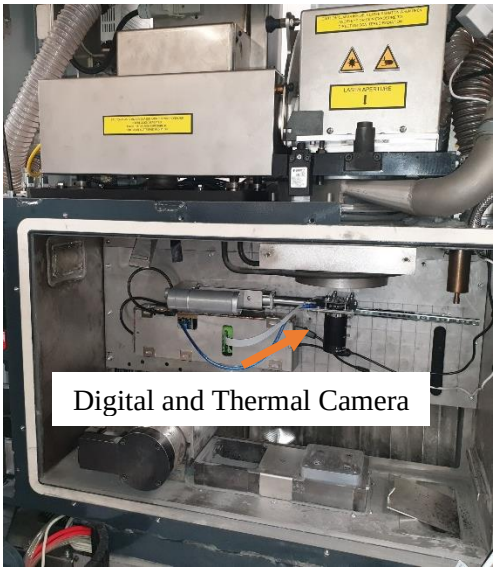

Figure 3-25 DMP ProX 100 printing chamber with retrofitted imaging system

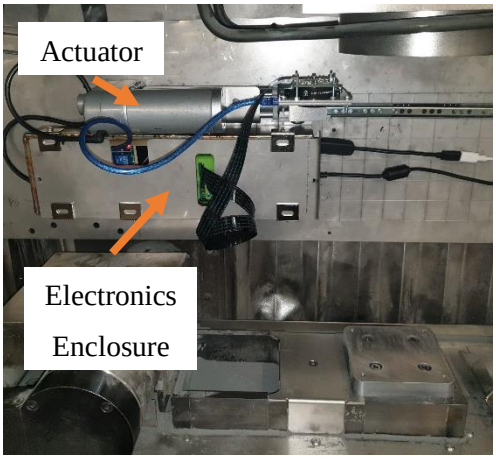

Figure 3-26 Front View of the DMP ProX 100 printing chamber with retrofitted imaging system

Python GUI to control thermal and digital camera imaging system

To operate the imaging system for capture, save images, adjust the camera settings and perform post processing of the thermal imaging video files, a unique Graphics User Interface (GUI) was created for the Digital Camera (Figure 3-27) and Thermal Camera (Figure 3-29). Additionally, the GUI enabled remote control (using TeamViewer to control the Raspberry Pi module) of the actuator and halogen lamp to move the cameras out of laser range. To geometrically correct the distortion of the digital images, a checkerboard camera calibration (Figure 3-28) with OpenCV image processing techniques, was used. The thermal imaging GUI script was designed using a modified version of pre-existing lepton developers code for the prethermal breakout. The post-processing GUI for the thermal camera (Figure 3-30), processed the thermal videos for frame-by-frame analysis of the thermal gradients and its change over time.

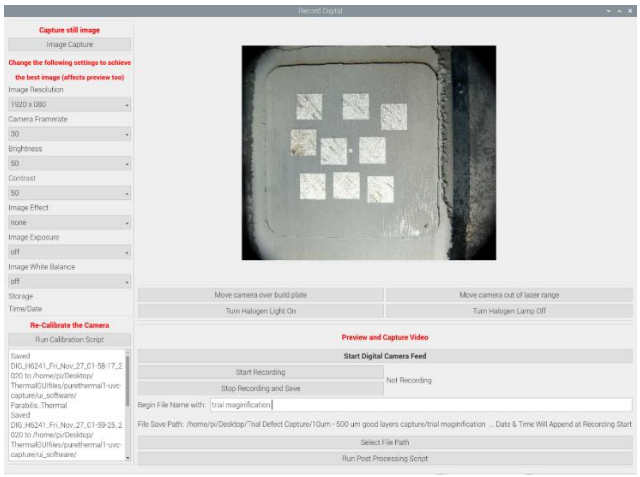

Figure 3-27 Digital Camera GUI

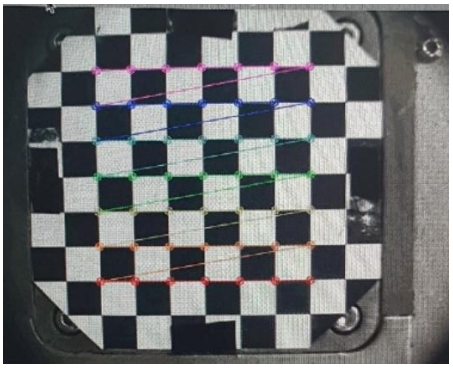

Figure 3-28 Digital Camera Checkerboard Calibration

Figure 3-29 Thermal Camera GUI video capture

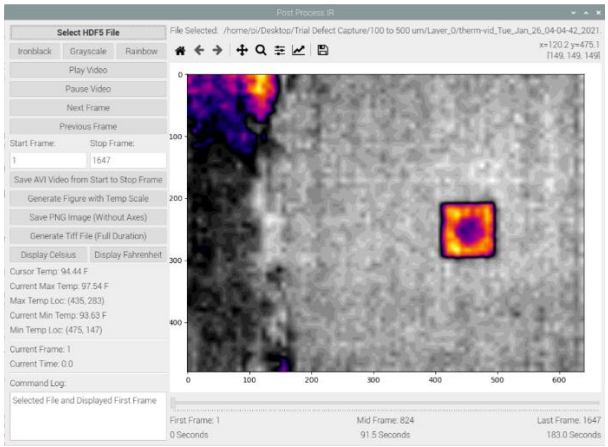

Figure 3-30 Thermal camera video post processing for image capture

Test Specimens

A simple square specimen (Figure 3-31 (a)) 15mm x 15mm x 0.5mm was designed in SolidWorks and manufactured in the DMP ProX 100 machine, where each printed layer was captured with the MV system described in section 0. Typical image processing studies involve training a deep-learning neural network to identify defects by studying the pixel density for each pixel in an image and feature matching algorithms. However, due to the time restriction and need to focus on progressing the research of image processing techniques in AM defect analysis, it was decided to stick to a simple data to capture two sample sets; one sample with the typical laser settings of the DMP ProX 100 and the other with synthesized defects (Figure 3-31 (b)). Ideally, more images would have been collected for analysis, but were not necessary in the proving the viability of the quality strategies presented in Chapter 5 and below. With the layer thickness of the printer set to 30 µm and an extrusion height of 0.25mm, each sample consisted of 16 sliced layers to capture. The width of the synthesized defects was set from 100 µm to 500 µm to exemplify the detection of typical defect sizes found in AM parts (Chapter 2 – Figure 2-9). Aside from the synthesized defects (imitating a crack) dimensionally justified above, the other types of defects studied included the typical surface profile (texture analysis) and real-time defects (pores, voids, unfused powder, burnt powder etc…) introduced into the part because of the typical process drawbacks.

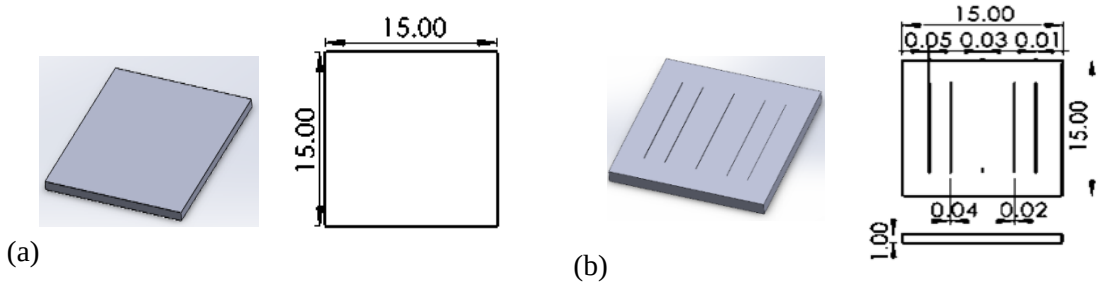

Figure 3-31 (a) Model of square test specimen representing the true sample specimen (dimensions in mm). (b) square specimen with synthesized defects in mm (widths: 0.01, 0.02, 0.03, 0.04, 0.05 and length: 10mm)

Pre-Processing of Images and Software

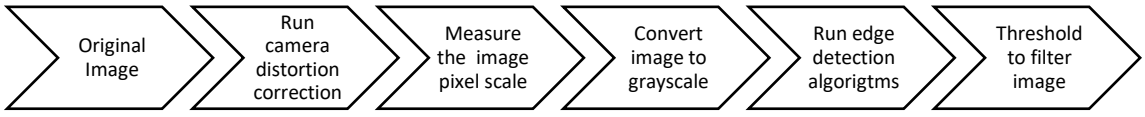

Figure 3-32 Typical process steps to extract key data points such as edges, colour gradients and more

Pre-processing of images follows the process steps in Figure 3-32. The initial GUI for image capture were designed on a Raspberry Pi 4B using the python programming language and OpenCV image processing toolbox. Following this, the pre-processing steps, surface manipulation and extrusion-based methods were performed using a combination of software.

These processes were performed on a Windows10 operating system, with an Intel(R) Core (TM) i7-7700HQ 2.80GHz CPU, a NVIDIA GeForce GTX 1050 GPU and 16GB RAM. A combination of Visual Studio 2019 (with python and OpenCV) and MATLAB 2021b (C++ and the Image Processing toolbox) was used. The code for pre-processing images up to edge-detection is readily available online. Because the aim of this experimentation was to focus on generating the 3D analysis model, aside from comparing the different edge detection techniques for each image, most of the development was focused on sizing the parts, defects and determining how to create the 3D representation of the layers, to be used for feedback to the DMP ProX 100 manufacturing software, the machine and to import the layers as a CAD file into Solidworks for analysis.

Raw Data and Grayscale Images

Figure 3-33 and Figure 3-34 illustrate the raw image captured with the digital camera for the standard layer and the defective layer. Below them Figure 3-35 and Figure 3-36 exemplify the digitally converted grayscale image (RGB to grayscale), used in the subsequent methods.

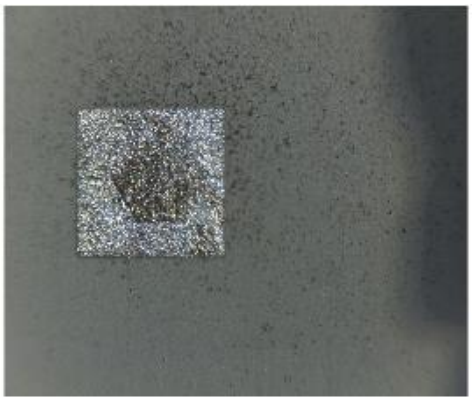

Figure 3-33 Original standard layer image with no processing

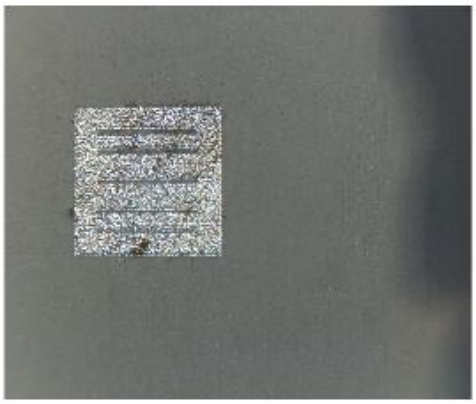

Figure 3-34 Original defective layer image with no processing

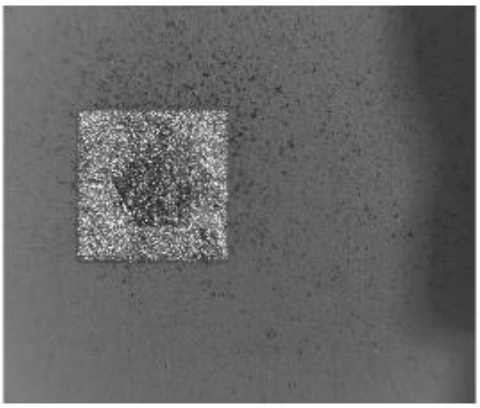

Figure 3-35 Grayscale standard layer image (MATLAB)

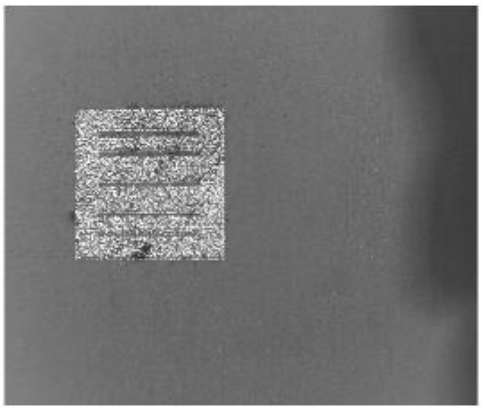

Figure 3-36 Grayscale defective layer image (MATLAB)

Edge-Detected Images

For the readers understanding and exemplification of the effect of various edge detection algorithms that can be used, illustrated below are in Table 3-10 are examples of five most common edge detection algorithms applied to the grayscale layer images shown previously. The different edge detection methods use various pixel comparison and line matching methods to detect illuminated outlines in an image. The gray powder existing in the background and in the synthesized defect areas are eliminated from the part. The scatter of detected edges around the part is partially due to the powder splatter created when the laser beam hits the powdered stainless steel.

The most common edge detector is the Canny operator, which was selected in some of the applications described ahead. Thresholding with erosion and dilation was applied to eliminate edges not part of the melted part area in both images.

Table 3-10 Edge detection algorithms applied to the grayscale images for the standard and defective part layer

Edge Detection algorithm	Standard Layer	Defective Layer
Canny	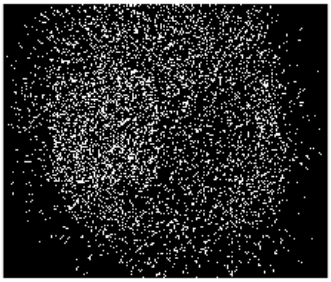	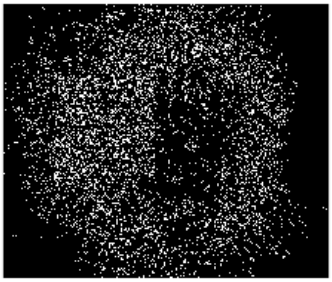
Sobel	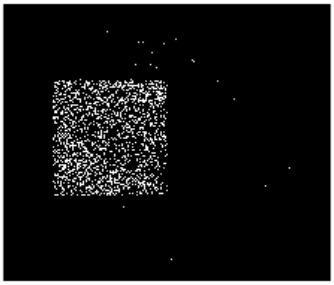	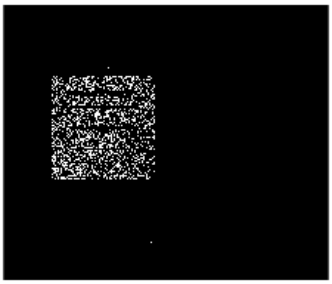
Roberts	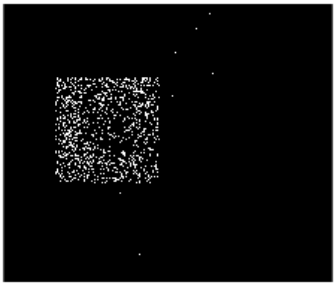	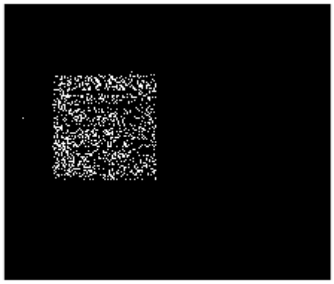

Log	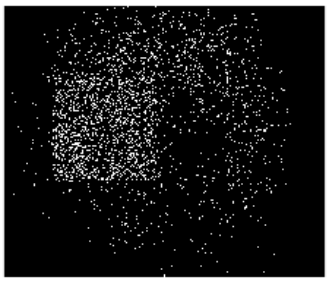	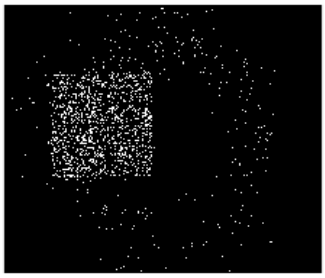

Method to digitally size the part and defects

A known and popular methodology is applied to this study to digitally size the manufactured part and defects within the captured image. This method surrounds the **findContours** function, a popular OpenCV tool used to detect changes in color and mark it as a contour. To add a metrical measurement to the images, the first step was to determine the number of pixels on one part edge. Because the size of the part edge is known (15mm), a digital image processing software called ImageJ was used to quantify the image. The measurement function within the software enables you to digital draw a line along the edge of the part and outputs a summary of the length of the line in px (pixels). The images captured in this study for each part were taken with the camera focused on the same dimensional area of the build platform. Regardless, to assure accuracy in this manual measurement process, several measurements were taken from different images and averaged to determine the average number of pixels in the 15mm edge was 405 px. Therefore, following this determination, basic arithmetic was used to calculate the px per mm for each image, i.e., 405 px was divided by 15 mm, resulting in the conversion factor for marking each edge, accordingly, knowing 1mm equates to 27 px. Similarly, for other sample sets of images where more than one part was printed, the same methodology to determine the px per mm was used.

The **findContours** function is dependent on the elimination of undesired pixels. Before the **findContours** function is applied, the process leading up to the edge detection shown beforehand is followed first. Thresholding (cv2.threshold()), eroding, (cv2.erode()) and dilating (cv2.dilate()) the edge detected image will affect the pixel density depending on the type of thresholding, and level of pixel erosion or dilation. The OpenCV library functions are called using cv2 (imported library). After the findContours function is applied, a **for** loop is used to check the size of contour found and used as an undesired pixel elimination strategy to clean up the image and detect only the contours surrounding the manufactured part. Then in combination with the calculation for px per mm, lines are drawn to enclose the part in a rectangular box and the height and width of the box is displayed in mm on the original image of the manufactured part (result displayed in Chapter 5). Once the size and pixels belonging to the manufactured part in the image

is known, it can be extracted cropping the image using the top left and bottom right points of the detected part profile. The programming code for each of these steps is detailed in the Appendix C. To assure the difference between the melted part area the SS powder, using a NumPy array and PIL functions, the pixels were set to either 0 or 255, white representing the melted areas and black for the powdered or defective areas. The cropped image is then gray scaled, with morphological operators applied, then edge detected. Before running the findContours function the image in inverted by subtracting each pixel from 255. to inverse the same contour detection process to now highlight and measure defective areas (synthesized and real) in the image. Altering the size of the dilation kernel and iterations impact the bounding box around the detected contour profile for the defects.

3D model extrusion methods

The end goal of the machine vision defect defection study was to develop a solution that could enable feedback to the DMP machine laser settings to remelt defective areas. To determine the method required to investigate a solution that could meet this end goal it was important to first consider what an output file required to enable the feedback to the DMP machine would look like. The DMP machine laser characteristics are controlled by a software dedicated to the 3D System DMP machines called DMP Manufacturing. The input file required for the manufacturing software is a STL file. The STL file is imported into the software and the model of the required part print is placed onto a replica of the 100mm x100mm build plate on which parts are additively manufactured. The part is then sliced into layers according to the layer thickness set on the machine which is by default 30 µm. Each of these sliced layers are imbedded with the laser scanning pattern (hexagonal) and laser melting settings.

Understanding this process, to create a laser scanning pattern file, created a point to work backward from. The end goal of this strategy could be more specifically defined to acquire an STL file that contains a 3D model reconstructed with the areas of the printed part that need more laser melting (unfused particles, voids, pores etc.). The steps detailed below reflect the thought process followed to reach the 3D model stage.

1) Capture the printed layer
2) Analyze the layer for variations in the surface profile and feature match areas of unfused powder where it should be fused.
3) Use this analysis to create a method to replicate the profile an exemplify the variation in a 2D grayscale spectrum.
4) Determine a method to take the 2D spectrum and extrude it the 30 µm height to match the layer thickness setting of the machine.

5) Use the extrusion for each layer, join them in an assembly and create a 3D representation of the printed part.
6) Having a 3D model creates the ability to generate an STL file that can be imported and sliced within the DMP manufacturing software.
7) Secondly, having a 3D model creates the opportunity to run a finite element analysis (FEA) on the part and provide the manufacturer with mechanical, thermal, flow, and life span analysis to determine the impact different sized defects have on an AM part.

A few strategies were considered take the model from an image analysis stage to digitally mapping or creating a replica of the surface profile. The white-light spectral reflectometry method was used to create a gradient of light on the surface of the DMP part. The gradient of light creates brighter pixel colours where there are peaks (higher points) and darker pixel colours where there are valleys (indentations). In addition, the darker tint to the powdered SS compared to the melted SS part was also affected by the gradient of light. For this reason, the steps leading to the edge detection (cropping the image, Gray scaling the image, setting the pixels to black or white) described, Table 3-11, in the defect detection methodology was used to change the darker pixels to represent the unfused powder to black and defective areas, and the brighter pixels representing the part to white.

Table 3-11 - Image analysis to process digital images

Original Image	Detect Part Size	Crop out part	Set peaks black
Layer 1 – Standard Part			
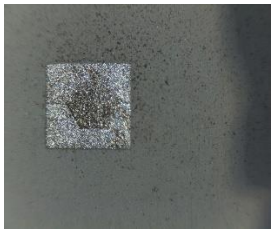	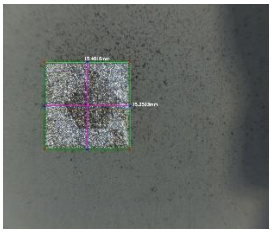	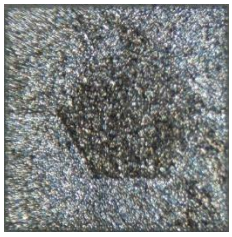	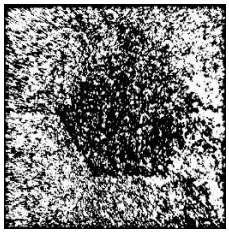
Layer 1 – Synthesized Defect part			
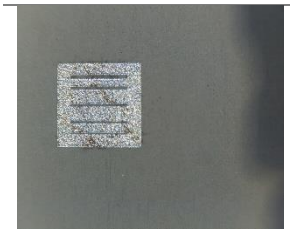	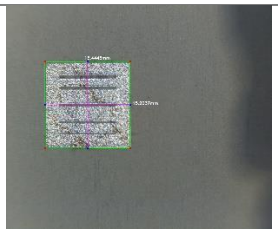	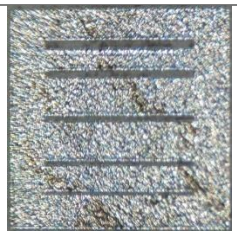	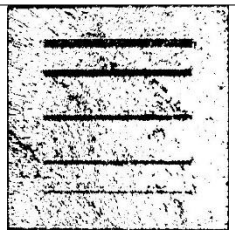

Having the gradient grayscale image and the white-black grayscale images of the printed parts, the next step was to decide how to extrude just the dark pixels and recreate the surface profile as a 3D layer. Generating 3D artifacts from images is an easy enough process with image

processing tools, and CAD software. But attempting to extrude just the contours of the defective edges was a difficult process. The defects were present on a micrometre level, this meant there were a lot of potential data points aside from the synthesized defects. Typically, you can import an image into Solidworks as a sketch and use the auto trace function on the black and white pixels to trace around the edges of the coloured pixels you select with the eye dropper tool. Several attempts to do this resulted in partial detection on the defect contours. Alternatively, you could use the in-built sketch tools to manually trace around the desired pattern. However, due to the sheer number of contours to trace, instead of continuing with manually tracing each layer for hours, which is not a viable method to recommend to other researchers or industry professionals, other methods were explored.

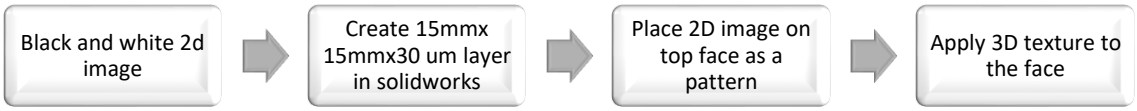

Figure 3-37 3D texture extrusion method

The second method (Figure 3-37 3D texture extrusion method) was the discovery of a new tool added in 2019 to Solidworks, called **3D texture**. **3D texture** works to create a texture profile of an imported image pattern onto a part face. The tool extracts the pixel definition, edges of the pattern profile and gradient of white or black for each pixel. The tool then extrudes out the whiter pixels and cuts into the part face where the black pixels are. You can specify the depth of the profile and the number of artifacts it detects down to the size of the defect. Using this tool, a 3D model of 15-part layers of the standard model was created and joined together in an assembly. The final rendering of the part resembled rough peak-like edges caused by the layering effect. This is not considered the most accurate method for reconstructing the printed part, and aside from providing a visual model, the FEA analysis on the assembly of layers was unsuccessful. The issues related to FEA analysis of the part, are discussed in depth in Chapter 5.

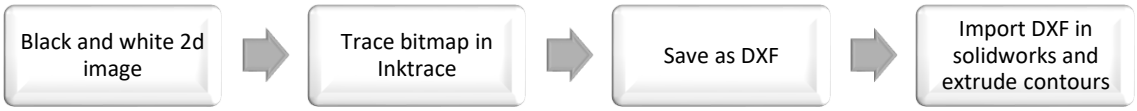

Figure 3-38 Bitmap Trace and DXF contour extrusion

Reaching another obstacle in creating the 3D model and layer files, importing a sketch was reconsidered. Only this time it was not a sketch, but a DXF file that had the contours and edges detected and drawn. Using a software called InkTrace, the grayscale layer images were imported into the workspace. InkTrace is a great software tool to quickly extract shape contours in an image and save the extracted features as a DXF file (importable into Solidworks). The steps to achieve the DXF, include using the **trace bitmap** function, setting your speckle amount,

smoothening level, and selecting trace. Then moving the mask created and deleting the original image. The user can size the image to the dimensions of the part as detected in the part sizing method, save the image as a DXF. Once all the DXF files were created, it was time to retry extruding the file as a 3D layer. The file was imported into Solidworks successfully, but upon selecting **extrude boss** to create the layer, the software was unable to compute all the contours in the DXF trace

Figure 3-39 Extrusion method using *svg file and Blender extrusion to create STL

The final method employed a combination of open-source software including InkTrace and Blender. Like the DXF method, Trace Bitmap was used on the images to extract the contours around the image, then the image was dimensioned, but the images were exported as a scalable vector graphic (*svg) instead. The *svg file was imported into Blender onto a generic 3D space and placed onto the X and Y plane. In **Object Mode**, selecting the **Object** toolbar, then clicking **set origin,** and finally selecting **Geometry to Origin**, moved the center of the part 2D contours file to the origin of the workspace. This step was performed to make it easier to locate the part and visualize the change once extruded. To extrude the part to the layer height (0.03µm) in Blender, the user must select **Object data properties,** then under **Geometry** type in the extrusion value in meters. Once this is done, the part can be exported as an STL file.

Layer Surface Profile Mapping

Having the STL file to reproduce the laser scanning file for part areas that were not melted or exhibit high peaks that influence the surface roughness (Ra and Rz values), was one aim of this research. The second aim is to consider a method that can digitally map the surface profile of each layer as it prints and develop an in-situ digital surface profilometry technique for AM parts. Typically, digital/optical profilometry follows a method of interferometry (popularly white light/Michaelson's Interferometry) or scattered light detection techniques. To use interferometry, a beam splitter is required to split a reference and incident ray both captured by a CCD camera. Chapter 5 and 6 further elaborate on the betterment of the layer profiling method using interferometry instead. In this study, reflectometry was used instead in combination with digital image processing. The surface of each printed part was illuminated by a halogen bulb sitting at a 45-degree angle to the surface of the part. The purpose of this was to create shadows that signified indented areas of the part profile. The work done to create a digital profile of the part within this study focused on mapping the difference in pixel intensity between pixels directly next to each other. The pixel intensity value represents the gray-level or color image numerical representation.

It stores as a single value for a grayscale image and 3 values for a color image (RGB). The pixel intensity is popularly used for classification because it contains the primary information stored within each pixel. In a grayscale image, the pixel intensity is represented by an integer ranging from 0 (Black) to 255 (White). Alternatively, multispectral imaging studies the pixel intensity of another image capture for the same area at a different wavelength. Though it was not used here, it would be the next step in spectral imaging to progress the surface profiling research by capturing the reflection of a different colored light (red or green) on the surface of the part.

The images captured as stated prior in the image processing section, were imported into MATLAB, and using the **Image Processing Toolbox**, manipulated to graph the pixel intensity on a 3D scale. More specifically, using the **surf(x,y,z)** function, which plots data sets in the form of an array, in this case plots the 2D image dimensions along the X and Y axis and the pixel intensity in the Z axis. This process is also achievable with python OpenCV, but the MATLAB method proved simpler to follow. The MATLAB code used to achieve this is detailed below.

```
%Read the images
orig=imread('image_path');

%Convert images to black and white
g_orig = im2gray(orig);

%x and y array sizes
hx = size(g_orig,1);
hy = size(g_orig,2);

%x and y mesh grid for the surface plots
[X,Y]=meshgrid(1:hx, 1:hy);

%Z represent the pixel gray value
Z = g_orig(X) + g_orig(Y);

%Convert X and Y pixels to mm, and Z to micromm
X = X/27;
Y = Y/27;

%plot image and grayvalues in 3D graph with contours
surfc(X,Y,Z)
colormap(pink)    % change color map
shading interp    % interpolate colors across lines and faces
xlabel('Width (mm)')
ylabel('Length (mm)')
zlabel('Pixel Intensity')
```

3.5 SUMMARY

This chapter has explored different methodologies in response to the research aim of each case study within this thesis. The chapter is sectioned to focus singularly on the two key cases studies that target surface finish improvement and surface finish monitoring. The surface finish improvement methodology details a strategy to in-situ laser polish the outline of DMP ProX 100 parts and determine if there is a significant improvement in surface RA, RZ, RSM, and layer thickness. Using Taguchi DOE, an experimental study was performed to test different laser parameters, part surface angles, and measure the change in surface profile parameters, mechanical hardness, and elemental analysis. This study is detailed in Chapter 4, with results, statistical analysis, and a discussion surrounding the impact the results have on surface finish improvement for metal AM parts.

Surface finish monitoring refers to an assessment of the layer topography through different NDT techniques. The progression of digital imaging technologies, image processing strategies and software has helped to quickly push this research from the image acquisition stage, to discovering the best method to represent the 2D layer image in terms of pixel intensity, defect detection and part detection with metrical sizing. This chapter details the work done with digital imaging, but thermal imaging and acoustic techniques were also briefly explored in this doctoral study. This is touched upon in the subsequent chapters, as the solutions explored were constructed with inexpensive hardware, but were not within the time scope of this doctoral research to significantly explore. Chapter 5 presents the results of image processing and segmentation described here in Chapter 3 and discusses the optimization of these strategies to create an in-situ NDT monitoring system, with digital image processing to access the surface profile of each layer and replicate areas that could potentially be improved by another laser scan.

CHAPTER 4

4 CHARACTERIZATION OF IN-SITU LASER-POLISHED DMP SS 17-4 PH SURFACES

Early literature review identified a shortage and inability of techniques to improve surface roughness on complex geometrical surfaces or channels inaccessible to subtractive tooling, for LBPF parts. Further research into possible solutions revealed two under-explored avenues as a starting point: post-processing the parts with a chemical solution and using electro-polishing or laser-polishing the parts during the build stage (in-situ). Based on novelty, laser-polishing was chosen as the experimental avenue in this research study. Laser-polishing is an established post-processing technique and a few research entities have explored and proven its ability to improve the surface finish of AM parts. However, during post-processing any enclosed channels/chambers is inaccessible. Consequently, this prompted the exploration of laser-polishing the part during the building stage. Laser-polishing was chosen over another subtractive-tooling hybrid-process, because LPBF parts are built on a bed of powder (a thin ~30μm layer is spread each layer), and any disruption to the powder would require respreading and any debris from the process could prevent the roller from spreading the powder, collide with the part and cause the part layer to delaminate.

A feature of the DMP ProX 100 printer is the ability to take the outline of each sliced layer in the DMP manufacturing software and outline only the edge of the part's surface as explained in Chapter 3. 3D Systems who manufacture the DMP ProX 100 (and other advanced versions of this AM machine) have experimented with the outline settings to determine the appropriate laser parameter compensations required to accurately aim the laser with the expected energy density to outline the edge of the building part-layer. However, no data or study could be found that explores controlling the laser parameters on the outline (with repetition), to characterize its effect on the surface roughness of LPBF parts. Consequently, the novelty of this research lies in proving in-situ laser-polishing the outline of the LPBF part can affect and improve (lower) the surface roughness. Furthermore, to characterize the solution's ability to improve surface roughness within a channel of a part. The experimental breakdown of this study and flow of results in this chapter can be summarized in the following 3 steps:

1) Control the DMP ProX 100 laser parameters independently to determine if a higher or lower laser power for laser-polishing improves the surface roughness of a flat surface.

2) Run a series of experiments to laser-polish the outline (walls) of the printed part controlling the machine laser parameters independently and rotating the part through different build orientations.
3) Apply the same experimental controls to see the difference in characteristics on the exterior wall vs the inner wall and a flat surface vs a rounded one.

An important factor in evaluating the performance of an AM machine is to measure the surface roughness of the printed part. Case Study (CS) 1, statistically examined the complex dependency of surface roughness, through independently controlling the DMP ProX 100 Metal AM process of SS 17-4 PH powder and proposing reliable regression equations to predict the surface roughness with respect to the build orientation. This chapter presents the results, with discussion, for the surface polishing Robust Parameter Design (RPD) experimental studies performed within the DMP ProX 100 to examine and characterize the significance of varying print orientation and print settings on the surface profile of SS 17-4 PH parts. The research objectives of this case study examine the correlation between laser power (P), scan speed (v), polishing iterations (N), and their influence on the surface profile on a metal AM part. The research hypothesis predicted controlling the machine parameters independently could lead to an improved surface roughness, creating novel design rules for achieving a better surface roughness with respect to the part edge build angle.

There are several testing strategies typically used to characterize the surface profile of a part, with focus on its texture, lustre, profile shape, and any surface anomalies. For metal AM parts, the laser welding line size and layer thickness greatly impacts the surface profile and measured surface roughness (Ra, Rsm, Rz etc…) of a part. The outcome of polishing the surface at different scan speeds and power could result in the formation of surface anomalies including variation in the weld line thickness, discolouration caused by high laser power, a change in mechanical hardness and the formation of surface defects.

The experimentation performed in this study to test the effect of in-situ laser polishing the outline as the part builds in different orientations, required several RPD set-ups. The RPD statistical design of experiment (DOE) was chosen to test the greatest number of factors whilst reducing the number of samples required, so more trials could be achieved. Metal AM is a time-consuming process; hence it was not within the scope of this study to complete a full factorial DOE. To account for any variation in printing consistency, in different locations on the build plate, the samples for each trial (identical print settings) were placed in randomized positions. The angled and vertically built samples were also rotated clockwise (axis perpendicular to the top face of the plate) at 90^{o} increments.

The manufactured tests specimens are presented first, followed by the RPD results, statistical analysis, and discussion. This is followed by qualitative results obtained through surface profilometry testing, SEM imaging, and EDX analysis.

4.1 SS 17-4PH DIRECT METAL PRINTED TEST SPECIMENS

Table 4-1 Test Specimen Abbreviation References

Test Specimen Abbreviation References

Sample Name	Ref.	Affected Surface
Top Surface	−T	Final Layer
Vertical Square Samples	∠SV	Vertical outline
Angled 20º	∠A20	Angled outline
Angled 40º	∠A40	Angled outline
Angled 60º	∠A60	Angled outline
Angled 80º	∠A80	Angled outline
Vertical Circle Samples	- IV	Inner Circular Profile

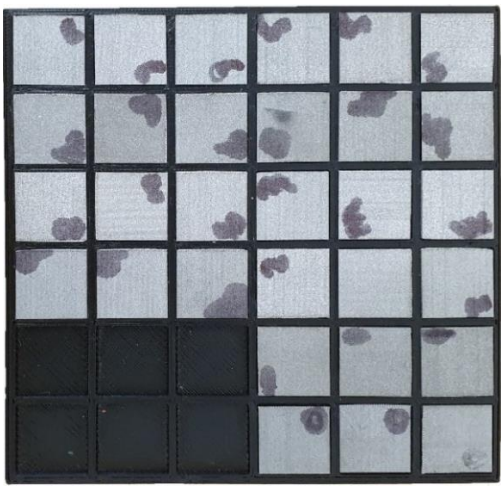

Figure 4-1 Vertical samples arranged with the affected surface perpendicular to measuring tool

The DMP test specimens were manufactured according to the RPD experimental set-up detailed in Chapter 3. Following removal from the DMP machine, the samples were removed from the build plate using a horizontal bandsaw with coolant running along its blade. The support material was removed using a linisher. The samples were cleaned in an ultrasonic bath (10% cleaning solution, 90% water) at 70 ºC for 10 minutes, to remove excess dirt, coolant, and excess metal powder from the surface. Most of the testing equipment used in the analysis of the test specimens required the surface to be ∠90º to beam/probe/camera. Therefore, custom sample holders were FDM printed to preserve and arrange the samples for inspection, particularly for the vertical (-V) and angled (∠A) samples.

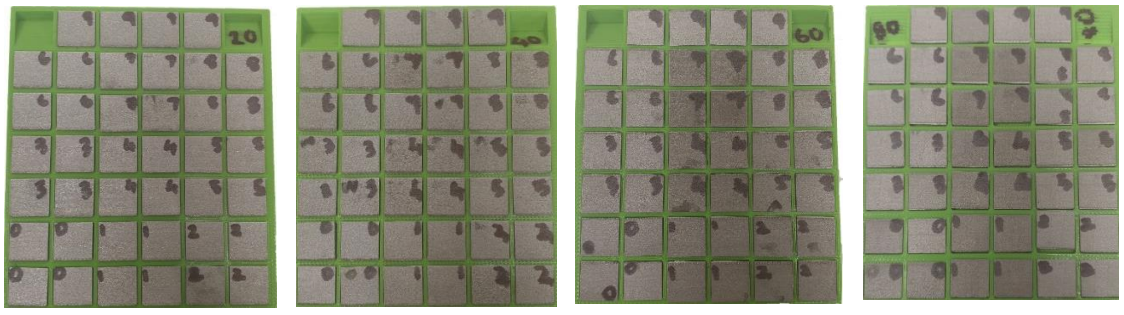

∠20 Samples ∠40 Samples ∠60 Samples ∠80 Samples

Figure 4-2 ∠20, ∠40, ∠60, ∠80 Samples arranged with the affected surface perpendicular to measuring tool

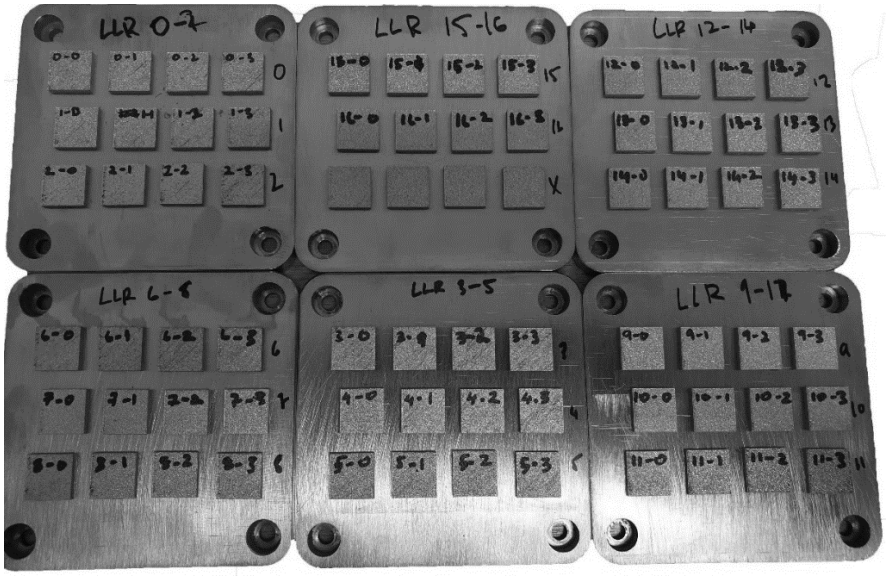

Figure 4-3 Horizontal samples as built before removal from the build plate

The top surface (− T) samples were left on the build plates (Figure 4-3) for the profilometry testing, as they were already perpendicular to testing probe. These samples were removed from the build plate by an EDM wire cutting machine, in preparation for the other testing measurements. Figure 4-1 illustrates the vertically built (-V) samples sitting within the FDM printed sample holder. Figure 4-2, captures the angled samples (∠A20, ∠A40, ∠A60, and ∠A80) in their respective FDM printed holder angled to bring the affected surface perpendicular to the testing equipment.

4.2 STATISTICAL RPD ANALYSIS OF – T SAMPLES

The unique low-powered laser required to bond the SS 17-4 PH powder, set the precedent for this study to determine the most effective range of laser power to alter the microstructure of the part and achieve a smoother surface profile. The surface profilometry testing revealed some improvement in surface roughness (Ra) (Table 4-2), proving the capability of the built-in laser to act as a laser polishing tool. The main effects plots for mean of means and mean of SN ratios (Figure 4-5 & Figure 4-4) for the – T samples show the higher spectrum of laser power (60%, 70% and 80% laser power) had a significantly positive result (9.4% improvement [Ra]), decreasing the surface roughness (Ra) for the SS 17-4 PH samples.

The scan speed was set to its default speed of 140mm/s. The outline tests analysed in the following section, use scan speed as an independently controlled variable, and the minimum speed recommended (by the manufacturer) for the DMP ProX 100 is 100 mm/s. The maximum speed is 1000 mm/s. The Ra values (-T tests) improved steadily in the higher spectrum of laser power but with a consistently lower scan speed (almost the minimum the machine could perform at). As

such, it was interesting to observe the performance (in the outline tests) of these 3 laser power settings, combined with higher scan speeds. A change in weld-line thickness on the surface of the samples was observed, but no statistical correlation can be made between the improvement and the influence of the corresponding input variables. The change in hatch spacing likely had the greatest effect on the weld-line thickness, however without at least one more independent variable, this statement cannot be made with some statistical confidence.

Figure 4-4 - T samples Mean of Means for Ra (Surface Roughness)

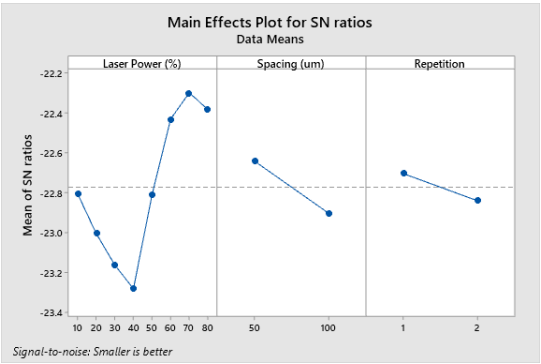

Figure 4-5 - T samples Mean of SN ratios for Ra (Surface Roughness)

The SEM visual inspection revealed voids on the surface of the printed parts that had a higher measured surface roughness value. There was some discoloration and burning on some of the samples corresponding with the repetition of lasering the surface twice. This experiment gave some insight into the inconsistency of the process for building in different sections off the build plate. In some test specimen corners there were defects present on the surface of the samples prior to the repolishing test. For this reason, in carrying out the outline experimentation, samples were placed in a randomized order and any samples which built with voids visible during the building phase were discarded and re-printed to ensure a fair test was carried out.

The surface of the test specimens was lightly sanded (smoothen the surface), to achieve a measurable indent required to test the mechanical hardness of the sample. The mechanical hardness of the samples (Table 4-2) did not show any significant drop or increase over the the standardized margin for mechanical hardness of SS 17-4PH parts. There could be some variation in mechanical hardness if all surfaces off the test specimen were to be repolished and this could change in respect to the specimen thickness. It was not within the scope of this study to examine the variation in tensile strength or fatigue strength, which would have provided further understanding of the effect of these repolishing tests on the mechanical properties of the altered test specimen. Further optimization of the following outline tests and a study of the consequence on layer-line thickness as an independent control variable (future work recommendation) could be a better point at which to perform and analyze these properties. Documented research

inferences a better surface roughness should result in higher mechanical strength and endurance with the reduction of surface defects.

Table 4-2 RPD L16(8^1 2^2) experimental design for horizontally printed samples (- T),

Ref.	Laser Power (%)	Spacing (um)	Repetition	Surface Roughness Ra (um)	Surface Roughness Rz (um)	Surface Roughness RSm (um)	Hardness (HV)	Weld-line Thickness (µm)
ORIGINAL				14.11	71.87	0.409	335.05	84
T1	10	50	1	13.64	71.19	0.409	335.3	81
T2	10	100	2	13.98	65.43	0.413	307.6	117
T3	20	50	1	13.69	74.58	0.436	357.9	86
T4	20	100	2	14.58	73.35	0.378	359.6	90
T5	30	50	1	14.03	75.61	0.426	349.2	90
T6	30	100	2	14.76	74.89	0.427	321.5	93
T7	40	50	1	14.26	75.37	0.406	328.4	137
T8	40	100	2	14.92	78.31	0.393	335.6	83
T9	50	50	2	13.69	77.21	0.404	340.3	56
T10	50	100	1	13.94	75.99	0.436	328.4	81
T11	60	50	2	13.68	78.91	0.451	348.4	61
T12	60	100	1	12.78	71.24	0.474	324.6	91
T13	70	50	2	12.69	68.89	0.438	335.8	68
T14	70	100	1	13.37	67.78	0.488	355.7	96
T15	80	50	2	12.79	69.37	0.576	348.5	69
T16	80	100	1	13.52	69.77	0.465	363.0	108

4.3 STATISTICAL ANALYSIS OF RPD L9 EXPERIMENTS AFTER LASER POLISHING THE OUTLINE OF THE EXTERNAL ANGLED WALLS FOR THE SS 17-4 PH TEST SPECIMENS

The following section analyses the statistical results of all experiments performed on the L9 RPD experiments including the vertical and angled outline experiments. The tablature results for these experiments can be found in Appendix B. The results documented in these tables columnize the final average taken from 4 trials for each RPD experiment to present quantitative data representing the surface profile, mechanical hardness and layer thickness captured with the testing equipment detailed in Chapter 3 the methodology. The study first begins with examining the results from the surface profilometry testing. Starting with the Ra and Rz measurements, but excluding the RSm values for all experiments, which was deemed insignificant as it did not meet the probability threshold ($\alpha \leq 0.05$) and was therefore pooled from the analysis. Figure 4-6 graphs the results for the Ra values measured for the vertical and angled experimentation. The graph confirms the vertical and $\angle 80^{o}$ angle samples (which align almost parallel to the laser) have a greater improvement in surface roughness than the flatter samples (angled closer to being perpendicular to the laser surface). This trend demonstrates that the range of scan speed (v), laser power (P) and repetition/polishing iterations (N) chosen for this study benefits the vertical (straight edge) orientation for laser polishing the samples to achieve a better surface roughness. Alternative experimentation with different independent control variables (ICV) (different laser power spectrum, or layer thickness) could result in better surface roughness for the angled -CV, $\angle 20^{o}$, $\angle 40^{o}$ and $\angle 60^{o}$ degree samples and would require more testing.

A consistent trend for the -SV, $\angle 20$ and $\angle 40$ experimentation can be observed, where identical peaks in surface roughness that align along the same ICV test format, such as T1, T4, and T7, correlating with an increase in Ra. These three peaks align with every test in which the scan speed was set to 100mm/s. And the reverse is seen for T2, T3, T5, T6, T8 and T9 where the Ra values decrease, and all align with a higher scan speed but also correlate in some way to the repetition and laser power. These experiments are designed to test the range of scan speed that would be most effective in decreasing the surface roughness, considering the laser power was already previously tested and the 1st RPD experiment presented in the study. There is no solid evidence or trend that can be stated with confidence to demonstrate that the repetition of the polishing settings (i.e., laser power and scan speed) had a major impact on the Ra value without examining the statistical data in Minitab 19 using ANOVA and RPD design analysis (this examination is presented in the following section). The values displayed in the graph shown in

Figure 4-6 are a total average taken from the four trials performed (for each L9 study) times the 5 measurements per sample.

The best improvement in surface roughness came from the ∠80 T2 sample set's total average, with a 16.7% decrease in Ra. The second-best improvement seen in the-SV T3 sample set's total average with a 10.7% decrease, however other combinations of scan speed, laser power and repolishing runs in the ∠80 L9 tests exhibited a higher percentage of improvement in surface roughness. Identical to the measured surface roughness Ra values, the Rz total averages also exhibit similar peaks and drops for each testing criteria (Figure 4-7). It is interesting to observe that even in the original samples the Rz values sit within 70 µm to almost 90 µm which means that the peaks and valleys in the surface profile range in height for about this much. As stated in the previous chapter methodology, typically a ratio range for Rz-to-Ra = 4:1 or 7:1. In the case of this study for the best sample set the ratio is ~7:1 and for the worst ~5:1 approximately.

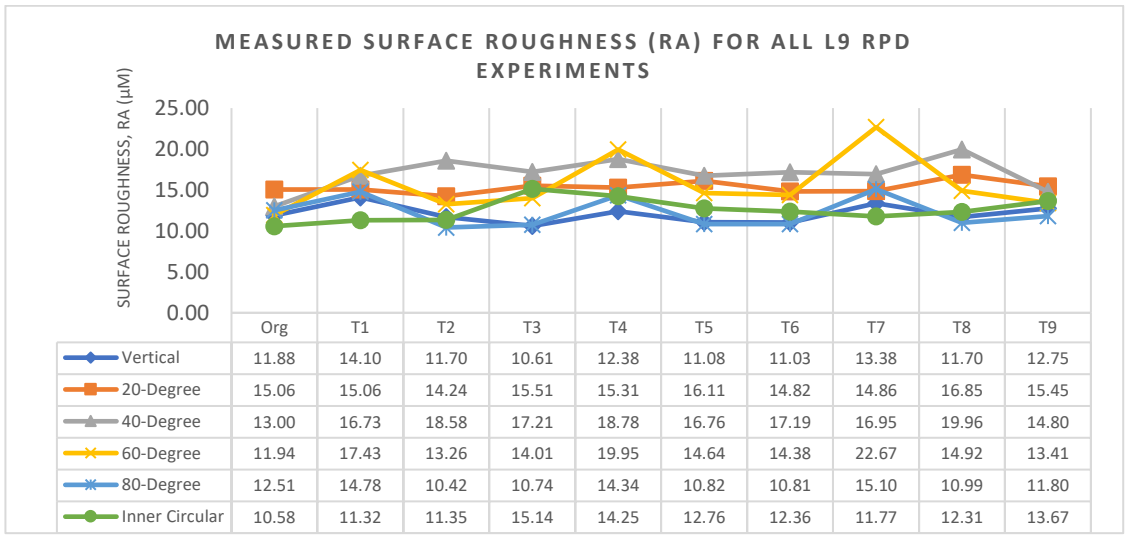

	Org	T1	T2	T3	T4	T5	T6	T7	T8	T9
Vertical	11.88	14.10	11.70	10.61	12.38	11.08	11.03	13.38	11.70	12.75
20-Degree	15.06	15.06	14.24	15.51	15.31	16.11	14.82	14.86	16.85	15.45
40-Degree	13.00	16.73	18.58	17.21	18.78	16.76	17.19	16.95	19.96	14.80
60-Degree	11.94	17.43	13.26	14.01	19.95	14.64	14.38	22.67	14.92	13.41
80-Degree	12.51	14.78	10.42	10.74	14.34	10.82	10.81	15.10	10.99	11.80
Inner Circular	10.58	11.32	11.35	15.14	14.25	12.76	12.36	11.77	12.31	13.67

Figure 4-6 Graphical Representation of measured Ra values for all L9 RPD experiments

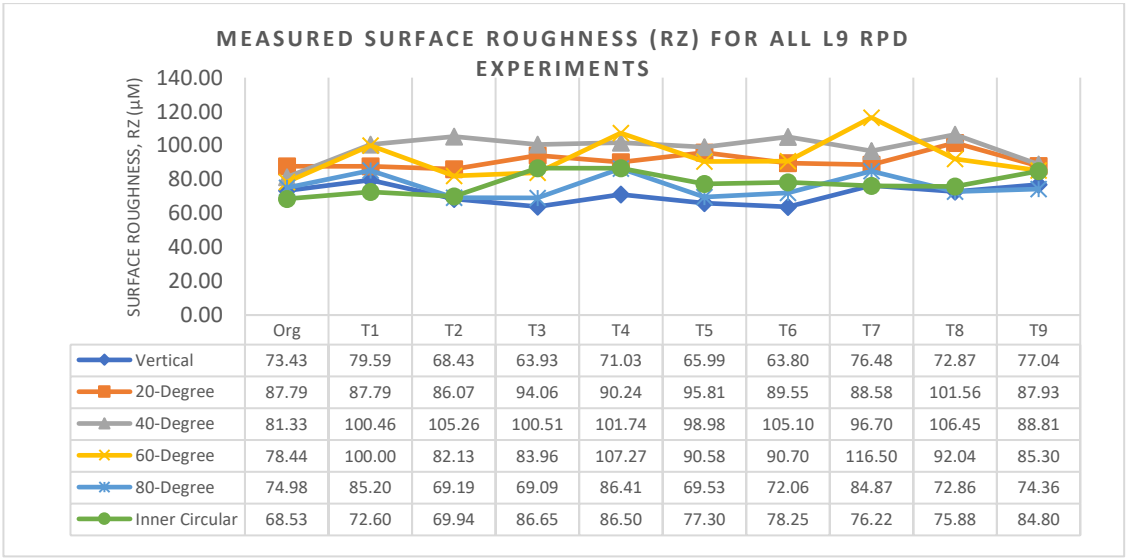

	Org	T1	T2	T3	T4	T5	T6	T7	T8	T9
Vertical	73.43	79.59	68.43	63.93	71.03	65.99	63.80	76.48	72.87	77.04
20-Degree	87.79	87.79	86.07	94.06	90.24	95.81	89.55	88.58	101.56	87.93
40-Degree	81.33	100.46	105.26	100.51	101.74	98.98	105.10	96.70	106.45	88.81
60-Degree	78.44	100.00	82.13	83.96	107.27	90.58	90.70	116.50	92.04	85.30
80-Degree	74.98	85.20	69.19	69.09	86.41	69.53	72.06	84.87	72.86	74.36
Inner Circular	68.53	72.60	69.94	86.65	86.50	77.30	78.25	76.22	75.88	84.80

Figure 4-7 Graphical Representation of measured Rz values for all L9 RPD experiments

The following data presented in Table 4-3 and Table 4-4 display the input variable ranking for the delta value based on the SN ratio and Means, taken from the RPD analysis for each L9 experiment that was performed in the study. The mean of SN ratios and mean of means for the Ra, Rz and Mechanical Hardness results, illustrating a difference in dependence on the input variables (*P*, *v*, and *N*), are displayed in Appendix B. The layer thickness and Rsm plots were determined to be insignificant due to a high P-value insinuating there is no significant difference between factors to void the null hypothesis, and therefore pooled from the study. Examining the rankings, the scan speed had the highest import on the surface roughness of the samples for the more vertically aligned samples such as the -SV, ∠80, ∠60, ∠40. Whereas the ∠20 samples were mostly affected by the repetition. Regarding the Rz values, scan speed was the most prominent for most sample sets. However, for the hardness testing, laser power had the greatest influence followed by repetition and scan speed on the average value of mechanical hardness taken from the samples.

Table 4-3 Input Variable Ranking for the Delta value based on SN ratio

	Ra			Rz			Hardness		
	Laser Power	Scan speed	Repetition	Laser Power	Scan speed	Repetition	Laser Power	Scan speed	Repetition
-SV	2	1	3	1	2	3	1	3	2
∠A20	2	3	1	3	2	1	1	3	2
∠A40	3	1	2	3	1	2	1	3	2
∠A60	2	1	3	2	1	3	1	2	3
∠A80	2	1	3	2	1	3	1	3	2
-CV	3	1	2	3	1	2	-	-	-

Table 4-4 Input Variable Ranking for the Delta value based on Means

	Ra			Rz			Hardness		
	Laser Power	Scan speed	Repetition	Laser Power	Scan speed	Repetition	Laser Power	Scan speed	Repetition
-SV	2	1	3	1	2	3	1	3	2
∠A20	3	2	1	3	2	1	1	3	2
∠A40	3	1	2	3	1	2	1	3	2
∠A60	2	1	3	2	1	3	1	2	3
∠A80	2	1	3	2	1	3	1	3	2
-CV	3	1	2	3	1	2	-	-	-

4.3.1 ANOVA FOR RA

Sources of variation: Factors, Trials, the Factors x Trials interaction, and the error terms.

Degrees of Freedom Calculation (DoF):

Factors = 3, Trials = 4

Table 4-5 Degrees of Freedom for each RPD study

	DoF for Factors	DoF for error of factors	DoF for Trials	DoF for Factors x Trials interaction	DoF for error of Trials
Calculation	3-1	8-6	4-1	2 x 3	2 x 3
Total	2	2	3	6	6

Equation 8 Formula to calculate the percentage of contribution from each input factor

$$\%\ contribution_{Factor} = \frac{Sum\ of\ Squares\ (Factor)}{Total\ Sum\ of\ Squares} \text{ x } 100$$

An analysis of variance (ANOVA) examines the significance of each result within the experimental study, so that the null hypothesis may be accepted or rejected for an alternative hypothesis. The sources of variation in each study contributes a level of noise that needs to be accounted for, especially in an RPD/Taguchi DOE. The L9 orthogonal arrays (OA) used in this case study depict a 3^3 (3 input parameters) OA, with a total of 6 Degrees of Freedom (DoF). Typically, a complete L9 Taguchi study will use a 3^4 (4 input parameters) OA and have 8 DoF. Therefore, there is 2 DoFs contributing toward the residual error in this study. the Table 4-6 provides the contribution of each control variable and its quantitative influence or %contribution on the final mean for surface roughness (Ra), including the contribution of residual error. As Equation 8, states the %contribution is a fraction of the sum of squares (SS Seq) for the individual factor divided by the total SS Seq for all factors (*P*, *v* or *N*), multiplied by 100 to achieve a percentage representation.

The values for the SS Seq column in Table 4-6, are taken from the Minitab 19 Taguchi Analysis, and the %contribution were calculated manually based on Equation 8. Reviewing the %contributions in Table 4-6, it is observed that the scan speed is shown to have the higher percentage of contribution for the -SV, ∠60, and ∠80 samples. There is a significant margin of error for the -CV, ∠20 and ∠40 samples; 46%, 46% and 56% respectively. This represents an ineffective margin and combination of *v*, *P* and *N* to improve Ra for these tests (further examination of these results is presented in the discussion section at the end of the chapter). Regarding the ∠80 sample set there is a 96% contribution from the *v*. The -SV samples are affected by a 59% *v* contribution and 18% contribution from the *P*. The *N* variable range (1 to 5

repetitions) shows no significant contribution in any of the Ra distributions for each of the RPD studies. The range of repetitions could be too few to have a significant impact on the part. There is no proof to show the increased repetitions alone were detrimental to the improvement in Ra.

Table 4-6 Summary of %contribution of independent control variables on the variation in Ra for each RPD.

Sample Set	Source	Sum of Squares (SS Seq)	% contribution
Square Vertical	Laser Power	0.9603	18%
	Scan speed	3.2446	59%
	Repetition	0.3974	7%
	Residual Error	0.8522	16%
	Total	5.4545	100%
20 Degree	Laser Power	0.2409	16%
	Scan speed	0.2266	15%
	Repetition	0.3487	23%
	Residual Error	0.698	46%
	Total	1.5143	100%
40 Degree	Laser Power	0.08892	2%
	Scan speed	1.5534	35%
	Repetition	0.33644	8%
	Residual Error	2.48161	56%
	Total	4.46037	100%
60 Degree	Laser Power	1.5593	7%
	Scan speed	18.0481	84%
	Repetition	1.0334	5%
	Residual Error	0.7995	4%
	Total	21.4403	100%
80 Degree	Laser Power	0.4391	3%
	Scan speed	13.645	96%
	Repetition	0.0004	0%
	Residual Error	0.1901	1%
	Total	14.2745	100%
Circle Vertical	Laser Power	0.3110	4.97%
	Scan speed	1.8714	29.93%
	Repetition	1.1778	18.84%
	Residual Error	2.8922	46.26%
	Total	6.2524	100.00%

Interaction plots graphically represent the relationship between the control variables used in the RPDs and the output measurements. Parallel lines in an interaction plot indicate no interaction, the greater the withdrawal of lines from the parallel state the higher the degree of interaction. Figure 4-8 and Figure 4-9 illustrate the interaction between *v*, *P* and *N* on the output Ra and Rz values for the ∠80 sample set. The interactive response between the variables is identical for both graphs, where the mid to higher range of *v* (500mm/s to 1000 mm/s) and the lower range of *P* (60%) perform as a better combination. The relationship between *P* and *N* shows the higher *P* and *N* are, the more Ra and Rz increases. This is visible across nearly all the

interaction plots for each RPD study (Table 4-7), except for the -CV experiments. Additionally, it is interesting to note that the lowest *P* setting (60%) combined with higher repetition, lowers the Ra and Rz means within the surface profile. Testing a lower spectrum of *P* (40% to 60%) with a similar or higher range of *N*, could produce better improvement in Ra and Rz.

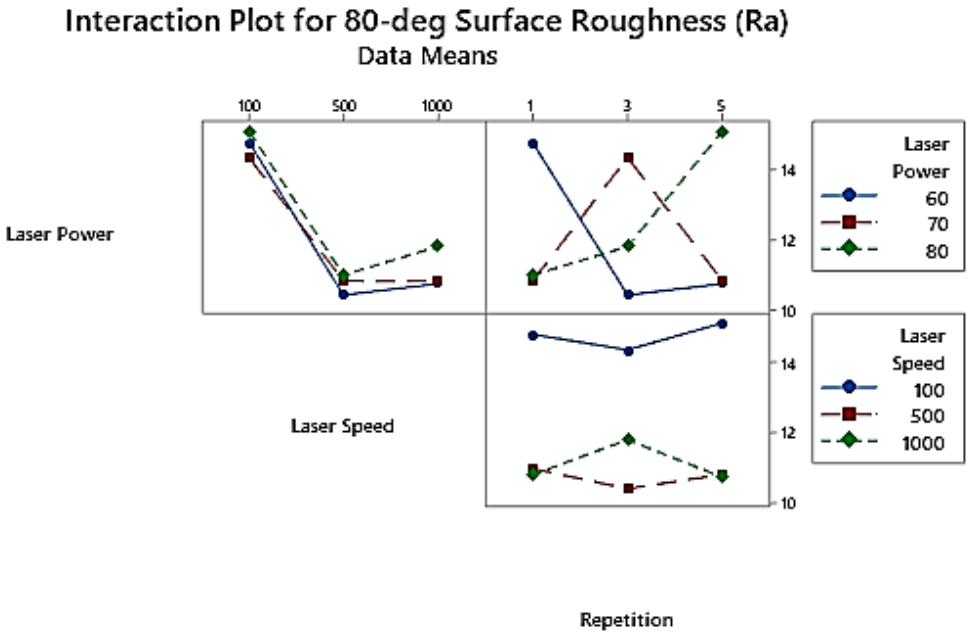

Figure 4-8 Interaction plot for ∠80° Surface Roughness (Ra)

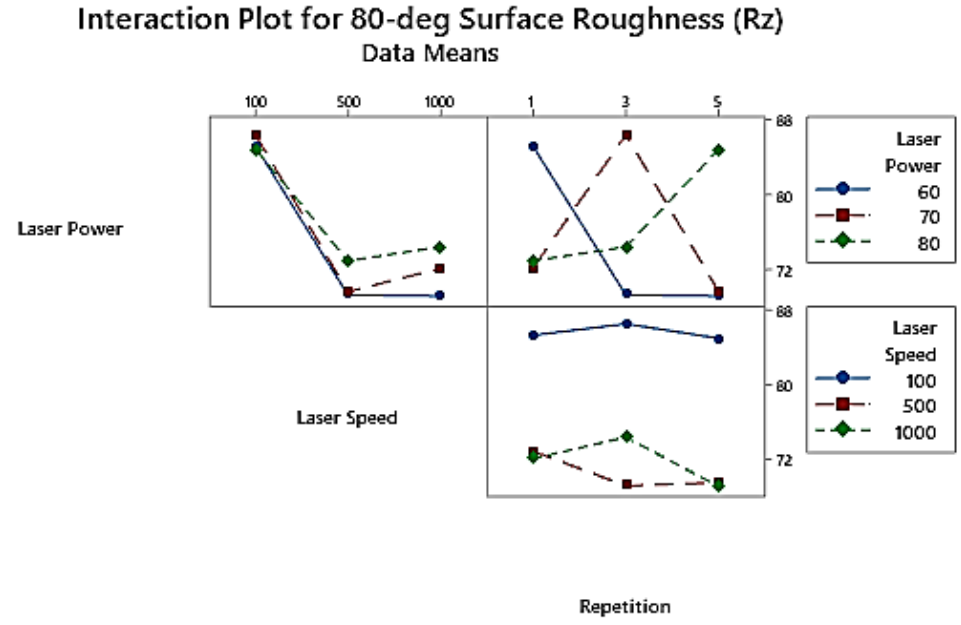

Figure 4-9 Interaction plot for ∠80° Surface Roughness (Rz)

Table 4-7 Interaction plots for the -SV, representing the correlation between *v*, *P* and *N* on the output roughness profile for the Ra and Rz measurements

	Ra	**Rz**
-SV	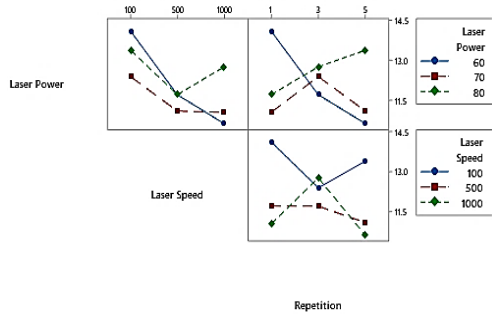	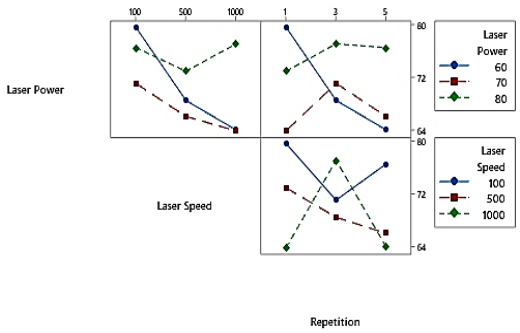
∠20	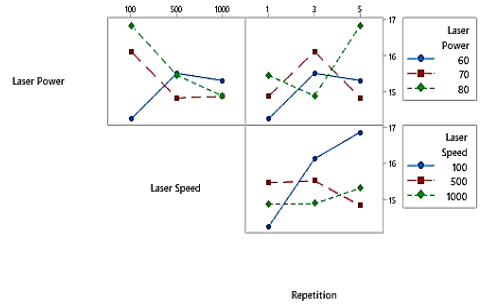	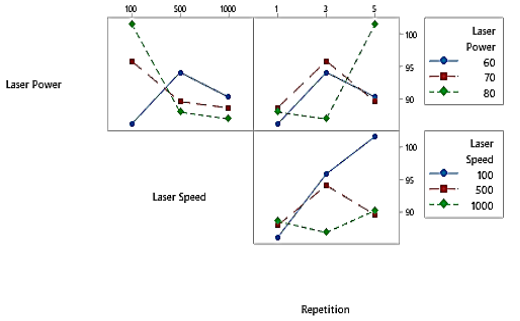
∠40	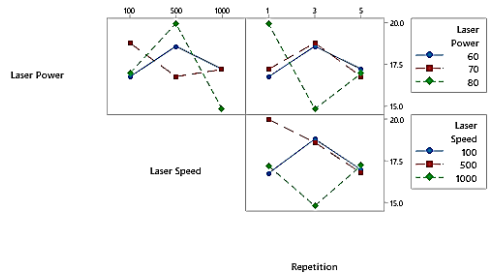	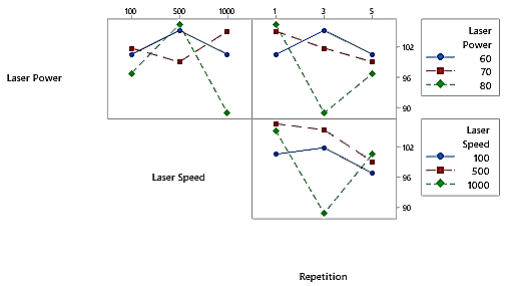
∠60	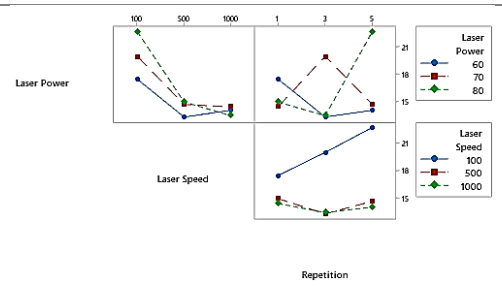	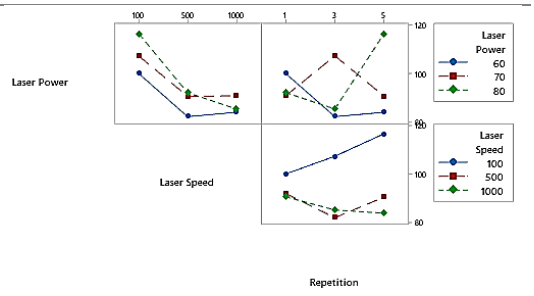
-CV	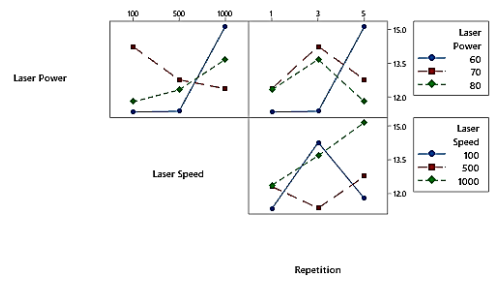	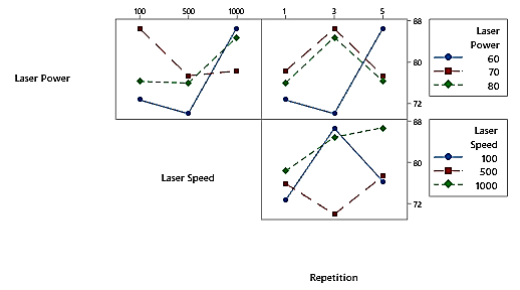

The following contour plots (Figure 4-10 and Figure 4-11) illustrate the influence of laser power and scan speed (the top 2 ranked influential parameters that affected the surface roughness in this experiment). Each plot demonstrates the spectrum of surface roughness within the range of *P* and *v* used in this study. The gradient of change in both contour plots show that despite the improvement in Ra, there is a significantly different relationship between the laser power and laser speed for each of these orientations. In Figure 4-10, it is observed that a reduction in Ra is achieved through a combination of higher laser speed and a lower laser power. Whereas, in Figure 4-11, a lower Ra is accomplished solely by a higher laser speed. Though they are not included in this thesis document, examining the contour plots for the other angled specimens exemplified the ∠60 sample had a similar interactive response to Ra (in-range of *P* and *v*) as the ∠80 sample. The ∠20 and ∠40 samples have a convoluted and disorganized gradient of change, possibly due to the level of error and lack of improvement in Ra. Similarly, as there was no inherent improvement in surface roughness for the -CV samples; the contour plot exemplifies the interaction between *P* and *v* (within the chosen maximum and minimum range) to adversely affect the Ra.

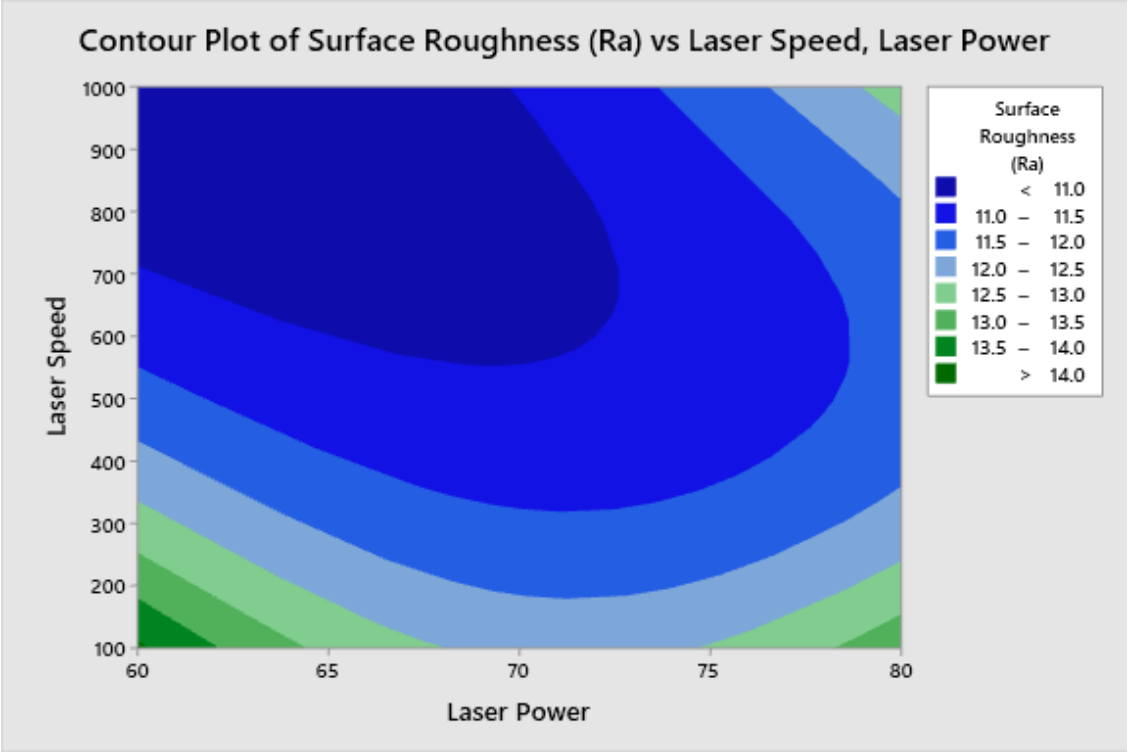

Figure 4-10 Contour Plot of Surface Roughness (Ra) vs *P* and *v* for the (a) -SV Outline test

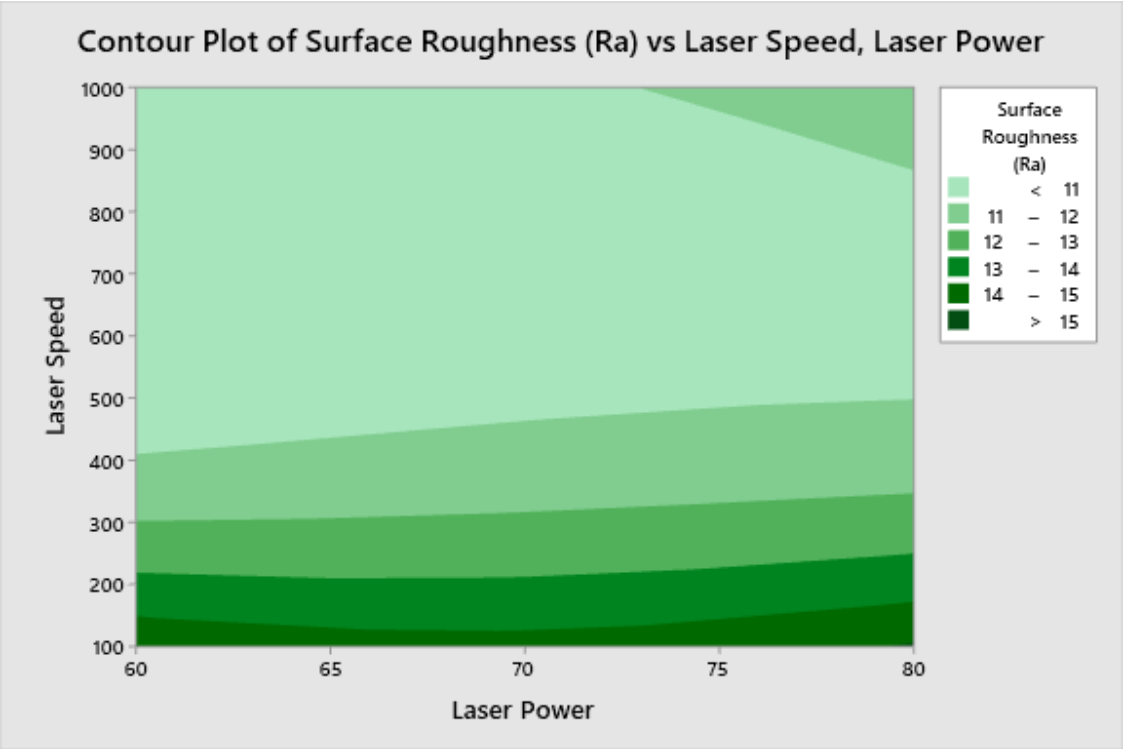

Figure 4-11 Contour Plot of Surface Roughness (Ra) vs *P* and *v* for the ∠A80 Outline test

4.3.2 REGRESSION ANALYSIS FOR EACH L9 RPD

The following equations summarize, the characterization of *P*, *v* and *N* and their influence on the surface profile parameter Ra for the DMP ProX 100 printed SS 17-4PH test specimens. The mathematical models are presented with the corresponding R^2 values below. The -CV model is excluded as no improvement was seen.

Print Orientation	**Regression Equation**
-SV	$Ra = 11.89 + 0.0238\,P - 0.001944\,v - 0.147\,N \;\; [R^2 = 84.38\%]$
∠A20	$Ra = 12.66 + 0.0355\,P - 0.000783\,v + 0.202\,N \;\; [R^2 = 53.90\%]$
∠A40	$Ra = 19.85 - 0.0137\,P - 0.00133\,v - 0.247\,N \;\; [R^2 = 44.36\%]$
∠A60	$Ra = 11.07 + 0.1047\,P - 0.00651\,v + 0.382\,N \;\; [R^2 = 96.27\%]$
∠A80	$Ra = 11.95 + 0.0325\,P - 0.00383\,v + 0.007\,N \;\; [R^2 = 98.67\%]$

4.3.3 SEM SURFACE DEFECTS AND LAYER THICKNESS ANALYSIS

The quantitative data presented thus far, provides a numerical characterization for the correlation between the 3 ICVs that were used in this study. The surface profile under visual inspection offers another analysis viewpoint to understand and interpret the consequence of repolishing the outline of a square specimens with different incident angles relative to the laser.

A study of the surface morphology exposed each angle had a different level of layer overlapping and essentially layer thickness. There are surface defects visible on all samples (balling and voids primarily). The following subsection presents observations from high-resolution images, captured from two different SEM imaging machines (Ziess EVO MA25 and Hiatchi TM3030Plus) and a chemical composition analysis performed with the built-in EDX analyzer.

Surface Morphology and Layer Orientation

Table 4-8 presents the SEM images, illustrating the surface morphology/topography, for the original (unaltered), best (lowest Ra) and worst (highest Ra) specimens for each angled print orientation. These images are a few picked from over 1000 images obtained to examine the layer thickness and defect sizing for each test specimen in this study. The images are a combination of captures taken from both SEM machines, some representing the layer thickness measurements and others the spectrum area measured using EDX analysis to determine the chemical composition within that section. The layer thickness for all experiments was set to 30µm (powder spread thickness) in the machine setting, however, due to the influence of the experimental laser parameters, a variation in the measured layer thickness (outline wall area) of the printed parts. An approximate average was obtained from the SEM images, measuring the visible overlap/layer thickness for unaltered samples printed at the different angles in this study. The samples with no slope/ a steeper slope had a layer thickness closer to the 30µm powder layer thickness [-SV ≈ 40 µm, ∠A80 ≈ 38 µm and ∠A60 ≈ 41µm]. Following on, the samples printed with a larger smaller incline (∠A20 ≈ 95 µm and ∠A40 ≈ 63 µm). This demonstrates an inverse variation between the measured layer thickness line and the print angle orientation. On the surface for most samples, voids, pores, and partially fused powder particles were visible contributing to the uneven profile wave.

EDX Chemical Composition Stability Confirmation

The composition analysis of residual debris and foreign particles using EDX analysis revealed the elemental distribution fell within the datasheet specification. There was some iron detected on the surfaces of the samples, which is expected from any processing done to the SS 17-4 PH parts and means the parts would need to be passivized to ensure corrosion resistance.

Table 4-8 SEM Images exemplifying the surface morphology in the original, best (Ra) and worst (Ra) with respect to each angled print orientation.

	Original	Best (Ra)	Worst (Ra)
-SV	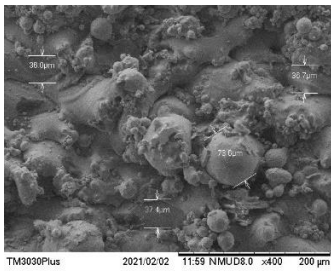	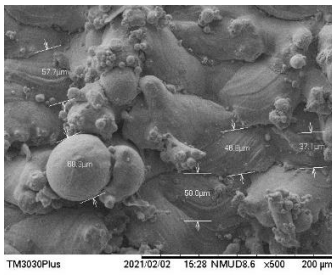	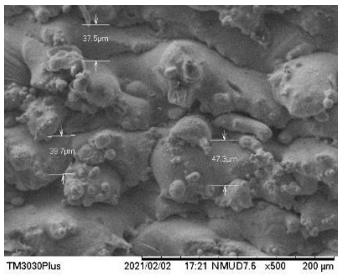
∠A20	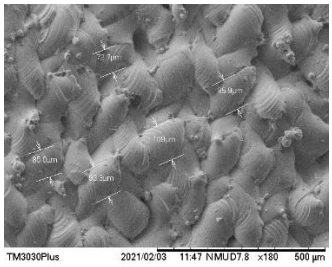	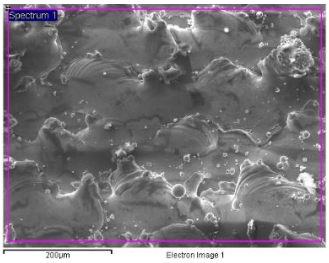	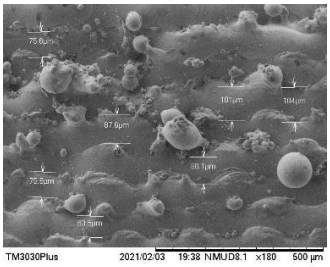
∠A40	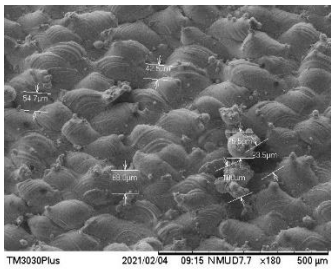		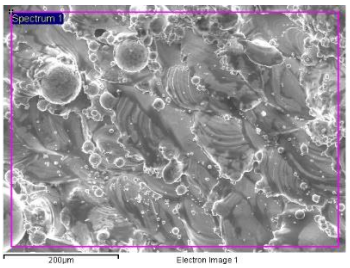
∠A60	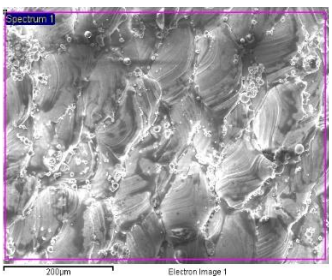	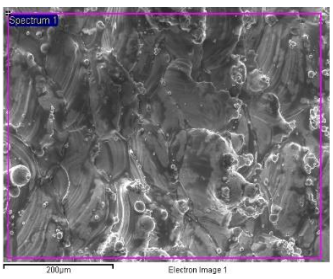	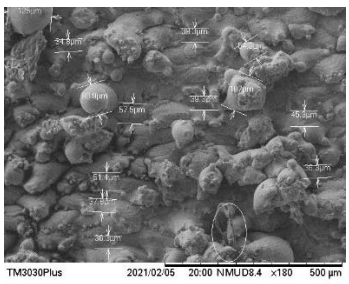
∠A80	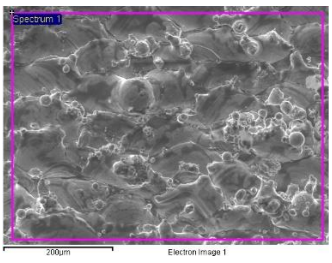	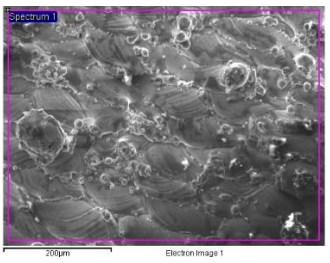	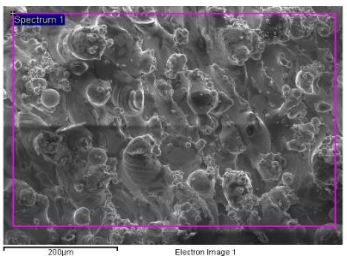

4.4 DISCUSSION

The experimentation performed to examine the characteristic alterations made by micro-laser-polishing the surface of a DMP ProX 100 printed SS 17-4 PH part, demonstrated improved surface roughness with respect to the surface position, relative lasering angle and curvature. Previously stated in Chapter 2, there are four primary surfaces of varying surface roughness in a metal AM part: top surface (flat), external walls, internal cavities, and support material bonded surfaces. This study examined methods with focus primarily on the flat surface (perpendicular to the laser), external walls and a minor study of the impact on internal cavities. The research questions at the introduction of this study sought to determine the effect of laser polishing (LP) the external surface of a metal AM part using the machine's in-built laser as it printed. Secondly, to discover which key input parameters (machine settings) positively affect the parts surface texture and mechanical aptitude.

Addressing the first part of the research question, it was evident to characterize the "effect", key topographic measurements were required. As such, a measure of the surface roughness profile (Ra, Rz and RSm), mechanical hardness, surface defects and layer thickness were the chosen output parameters in the experimental study. Consequently, the independent control variables (input parameters), were the machine's settings for laser power (P), scan speed (v), polishing iterations (N). In addition to these control variables, it was important to observe the impact of varying the wall angles and the consequential impact of the same trials on each angled specimen. The results presented in this chapter provided a detailed overview of the affected surface characteristics (output parameters), that may have been altered due to the different trial formulations used in the LP tests (input parameters) of each test specimen and, bring to light new areas of research focusing on developing new in-situ LP methods customized to consider the wall angle and curvature.

Summary of experimental work

Preceding the experimental work in this study, the academic review of previous work related to LP for AM parts revealed most work performed was to affect a flat square shaped surface after the specimen was printed and removed from the build chamber [58, 76, 80]. This led to the initial work performed to prove the capability of in-situ laser polishing for the "top surface (flat)". The focus of this minor study examined the impact that the higher and lower spectrum of laser power (5W to 45W) had on the top surface of the samples. Contrary to the laser parameters used by other researchers, who use a 150W or higher laser power, the maximum energy output for this laser is 50W. As expected, the lower range of laser power (5W to 25W) had a detrimental effect on the surface texture of the affected specimen face, measuring at a higher Ra value than

the original samples with notably sized surface pores and powder discoloration. It is speculated that this phenomenon might be due to existing gas pores that were potentially released or opened with the remelting. As previously noted in the results, the discoloration and surface defects also occurred post-built before the remelting operation was conducted. Voids of notable size (visible to the human eye) were present on samples printed in the bottom-left hand corner of the plate. The study did prove fruitful, demonstrating the ability of the DMP ProX 100's laser to improve the surface finish (Ra whilst staying within the expected Rz range) of the printed part. This was the main purpose of this case study, and the percentage of improvement was significant. The DMP ProX 100 is a research grade printer, that has now been surpassed by newer models that produce parts with an improved surface roughness.

The DMP ProX 300 (the highest model that uses SS 17-4 PH) parts exhibit an average roughness value of 6 µm, compared to the 14 µm average Ra value of the DMP ProX 100 parts. These estimates do not apply to all shapes and part faces produced by these machines, and it is due to this concern that AM manufacturers are interested in methods to improve the surface finish. The inherent difference between the two machines (research vs commercial) is the build capacity and laser power, where the ProX 300 is higher in both regards. Oftentimes, AM specialists will criticize a singular value of surface roughness due to the inconsistency along each surface of a printed part, yet datasheets for AM machines tend to provide a range of Ra standardized for the entire printed part. This study illustrates the differences in surface texture (top flat surface laser melting lines vs side wall layer lines) for the different part surfaces, including the impact of the surface print angle and the curvature. Therefore, the next stage of this research progressed to examine LP on non-flat surfaces to determine the impact the fixed laser would have on the surface profile for the 'walls' of the printed part.

The subsequent tests on a flat wall surface (square shape) straight edge part outline sought to determine the range of laser settings (*P*, *v* and *N*) that had a positive impact on the surface profile of the flat wall surface. These settings were pre-determined to have the biggest influence in previous studies for LP on the surface profile. The results revealed the change in *v* had the greatest response on the measured outputs (Ra, Rz and mechanical hardness). At 100mm/s *v* the walls of the printed parts deteriorated and exhibited a higher surface roughness. There were more partially fused powder particles on the surface, the surface appearing a darker shade compared to the other samples with test parameters including a higher *v*. It was determined, with confidence, that the higher *v* had the most positive impact on the printed part irrespective of the print angle. However, one criticism of this study would be the limited range of *P* used (*P* 60%, *P* 70%, *P* 80%), rather than a broader range (*P* 10%, *P* 50%, *P* 90%). A lower spectrum of power might have shown a more significant impact on the measured surface finish. Nevertheless, the reason was pursuing the experimental make-up with the 60 – 80% *P* was based on the results of the flat

surface LP study, and the purpose of the limited range was to compare the output with the results of the flat top surface experiments where the higher range of *P* had a better impact of the printed part. It is important to consider, that each AM machine manufactures parts with changing recommended settings, the laser settings are specifically calibrated. These different settings will surely impact the build characteristics, should the methodology for outlining the part's exterior profile be applied. Furthermore, there are many notable settings that can be varied to affect the built part, one of which is the layer thickness. Experimenting with the layer thickness setting of the build should result in an improved Ra with a less erratic surface profile.

There is research documenting the positive effect of a small layer thickness on the Ra of the finished part. For this case study, the default layer thickness (30 µm) for the DMP ProX100 was set by the manufacturer following rigorous testing to achieve the best part properties when built. It was not within the scope of this study to vary the layer thickness and assess the impact of it on the parts Ra, as preliminary work to study the impact of the variation on the part's mechanical strength, dimensional accuracy and perfect laser parameters would be required. It was the complexity of the process and time spent on the preliminary work vs the output related to improving the Ra which was considered too time-consuming compared to the experiments performed in this study. In reflection and retrospect, more efficient experimental set-ups including other printer parameters varied in parallel to the ones mentioned in this case study could be considered, that would equate to a slightly higher print time but deliver a more detailed report with consideration of these other variables (layer thickness, offsetting the laser outline, the laser jump speed, layer cooling time and more).

Summary of material characterization

The material used in this study is SS 17-4 PH, an austenitic stainless steel, with a relatively low cost, great ductility, high mechanical strength, and advantageous corrosion resistance. It is considered a high-quality material, used in the production of bio-medical devices, dental implants, aeronautical parts, food manufacturing plants and more. The high corrosion resistance makes the material an excellent choice in the fabrication of orthopedic implants both by AM and traditional manufacturing methods. However, the biggest drawback for SS, not unlike other metals, is the high surface roughness which requires post-processing to optimize the part's surface, whilst ensure the materials corrosion resistance is not compromised. The corrosion resistance of SS 17-4 PH is achieved through passivation, where the material is immersed in nitric/citric acid bath to remove the free iron particles (to prevent it oxidizing and rusting), whilst leaving the chromium (unaffected by the acid bath) to oxidize when exposed to air and form a protective layer around the exposed areas of the part. Passivation of SS is done following any post-processing method to ensure the protective chromium oxide layer is present to maintain its

“corrosion-resistance”. Manufacturing SS 17-4 PH using the DMP ProX 100 requires a nitrogen inerted chamber, to reduce the possibility of the oxygen within the chamber fusing with the powdered material as it is melted. While no machine has proven capability to inert a chamber completely free of oxygen, more advanced machines currently employed in industry have a much lower threshold of parts per million of oxygen. Secondly, some research suggests only a hydrogen inerted chamber provides a degree of corrosion resistance, whereas there is an inferior corrosion resistance caused by powder filed pores and voids [126]. Passivation can be used to ensure the corrosion-resistance of the AM SS 17-4 PH part, and as a supporting curiosity, included in this research, were observations of the chemical composition for the affected LP surface of the test specimens to study the exposure of iron on the surface.

Comparative measure of experimental output

Shortly after the commencement of this thesis work, Obeidi et al published an article to demonstrate LP with CO2 laser beam irradiation on SS 316L [127]. The author shares a common opinion with the basis of this research study and discusses the potential of LP to become an automated process that could be integrated within the AM machine and reduce the labor intensive and costly post-processing methods. Near the end of this research work, further articles were published, detailing work done to use LP, electropolishing and chemical solvents to improve the overall surface roughness of a metal AM part [76, 79, 80, 128]. The flexibility and high dimensional accuracy of the AM process is a huge benefit to the LP process, where complex geometric shapes unique to the AM process often requires a multitude of different subtractive processing strategies. Furthermore, various levels of processing are required for certain areas where the roughness varies.

Comparatively, techniques commonly used like abrasive-blasting and electropolishing are ineffective in certain cases due to the lack of dimensional accuracy. Whereas LP offers an ecologically friendly method to achieve an improved surface finish without compromising the dimensional accuracy. Tyagi et al [129] combined abrasive-blasting with electropolishing post-processing of a lattice SS structure, similarly, arguing that the inherent porosity and rough surface texture of AM SS parts is one of the biggest hurdles to overcome and assure fatigue strength. However, the preliminary results of the study demonstrated an increase in Ra possibly caused by the microcracks induced on the surface following the electropolishing process. Other studies also confirmed the deterioration of SS part surface when electropolishing was applied [70, 79, 129-131]. Other chemical bath methods have been more effective, where local temperature plasma-nitriding has been proven to reduce surface porosity and improve wear and corrosion resistance of a part.

LP within an AM machine offers a unique solution to selectively melt/sinter affected areas. The isotropic profile in SS AM parts creates visible peaks and valleys that influence the surface profile (especially the Rz parameter). Combining LP with a machine vision technique which identifies the peak areas and creating layer slices that target these peaks selectively could result in the best LP method where the softened molten steel is relocated into the valleys smoothening the surface in the process. However, with the LPBF process this could incur some limitations due to the powder surrounding the part. To summarize, this case study confirmed the ability of LP to improve Ra for SS 17-4 PH parts during the DMP ProX 100 manufacturing process. The study has revealed the potential for further research that will progress the work done here, to possibly realize a selective laser melting solution aimed at sections with a higher surface roughness. This could be accomplished with an integrated laser optics or detector system and feedback control. This approach was considered in case study 2, which is related to the digital layer capture and surface reconstruction.

CHAPTER 5

5 QUALITY MONITORING STRATEGIES USING NON-DESTRUCTIVE TESTING SYSTEMS

Non-destructive testing (NDT) techniques are established methods that focus on detect detection. Futuristic NDT technologies have narrowed to focus on methods used to assure accuracy and quality in automated processes. At its birth, NDT technologies were revolutionary in producing signals that imitated or correlated to defects within a part inspected by visual, electrical, acoustic, or thermal based methods. The rapid production of microelectronics has revolutionized the state of art for NDT technologies and the vast number of methods that can be used to detect defects is pertinent in many applications. The groundwork in creating a multitude of sensing apparatus has paved the way for researchers to focus on data manipulation by exploiting the raw data collected from these sensors in the form of pixel arrays, sound signals, electrical signals, and heat signatures.

The size of sensors, accuracy of lasers and material deposition strategies have surpassed the micrometer scale or smaller. Most importantly, this is all prevalent in AM technologies which exhibit micrometer accuracy for L-BPF parts. With micrometer accuracy required defects are created on the same scale or larger and the presence of the defect can impact the structural makeup off the AM part as it is manufactured layer-by-layer. Detecting porosity, cracks and other typical defects within an AM part is just as important as assuring dimensional accuracy where the part could be affected by other defects such as delamination and thermal stresses.

Understanding the depth of knowledge behind each type of NDT technology takes a considerable amount of time. In addition to that, manipulating existing sensors in a new application requires new raw data. This data needs to identify what a defect looks like in this application and more importantly note how does the size and type of artifact affect the desired part qualities whether it be through mechanical, electrical, thermal, or fluid dynamic analysis. The variety of research focus within this doctoral study for surface finish improvement and exploring a solution for defect detection, took a considerable amount of time. Optimizing the DMP ProX 100, trying to research 3 NDT techniques alongside developing a strategy to laser polish the outline of the printed, meant several techniques were explored but limited development time was available to provide an in-depth solution. However, exploring each of these solutions has revealed key information in moving the research for NDT past data acquisition and toward data processing with feedback.

The end goal for NDT research is to achieve a real-time detection system with feedback control. This chapter details the results for the NDT methods used to assess defects found in metal AM parts, dimensional accuracy of the print file and create a feedback strategy to remelt defective areas. The engineered mechatronic solutions presented in Chapter 3, were created to first acquire the digital images, then process the images using image objectification techniques, classifying defective areas by its pixel intensity. The techniques demonstrated in this doctoral study range in speciality including product development, design optimization, manufacturing, machine vision, and more. Where necessary the author has further explained relevant theory to demonstrate understanding and aid the readers interpretation of the results presented and decisions made toward the final solutions. In some cases, further reading material is referenced to provide a more in-depth explanation of certain theories and mechanisms developed by other researchers or commercially available systems.

5.1 PRACTICAL DEVELOPMENTS WITH NDT TESTING METHODS

5.1.1 DIGITAL AND THERMAL IN-SITU MONITORING SYSTEM

This case study began with the development of a digital layer-wise capture system that actuated under the laser scanning lens and print bed area to capture the layer profile after the melting stage of the direct-melting-printing process. Key considerations in developing this solution included:

- Reversable retro fitment of the monitoring system
- Remote access to control the system from an external computer
- A digital camera and thermal sensor
- Using stainless steel as the material to enclose the electronics, for any mounting brackets, and replacing the back plate of the printer.
- Supplying power to the electronics without compromising the anti-air leak sealed nature of the DMP machine
- Being aware of the powder spreader as it moves during print, the vacuum nozzle, and the heating element within the chamber, ensuring to keep parts from colliding or being heated by these two obstacles.

Taking into consideration these design specifications, the in-situ monitoring system was developed as shown in chapter 3. The author was responsible for the design and manufacturing of the entire system with some instruction and supervision from the university workshop assistants. The design of the monitoring system was done in Solidworks, using the sheet metal toolbox to work with flat sheets of metal and bend it into shape for encasing the components going

into the printer in SS. The enclosed SS design elements included the replicated ‘back plate’ of the DMP printer, the electronics box enclosure, mounting bracket to hold the linear actuator, end-effector cube on the actuator arm to hold the digital camera and thermal camera mounts, and the bracket for the camera mounts (Appendix A). The manufacturing components within the chamber of the DMP, where the metal powder, build station and powder recycling canisters are placed, is almost entirely constructed out of SS. The exceptions include the two light bulbs covers placed on either side of the chamber at the top and the crimped coversheet which is exposed under the ‘back plate’ of the printer that moves with the powder spreader.

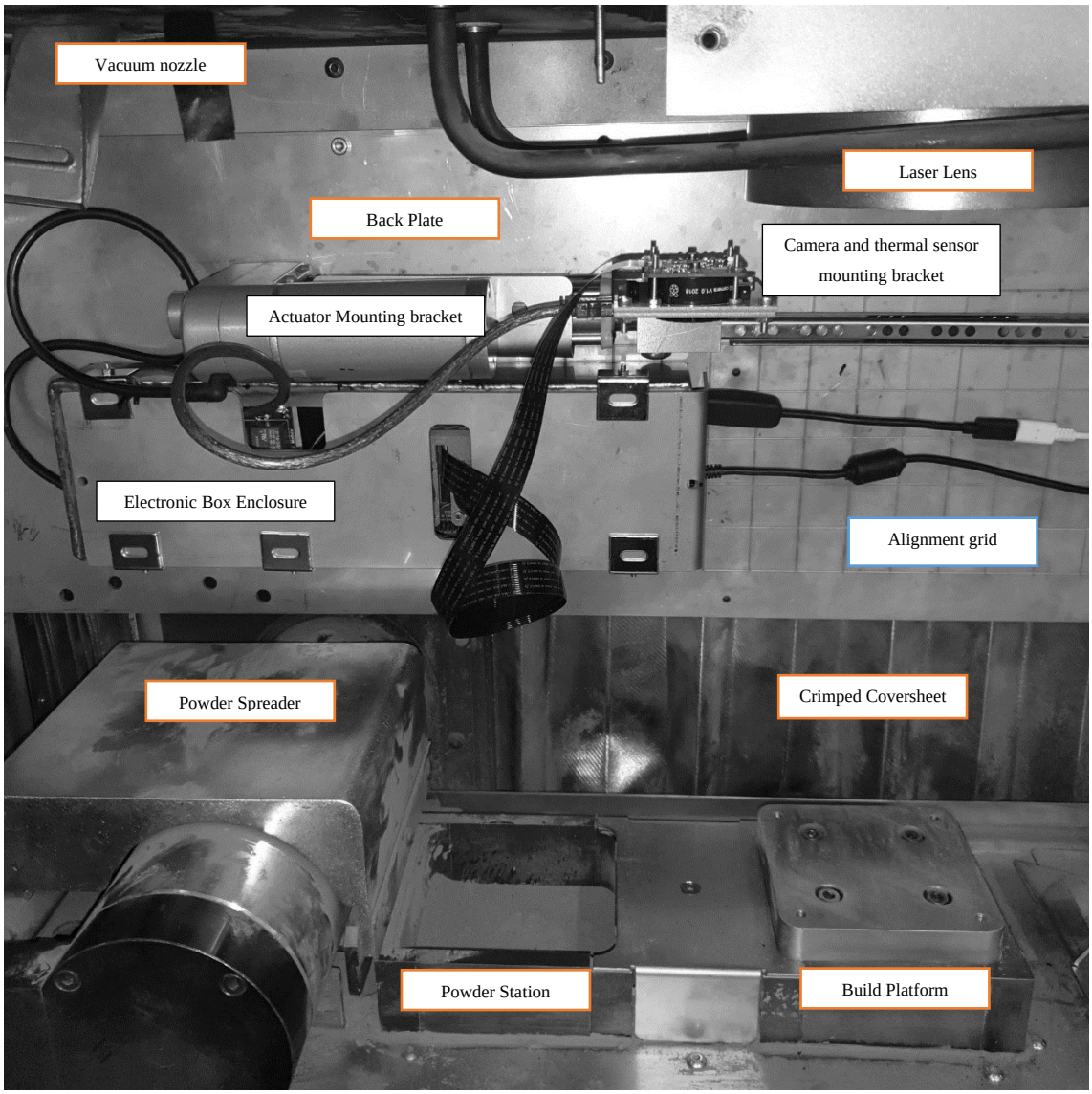

Figure 5-1 Final manufactured in-line monitoring system installed inside the DMP ProX 100 chamber

All these parts are as labelled inFigure 5-1, the orange outlined boxes are labels for existing parts within the machine, the black outline boxes are labels for parts added as part of the digital and thermal monitoring system. The purpose of using SS and covering the electronics in it, is to reduce contamination to the recycled SS 17-4 PH powder. The only exposed non-SS elements in the monitoring system were the camera, lens, thermal sensor, and electronics wiring cables (power and camera data cables).

The movement of nitrogen gas coming into the printing chamber, the suction of air out of the chamber (into the air filtration system attached to the printer), and airflow created by the movement of the powder spreader, all cause particles of SS powder to fly within the chamber. Considering this and the exposure hole in the electronics box (where the camera and thermal sensor cables connect through to the Raspberry Pi inside), it had to be wide enough to allow easy movement of the cables as the actuator moves in and out. Knowing the holes expose the electronics to the flying powder within the chamber, fans were installed with a dual purpose. Firstly, to blow air away from the holes and secondly to take any heat out of the electronics box to ensure the electronic hardware within did not overheat.

The design was made with robust engineering considerations to ensure limited maintenance was required. It is a time-consuming process to open the printing chamber and re-inert it for every print. The only instances for opening the printer, in relation to the installed monitoring system, was to perform the checkboard calibration and remove the camera and thermal sensor for developing the coded application to control the system. For the checkboard calibration, a 100mm x 100mm cut out of a black and white checkerboard (10x10mm squares) was taped to the build plate (Figure 3-28). Then the printer calibration process was performed to level the build plate at the first sintering position. This position is consistent for the entire print, where the top layer sinters in the same position as the build plate moves down. This was advantageous for focusing the camera lens, knowing the depth of detection would not change. The SS mount holding the camera and thermal sensor was attached to the end of the actuator with a custom-made cube, and the mount was held in place by 4 screws at the top of the cube. It was a straight-forward process to remove and replace the mount within the printer.

Several iterations were made of various parts to ensure accurate alignment of the cameras to move out of the laser range and move in over the center of the build platform. The manufacturing methods involved to produce the components included waterjet cutting the flat SS metal sheets, folding the metal into shape with a bending machine (and sometime vice), welding some of the flat metal pieces together, drilling custom holes not included in the back plate design file sent to the waterjet, and using hand tools to attach the components with nuts, bolts, and washers. The original screws (~12 of them), that hold the original machine back plate, were used to mount in

the replicated plate created for the system. Creating this mounting system was an excellent learning process and application of engineering design and manufacturing skills. Some iterations to reproduce defective parts, was due to poor tolerance considerations, as the author had never worked with bending sheet metal prior to this application. The 'alignment grid' labelled in Figure 5-1 (blue box outline), was etched onto the backplate when it was waterjet cut. The center of the build plate aligned with one of the lines etched onto the plate, which was used to align and tighten the camera mount cube in place to the runner guiding the movement of the cube.

The electronics within the SS electronics box are as described in Chapter 3; the Raspberry Pi 4B+, the relays and custom PCB. An ABS plastic case was FDM printed to encase the Raspberry Pi 4B+ and a layer of MDF was placed as insulation between the electronic components and the SS enclosure. The linear actuator and halogen lamp added to the system were controlled by individual relays. When considering the method to operate the electronics the following considerations were noted:

- Turning the actuator on and off.
- Turning the halogen lamp on and off
- Controls to capture images from the Raspberry Pi digital camera with image pre-processing options.
- Controls to capture video for the FLIR Lepton thermal sensor
- Saving the images for each layer and seeing the digital and thermal sensor feeds in a livestream.

The programming development to achieve these steps and make them work together for efficient control of the monitoring system took some time to achieve. A user interface was required and developed as shown in Figure 3-27, chapter 3. This was the first time the author had worked a Raspberry Pi development environment and thermal sensor. The immense amount of online support material for the Raspberry Pi board, GUI development, digital camera development with Raspberry Pi and the FLIR Lepton Purethermal breakout board, aided the process to achieve the desired solution. The programming was performed on the Raspberry Pi 4B+ using Team Viewer and VNC viewer (depending on the internet connection).

TeamViewer is a popular remote-desktop management tool that is free for personal use. It was used to connect and work on the coding development outside of the university building. The connection was slower than VNC viewer, but selecting the speed focused performance option, helped a bit. VNC Viewer only worked while both devices were connected to the same network. The Raspberry Pi would not remotely connect to a double stage internet verification process typically used by university Wi-Fi connections (requires username and password) and a research Wi-Fi modem had to be used instead. The best connection method would be to run an

HDMI cable from the Raspberry Pi 4B+ out to a monitor outside the system, with a wireless keyboard and mouse. Initially, it was thought that the system would be powered using a battery cell rather than running mains power into the printer. However, the solution was bulky and proved tedious. By the time it was decided that the cables were going to run out of the air pipe and be sealed, the rest of the components had been positioned to minimize the space required for the electronics box. That is, there was no room for the HDMI cable to fit into the HDMI port on the Raspberry Pi. This is something that could be improved in the next design upgrade for the monitoring system.

The final GUIs for the digital camera capture, the thermal video capture and post-processing script to individual frames from the thermal video was design using the QT GUI development software. The PyQT5 package enabled easy cross-platform programming to define the functions for each GUI widget (push buttons, images, text lines etc…). Once the layout for the widgets was determined, the QT development file was saved as a UIC file type, then imported into the Python programming environment for development. Three separate GUI platforms were created, because a solution was not found in the time allocated for the development, to run the two camera streams (digital and thermal) scripts together and to accelerate opening and closing both platforms over the Wi-Fi streams. The programming scripts for each GUI can be found in Appendix C. The controls for the linear actuator and halogen lamp were built into the Digital capture GUI and the thermal camera to control the system from either capture environment.

The layer-wise capture process is as detailed below, using the system described above, starting at the first layer:

1) Wait till the laser melts the first part scanning pattern and has turned off.
2) Open the digital camera GUI.
3) Click the ‘Actuate out’ push button to move the sensors over the build plate
4) Click ‘Start camera feed’ to display the live feed into the image widget box.
5) Click the ‘Turn on Halogen lamp’ push button to illuminate the build plate with the halogen lamp.
6) Adjust the camera settings on the left panel of the GUI, then select the file save path and navigate to the folder you wish to save the images.
7) In the text line, label the file
8) Then either click the ‘Image Capture’ button for a still JPEG image, or ‘Start recording’ to record a video and ‘Stop recording’ to finish the video and save the tiff file to the chosen file directory.

9) The quit the digital camera GUI and open the thermal sensor GUI, to record a video of the part's thermal gradient over time. Follows much the same process as the digital camera GUI.
10) Finally, in the thermal camera GUI, click 'Actuate In' to move the camera out of the laser range and begin the next printer

After some confusion in remembering the purpose of the 'actuate in' and 'actuate out' button labels, they were changed to read as, 'move camera away out of laser range' and 'move camera over build plate'. Future work for the user interface could see the implementation of the part sizing, defect sizing, and laser scanning file creation done in real-time. Furthermore, eliminate or speed up the manual actuation process to reduce the image acquisition time (unfeasible for 100 layers, which takes around 3 hours to manufacture without the added NDT process).

After the images were captured for each layer, the development environment moved from the Raspberry Pi 4B+ to a personal laptop (specifications as described in Chapter 3). The results for the image processing methods described in Chapter 3 for the digital images are presented further on.

5.2 SOFTWARE DEVELOPMENT FOR NDT STRATEGIES

This section details the results with discussion for the image processing techniques, feature detection, sizing and 2D to 3D layer modelling results achieved within this doctoral study. The layout of results correlates to the methodology as described in Chapter 3: Case Study 2 Methodology. The results first detail the output from the developmental code written to size the part within the 2D image capture of each layer, crop out the part and then process the image to reveal possible defects. The accompanying discussion reviews the capability of the part-and-defect sizing method to work with other shapes and more complex contours typically seen in AM parts. The second result section focuses on the 2D to 3D extrusion method applied, and displays the progress made in applying the extrusion using bitmap tracing and extrusion of the scalable vector graphic to create an STL file. The chapter ends with an overview of the NDT quality assurance methodologies that were investigated within this thesis, in comparison to research done in parallel to this doctoral study period by other AM researchers and commercial entities.

5.2.1 DETECTION OF PARTS AND DEFECT WITH METRIC SIZING

The image acquisition process used to capture every layer in the test specimen specified in chapter 3 involved a stationary camera mounted to a linear actuator that moved into place over

the build plate iteratively stopping in the same position. Every layer of the part was captured with the same lens focus. The images were all captured as a 1980 x 1080 image array size by the Raspberry Pi 12.3 megapixels high resolution camera. Notably, the maximum image size can be set to 4056 x 3040 pixels (5K), with a minimum pixel size of 1.55µm x 1.55µm (~6 MB JPEG file size). The layers were captured with the entire build plate in focus, to investigate if one camera is enough to detect multiple parts on the build plate and if micrometer defects were still visible and detectable. Chapter 3 describes the acquisition of a single test specimen printed, but another print was captured with multiple test specimens (Figure 5-2) manufactured with parts placed randomly on the build plate. By comparison, other image acquisition methods focus on a portion of the build plate and use an array of imaging sensors (digital, thermal, electron beam, radiography etc.) with the images stitched together. The 100 mm x 100 mm build space is a relatively small area to capture compared to AM machine with print beds ranging above the millimeter scale into the meter size metric. With the image size identical for every capture, and a reference image with the exact part size, a well-known pixel measuring method (ImageJ with the line measurement) was used to mathematically convert the image feature size from pixels to mm.

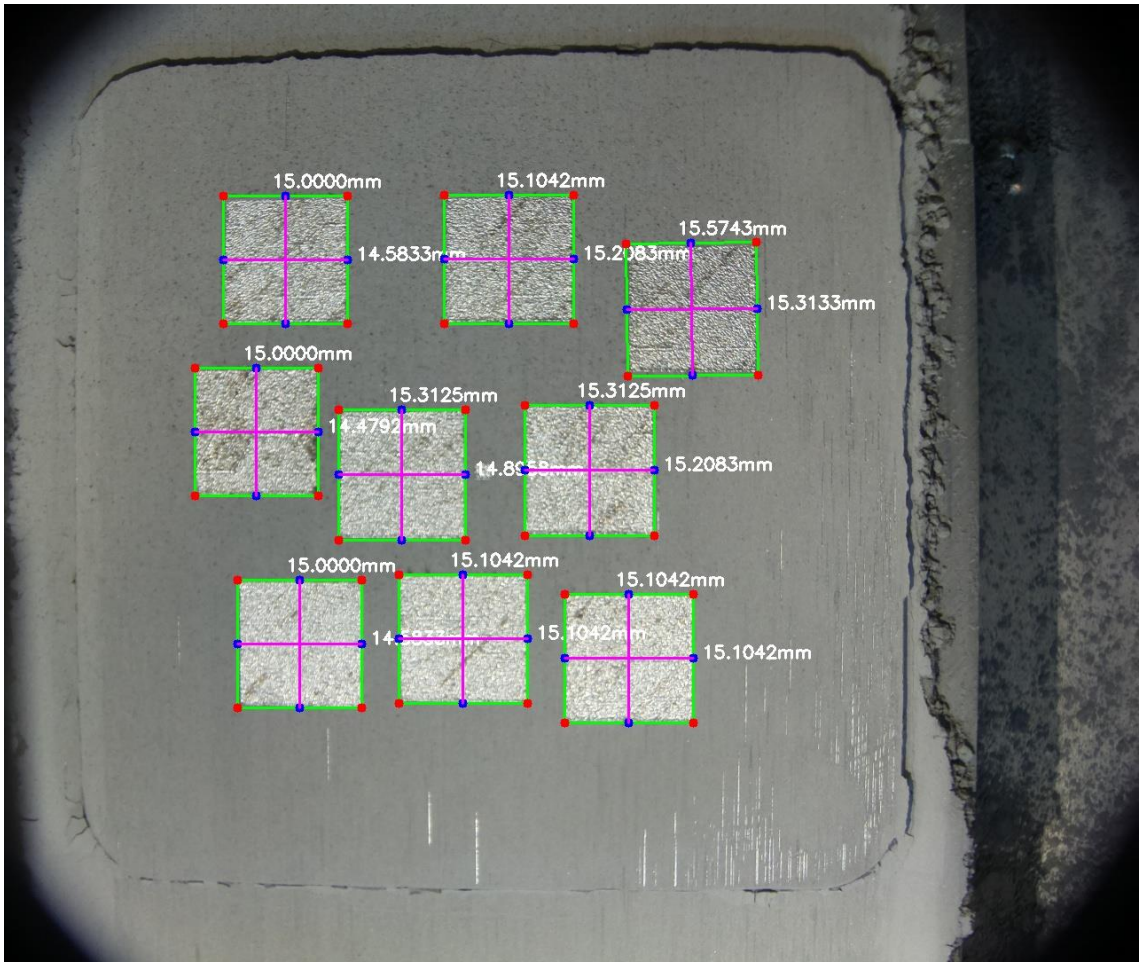

Figure 5-2: Part sizing algorithm applied to a print with nine 15mm x 15mm squares

Figure 5-2 illustrates the contours detected in the same 2D layer image, but to filter out other edges detected by the Canny detector (lower threshold set to 50 and max to 100), the following conditions were written into the coding algorithm.

```
for c in cnts:
	# if the contour is not sufficiently large or too big, ignore it
	if cv2.contourArea(c) < 3000:
		continue
	if cv2.contourArea(c) > 25000:
			continue
```

Following the detection of the part size (code available in Appendix C), each part contour is cropped along the draw on contour lines. The cropped images highlight instances in which the edge detection algorithm included 'false' edges due to partially fused powder around the part. Therefore, the height and width of the part is not always accurate to the true boundary of the part. The only shape tested by this process was the square test specimen, however this method is still viable for circular and more complex geometry shapes. Drawing the box around the contours detected presents the user with a simple bounding box defined by its max height and width. The code below specifies the parameters used in the **findContours** function. The RETR_EXTERNAL parameter returns only the outer most contours of an image after sorting the contours and their relationship to each other in a nested array. The CHAIN_APPROX_SIMPLE parameter works to organize and compact the horizontal, vertical, and diagonal segments of the contours found return the end points. If relevant contours in a complex geometrical shape are not found, then CHAIN_APPROX_NONE can be used to returns all detected contours.

```
cnts = cv2.findContours(edged.copy(), cv2.RETR_EXTERNAL,
			cv2.CHAIN_APPROX_SIMPLE)
```

To assess each part individually, the cropped images are processed so that the image greyscale values are inverted (black-to-white, white-to-black), to now detect defects in each individual part. The synthesized defects that were cut out of the original test specimen to imitate a flaw (unsintered area), were detected by the darker hue of the unsintered powder. It is interesting to observe that the 'burnt' areas where the laser power might have been too strong, also presents as a darker hue than the correctly sintered areas. This method is useful in many applications; inspection to assure file security, inspection to detect sizable flaws, creating a laser scanning file based on including areas of the cropped image based on a set pixel intensity and more. These are notably the biggest issues highlighted in NDT literature reviews investigating the state of art for NDT. Continued improvement and development of this method could see this solution integrated into the GUIs used to capture the image. Real-time processing of the images with a report created to point out defective layers for the end-user could prove useful as a quality assurance strategy. With contour predictors and conditioning the method could be automated to disregard any 'good' layers but save the 'bad' ones for inspection or inspect them and report on key flaws identified.

The synthesized defects ranged from 100µm to 500µm (0.1mm to 0.5mm), which represent the largest flaws typically detected within the part. The aim of the defect detection process was to determine if these typical flaws could be identified and measured in the same process as the method described above. While detecting the part within the original image required only adjustment to the Canny detector parameters and contour sizing, the defect sizing method needed adjustment to other parameters. This included varying the dilation kernel and iteration to overlap more of the detected edges. Adjusting the canny detector threshold and dilation parameters, resulted with the 0.2mm to 0.5mm defects being detected and sized correctly, but while the 0.1mm defect would be visible in the edge detection image, the contour detection and sizing would be wrong. The contour would include other pixel intensities detected in the grey value threshold region and set the contour corners around the topmost and bottom most edged of the detected pixel. The similarity in colour between the SS unsintered powder and the SS melted region makes it difficult for digital distinguishment between the small pixel intensity differences. Some researchers believe one solution to solve this issue could be the use of an added pigment to the powder, which would evaporate when the laser melts the part. This is unnecessary, as using a thermal sensor provides that high contrast. The captured thermal images using the rainbow temperature gradient, exemplified this contrast but due to the quality of the images in re-sizing them it is recommended a camera with a bigger pixel map be used.

5.2.2 2D TO 3D LAYER EXTRUSION

This research study surrounds quality strategies for surface finish improvement. Inter-layer defects affect the overall surface roughness of the exterior walls of the printed part. Case Study 1 tested polishing the outer wall of the printed part and the outline definition is a feature built into the manufacturing software. Remelting the entire layer of printed part could possibly negatively impact areas that are perfectly melted.

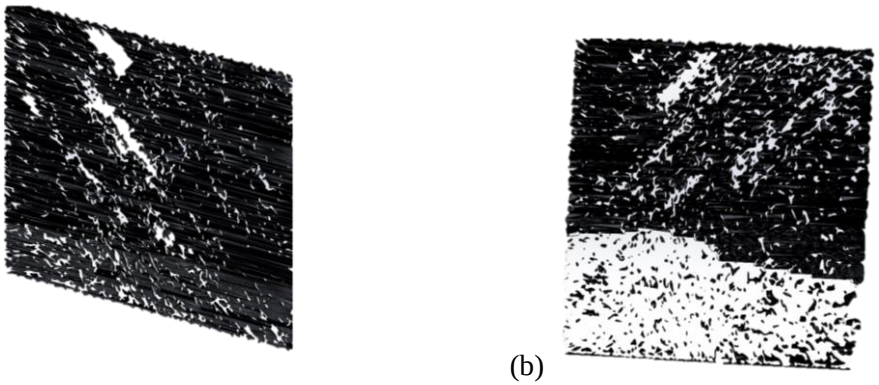

(a) (b)

Figure 5-3 (a) Correct extrusion of bitmap contour profile of the part (b) Missing bitmap contour profile, inverted bottom part when imported into Blender

Therefore, the application tied to surface finish improvement and feedback control using NDT technologies, was to selectively melt imperfect regions detected by the in-situ monitoring system. It was known that the DMP manufacturing software requires an STL file input, combined with the layer slicing thickness applied for each layer laser scanning pattern. Problem-solving a solution leading to achieving a STL file required taking the 2D image from the image acquisition software, detecting the defective areas as described above and creating a 2D contour profile by tracing around the bunch of pixels part of the defect. As the methodology in Chapter 3 describes the contour profile was achieved by using a bitmap trace, followed by saving the profile as a scalable vector graphic. This vector graphic was imported into Blender in which the profile was extruded. Most of the layers imported with no issues (Figure 5-3 (a)), but in some layers had portions of the image where the trace bitmap inversed the contour fill (Figure 5-3 (b)). It was later discovered this issue can be rectified by using the stroke to part tool in Inkscape where the contour trace was performed.

The images were separated by its pixel intensities, the black pixels define the area contour to trace around and will be extruded when the part is placed in Blender. The first extrusion files were made by setting the defective areas to black and creating (30μm) STL layers for the print file to feed back into the DMP manufacturing software. Following a manual application method, the operator must import the defective layer STL file, slice it and transfer the file to the printer. Prints can be interrupted, and a new print file introduced mid-print. Unfortunely, a study could not be performed to test this process during the doctoral study but is suggested as further work.

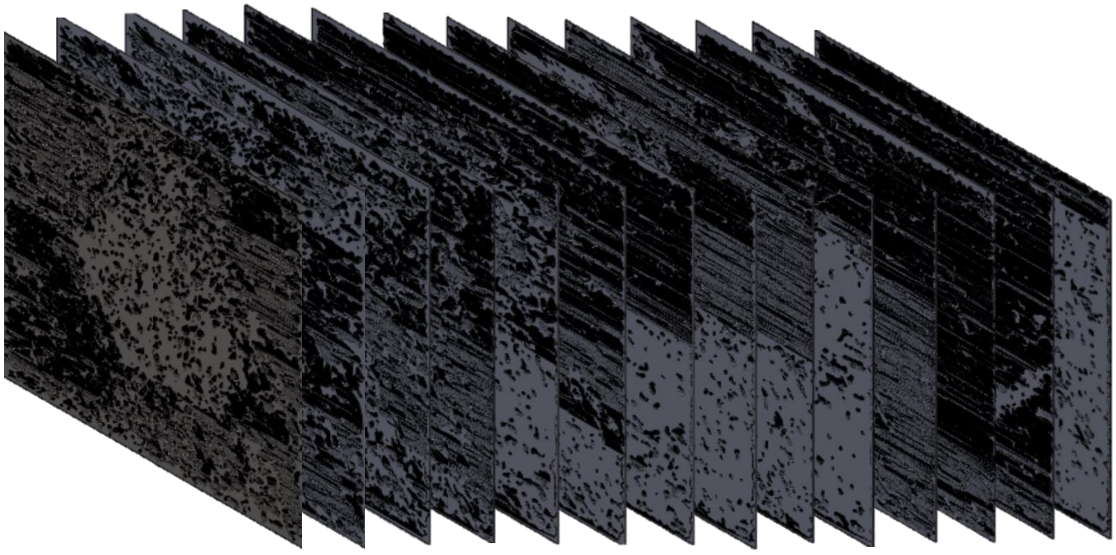

Figure 5-4 Extruded layers with the brighter pixel intensities visible on top

The second application and aim of creating the 3D extrusion of the layers was to digitally reconstruct the printed part and run FEA analysis on the part. In this case, the brighter (whiter) intensity pixels in the greyscale were set to black and the darker pixel intensities to white. The layer was extruded 10 µm and added to a 20 µm extruded square in Solidworks (Figure 5-4) to make up the total layer height. Without, a depth detection method applied to detect the peak and valley depth, an assumption was made to set the highest points to 10 µm. Having a 3D model meant an FEA analysis could be performed. Confirming the possibility of creating an analysis output for the study, the next stage is to capture standardized fatigue test specimen and compare the simulated analysis to a traditional fatigue and fracture test.

5.2.3 LAYER SURFACE PROFILE MAPPING

The 2D to 3D extrusion method describes using the grayscale pixel intensity of the captured image to distinguish between the peaks and valleys. To illustrate the variation in pixel intensity, a MATLAB script (included in chapter 3) was written and examples for a few layers are displayed in Figure 5-5. This provides the range of grayscale pixels (0 to 255) for each image and helps with thresholding the image. Studying the graphs, it is clear there is little variation in between the smallest gray value and the highest (~150 to 220).

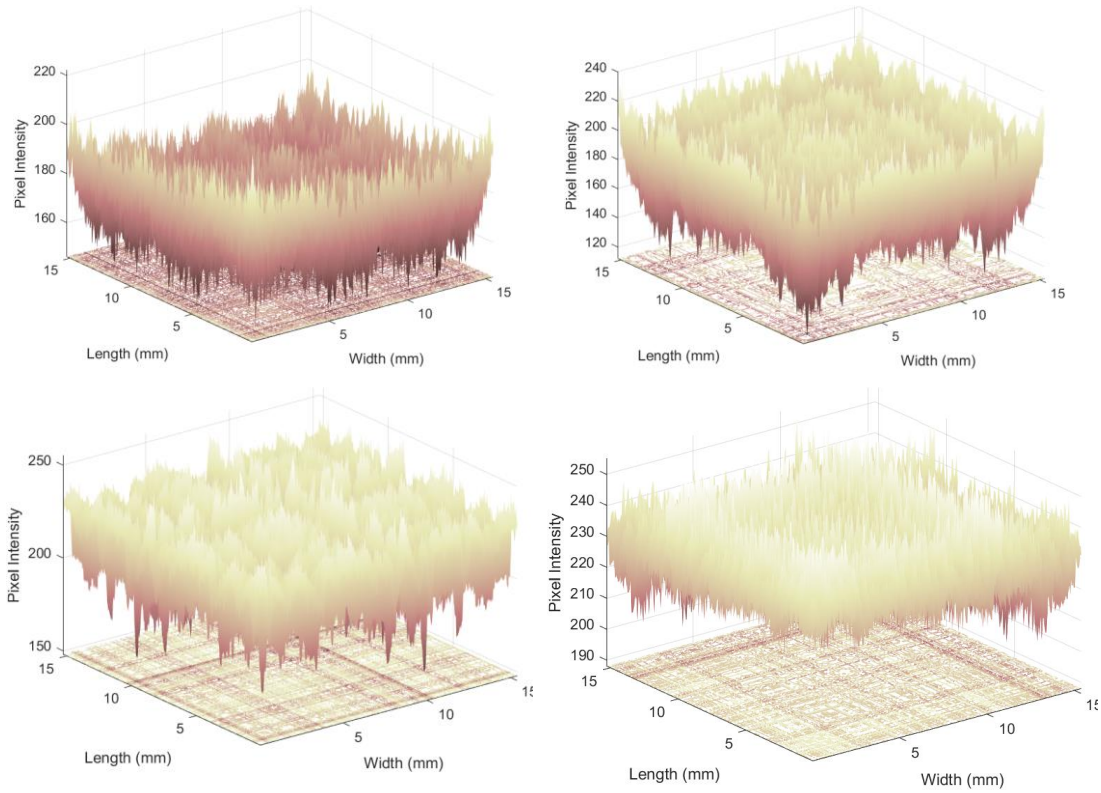

Figure 5-5 MATLAB Surface plots (with contour mapping) for 4 different layers captured in this case study

5.3 NDT CALIBRATION AID FOR DMP PROX 100

Printer calibration is an important maintenance process for every AM machine. With L-PBF printers the main calibration adjustment provided by the user is the optimal laser defocus. Laser defocus refers to the height in mm (increments of ± 1 mm) the build plate is moved from the origin to achieve the best laser focus and powder splatter (as the laser hits the powder). The process to run the laser defocus calibration is detailed in Chapter 3. Usually, the AM machine operator will watch the laser melting stage to see which parts have the higher powder splatter (good) and which have next to none (bad). The in-situ digital monitoring system also provides a great method to detect which defocus is too intense and burning the metal powder.

Figure 5-6 provides an example of the first calibration layer captured by the in-situ monitoring system. The red bounding boxes indicate parts that in which the laser focus caused the powder to burn and had no powder splatter. Based on this information, the calibration settings for the parts in the red boxes are removed from the rest of the print. The yellow boxes indicate calibration settings with some burning to keep an eye on and remove further on if the burning persists. Aside from the other applications mentioned in this study, calibration is an essential process for every AM machine. Instead of continuing to perform the calibration through the method just described, using the monitoring system, real-time assessment of the best laser defocus could be done. The laser defocus can influence the final part quality if different areas are deformed due to burning. Checking the layers in real-time to see if the current laser defocus is burning the part or creating a significant number of partially-fused-powder areas, is a useful strategy. The burning could indicate the laser lens has not been cleaned properly, or an unevenness in the build plate surface.

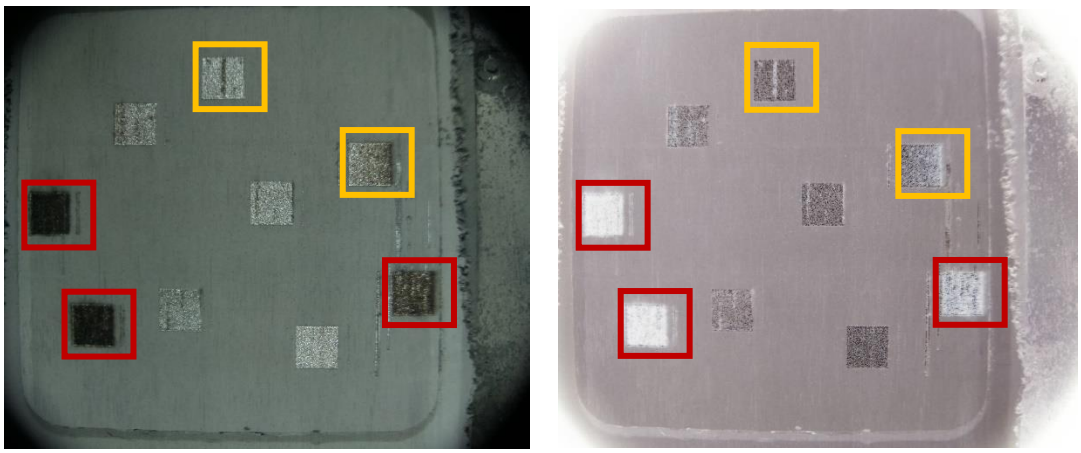

Figure 5-6 Capture of the calibration print layers

5.4 ALTERNATIVE NDT METHODS

Aside from the digital in-situ monitoring system case study 2 focuses on, there were other NDT technologies explored but due to time constraints were not viable to further pursue in this research period. These NDT techniques are Laser Scanning, Acoustic Resonance and Acoustic Imaging. In the initial stages of this study, E8 subsize tensile specimens were printed in the DMP Pro X 100 printer. Unfortunely, at this stage the printer had been moved from its calibrated position and this caused issues with the printing process resulting in failed builds. These failed specimens are seen in (Figure 2-9). Once removed from the build plate (with a hammer and chisel, not the horizontal bandsaw which was part of the part removal research to optimize the post-processing for the DMP ProX 100 prints), the parts were deformed and bent out of shape. These presented as the first defective specimens studied using Laser Scanning and Acoustic Resonance testing.

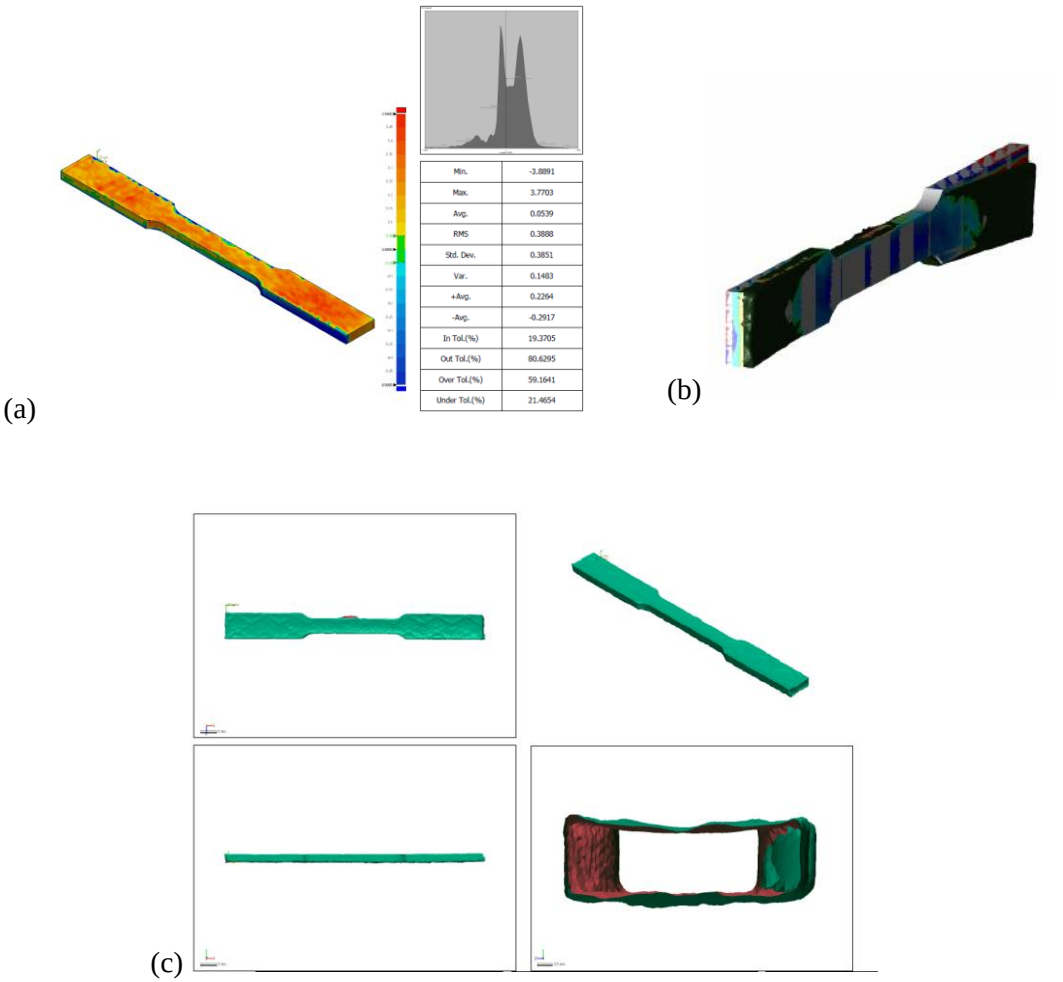

Figure 5-7 (a) Stress distribution on CAD model of E8 subsize Tensile testing specimen (b) displacement of laser scanned printed sample with respect to the original CAD specimen (c) Surface mapping with laser scanner to demonstrate surface texture

Laser Scanning

A Laser Scanner is an advanced 3D model reconstruction tool, that collects detailed point clouds, which is processed in a point cloud software to create digital 3D models. Popularly, laser scanners are used in large scale scanning applications where the scanning accuracy used to be in the millimetre accuracy range. But the rapid development of laser scanning methods using laser beams, advanced sensors, Global Positioning Systems (GPS), Inertial Measurement Units (IMU), receiver electronics, and photodetectors, has reached micrometre scanning capability. With this development manufacturers are expanding the application of laser scanners to include surface profile of parts to measure and model the surface texture and read the overall roughness measurements. To succinctly summarize the methodology for laser scanning, the system uses a 'time of flight' measurement system, by sending out multiple light waves that reflect of the part surface into the detector on the scanner. The sensor then calculates the distance to the reflection of the beam (part surface) by measuring the time taken to send and receive the reflected signal. It is a quick (seconds) method, with a huge amount of data stored in each measurement.

Early in this research study, when exploring NDT techniques and methods to measure the surface profile of a part, laser scanning was considered. 3D systems offered to scan some defect parts while they were in position of a Kreon laser scanner. Figure 5-7 illustrates the scans taken by the scanner to replicate the deformation and rough surface indentation profile caused by the failed print and bad part removal technique. This illustration demonstrated that laser scanning was indeed a viable NDT technique to remodel a 3D printed part and performed simulated analysis on the part. But quality inspectors in the AM space want to inspect microdefects with each printed part. One strategy to consider, is in-situ laser scanning of every 2D layer, to map the surface profile, which will provide more accurate contours than the method employed in this study.

Acoustic Resonance and Acoustic Imaging

There was a brief exploration of acoustic-based NDT techniques, performed in parallel to the digital and thermal monitoring system development. As chapter 2 highlights, limited research has been done to this space and there exists a possibility to develop a novel contraption and quality strategy. Initial discussion with between the author and the supervisory panel, focused on exploring acoustic ultrasound and acoustic resonance. The first strategy was to put a microphone into the printer and record the various acoustic signals (sounds made by the inertion gas coming into the chamber, roller spreading powder and the laser as it melted the stainless-steel powder), then isolate and filter out these sounds to focus the sensitivity of the sound of the building stage (to possibly detect signals indicating thermal stresses forming, or cracking occurring). As the methodology for this solution was being developed and parts obtained for the experimental set-up, a doctoral thesis and conference publications were made public to detailing

the same methodology in a LPBF system. The study concluded the complexity of distinguishing between the overlapping signals and the difficultly to listen for crack initiation without having a reference signal to compare the study too. This reference signal is the key piece of data required to pursue acoustic signal processing. As such other researchers also attempted to record the acoustic emission of an AM part undergoing a 3-point bend test, to capture the crack initiation leading to part failure. They hoped this would provide a starting basis for acoustic signal processing.

The second in-situ acoustic solution was an ultrasound technique (using a high frequency (MHz) transducer), with a concept developed to replace the DMP ProX 100 build station jig to which the build plate attaches to. In doing so, this creates a cavity for a flat disc transducer to fit into surrounded by an ultrasonic gel couplant. This method was discarded, based on its potential to disrupt the levelness of the build plate.

The third solution was an ultrasound-based method, which could scan and possibly display defects. An ultrasound research group with opensource material posted on Git, described a low-cost development board designed to use a common transducer thickness gauge, combined with the board signal processing and amplification, controlled by a microcontroller (Arduino), and display the image on an LCD device. Their application was for a portable human ultrasound scanner. The first stages of this solution investigated the capability the thickness gauge to determine if the gauge could pick up defects in a part considering the powder was still compacted inside it. Put simply, the thickness gauge works by emitting a 5 MHz frequency down the transmitter end of the transducer and reads the reflected signal from the receiver half. The gauge was successful in detecting large defects (1mm +) but not microdefects. This method showed a lot of promise and with further research into the speed of sound within the melted part, vs the speed of sound through the compacted powder in the defects, this could prove an effective NDT technique for defect detection and mapping. If this were the sole focus of the research study, or more time was available, this research could have produced useful data.

5.5 DISCUSSION

This research began with a focus to investigate the capability of NDT methods to replace traditional destructive testing (TDT). Material wastage and the inconsistency in the processes surrounding AM technologies (feedstock, machines components, printed part properties) was deemed problematic and TDT methods too expensive and unreliable to assure quality in every manufactured 'batch' of an AM process. A huge focus on developing NDT quality strategies stemmed from a need to assure the integrity of load bearing components commonly used in high-end product industries. As such, several successful AM machine manufacturers began exploring NDT quality strategies and developing in-situ monitoring sensors built into processing line. These companies include TWI, Zeiss, Renishaw, EOS, 3D Systems and other leading AM machine manufacturers.

Most of these companies are focused on in-situ real time monitoring of AM parts using optics and thermal sensors. To date, EOS and Renishaw were noted for working on separate in-situ monitoring systems, EOSTATE for EOS and InfiAM Spectral for Renishaw. These in-situ monitoring systems work similarly to the solution presented within this thesis work. The software package alone was deemed "too expensive" by several smaller AM manufacturers and criticized for its ability to work solely on their own machines alone [31]. More importantly, both systems were collecting sizeable data, but struggling with the metallurgical interpretation. This year (2021) EOS and Zeiss (metallurgy analysis company) announced a joint research venture [132] to create a new on-line monitoring system that helps EOS technicians to characterize the data from the EOSTATE system digitally. As this research study highlights, understanding the metallurgy characteristics of the printed part is important to defining critical or failure initiating defects.

Renishaw has also announced they are expanding their software to work with Verisurf (CAD [133], Model-Based Inspection and Measurement software developers amongst other things). Companies have realized what this doctoral thesis highlights as the potential method for characterizing defects in AM parts. That is, to find a method of compatibility between existing monitoring techniques and existing CAD simulation analysis software. It is important to focus on a single NDT research tool and collect data for different machines the tool is suitable for. That is, providing researchers with base data to progress machine development, material standards, part printing accuracy and more.

Computed tomography (CT) was noted as the prevalent technology in defect detection due to its easy adaptation to assessing AM parts. AM specialists and manufacturers who believe in the necessity of NDT technologies, began to explore alternative imaging methods, to CT, to model

and size the defects within the part. One notable method is digital radiography, a faster in-line approach that captures a 2-dimensional rendering of the density and material thickness for predetermined regions of interest. For example, TWI additive manufacturing is one company focused on this line of research, and are also investigating optical, ultrasound and laser ultrasound techniques too. The NDT imaging solution described in this research lacks depth analysis which is essential in determining the placement of defects in the Z-axis to map an accurate representation of the part. When the system was being designed, the FLIR thermal sensor was integrated with the aim to provide the depth analysis, but without proper calibration and strong enough excitation on the surface this method failed, aside from viewing the part surface thermal data. The future work section that follows describes further development of the in-situ system to properly integrate a depth sensing thermal solution.

Micrometer defects in L-PBF parts

Before the NDT experimental work stated in Case Study 2 was done, a study was performed to assess the impact of micro defects on the mechanical characteristics of the DMP parts. In collaboration with an undergraduate student, completing their final year individual research study, a Taguchi designed study was done to add synthetic micrometer sized defects ASTM E8 subsize tensile dog bones. During this period of experimentation, the DMP ProX 100 was used to manufacture the dog bones (30 prints with 3 dog bones per print). The defects ranged in size from 100 µm to 500 µm, and were placed in varying X, Y and Z positions along the neck of the dog bone. The tensile results from the study revealed no significant impact of the tensile strength of the part compared the machine data sheet average tensile strength using SS 17-4PH. However, examining the break revealed the breakage following necking occurred through the defect position. In some cases, the separation initiated at the micrometer void, and in others the crack travelled toward the void (Figure 5-8).

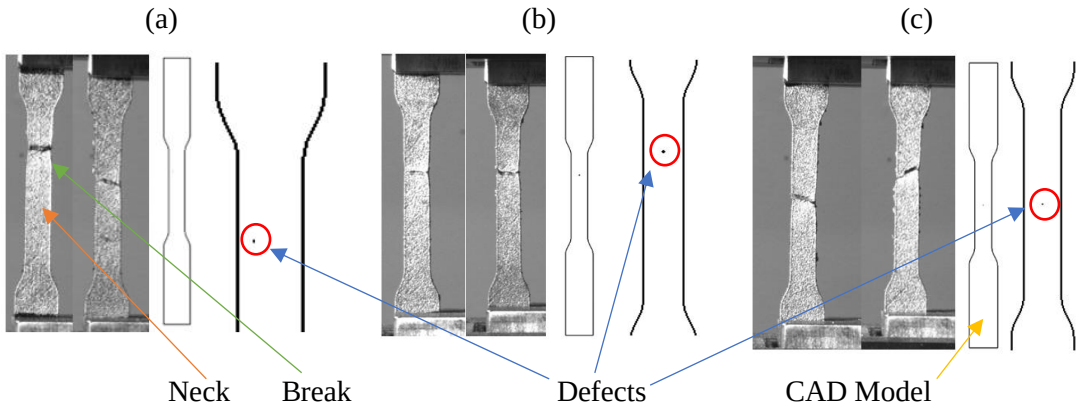

Figure 5-8 Each example consists of 2 photos of tensile failure, the CAD model of the tensile sample and the placement of the void in the sample (a) Left tensile specimen shows breaking along the placed void and the right shows breaking veering toward the placed void. (b) both specimens cracked along the void. (c) the cracks occurred through the void but at different angles

Microdefects do not really affect the tensile strength of an AM part but would highly impact the part fatigue failure when loaded. A study was not performed to print and test fatigue failure through standardized fatigue cyclic testing. There have been other works confirming the impact of microdefects on the fatigue failure of AM parts [87]. The impact of microdefects is what prompted the exploration of NDT techniques, and creating a database linking defect size, placement and failure impact in a part could provide NDT researchers with a basis for characterizing the defects detected.

Low-Cost analysis for the In-situ Monitoring system

The monitoring system was designed to be within a 'reasonable' budget for other researchers to replicate in a similar fashion for other AM machines. The total cost of the electronic hardware used in the monitoring system is detailed in Table 5-1.

Table 5-1 Cost analysis of hardware used in In-situ monitoring system

Component	Model	Quantity	Price per item
Digital Camera	Raspberry Pi Hi Res Camera	1	$80.27
Camera Lens	Raspberry Pi 16mm 10MP Telephoto lens with a C or CS-mount	1	$82.14
Thermal sensor	FLIR Radiometric Lepton 2.5	1	$379.91
	Pure Thermal 2 breakout board	1	$203.30
Linear Actuator	Linear Actuator 100mm Stroke 12V 20mm/s with a 60kg LFHB	1	$135.00
Microcontroller	Raspberry Pi 4B+ with 4GB RAM and in-built WIFI	1	$86.06
Relay	Relay Module 2 Channel Isolated 3.3V or 5V input	2	$4.95
Halogen Lamps	OSRAM Halogen Lamp	5	$~3.28 to $19.72
		TOTAL	**$ 1,018.43**

The cost analysis in Table 5-1 excludes the cost of the SS 17-4PH sheet metal that was purchased to make the back plate, enclosure, and mounting brackets for the electronic hardware. But the metal requirement was unique to this application. Other miscellaneous items such the ribbon cable and connection cables for the electronics are also not included but are relatively inexpensive.

Summary of Experimental NDT work

The experimental work conducted in case study 2, has produced an in-situ digital and thermal monitoring system to perform layer-wise capture of a printed part. It has created image processing strategies to digitally size the printed parts and defects (smallest size being around 0.2 mm), and 2D-to-3D extrusion strategies to digitally replicate a 3D model of the printed part. The part sizing and defect sizing methodology is easily adaptable to an online detection feed for continuous sizing and part/defect identification. Provided the camera lens remains focused on the same area, little needs to change in the method. If not, it is simple to recalculate the px per mm for an image using the free research tool ImageJ or even the built line measurement tool in OpenCV or MATLAB. While feature matching and defect sizing are a great research tool, this research needs to focus further on the reconstruction of the defects within a 3D model for both simulated analysis and a study of fatigue failure for DMP ProX 100 SS 17-4 PH parts to determine a correlation between the two or improve mesh analysis in simulation to achieve an accurate analysis of the part failure. Secondly, to work toward feedback control to target defective areas on the printed part and re-melt them.

This study has stated the inclusion of the FLIR Lepton thermal imaging sensor in the in-situ monitoring system. Thermal imaging was included in the monitoring system because residual stresses was highlighted as one of the 3 key issues for quality assurance in NDT. There has been a significant amount of investigation by other researchers documenting thermal image/sensing capture, with residual stress and heat-affected-zone analysis. The image acquisition GUIs worked well to capture the thermal images of the printed layers, and while the images did not provide any depth information, the rainbow spectrum of colour provided a good contrast between the melted and unmelted powder. But the image captured was too blurry to use for processing. This provided a better spectrum of pixel intensity to threshold in the defect detection methodology. Future development of a similar methodology to the digital image processing steps, could be adapted to processing the thermal images for sizing defects. The thermal camera temperature capture was inadmissible as an accurate measurement of the surface temperature, because calibration to test the emissivity of the powder, vs the melted part with reference to a thermal black tape was not performed (standard calibration process for thermal detectors).

Improvements to the image acquisition system and capture stage would greatly help, with an increased number of images taken for each layer, placement of more lights or different colored lights, a beam splitter, and mirrors to try an interferometer approach or laser scanning approach instead. Interrupting the print for every layer to actuate the camera over the build platform is inefficient, and while it is ideal for an interferometry set-up, an improved solution would be to

angle a camera at the build plate, and using the checkerboard calibration, level the image accordingly.

CHAPTER 6

6 FUTURE WORK AND RECOMMENDATIONS

The time limitations of each research study only allow for a degree of progression in the pursuit of a novel research methodology, technology, or research data. This study began in the exploration of NDT techniques to verify the accuracy of AM parts. The area of interest was widened to include exploration of techniques to improve surface finish in AM parts too. As a result, in-situ laser polishing and machine vision surface profiling were considered to a degree, with experimentation conducted to explore the validity of the suggested methodologies to satisfy the interest in both areas. The result of this study has revealed the merit in the solutions explored and created an opportunity for further research and the growth to perfect a solution that assures the quality of AM parts. The end goal being the introduction of AM technologies into product categories that manufacture load bearing parts with complex geometries. This chapter explores the future work required to do this and recommends adaptations to the methodologies presented based on the results discussed in the previous two chapters.

The potential of in-situ laser polishing to significantly improve the surface finish of L-PBF parts

This thesis has presented an in-situ laser polishing method with quantitative justification to improve the surface finish of metal AM parts. The proof applied specifically to the L-PBF method of direct metal printing in case study 1. However, there is reasonable proof that in-situ laser polishing provides a degree of improvement to the manufactured part and may be relevant to other L-PBF machines too. The significant improvement in the outline of the part exteriors wall, recommends the technique to be pursed in further research studies. Future work would be beneficial, to not only realize the potential of this method but possibly expand the methodology to work in combination with chemical-based techniques which have been proven effective by other research groups [130, 131, 134].

Further research into examining other laser parameters within DMP technologies or even other Laser-Powder Bed Fusion technologies could see further improvement in the surface profile smoothening. The discussion in chapter 4 states the DMP ProX 100 to be a ‘research-grade’ printer, where commercially employed L-PBF machines outperform this machine with an improved surface finish on the printed part. Design an experimental study to compare the data captured in this research with a similar experimental study and adjusting the min-to-max laser speed, laser power and the same repetition scale (parameters used in this study) performed on a commercial grade printer. This would hopefully demonstrate the percentage of improvement laser

polishing can affect commercial grade printers by and add to the confirmation that LP can be used to improve the surface finish of metal AM parts.

However, one concern resulting from this study, is the realization that LP smoothens the surface marginally, but still exhibits an erratic surface profile. The future work will also focus on testing other printer parameters such as laser scanning profile offset, jump speed, layer thickness, and more. Adjusting the laser scanning profile by offsetting it, is suggested due to the partial melting of powder surrounding the part. This phenomenon creates inclusions of powder on the surface off the printed part affecting the overall surface finish. By offsetting the laser outline to scan slightly within the part it is expected that this issue can be solved.

The experimental work with LP in this doctoral study focused on the outline of the printed part, however as case study 2 discusses, there is potential to create laser scanning strategies based on the pixel intensity created by light-based detection methods to isolate peaks and potentially remelt them to smoothen the surface.

The potential of digital and thermal imaging to provide defect detection and part failure analysis

Several NDT solutions were explored in this thesis, including digital imaging with machine vision, thermal imaging, acoustic resonance, laser scanning and acoustic imaging with ultrasound. The study presents methodologies for parts sizing and defect detection within the DMP ProX 100 printer and has created opportunity for future work in exploring these NDT solutions. Firstly, regarding the digital imaging system, there are improvements that can be made to acquire data more efficiently without interrupting the printing process. Removing the linear actuator from the system and creating an angled mount extruding from the backplate to hold the digital camera with its lens focused on the build plate, is one possible solution. Chapter 5 discusses the robustness of the system built in the printer where the printer only needed to be open for calibration. The current calibration process requires a square cut out of a checkerboard to be taped onto the build plate by opening the printer. A suggestion for eliminating this process is to integrate a light-based checkerboard projection, with a grid blocking out the black squares, always aimed at the surface. This grid could also be used as a measurement reference for defining the location of a part and its size on a build plate.

Methods to accurately map the surface profile of the printed part have been described to use an interferometry optical-based application or laser scanning. However, there is an alternative digital camera method that was considered but required more time to implement. That is using two digital cameras placed next to each other with the known location for the center of the camera detector. This application is referred to as stereo vision. Stereo vision could be used to accurately measure surface profile parameters in real-time what's dual microscopic-camera-vision.

Future work to process the thermal images taken by the thermal sensor in the in-situ monitoring system is required. The digital images that were processed for defect detection proved ineffective due to the high similarity between the melted-part pixel color and the unmelted-powder pixel color. Visual inspection of the thermal images shows a huge discrepancy between the melted-part pixel color and the unmelted-powder pixel color. In addition, lock-in thermography as described in chapter 2 has the potential to provide 3D data for the thermal images that could be used to map the depth of defects more accurately within each layer of the part and highlight the interaction between layers. In this study a halogen lamp (excitation source) was integrated into the monitoring system, and the thermal sensor recorded the thermal gradient on the surface of the part with respect to time to capture a change in gradient over time. Unfortunately, no change was observed over the (10, 20 or 30 second mark). Using a light-based method, the excitation being captured is the spread of light/heat over the part. Therefore, the capturing implementation in this experiment was incorrect. Further work would have to use frequency-modulated thermal-wave imaging, where the frequency of the excitation (light) signal changes monotonically with time instead.

CHAPTER 7

7 SUMMARY OF RESEARCH OUTPUTS

This doctoral study features two key areas of research, that were explored in an engineering capacity to determine new quality assurance strategies, firstly, to improve surface finish in L-PBF SS 17-4 PH parts. Secondarily, to explore Non-Destructive testing technologies, to determine new methods of defect detection and mechanical property characterization for metal AM parts. More specifically, the experimentation surrounds the DMP ProX 100 AM machine. The experimental work was divided into two case studies. The first case study examined in-situ laser polishing the SS 17-4 PH specimens, in pursuit of a surface finish improvement technique. An improvement in surface finish was linked to the betterment of mechanical properties and significantly reduces the risk of fatigue failure due to defect initiation or elongation. The literature review and industry surveying summary highlighted 3 key issues faced in metal AM at the commencement of this research. The first was an improvement in surface finish, the second inspecting residual stresses and lastly defect detection within printed parts. These were not the only issues identified, where other gaps in research could have been pursued to focus on an economic-based strategy, design for AM strategy, material research or even explore a new AM technology. Research into these areas is key to progressing the state-of-art for AM but improving the quality of AM parts is arguably the most crucial area of research. This doctoral thesis demonstrates how important quality assurance for AM parts is to progress the industry and product capability into manufacturing load bearing components. The inspiration behind a surface-finish-improvement and NDT technology focus stemmed from the discovery of inconsistency within AM prints process-to-process.

Chapter 2 provides a very succinct summary of NDT technologies that were considered after reviewing several published works that have begun research efforts in the NDT research space for AM technologies. The vast amount of NDT research already conducted to date, provided an excellent starting point to pick research in one of the many explored technologies. To date the most popular technology used is X-ray in combination with computed tomography (CT) to scan AM parts post-print. To reiterate, while this method has proven mostly successful in defect detection, there are some drawbacks that have justified the investigation of other techniques. These drawbacks include the high-cost, high-processing time, lack off thermal stress information (residual stresses), and failure to detect some defects in particular orientations or pores filled with unsintered powder. The study has revealed the depth of solutions required to address the multitude of issues in an AM process. It is clear there is no single solution that will work entirely to assure

quality of the machine feedstock, machine parameters, part defects, and more. Therefore, several research methods exist in this study with different technologies studied.

Practical Implementations and Engineering solution outcomes

This doctoral study has included the practical development of supporting mechanisms used to collect the novel data for the methodologies created. Many of the methods and mechanisms created was to improve the DMP ProX manufacturing and maintenance processes by increasing process efficiency and reducing print failure. These mechanisms are listed below:

1) Training, operation, and maintenance of the DMP ProX 100 printer

Operating the DMP ProX 100 was a laborious task considering the work required in the pre-printing, printing, and post-printing operations. The parts of the printer were made of SS and were considerably heavy. The pre-printing process was primarily software based aside from loading the new build plate and topping up the SS powder. The printing process began with loading the SS 17-4PH build plate onto the build station and securing the plate with 4 screws, this was done using gloves and looking through a small viewing window. The powder is held in SS canisters that are used to capture the recycled powder swept into the powder overflow station and in the external powder sifting machine. The laser lens must be cleaned before every print using isopropyl alcohol. Then the printer is inerted with nitrogen. The nitrogen is supplied from individual canisters that last for 2 to 3 prints depending on the length of the print.

The printing process is almost entirely automated unless the powder spreader gets stuck on a layer, which initially happened a lot. If the collision sensor in the printer was triggered, then the powder spreader had to be manually pushed back to its origin. The reason for the powder spreader getting stuck was often due to unevenness on the surface of the build plate caused by the plate recycling process. The post-printing process involves removing the build part, then removing the parts from the build plate, performing the recycling process described below and sifting the recycled power.

Maintenance of the printer, included opening the printer chamber door (secured by 14 screws), brushing powder around the build station into the overflow station and vacuuming the rest and cleaning the plate in the build station where powder would sometimes build up in the screw holes that secure the plate to the machine. Notable issues encountered in the manufacturing process that required new methods to be developed was the unevenness caused by the build-plate recycle process, the way the parts were removed from the build plate and powder spreader getting stuck by melting every layer of the support layers. The strategies to improve these issues follows.

2) Resolving issues related to the powder spreader catching

The two issues causing the powder spreader to catch was the unevenness of the build plate surface and melting every support layer. Initially, following the advice provide by the previous machine operator, the build plates were recycled using the CNC machine and roughened (to help the powder spread for the first layer and not slide off) using a horizontal linisher. The linisher was too powerful and done manually caused the part to strip areas unevenly. This process was replaced by sanding the CNC'd part by hand with sandpaper, moving in one direction. The issue with the support layers was realized following a visit from the 3D systems service technician, who upgraded the machine software and said they realized the part encounters no issues when every second support layer is spread, instead of every layer. The only other consideration for every print was, to prevent delamination the first layer had to be sintered twice and the powder for the first part layer had to be spread twice.

3) Improved part removal process

Initially the process to remove the parts from the build plate was done using a hammer, chisel, and vice to remove the parts. This resulted in the bending deformation shown in the laser scanning illustration in Chapter 5 (Figure 5-7). To solve this issue, it was important to consider a machinery that had coolant applied to prevent the parts from deforming due to friction created by a fast-moving blade. Therefore, a custom jig was created to mount the DMP build plate in the horizontal bandsaw grips and saw the parts off. The horizontal bandsaw has coolant running along the blade, with adjustable speed and descent which enables the operator to monitor the process and stop it if the blade is cutting into the build plate or the part surface. Establishing this method for the part removal, meant the support material height was always set to 3mm at the minimum part face/vertices. The part removal was followed by linishing the remaining support material off.

4) Manufacturing of laser polished test specimens

Manufacturing the test specimens for case study 1 took a considerable amount of time, following the operation methods described above. The computer linked to the DMP manufacturing software was extremely slow when trying to change the laser settings for each part in the print. Remote control of the software was done, to work whilst waiting for every command to take effect (20 to 40 seconds). Trial and testing were required to figure out how to apply the **outline** function in this application, as the only information source was the DMP manufacturing manual that briefly describes the existence of the tool and selecting it in the part scanning method (replacing the usual hexagonal file with the outline).

5) Design, manufacture, and installation of the digital and thermal monitoring system and the creation of novel GUIs to electronically control the hardware elements inside the monitoring system and used for digital and thermal image acquisition

The largest engineered solution was the development of the mechatronic monitoring system as described in Chapter 3 and 5. The author applied her mechatronic knowledge and skills to create the solution combining CAD, manufacturing, installation, and software development skills.

Due to the restrictive nature in accessing the inside of the printing chamber, most of the development time was spent on this practical implementation, especially creating the image capture GUIs. But the output was worth the time to create a reliable research tool that can now be used to gather more defect data in fatigue test specimens and find a correlation between defect placement, simulated analysis, and the destructive testing process. Secondly, to focus on improving the LP process by tying the 2D layer analysis and DMP laser scanning file creation together. As described in Chapter 5, the in-situ monitoring system helped with the laser defocus calibration process by visually inspecting each calibration layer to clearly detail failed settings.

6) Digital image processing strategies

The code written for the image processing in Visual Studio using Python 3 and OpenCV and MATLAB, was created specific to the applications in this study. Online support for the key functions used in each program, made it easier to manipulate the functions and achieve the results presented in Chapter 5.

Experimental summary

The experimental summary is split by the two case studies. Case study 1 used the laser within the DMP ProX 100 printer to polish the outline of each part for every layer, building at different slope angles with varying laser parameters (laser power, laser speed and polishing iterations). The research questions surrounding this study sought a method to improve surface finish and determine if in-situ laser polishing could achieve this. The research hypothesis was detailed around the research questions and was satisfied by the proven improvement of Ra in the DMP ProX 100 SS 17-4PH printed parts. Case Study 2 explored the use of machine vision with image processing to perform layer-wise capture and digital processing of a DMP ProX 100 SS 17-4 printed part. The research questions for this study enquired about the capability of NDT methods to detect defects in L-PBF parts, provide file security to detect and measure the dimensions of the part being printed vs the print file supplied to the printer. The solutions described in Chapter 5, prove successful detection of parts with metric measurement of the square, for multiple parts in a print. Secondly, defect detection of microdefects typically found in L-PBF

parts were partially detected and combining the digital and thermal images together could provide a completely successful solution.

Research contributions

The major research contribution of this thesis work are the multiple quality assurance strategies developed around the DMP ProX 100 machine with SS 17-4PH powder. The data and analysis presented in this thesis work highlights novel contributions to the L-PBF process research space. The research tools created were made with adaptability in mind, to help other researchers further the data processing side of NDT research in the AM space. The publications noted at the start of this thesis are formal public contributions from this research study.

8 CONCLUSION

This doctoral research set out to examine and investigate quality assurance strategies for the DMP ProX 100. The overarching aim of this pursuit was to determine new methods that would improve the surface finish of DMP parts and examine the ability of NDT techniques to replace common destructive testing techniques and determine if an AM part is fit for purpose.

The surface finish improvement study sought examine the ability of in-situ laser polishing to improve the surface finish texture and roughness profile without compromising the mechanical integrity of the part. The aim was successfully met, with an improvement of Ra by 16.7% when the part's exterior surface was angled ∠80 relative to the build plate. The study proved the CS1 hypothesis true; the part angled in different orientations was affected to a different degree by the laser polishing strategies. With the right laser parameters and print orientation, in-situ laser polishing is a viable method to improve surface roughness in metal AM parts.

A low-cost digital and thermal monitoring system was successfully installed into the DMP ProX 100 machine. The monitoring system was created with the aim to capture each layer of a print as a 2D image and successfully did so. The main objective of the system was to produce NDT acquired data and use image processing to measure the printed part as a verification against the inputted part file for the operator and digitally detect, with measurement, synthetic defects produced in the printed part. The digital camera was successful in classifying the part size but every image with the synthesized defects needed individual adjustment to the thresholding range the dilation kernel size and iterations.

The greyish-silver colouring of the SS 17-4 PH powder and melted part were close in pixel intensity variability, which interfered with the feature separation algorithm to isolate the

powder (defective areas) with the square part shape and the solid metal layer. The powder pixel intensity also closely resembled the indented areas of the printed part when lit by the halogen lamp, which was great for creating the zones for remelting, but not quite for isolating the defects. The thermal sensor helped with this issue by providing a higher contrast of pixel intensity. This confirmed the need to combine NDT technologies to better detect microdefects in metal AM parts. The 2D layer capture focused on the entire 100mm x 100mm print bed, including the printed parts and surrounding powder. After isolating the part from the powder, and thresholding the image based on the pixel intensity of different areas, the extracted contour profiles were traced and extruded to 30 μm to mimic the layer thickness of each layer in the printed part. There were many practical engineering, manufacturing, design, and software elements, created in the pursuit of creating quality assurance methods for the DMP ProX 100 machine. The use of existing technologies in novel applications has resulted in the successful creation of a low-cost in-situ monitoring system, unique methods to provide feedback to the DMP ProX 100 machine and created the opportunity for further research to improve on the solutions presented in this study.

REFERENCES

[1] Gausemeier, J., et al., *Thinking ahead the Future of Additive Manufacturing–*. Future Applications, 2011.

[2] Bourell, D.L., M.C. Leu, and D.W. Rosen, *Roadmap for additive manufacturing: identifying the future of freeform processing.* The University of Texas at Austin, Austin, TX, 2009: p. 11-15.

[3] Faludi, J., et al., *Comparing environmental impacts of additive manufacturing vs traditional machining via life-cycle assessment.* Rapid Prototyping Journal, 2015. **21**(1): p. 14-33.

[4] Gao, W., et al., *The status, challenges, and future of additive manufacturing in engineering.* Computer-Aided Design, 2015. **69**: p. 65-89.

[5] Atzeni, E. and A. Salmi, *Economics of additive manufacturing for end-usable metal parts.* The International Journal of Advanced Manufacturing Technology, 2012. **62**(9-12): p. 1147-1155.

[6] Tofail, S.A., et al., *Additive manufacturing: Scientific and technological challenges, market uptake and opportunities.* Materials Today, 2017.

[7] Da Silveira, G., D. Borenstein, and F.S. Fogliatto, *Mass customization: Literature review and research directions.* International journal of production economics, 2001. **72**(1): p. 1-13.

[8] Wohlers, T., *Wohler's report 2013.* 2013.

[9] Kalpakjian, S., K. Vijai Sekar, and S.R. Schmid, *Manufacturing engineering and technology*. 2014: Pearson.

[10] Unger, A.S., R.J. Lewis, and T. Gruen, *Evaluation of a porous tantalum uncemented acetabular cup in revision total hip arthroplasty: clinical and radiological results of 60 hips.* The Journal of arthroplasty, 2005. **20**(8): p. 1002-1009.

[11] Excell, J. and S. Nathan, *The rise of additive manufacturing.* The engineer, 2010. **24**.

[12] Ventola, C.L., *Medical applications for 3D printing: current and projected uses.* Pharmacy and Therapeutics, 2014. **39**(10): p. 704.

[13] Pine, B.J., B. Victor, and A.C. Boynton, *Making mass customization work.* Harvard business review, 1993. **71**(5): p. 108-11.

[14] Eastwood, M.A., *Implementing mass customization.* Computers in industry, 1996. **30**(3): p. 171-174.

[15] Tseng, M.M., J. Jiao, and M.E. Merchant, *Design for mass customization.* CIRP Annals-Manufacturing Technology, 1996. **45**(1): p. 153-156.

[16] Joffe, L., *Current Products and Practice Invisalign®: early experiences.* J orthod, 2003. **30**(4): p. 348-52.

[17] Reeves, P., C. Tuck, and R. Hague, *Additive manufacturing for mass customization*, in *Mass Customization*. 2011, Springer. p. 275-289.

[18] Conner, B.P., et al., *Making sense of 3-D printing: Creating a map of additive manufacturing products and services.* Additive Manufacturing, 2014. **1**: p. 64-76.

[19] Hopkinson, N. and P. Dicknes, *Analysis of rapid manufacturing—using layer manufacturing processes for production.* Proceedings of the Institution of Mechanical Engineers, Part C: Journal of Mechanical Engineering Science, 2003. **217**(1): p. 31-39.

[20] Ruffo, M., C. Tuck, and R. Hague, *Make or buy analysis for rapid manufacturing.* Rapid Prototyping Journal, 2007. **13**(1): p. 23-29.

[21] Levy, G.N., R. Schindel, and J.-P. Kruth, *Rapid manufacturing and rapid tooling with layer manufacturing (LM) technologies, state of the art and future perspectives.* CIRP Annals-Manufacturing Technology, 2003. **52**(2): p. 589-609.

[22] Petrick, I.J. and T.W. Simpson, *3D printing disrupts manufacturing: how economies of one create new rules of competition.* Research-Technology Management, 2013. **56**(6): p. 12-16.

[23] Ulrich, K. and S. Eppinger, *1995, Product Design and Development, McGraw Hill.* Inc., New York.
[24] Boothroyd, G., P. Dewhurst, and W.A. Knight, *Product Design for Manufacture and Assembly, revised and expanded*. 2001: CRC press.
[25] Gero, J., *Recent advances in computational models of creative design.* Computing in civil and building engineering, balkema, 1995. **21**.
[26] Lyons, B., *Additive manufacturing in aerospace: Examples and research outlook.* The Bridge, 2014. **44**(3).
[27] Zuniga, J.M., et al., *The development of a low-cost three-dimensional printed shoulder, arm, and hand prostheses for children.* Prosthetics and orthotics international, 2017. **41**(2): p. 205-209.
[28] Kruth, J.-P., M.-C. Leu, and T. Nakagawa, *Progress in additive manufacturing and rapid prototyping.* CIRP Annals-Manufacturing Technology, 1998. **47**(2): p. 525-540.
[29] Stein, A., *Disadvantages of 3D printers. eHow TECH*. 2012.
[30] Berman, B., *3-D printing: The new industrial revolution.* Business horizons, 2012. **55**(2): p. 155-162.
[31] 3Ders. *Price compare - 3D printers*. 3D printer and 3D printing news 2018 [cited 2018 05/06/2018]; Available from: https://www.3ders.org/pricecompare/3dprinters/.
[32] Thomas, D.S. and S.W. Gilbert, *Costs and cost effectiveness of additive manufacturing.* NIST Special Publication, 2014. **1176**: p. 12.
[33] Russell, J.P. *What are quality assurance and quality control?* Learn about Quality 2017 [cited 2017 15/08]; Available from: http://asq.org/learn-about-quality/quality-assurance-quality-control/overview/overview.html.
[34] Diegel, O., et al., *Tools for sustainable product design: additive manufacturing.* 2010.
[35] Newman, S.T., et al., *Process planning for additive and subtractive manufacturing technologies.* CIRP Annals, 2015. **64**(1): p. 467-470.
[36] Everton, S.K., et al., *Review of in-situ process monitoring and in-situ metrology for metal additive manufacturing.* Materials & Design, 2016. **95**: p. 431-445.
[37] Sharratt, B.M., *Non-destructive techniques and technologies for qualification of additive manufactured parts and processes.* no. March, 2015.
[38] Rajkolhe, R. and J. Khan, *Defects, causes and their remedies in casting process: A review.* International Journal of Research in Advent Technology, 2014. **2**(3): p. 375-383.
[39] Kim, F.H. and S.P. Moylan, *Literature Review of Metal Additive Manufacturing Defects*. 2018.
[40] Lloyd's Register Group Limited, T.L., *Guidance Notes for the Certification of Metallic Parts made by Additive Manufacturing*. 2017, Lloyd's Register Group Limited: 71 Fenchurch Street, London, EC3M 4BS, United Kingdom. p. 22.
[41] Pereira, T., J. Potgieter, and J.V. Kennedy. *A fundamental study of 3D printing testing methods for the development of new quality management strategies*. in *Mechatronics and Machine Vision in Practice (M2VIP), 2017 24th International Conference on*. 2017. IEEE.
[42] Technologies, A.C.F.o.A.M. and A.C.F.o.A.M.T.S.F.o. Terminology, *Standard terminology for additive manufacturing technologies*. 2012: ASTM International.
[43] Lucideon. *Additive Manufacturing Testing*. Testing & Characterization 2017 [cited 2017 4/08]; Testing methods for quality assurance of additive manufactured parts]. Available from: https://www.lucideon.com/testing-characterization/additive-manufacturing-testing.
[44] Frazier, W.E., *Metal additive manufacturing: a review.* Journal of Materials Engineering and Performance, 2014. **23**(6): p. 1917-1928.
[45] Czichos, H., *Handbook of technical diagnostics: fundamentals and application to structures and systems*. 2013: Springer Science & Business Media.
[46] Wing, I., R. Gorham, and B. Sinderman, *3D Opportunity for Quality Assurance and Parts Qualification. Additive Manufacturing Clears the Bar*. 2015, Deloitte University Press.

[47] Dongarra, J.J., H.W. Meuer, and E. Strohmaier, *Top500 supercomputer sites*. 1994, Technical Report RUM 40/94, Computing Centre, Univ. of Mannheim, 68131 Mannheim, Germany.
[48] Dutta, B. and F.H.S. Froes, *The additive manufacturing (AM) of titanium alloys*, in *Titanium powder metallurgy*. 2015, Elsevier. p. 447-468.
[49] Gibson, I. and D. Shi, *Material properties and fabrication parameters in selective laser sintering process.* Rapid Prototyping Journal, 1997. **3**(4): p. 129-136.
[50] Beyer, C., *Strategic implications of current trends in additive manufacturing.* Journal of Manufacturing Science and Engineering, 2014. **136**(6): p. 064701.
[51] King, W., et al., *Overview of modelling and simulation of metal powder bed fusion process at Lawrence Livermore National Laboratory.* Materials Science and Technology, 2015. **31**(8): p. 957-968.
[52] Calignano, F., et al., *Influence of process parameters on surface roughness of aluminum parts produced by DMLS.* The International Journal of Advanced Manufacturing Technology, 2013. **67**(9-12): p. 2743-2751.
[53] Islam, N.K.M.S., et al. *Physical properties and microstructure study of stainless steel 316L alloy fabricated by selective laser melting*. in *AIP Conference Proceedings*. 2017. AIP Publishing.
[54] Mercelis, P. and J.-P. Kruth, *Residual stresses in selective laser sintering and selective laser melting.* Rapid prototyping journal, 2006. **12**(5): p. 254-265.
[55] Glardon, R., et al., *Influence of Nd: YAG parameters on the selective laser sintering of metallic powders.* CIRP Annals, 2001. **50**(1): p. 133-136.
[56] Jhabvala, J., et al., *On the effect of scanning strategies in the selective laser melting process.* Virtual and physical prototyping, 2010. **5**(2): p. 99-109.
[57] Parry, L., I. Ashcroft, and R.D. Wildman, *Understanding the effect of laser scan strategy on residual stress in selective laser melting through thermo-mechanical simulation.* Additive Manufacturing, 2016. **12**: p. 1-15.
[58] Giorleo, L., E. Ceretti, and C. Giardini. *Ti surface laser polishing: effect of laser path and assist gas*. in *CIRP ICME'14-9th CIRP Conference on Intelligent Computation in Manufacturing Engineering*. 2015. Elsevier.
[59] Shamsaei, N., et al., *An overview of Direct Laser Deposition for additive manufacturing; Part II: Mechanical behavior, process parameter optimization and control.* Additive Manufacturing, 2015. **8**: p. 12-35.
[60] Kainer, K.U., *Metal matrix composites: custom-made materials for automotive and aerospace engineering*. 2006: John Wiley & Sons.
[61] Additively. *Overview over 3D printing technologies*. 2020 [cited 2018; Available from: https://www.additively.com/en/learn-about/3d-printing-technologies#read-more.
[62] Gu, D. and Y. Shen, *Balling phenomena in direct laser sintering of stainless steel powder: Metallurgical mechanisms and control methods.* Materials & Design, 2009. **30**(8): p. 2903-2910.
[63] Tolochko, N.K., et al., *Absorptance of powder materials suitable for laser sintering.* Rapid Prototyping Journal, 2000.
[64] Lide, D.R., *CRC handbook of chemistry and physics*. Vol. 85. 2004: CRC press.
[65] Arafune, K. and A. Hirata, *Thermal and solutal Marangoni convection in In–Ga–Sb system.* Journal of Crystal Growth, 1999. **197**(4): p. 811-817.
[66] Meier, C., et al., *Thermophysical phenomena in metal additive manufacturing by selective laser melting: fundamentals, modeling, simulation, and experimentation.* Annual Review of Heat Transfer, 2017. **20**.
[67] Yadroitsev, I. and I. Smurov, *Surface morphology in selective laser melting of metal powders.* Physics Procedia, 2011. **12**: p. 264-270.
[68] Gong, H., et al., *Analysis of defect generation in Ti–6Al–4V parts made using powder bed fusion additive manufacturing processes.* Additive Manufacturing, 2014. **1**: p. 87-98.
[69] Zhao, C., et al., *Real-time monitoring of laser powder bed fusion process using high-speed X-ray imaging and diffraction.* Scientific Reports, 2017. **7**.

[70] Yang, L., H. Gu, and A. Lassell. *Surface treatment of Ti6al4V parts made by powder bed fusion additive manufacturing processes using electropolishing*. in *Proceedings of the Solid Freeform Fabrication (SFF) Symposium, Austin, TX, USA*. 2014.
[71] Kumbhar, N. and A. Mulay, *Post processing methods used to improve surface finish of products which are manufactured by additive manufacturing technologies: a review.* Journal of The Institution of Engineers (India): Series C, 2016: p. 1-7.
[72] Classification, A.S.o.M.E.S.C.B. and D.o.S. Qualities, *Surface texture: Surface roughness, waviness and lay*. 2003: Amer Society of Mechanical.
[73] Poon, C.Y. and B. Bhushan, *Comparison of surface roughness measurements by stylus profiler, AFM and non-contact optical profiler.* Wear, 1995. **190**(1): p. 76-88.
[74] O'Regan, P., et al., *Metal based additive layer manufacturing: variations, correlations and process control.* Procedia Computer Science, 2016. **96**: p. 216-224.
[75] AlMangour, B. and J.-M. Yang, *Improving the surface quality and mechanical properties by shot-peening of 17-4 stainless steel fabricated by additive manufacturing.* Materials & Design, 2016. **110**: p. 914-924.
[76] Dadbakhsh, S., L. Hao, and C.Y. Kong, *Surface finish improvement of LMD samples using laser polishing.* Virtual and Physical Prototyping, 2010. **5**(4): p. 215-221.
[77] Luong, H. and M.R. Hill, *The effects of laser peening and shot peening on high cycle fatigue in 7050-T7451 aluminum alloy.* Materials Science and Engineering: A, 2010. **527**(3): p. 699-707.
[78] Jamal, M. and M.N. Morgan, *Design Process Control for Improved Surface Finish of Metal Additive Manufactured Parts of Complex Build Geometry.* Inventions, 2017. **2**(4): p. 36.
[79] Urlea, V. and V. Brailovski, *Electropolishing and electropolishing-related allowances for powder bed selectively laser-melted Ti-6Al-4V alloy components.* Journal of Materials Processing Technology, 2017. **242**: p. 1-11.
[80] Krishnan, A. and F. Fang, *Review on mechanism and process of surface polishing using lasers.* Frontiers of Mechanical Engineering, 2019: p. 1-21.
[81] Czichos, H., T. Saito, and L.E. Smith, *Springer handbook of metrology and testing*. 2011: Springer Science & Business Media.
[82] Rombouts, M., et al., *Surface finish after laser metal deposition.* Physics Procedia, 2013. **41**: p. 810-814.
[83] Slotwinski, J.A. and E.J. Garboczi, *Metrology needs for metal additive manufacturing powders.* Jom, 2015. **67**(3): p. 538-543.
[84] Slotwinski, J.A., et al., *Characterization of metal powders used for additive manufacturing.* Journal of research of the National Institute of Standards and Technology, 2014. **119**: p. 460.
[85] Campbell, J., *Complete casting handbook: metal casting processes, metallurgy, techniques and design*. 2015: Butterworth-Heinemann.
[86] Jin, M., T. Zhao, and C. Chen, *The effects of micro-defects and crack on the mechanical properties of metal fiber sintered sheets.* International Journal of Solids and Structures, 2014. **51**(10): p. 1946-1953.
[87] Wycisk, E., et al., *Effects of defects in laser additive manufactured Ti-6Al-4V on fatigue properties.* Physics Procedia, 2014. **56**: p. 371-378.
[88] Slotwinski, J.A., E.J. Garboczi, and K.M. Hebenstreit, *Porosity measurements and analysis for metal additive manufacturing process control.* Journal of research of the National Institute of Standards and Technology, 2014. **119**: p. 494.
[89] Ning, J., et al., *Analytical modeling of part porosity in metal additive manufacturing.* International Journal of Mechanical Sciences, 2020. **172**: p. 105428.
[90] Ning, J., et al., *Analytical modeling of lack-of-fusion porosity in metal additive manufacturing.* Applied Physics A, 2019. **125**(11): p. 1-11.
[91] Wu, J., et al., *Infill optimization for additive manufacturing—approaching bone-like porous structures.* IEEE transactions on visualization and computer graphics, 2017. **24**(2): p. 1127-1140.

[92] Du Plessis, A. and E. Macdonald, *Hot isostatic pressing in metal additive manufacturing: X-ray tomography reveals details of pore closure.* Additive Manufacturing, 2020. **34**: p. 101191.
[93] Kumar, A.Y., et al., *The effects of Hot Isostatic Pressing on parts fabricated by binder jetting additive manufacturing.* Additive Manufacturing, 2018. **24**: p. 115-124.
[94] Chen, C., et al., *Effect of hot isostatic pressing (HIP) on microstructure and mechanical properties of Ti6Al4V alloy fabricated by cold spray additive manufacturing.* Additive Manufacturing, 2019. **27**: p. 595-605.
[95] Chetiyar, S., et al., *Measurement of Surface Defects in 3D Printed Models*. 2016.
[96] Li, C., et al., *Residual stress in metal additive manufacturing.* Procedia Cirp, 2018. **71**: p. 348-353.
[97] Zaeh, M.F. and G. Branner, *Investigations on residual stresses and deformations in selective laser melting.* Production Engineering, 2010. **4**(1): p. 35-45.
[98] Czichos, H., *Introduction to Metrology and Testing*, in *Springer Handbook of Metrology and Testing*. 2011, Springer. p. 3-22.
[99] Baldi, A., *Residual stress measurement using hole drilling and integrated digital image correlation techniques.* Experimental Mechanics, 2014. **54**(3): p. 379-391.
[100] Schajer, G.S., *Advances in hole-drilling residual stress measurements.* Experimental mechanics, 2010. **50**(2): p. 159-168.
[101] Goldstein, J., et al., *Scanning electron microscopy and X-ray microanalysis: a text for biologists, materials scientists, and geologists*. 2012: Springer Science & Business Media.
[102] Goodge, J. *Energy-Dispersive X-Ray Spectroscopy (EDS)*. Geochemical Instrumentation and Analysis 2017 April 26, 2017 [cited 2017 01/08]; What is EDS; how it works, Strengths, limitations, Results]. Available from: https://serc.carleton.edu/research_education/geochemsheets/eds.html.
[103] Cheruvathur, S., E.A. Lass, and C.E. Campbell, *Additive manufacturing of 17-4 PH stainless steel: post-processing heat treatment to achieve uniform reproducible microstructure.* Jom, 2016. **68**(3): p. 930-942.
[104] Garnier, C., et al., *The detection of aeronautical defects in situ on composite structures using Non Destructive Testing.* Composite structures, 2011. **93**(5): p. 1328-1336.
[105] Hirsch, M., et al., *Assessing the capability of in-situ nondestructive analysis during layer based additive manufacture.* Additive Manufacturing, 2017. **13**: p. 135-142.
[106] Erhard, A., *Non-destructive evaluation*, in *Handbook of Technical Diagnostics*. 2013, Springer. p. 161-174.
[107] Shah, P., R. Racasan, and P. Bills, *Comparison of different additive manufacturing methods using computed tomography.* Case studies in nondestructive testing and evaluation, 2016. **6**: p. 69-78.
[108] Strantza, M., et al., *Evaluation of SHM system produced by additive manufacturing via acoustic emission and other NDT methods.* Sensors, 2015. **15**(10): p. 26709-26725.
[109] Strantza, M., et al., *Evaluation of SHM system produced by additive manufacturing via acoustic emission and other NDT methods.* Sensors, 2015. **15**(10): p. 26709-26725.
[110] Baumann, F.W., et al., *Trends of machine learning in additive manufacturing.* International Journal of Rapid Manufacturing, 2018. **7**(4): p. 310-336.
[111] Caggiano, A., et al., *Machine learning-based image processing for on-line defect recognition in additive manufacturing.* CIRP Annals, 2019. **68**(1): p. 451-454.
[112] Wang, C., et al., *Machine learning in additive manufacturing: State-of-the-art and perspectives.* Additive Manufacturing, 2020: p. 101538.
[113] Qi, X., et al., *Applying neural-network-based machine learning to additive manufacturing: current applications, challenges, and future perspectives.* Engineering, 2019. **5**(4): p. 721-729.
[114] Zhu, Y.-K., et al., *A review of optical NDT technologies.* Sensors, 2011. **11**(8): p. 7773-7798.

[115] Lv, C., et al., *Edge detection of internal defects based on the hidden singularity of gradient streamlines obtained by continuous wavelet transform.* Optical Engineering, 2019. **58**(3): p. 033105.
[116] Bayle, F. and M. Doubenskaia. *Selective laser melting process monitoring with high speed infra-red camera and pyrometer*. in *Fundamentals of laser assisted micro-and nanotechnologies*. 2008. International Society for Optics and Photonics.
[117] Furumoto, T., et al., *Monitoring of laser consolidation process of metal powder with high speed video camera.* Physics Procedia, 2012. **39**: p. 760-766.
[118] Gao, F., et al., *Surface measurement errors using commercial scanning white light interferometers.* Measurement Science and Technology, 2007. **19**(1): p. 015303.
[119] Chua, Z.Y., I.H. Ahn, and S.K. Moon, *Process monitoring and inspection systems in metal additive manufacturing: Status and applications.* International Journal of Precision Engineering and Manufacturing-Green Technology, 2017. **4**(2): p. 235-245.
[120] Krauss, H., C. Eschey, and M. Zaeh. *Thermography for monitoring the selective laser melting process*. in *Proceedings of the Solid Freeform Fabrication Symposium*. 2012.
[121] Maldague, X. and S. Marinetti, *Pulse phase infrared thermography.* Journal of applied physics, 1996. **79**(5): p. 2694-2698.
[122] Breitenstein, O. and M. Langenkamp, *Lock-in thermography*, in *Basics and Use for Functional Diagnostics of Electronics Components*. 2003, Springer.
[123] Gaussorgues, G. and S. Chomet, *Infrared thermography*. Vol. 5. 1993: Springer Science & Business Media.
[124] Krauss, H., T. Zeugner, and M.F. Zaeh, *Layerwise monitoring of the selective laser melting process by thermography.* Physics Procedia, 2014. **56**: p. 64-71.
[125] Simchi, A., *Direct laser sintering of metal powders: Mechanism, kinetics and microstructural features.* Materials Science and Engineering: A, 2006. **428**(1-2): p. 148-158.
[126] Murr, L., *Metallurgy principles applied to powder bed fusion 3D printing/additive manufacturing of personalized and optimized metal and alloy biomedical implants: an overview.* Journal of Materials Research and Technology, 2020. **9**(1): p. 1087-1103.
[127] Obeidi, M.A., et al., *Laser polishing of additive manufactured 316L stainless steel synthesized by selective laser melting.* Materials, 2019. **12**(6): p. 991.
[128] Rosa, B., P. Mognol, and J.-Y. Hascoët, *Laser polishing of additive laser manufacturing surfaces.* Journal of Laser Applications, 2015. **27**(S2): p. S29102.
[129] Tyagi, P., et al., *Reducing the roughness of internal surface of an additive manufacturing produced 316 steel component by chempolishing and electropolishing.* Additive Manufacturing, 2019. **25**: p. 32-38.
[130] Kim, U.S. and J.W. Park, *High-quality surface finishing of industrial three-dimensional metal additive manufacturing using electrochemical polishing.* International Journal of Precision Engineering and Manufacturing-Green Technology, 2019. **6**(1): p. 11-21.
[131] Ambrosi, A. and M. Pumera, *3D-printing technologies for electrochemical applications.* Chemical Society Reviews, 2016. **45**(10): p. 2740-2755.
[132] News, M. *ZEISS and EOS Collaborate In Metal Powder Bed In-Process Monitoring*. 2021 [cited 2021; Available from: https://metrology.news/zeiss-and-eos-collaborate-in-metal-powder-bed-in-process-monitoring/.
[133] News, M. *Renishaw Expand CMM Software Offering with Verisurf*. 2021; Available from: https://metrology.news/renishaw-announces-expanded-cmm-software-offering-with-verisurf-agreement/.
[134] Çakır, O. *Study of etch rate and surface roughness in chemical etching of stainless steel*. in *Key Engineering Materials*. 2008. Trans Tech Publ.

APPENDIX

APPENDIX A – CHAPTER 3 PARTS IN IN-SITU MONITORING SYSTEM

8.1.1 FINAL DESIGN HARDWARE

Imaging System Electronics and Hardware List

Hardware	Illustration	Product Specifications	Design Specifications	Custom SS Mounts
Digital Camera		Raspberry Pi High Resolution Camera with a Sony IMx477R stacked, back-illuminated sensor. 12.3 megapixels, 7.9mm sensor diagonal (1.55µm x 1.55µm pixel size).	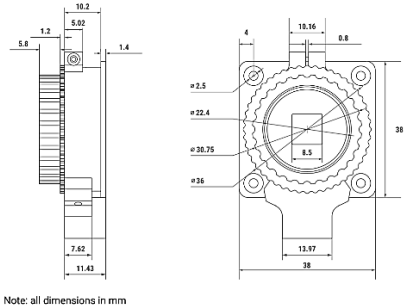	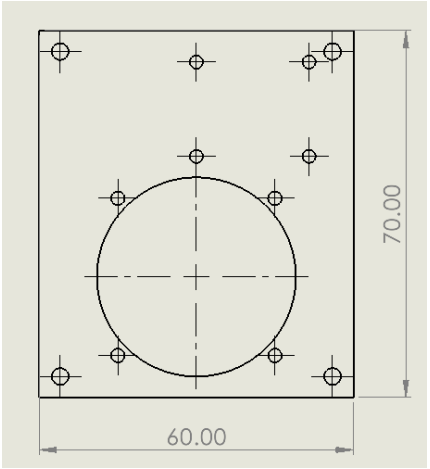
Camera Lens		Raspberry Pi 16mm 10MP Telephoto lens with a C or CS-mount	Dimensions: 39mmx50mm	
Thermal Sensor		FLIR Radiometric Lepton 2.5 with the Pure Thermal 2 breakout board.	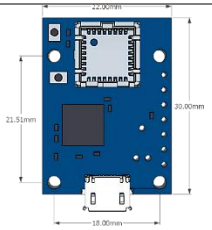	

Linear Actuator		Instant Panel – Linear Actuator 100mm Stroke 12V 20mm/s with a 60kg LFHB	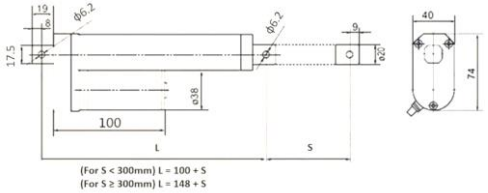	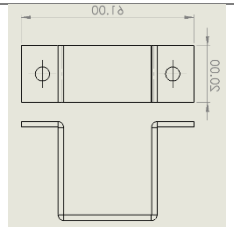
Raspberry Pi		Raspberry Pi 4B+ with 4GB RAM and in-built WIFI	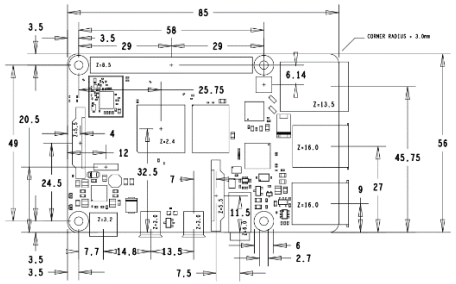	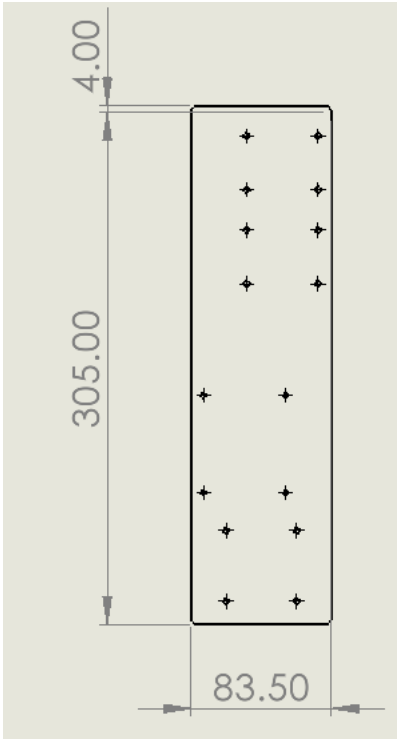
Relays		Relay Module 2 Channel Isolated 3.3V or 5V input	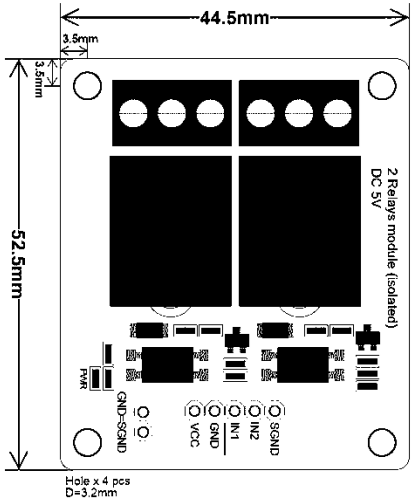	

PCB	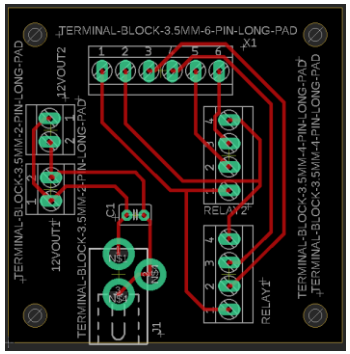	Custom PCB with terminal blocks to connect	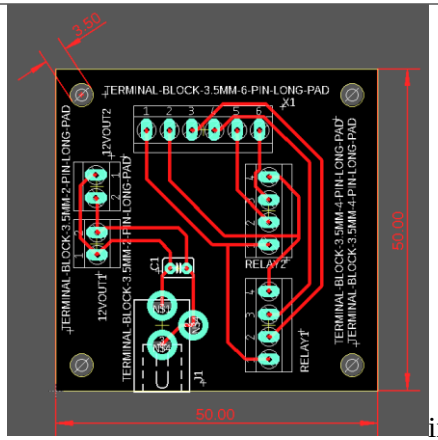 in mm
Halogen Lamps		OSRAM Halogen Lamp (25W, 30W and 50W)	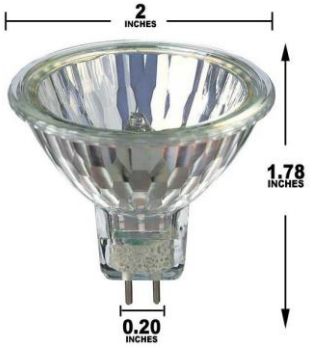

APPENDIX B – CHAPTER 4 – LASER POLISHING RESULTS

Tablature Results for vertically built samples, effect of polishing the outline of the −V samples

Ref.	Laser Power (%)	Spacing (um)	Repetition	Surface Roughness Ra (um)	Surface Roughness Rz (um)	Surface Roughness RSm (um)	Hardness (HV)	Layer Thickness (µm)
		ORIGINAL		11.88	73.4306	0.21055	342.84	51
T1	60	100	1	14.097	79.5903	0.230833	323.520	52
T2	60	500	3	11.6963	68.4341	0.213500	304.180	46
T3	60	1000	5	10.6056	63.9281	0.214556	331.080	49
T4	70	100	3	12.3804	71.0264	0.262389	339.267	47
T5	70	500	5	11.0817	65.9919	0.246222	377.500	50
T6	70	1000	1	11.0323	63.7971	0.228111	387.500	49
T7	80	100	5	13.3764	76.4755	0.219778	391.400	44
T8	80	500	1	11.6984	72.8696	0.228167	371.800	51
T9	80	1000	3	12.7503	77.0398	0.232167	364.200	52

Tablature Results for 20-degree angled samples, effect of polishing the outline of the ∠A20 samples

Ref.	Laser Power (%)	Spacing (um)	Repetition	Surface Roughness Ra (um)	Surface Roughness Rz (um)	Surface Roughness RSm (um)	Hardness (HV)	Layer Thickness (µm)
		ORIGINAL		15.06204	87.7908	0.294250	331.06	103
T1	60	100	1	15.06204	87.79088	0.29425	355.500	101
T2	60	500	3	14.23529	86.06896	0.297292	377.400	88
T3	60	1000	5	15.50587	94.05521	0.335708	357.700	46
T4	70	100	3	15.30538	90.24492	0.358208	334.840	56
T5	70	500	5	16.109	95.8115	0.344458	298.720	55
T6	70	1000	1	14.82025	89.55021	0.326958	344.200	43
T7	80	100	5	14.86304	88.57529	0.316917	318.904	72
T8	80	500	1	16.8495	101.5579	0.37525	371.840	47
T9	80	1000	3	15.45125	87.9265	0.370083	367.120	45

Tablature Results for 40-degree angled samples, effect of polishing the outline of the ∠A40 samples

Ref.	Laser Power (%)	Spacing (um)	Repetition	Surface Roughness Ra (um)	Surface Roughness Rz (um)	Surface Roughness RSm (um)	Hardness (HV)	Layer Thickness (µm)
		ORIGINAL		13.001	81.3319	0.254666	329.58	69
T1	60	100	1	16.7337	100.457	0.321000	318.60	60
T2	60	500	3	18.5824	105.256	0.328792	346.40	51
T3	60	1000	5	17.2065	100.507	0.333458	328.92	51
T4	70	100	3	18.7848	101.738	0.370042	328.02	42
T5	70	500	5	16.7558	98.983	0.328542	304.06	40
T6	70	1000	1	17.1859	105.102	0.347375	335.74	46
T7	80	100	5	16.9460	96.695	0.322375	333.30	45
T8	80	500	1	19.9575	106.451	0.339417	318.52	49
T9	80	1000	3	14.7991	88.810	0.290458	315.10	38

Tablature Results for 60-degree angled samples, effect of polishing the outline of the ∠A60 samples

Ref.	Laser Power (%)	Spacing (um)	Repetition	Surface Roughness Ra (um)	Surface Roughness Rz (um)	Surface Roughness RSm (um)	Hardness (HV)	Layer Thickness (µm)
	ORIGINAL			11.9392	78.44062	0.2334	323.9	50
T1	60	100	1	17.4327	100.004	0.303583	325.887	48
T2	60	500	3	13.2644	82.134	0.273792	311.600	43
T3	60	1000	5	14.0120	83.957	0.286750	317.950	45
T4	70	100	3	19.9465	107.267	0.326375	371.050	41
T5	70	500	5	14.6378	90.578	0.305833	333.300	43
T6	70	1000	1	14.3846	90.697	0.283333	344.000	45
T7	80	100	5	22.6677	116.497	0.398333	334.925	50
T8	80	500	1	14.9170	92.036	0.286708	328.000	46
T9	80	1000	3	13.4075	85.298	0.262958	332.450	46

Tablature Results for 80-degree angled samples, effect of polishing the outline of the ∠A80 samples

Ref.	Laser Power (%)	Spacing (um)	Repetition	Surface Roughness Ra (um)	Surface Roughness Rz (um)	Surface Roughness RSm (um)	Hardness (HV)	Layer Thickness (µm)
	ORIGINAL			12.51033	74.98329	0.249166	338.325	45
T1	60	100	1	14.7767	85.1962	0.252833	334.550	40
T2	60	500	3	10.4206	69.1894	0.219917	331.100	34
T3	60	1000	5	10.7414	69.0885	0.229542	330.825	37
T4	70	100	3	14.3392	86.4083	0.227875	353.800	38
T5	70	500	5	10.8223	69.5266	0.212792	357.075	39
T6	70	1000	1	10.8146	72.0625	0.228083	351.550	40
T7	80	100	5	15.0978	84.8689	0.235750	340.100	37
T8	80	500	1	10.9875	72.8648	0.225375	308.975	38
T9	80	1000	3	11.8020	74.3602	0.236333	327.315	39

Tablature Results for inner cylindrical samples build vertically, effect polishing the outline for a circular profile – IC samples

Ref.	Laser Power (%)	Spacing (um)	Repetition	Surface Roughness Ra (um)	Surface Roughness Rz (um)	Surface Roughness RSm (um)
	ORIGINAL			10.57817	68.52967	0.198333
T1	60	100	1	11.32167	72.59933	0.209167
T2	60	500	3	11.35417	69.93767	0.208833
T3	60	1000	5	15.14133	86.64783	0.291167
T4	70	100	3	14.2525	86.49533	0.258333
T5	70	500	5	12.75733	77.303	0.251167
T6	70	1000	1	12.36133	78.25	0.232833
T7	80	100	5	11.77033	76.22066	0.238167
T8	80	500	1	12.30583	75.88217	0.235333
T9	80	1000	3	13.66783	84.79717	0.256667

Main Effects Plots for Mean Data Means and SN ration Data means with respect to Ra

	Main Effects Plot for Mean Data Means	Main Effects Plot for SN ratios Data Means
-V	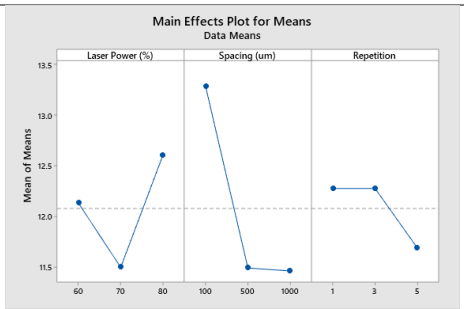	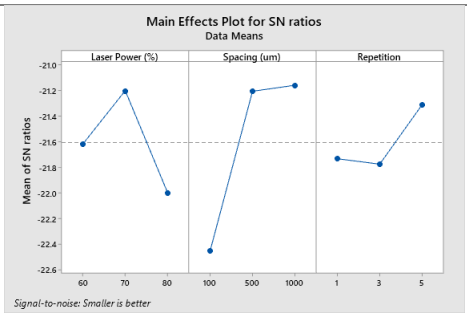
∠A20		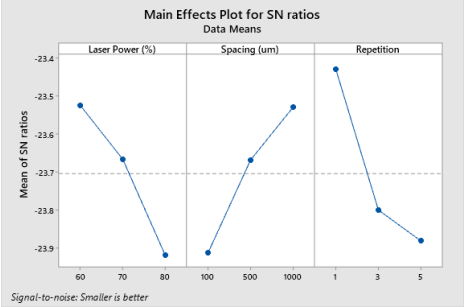
∠A40		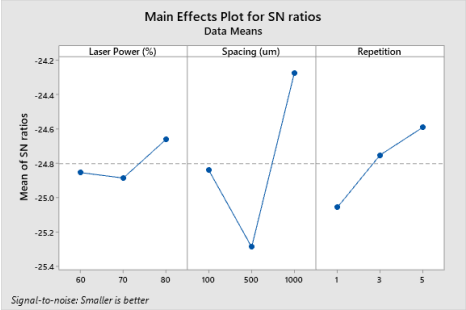
∠A60	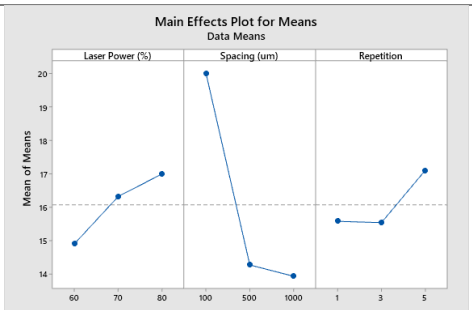	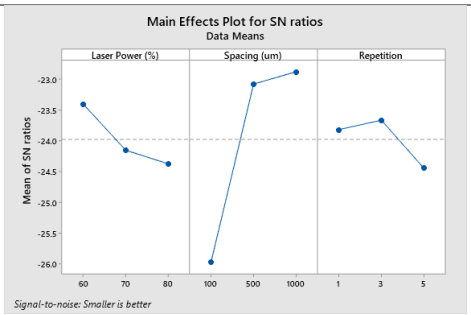
∠A80	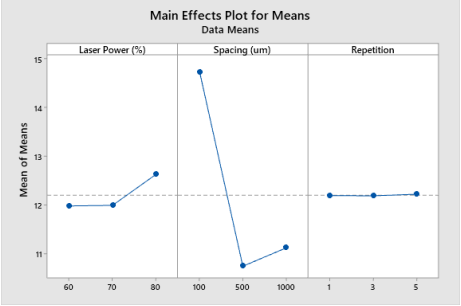	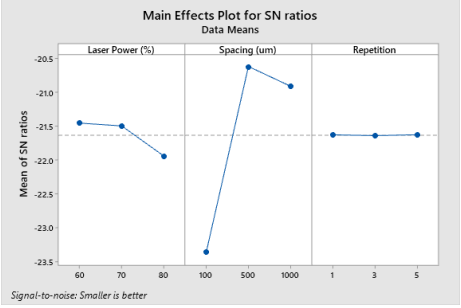

Main Effects Plots for Mean Data Means and SN ration Data means with respect to Rz

	Main Effects Plot for Mean Data Means	Main Effects Plot for SN ratios Data Means
-V	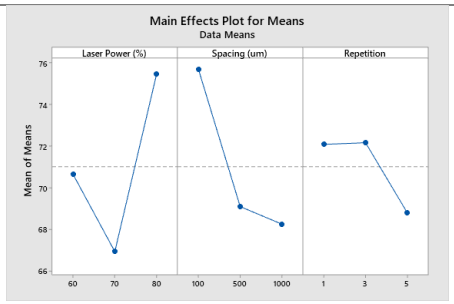	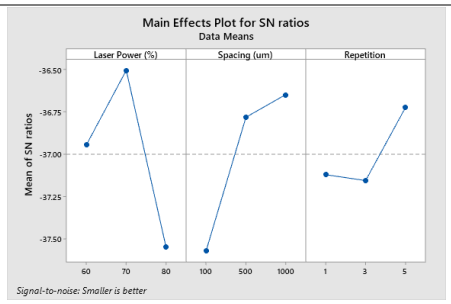
∠A20	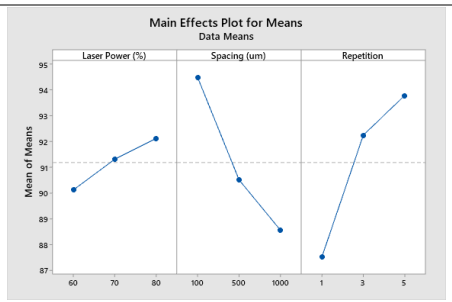	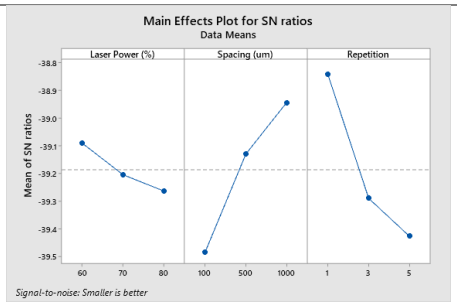
∠A40	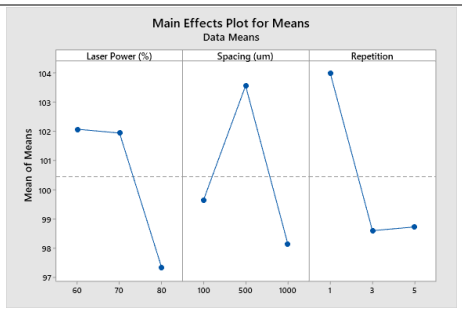	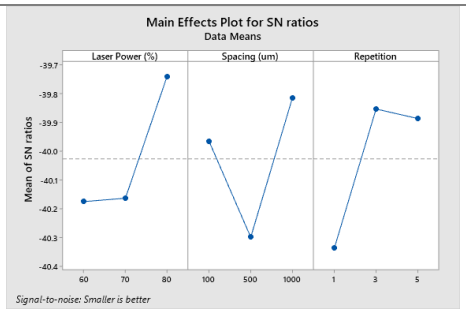
∠A60	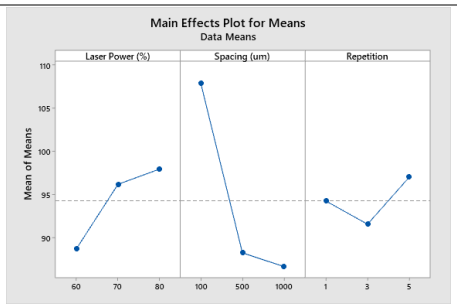	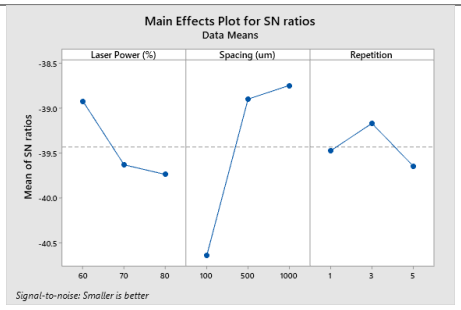
∠A80	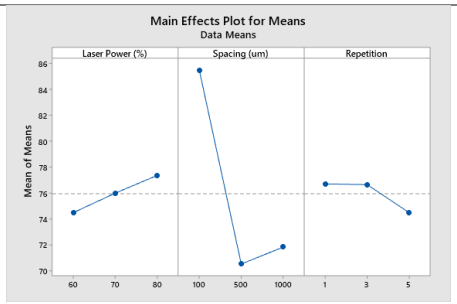	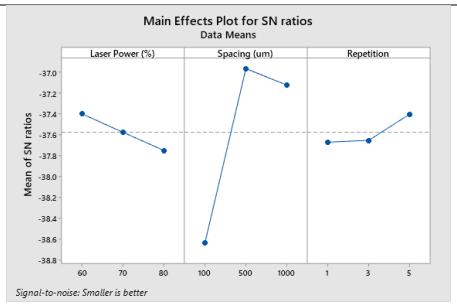

Main Effects Plots for Mean Data Means and SN ration Data means with respect to Mechanical Hardness

	Main Effects Plot for Mean Data Means	Main Effects Plot for SN ratios Data Means
-V	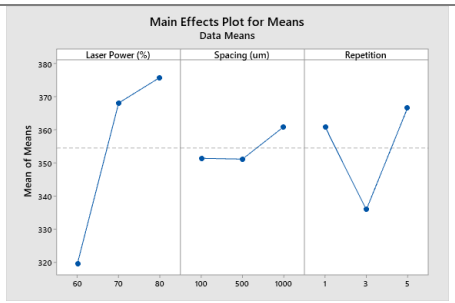	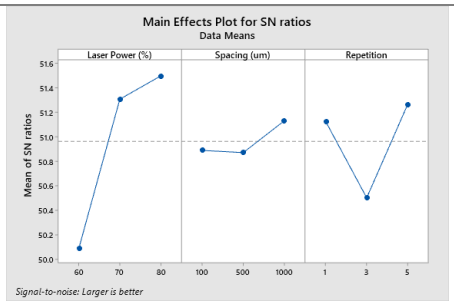
∠A20	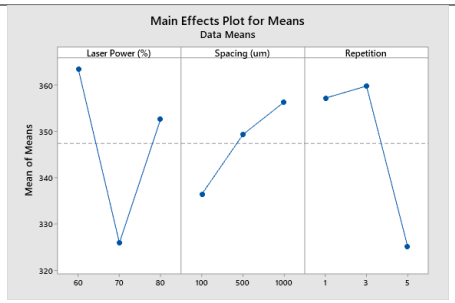	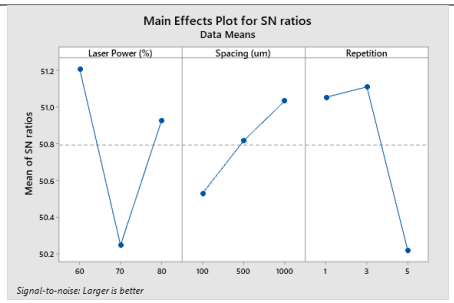
∠A40	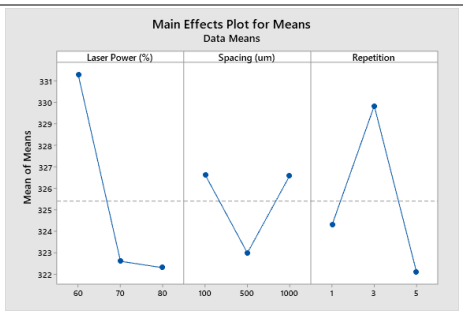	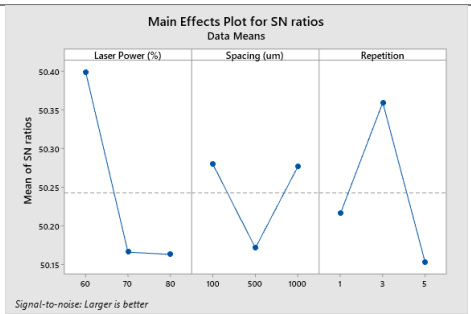
∠A60	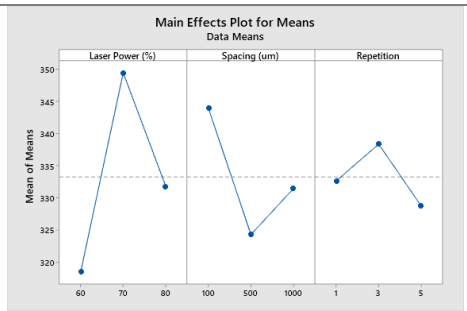	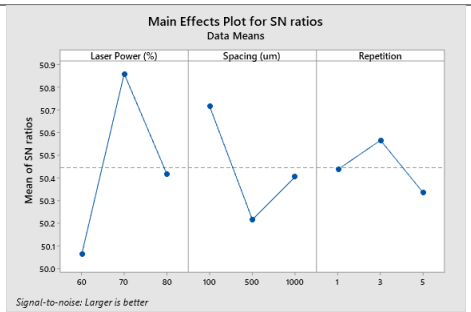
∠A80	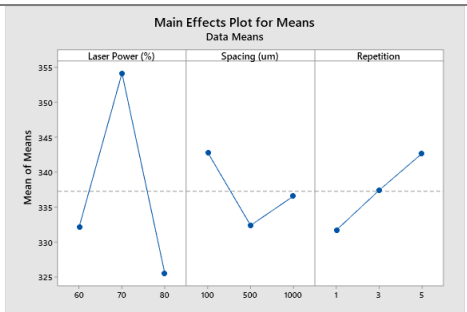	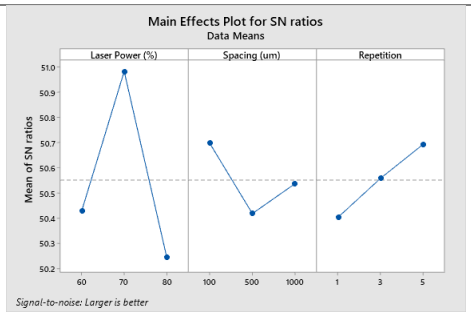

Statistical representation of the relationship between laser power, laser speed and polishing iterations on the Ra and Rz outputs for each sample type

Interaction Plots		
	Ra	**Rz**
-V	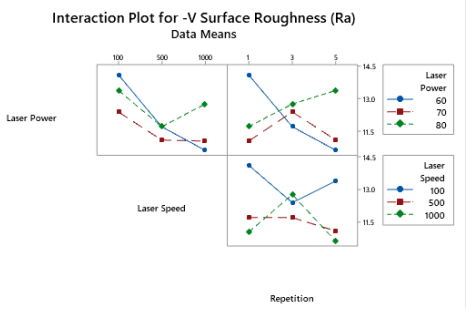	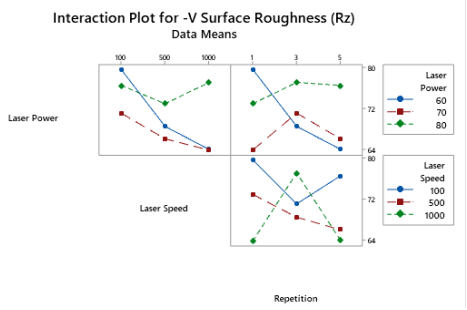
∠A20	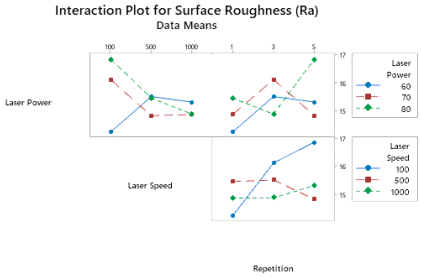	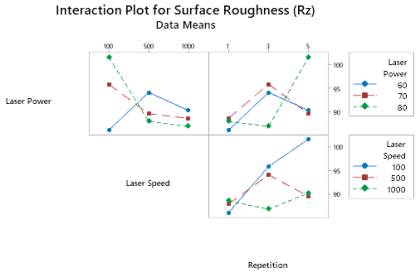
∠A40	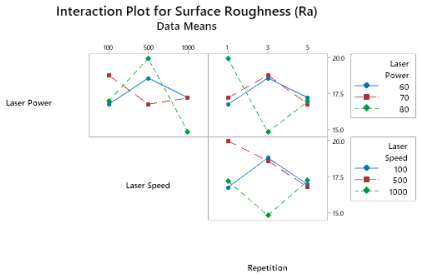	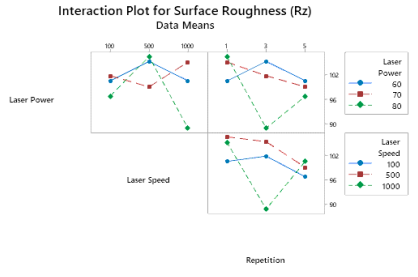
∠A60	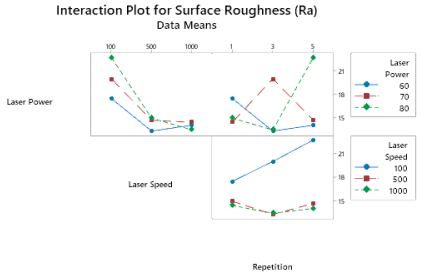	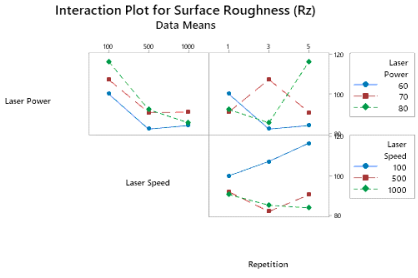

APPENDIX C – CHAPTER 3 – CODE DEVELOPED FOR IN-SITU MONITORING GUIS AND IMAGE PROCESSING

Code developed in Visual Studio 2019 using python 3 and OpenCV

Digital Camera GUI:

```
from PyQt5 import QtWidgets as qtw
from PyQt5 import QtCore as qtc
from PyQt5 import QtGui as qtg
from PyQt5 import uic
print('Successful import of uic') #often reinstallation of PyQt5 is required


from PyQt5.QtCore import (QCoreApplication, QThread, QThreadPool, pyqtSignal, pyqtSlot, Qt, QTimer,
QDateTime)
from PyQt5.QtGui import (QImage, QPixmap, QTextCursor)
from PyQt5.QtWidgets import (QWidget, QMainWindow, QApplication, QLabel, QPushButton, QVBoxLayout,
QGridLayout, QSizePolicy, QMessageBox, QFileDialog, QSlider, QComboBox, QProgressDialog)
from picamera.array import PiRGBArray
from picamera import PiCamera
import sys
import os.path
import cv2
from tifffile import imsave
import numpy as np
import RPi.GPIO as GPIO
import h5py
import time
import psutil
from multiprocessing  import Queue
import threading
from subprocess import call

print('Loaded Packages and Starting Pi Camera Data...')
GPIO.setmode(GPIO.BCM)
pinList = [2, 3, 17, 27]
qtCreatorFile = "digCam.ui"  # Enter file here.
postScriptfilePathDisp = "PostProcessDig.py"
camera = PiCamera()
time.sleep(0.1)
camera.resolution = (1280,1080)
camera.framerate = 30
rawCapture = PiRGBArray(camera, size=(1280, 1080))
Dig_Capture, baseClass = uic.loadUiType(qtCreatorFile)

def getFrame():
    global tiff_frame
    global camState
    global maxVal
    global minVal
    data = rawCapture
    if data is None:
        print('No Data')
    if camState == 'recording':

        camera.create_dataset(('image'+str(tiff_frame)), data=data)
        tiff_frame += 1
    #Cannot you cv2.resize on raspberry pi 3b+. Not enough processing power.
    #data = cv2.resize(data[:,:], (640, 480))

    img = cv2.LUT(raw_to_8bit(data), generate_colour_map())

    return img
class ThreadDig(qtc.QThread):

    changePixmap = qtc.pyqtSignal(qtg.QImage)

    def run(self):
        for frame in camera.capture_continuous(rawCapture, format="bgr", use_video_port=True):
            # grab the raw NumPy array representing the image, then initialize the timestamp
            # and occupied/unoccupied text
            image = frame.array
            # show the frame
            #cv2.imshow("Frame", rgbimage)
            # clear the stream in preparation for the next frame
            rgbImage = cv2.cvtColor(image, cv2.COLOR_BGR2RGB)
            h, w, ch = rgbImage.shape
            bytesPerLine = ch * w
            convertToQtFormat = qtg.QImage(rgbImage.data, w, h, bytesPerLine,
qtg.QImage.Format_RGB888)
            p = convertToQtFormat.scaled(640, 480, qtc.Qt.KeepAspectRatio)
            self.changePixmap.emit(p)
            rawCapture.truncate(0)

thread = "unactive"
saveFilePath = ""
```

```
fileNamingFull = ""
fileNamingFull1 = ""
bFile = ""
camState = 'not_recording'
tiff_frame = 1

class MainWindow(baseClass):

    def __init__(self, *args, **kwargs):

        super().__init__(*args, **kwargs)
        self.ui = Dig_Capture()
        self.ui.setupUi(self)
        global fileNamingFull
        self.ui.startRec.clicked.connect(self.startRec2)
        self.ui.stopRec.clicked.connect(self.stopRecAndSave)
        self.ui.startRec.clicked.connect(self.displayRec)
        self.ui.stopRec.clicked.connect(self.displayNotRec)
        self.ui.startStreamBut.clicked.connect(self.StartStream)
        self.ui.brightness.currentTextChanged.connect(self.setBrightness)
        self.ui.contrast.currentTextChanged.connect(self.setContrast)
        self.ui.img_effect.currentTextChanged.connect(self.setImgEffect)
        self.ui.img_exp.currentTextChanged.connect(self.setImgExp)
        self.ui.ActuateIn.clicked.connect(self.ActuateIn)
        self.ui.ActuateOut.clicked.connect(self.ActuateOut)
        self.ui.LampOn.clicked.connect(self.LampOn)
        self.ui.LampOff.clicked.connect(self.LampOff)
        self.ui.framerate.currentTextChanged.connect(self.setFramerate)
        self.ui.img_wht_bal.currentTextChanged.connect(self.setWhiteBal)
        self.ui.img_capture.clicked.connect(self.imageCap)
        defaultName = 'DIG_H624'
        fileNamingFull = defaultName
        self.ui.fileName.setText(defaultName)
        self.ui.fileName.textChanged.connect(self.fileNaming)
        self.ui.w = QWidget()
        self.ui.filePathBut.clicked.connect(self.getFiles)

    def LampOn(self):
        GPIO.setmode(GPIO.BCM)
            # init list with pin numbers
        pinList1 = [17, 27]
        # loop through pins and set mode and state to 'high'
        for i in pinList1:
            GPIO.setup(i, GPIO.OUT)
            GPIO.output(i, GPIO.HIGH)
        try:
            GPIO.output(27, GPIO.LOW)
            GPIO.output(17, GPIO.HIGH)
            print ("Halogen Lamp ON")
        except KeyboardInterrupt:
            print ("  Quit")
            # Reset GPIO settings
            GPIO.cleanup()
    def LampOff(self):
        GPIO.setmode(GPIO.BCM)
            # init list with pin numbers
        pinList1 = [17, 27]
        # loop through pins and set mode and state to 'high'
        for i in pinList1:
            GPIO.setup(i, GPIO.OUT)
            GPIO.output(i, GPIO.HIGH)
        GPIO.output(27, GPIO.HIGH)
        GPIO.output(17, GPIO.LOW)
        print ("Halogen Lamp OFF")
        GPIO.cleanup()
    def ActuateOut(self):
        GPIO.cleanup()
        GPIO.setmode(GPIO.BCM)
            # init list with pin numbers
        pinList1 = [2, 3]
        # loop through pins and set mode and state to 'high'
        for i in pinList1:
            GPIO.setup(i, GPIO.OUT)
            GPIO.output(i, GPIO.HIGH)
        try:
            GPIO.output(2, GPIO.LOW)
            GPIO.output(3, GPIO.HIGH)
            print ("Actuated out - camera in laser range")
        except KeyboardInterrupt:
            print ("  Quit")
            # Reset GPIO settings


    def ActuateIn(self):
        GPIO.cleanup()
        GPIO.setmode(GPIO.BCM)
            # init list with pin numbers
        pinList1 = [2, 3]
        # loop through pins and set mode and state to 'high'
        for i in pinList1:
            GPIO.setup(i, GPIO.OUT)
            GPIO.output(i, GPIO.HIGH)
        GPIO.output(2, GPIO.HIGH)
        GPIO.output(3, GPIO.LOW)
        print ("Actuated camera system in - camera out of laser range")
    def startRec2(self):
        global thread
        global camState
        global saveFilePath
        global fileNamingFull
```

```
        if thread == 'active':
            if camState == 'recording':
                print('Already Recording')
            else:
                if fileNamingFull != "":
                    dateAndTime = str(QDateTime.currentDateTime().toString())
                    dateAndTime = dateAndTime.replace(" ", "_")
                    dateAndTime = dateAndTime.replace(":", "-")
                    filePathAndName = str(fileNamingFull + '_' + dateAndTime)
                    print(filePathAndName)
                    self.ui.filePathDisp.setText(filePathAndName)
                    try:
                        camera.start_recording(filePathAndName, format='h264')
                        camState = 'recording'
                        print('Started Recording')
                        if saveFilePath == "":
                            self.ui.history.insertPlainText('Saved ' + str(filePathAndName) + ' to '
+ os.path.dirname(os.path.abspath(__file__)) + '\n')
                            self.ui.history.moveCursor(QTextCursor.End)
                        else:
                            self.ui.history.insertPlainText('Saved to ' + str(filePathAndName) +
'\n')
                            self.ui.history.moveCursor(QTextCursor.End)
                    except:
                        print('Incorrect File Path')
                        camState = 'not_recording'
                        print('Did Not Begin Recording')
                else:
                    print('No FileName Specified')
        else:
            print('Remember to Start Stream')
            self.ui.history.insertPlainText('Remember to Start Stream\n')
            self.ui.history.moveCursor(QTextCursor.End)
    def displayRec(self):
        if camState == 'recording':
            self.ui.recLabel.setText('Recording')
        else:
            self.ui.recLabel.setText('Not Recording')

    def displayNotRec(self):
        if camState == 'not_recording':
            self.ui.recLabel.setText('Not Recording')
        else:
            self.ui.recLabel.setText('Recording')
    def stopRecAndSave(self):
        global fileNum
        global tiff_frame
        global camState
        global dataCollection
        if tiff_frame > 1:
            print('Ended Recording')
            camState = 'not_recording'
            try:
                camera.stop_recording()
                print('Saved Content to File Directory')
                #fileNum += 1
            except:
                print('Save Failed')
            tiff_frame = 1
        else:
            camState = 'not_recording'
            print('Dont Forget to Start Recording')
            self.ui.history.insertPlainText('Dont Forget to Start Recording\n')
            self.ui.history.moveCursor(QTextCursor.End)
    def setImageDig(self, image):
        self.ui.displayFrame.setPixmap(qtg.QPixmap.fromImage(image))
    def setBrightness(self,value):
        value = self.ui.brightness.currentText()
        print("Brightness is set to")
        print (int(value))
        camera.brightness = int(value)
    def setContrast(self,value):
        value = self.ui.contrast.currentText()
        print("Contrast is set to")
        print (int(value))
        camera.contrast = int(value)

    def setFramerate(self,value):
        value = self.ui.framerate.currentText()
        print = (int(value))
        camera.framerate = int(value)
    def setImgEffect(self,value):
        value = self.ui.img_effect.currentText()
        print("Image effect is set to")
        print (value)
        camera.image_effect = value
    def setImgExp(self,value):
        value = self.ui.img_exp.currentText()
        print("Image exposure is set to")
        print (value)
        camera.image_exposure = value
    def setWhiteBal(self,value):
        value = self.ui.img_wht_bal.currentText()
        print("Image white balance is set to")
        print (value)
        camera.awb_mode = value
    def StartStream(self):
        global thread
        try:
            if thread == "unactive":
```

```
                try:

                    th = ThreadDig(self)
                    th.changePixmap.connect(self.setImageDig)
                    th.start()
                    thread = "active"
                    print('Starting Thread')
                except:
                    print('Failed!!!!')
                    exit(1)
            else:
                print('Already Started Camera')
        except:
            msgBox = QMessageBox()
            reply = msgBox.question(self, 'Message', "Error Starting Camera - Plug or Re-Plug Camera
into Computer, Wait at Least 10 Seconds, then Click Ok and Try Again.", QMessageBox.Ok)
            print('Message Box Displayed')
            if reply == QMessageBox.Ok:
                print('Ok Clicked')
            else:
                event.ignore()

    def fileNaming(self):
        global fileNamingFull
        bFile = str(self.ui.fileName.text())
        if saveFilePath == "":
            fileNamingFull = bFile
            self.ui.filePathDisp.setText('/' + bFile + ' ... Date & Time Will Append at Recording
Start')
        elif saveFilePath != "":
            fileNamingFull = saveFilePath + '/' + bFile
            self.ui.filePathDisp.setText(saveFilePath + '/' + bFile + ' ... Date & Time Will Append
at Recording Start')
        else:
            print('I am Confused')
    def getFiles(self):
        global saveFilePath
        saveFilePath = QFileDialog.getExistingDirectory(self.ui.w, 'Open File Directory', '/')
        self.ui.filePathDisp.setText(saveFilePath)
        self.fileNaming()
    def imageCap(self):
        global thread

        global saveFilePath
        global fileNamingFull
        if thread == 'active':

            if fileNamingFull != "":
                dateAndTime = str(QDateTime.currentDateTime().toString())
                dateAndTime = dateAndTime.replace(" ", "_")
                dateAndTime = dateAndTime.replace(":", "_")
                filePathAndName = str(fileNamingFull + '_' + dateAndTime)
                print(filePathAndName)
                self.ui.filePathDisp.setText(filePathAndName)
                try:
                    camera.capture(filePathAndName + '.jpg')
                    print('Picture Captured')
                    if saveFilePath == "":
                        self.ui.history.insertPlainText('Saved ' + str(filePathAndName) + ' to ' +
os.path.dirname(os.path.abspath(__file__)) + '\n')
                        self.ui.history.moveCursor(QTextCursor.End)
                    else:
                        self.ui.history.insertPlainText('Saved to ' + str(filePathAndName) + '\n')
                        self.ui.history.moveCursor(QTextCursor.End)
                except:
                    print('Incorrect File Path')

            else:
                print('No FileName Specified')
        else:
            print('Remember to Start Stream')
            self.ui.history.insertPlainText('Remember to Start Stream\n')
            self.ui.history.moveCursor(QTextCursor.End)



    def closeEvent(self, event):
        print("Close Event Called")
        if camState == 'recording':
            reply = QMessageBox.question(self, 'Message', "Recording still in progress. Are you sure
you want to quit?", QMessageBox.Yes, QMessageBox.No)
            print('Message Box Displayed')
            if reply == QMessageBox.Yes:
                print('Exited Application, May Have Lost Raw Data')
                event.accept()
            else:
                event.ignore()
        else:
            print('Exited Application')
            event.accept()

if __name__ == "__main__":
    app = qtw.QApplication([])
    widget = MainWindow()
    widget.show()
    sys.exit(app.exec_())
```

Thermal Sensor code:

```
#!/usr/bin/env python3
# Author: Karl Parks, 2018

from PyQt5 import QtCore, QtGui, uic
print('Successful import of uic') #often reinstallation of PyQt5 is required

from PyQt5.QtCore import (QCoreApplication, QThread, QThreadPool, pyqtSignal, pyqtSlot, Qt, QTimer, QDateTime)
from PyQt5.QtGui import (QImage, QPixmap, QTextCursor)
from PyQt5.QtWidgets import (QWidget, QMainWindow, QApplication, QLabel, QPushButton, QVBoxLayout, QGridLayout,
QSizePolicy, QMessageBox, QFileDialog, QSlider, QComboBox, QProgressDialog)

import sys
import os.path
import cv2
from tifffile import imsave
import numpy as np
import h5py
import time
import psutil
from uvctypesParabilis_v2 import *
from multiprocessing  import Queue
import threading
from subprocess import call
import RPi.GPIO as GPIO
print('Loaded Packages and Starting IR Data...')

qtCreatorFile = "ir_v11.ui"  # Enter file here.
postScriptFileName = "PostProcessIR_v11.py"

Ui_MainWindow, QtBaseClass = uic.loadUiType(qtCreatorFile)

BUF_SIZE = 2
q = Queue(BUF_SIZE)
colorMapType = 0

def py_frame_callback(frame, userptr):
    array_pointer = cast(frame.contents.data, POINTER(c_uint16 * (frame.contents.width * frame.contents.height)))
    data = np.frombuffer(
        array_pointer.contents, dtype=np.dtype(np.uint16)).reshape(frame.contents.height, frame.contents.width)
    if frame.contents.data_bytes != (2 * frame.contents.width * frame.contents.height):
        return
    if not q.full():
        q.put(data)

PTR_PY_FRAME_CALLBACK = CFUNCTYPE(None, POINTER(uvc_frame), c_void_p)(py_frame_callback)

def generate_colour_map():
    """
    Conversion of the colour map from GetThermal to a numpy LUT:

https://github.com/groupgets/GetThermal/blob/bb467924750a686cc3930f7e3a253818b755a2c0/src/dataformatter.cpp#L6
    """

    lut = np.zeros((256, 1, 3), dtype=np.uint8)

    #colorMaps
    colormap_grayscale = [0, 0, 0, 1, 1, 1, 2, 2, 2, 3, 3, 3, 4, 4, 4, 5, 5, 5, 6, 6, 6, 7, 7, 7, 8, 8, 8, 9, 9, 9,
10, 10, 10, 11, 11, 11, 12, 12, 12, 13, 13, 13, 14, 14, 14, 15, 15, 15, 16, 16, 16, 17, 17, 17, 18, 18, 18, 19, 19,
19, 20, 20, 20, 21, 21, 21, 22, 22, 22, 23, 23, 23, 24, 24, 24, 25, 25, 25, 26, 26, 26, 27, 27, 27, 28, 28, 28, 29,
29, 29, 30, 30, 30, 31, 31, 31, 32, 32, 32, 33, 33, 33, 34, 34, 34, 35, 35, 35, 36, 36, 36, 37, 37, 37, 38, 38, 38,
39, 39, 39, 40, 40, 40, 41, 41, 41, 42, 42, 42, 43, 43, 43, 44, 44, 44, 45, 45, 45, 46, 46, 46, 47, 47, 47, 48, 48,
48, 49, 49, 49, 50, 50, 50, 51, 51, 51, 52, 52, 52, 53, 53, 53, 54, 54, 54, 55, 55, 55, 56, 56, 56, 57, 57, 57, 58,
58, 58, 59, 59, 59, 60, 60, 60, 61, 61, 61, 62, 62, 62, 63, 63, 63, 64, 64, 64, 65, 65, 65, 66, 66, 66, 67, 67, 67,
68, 68, 68, 69, 69, 69, 70, 70, 70, 71, 71, 71, 72, 72, 72, 73, 73, 73, 74, 74, 74, 75, 75, 75, 76, 76, 76, 77, 77,
77, 78, 78, 78, 79, 79, 79, 80, 80, 80, 81, 81, 81, 82, 82, 82, 83, 83, 83, 84, 84, 84, 85, 85, 85, 86, 86, 86, 87,
87, 87, 88, 88, 88, 89, 89, 89, 90, 90, 90, 91, 91, 91, 92, 92, 92, 93, 93, 93, 94, 94, 94, 95, 95, 95, 96, 96, 96,
97, 97, 97, 98, 98, 98, 99, 99, 99, 100, 100, 100, 101, 101, 101, 102, 102, 102, 103, 103, 103, 104, 104, 104, 105,
105, 105, 106, 106, 106, 107, 107, 107, 108, 108, 108, 109, 109, 109, 110, 110, 110, 111, 111, 111, 112, 112, 112,
113, 113, 113, 114, 114, 114, 115, 115, 115, 116, 116, 116, 117, 117, 117, 118, 118, 118, 119, 119, 119, 120, 120,
120, 121, 121, 121, 122, 122, 122, 123, 123, 123, 124, 124, 124, 125, 125, 125, 126, 126, 126, 127, 127, 127, 128,
128, 128, 129, 129, 129, 130, 130, 130, 131, 131, 131, 132, 132, 132, 133, 133, 133, 134, 134, 134, 135, 135, 135,
136, 136, 136, 137, 137, 137, 138, 138, 138, 139, 139, 139, 140, 140, 140, 141, 141, 141, 142, 142, 142, 143, 143,
143, 144, 144, 144, 145, 145, 145, 146, 146, 146, 147, 147, 147, 148, 148, 148, 149, 149, 149, 150, 150, 150, 151,
151, 151, 152, 152, 152, 153, 153, 153, 154, 154, 154, 155, 155, 155, 156, 156, 156, 157, 157, 157, 158, 158, 158,
159, 159, 159, 160, 160, 160, 161, 161, 161, 162, 162, 162, 163, 163, 163, 164, 164, 164, 165, 165, 165, 166, 166,
166, 167, 167, 167, 168, 168, 168, 169, 169, 169, 170, 170, 170, 171, 171, 171, 172, 172, 172, 173, 173, 173, 174,
174, 174, 175, 175, 175, 176, 176, 176, 177, 177, 177, 178, 178, 178, 179, 179, 179, 180, 180, 180, 181, 181, 181,
182, 182, 182, 183, 183, 183, 184, 184, 184, 185, 185, 185, 186, 186, 186, 187, 187, 187, 188, 188, 188, 189, 189,
189, 190, 190, 190, 191, 191, 191, 192, 192, 192, 193, 193, 193, 194, 194, 194, 195, 195, 195, 196, 196, 196, 197,
197, 197, 198, 198, 198, 199, 199, 199, 200, 200, 200, 201, 201, 201, 202, 202, 202, 203, 203, 203, 204, 204, 204,
205, 205, 205, 206, 206, 206, 207, 207, 207, 208, 208, 208, 209, 209, 209, 210, 210, 210, 211, 211, 211, 212, 212,
212, 213, 213, 213, 214, 214, 214, 215, 215, 215, 216, 216, 216, 217, 217, 217, 218, 218, 218, 219, 219, 219, 220,
220, 220, 221, 221, 221, 222, 222, 222, 223, 223, 223, 224, 224, 224, 225, 225, 225, 226, 226, 226, 227, 227, 227,
228, 228, 228, 229, 229, 229, 230, 230, 230, 231, 231, 231, 232, 232, 232, 233, 233, 233, 234, 234, 234, 235, 235,
235, 236, 236, 236, 237, 237, 237, 238, 238, 238, 239, 239, 239, 240, 240, 240, 241, 241, 241, 242, 242, 242, 243,
243, 243, 244, 244, 244, 245, 245, 245, 246, 246, 246, 247, 247, 247, 248, 248, 248, 249, 249, 249, 250, 250, 250,
251, 251, 251, 252, 252, 252, 253, 253, 253, 254, 254, 254, 255, 255, 255];

    colormap_rainbow = [1, 3, 74, 0, 3, 74, 0, 3, 75, 0, 3, 75, 0, 3, 76, 0, 3, 76, 0, 3, 77, 0, 3, 79, 0, 3, 82, 0,
5, 85, 0, 7, 88, 0, 10, 91, 0, 14, 94, 0, 19, 98, 0, 22, 100, 0, 25, 103, 0, 28, 106, 0, 32, 109, 0, 35, 112, 0, 38,
116, 0, 40, 119, 0, 42, 123, 0, 45, 128, 0, 49, 133, 0, 50, 134, 0, 51, 136, 0, 52, 137, 0, 53, 139, 0, 54, 142, 0,
55, 144, 0, 56, 145, 0, 58, 149, 0, 61, 154, 0, 63, 156, 0, 65, 159, 0, 66, 161, 0, 68, 164, 0, 69, 167, 0, 71, 170,
0, 73, 174, 0, 75, 179, 0, 76, 181, 0, 78, 184, 0, 79, 187, 0, 80, 188, 0, 81, 190, 0, 84, 194, 0, 87, 198, 0, 88,
200, 0, 90, 203, 0, 92, 205, 0, 94, 207, 0, 94, 208, 0, 95, 209, 0, 96, 210, 0, 97, 211, 0, 99, 214, 0, 102, 217, 0,
103, 218, 0, 104, 219, 0, 105, 220, 0, 107, 221, 0, 109, 223, 0, 111, 223, 0, 113, 223, 0, 115, 222, 0, 117, 221, 0,
118, 220, 1, 120, 219, 1, 122, 217, 2, 124, 216, 2, 126, 214, 3, 129, 212, 3, 131, 207, 4, 132, 205, 4, 133, 202, 4,
134, 197, 5, 136, 192, 6, 138, 185, 7, 141, 178, 8, 142, 172, 10, 144, 166, 10, 144, 162, 11, 145, 158, 12, 146, 153,
13, 147, 149, 15, 149, 140, 17, 151, 132, 22, 153, 120, 25, 154, 115, 28, 156, 109, 34, 158, 101, 40, 160, 94, 45,
162, 86, 51, 164, 79, 59, 167, 69, 67, 171, 60, 72, 173, 54, 78, 175, 48, 83, 177, 43, 89, 179, 39, 93, 181, 35, 98,
183, 31, 105, 185, 26, 109, 187, 23, 113, 188, 21, 118, 189, 19, 123, 191, 17, 128, 193, 14, 134, 195, 12, 138, 196,
10, 142, 197, 8, 146, 198, 6, 151, 200, 5, 155, 201, 4, 160, 203, 3, 164, 204, 2, 169, 205, 2, 173, 206, 1, 175, 207,
1, 178, 207, 1, 184, 208, 0, 190, 210, 0, 193, 211, 0, 196, 212, 0, 199, 212, 0, 202, 213, 1, 207, 214, 2, 212, 215,
3, 215, 214, 3, 218, 214, 3, 220, 213, 3, 222, 213, 4, 224, 212, 4, 225, 212, 5, 226, 212, 5, 229, 211, 5, 232, 211,
6, 232, 211, 6, 233, 211, 6, 234, 210, 6, 235, 210, 7, 236, 209, 7, 237, 208, 8, 239, 206, 8, 241, 204, 9, 242, 203,
9, 244, 202, 10, 244, 201, 10, 245, 200, 10, 245, 199, 11, 246, 198, 11, 247, 197, 12, 248, 194, 13, 249, 191, 14,
250, 189, 14, 251, 187, 15, 251, 185, 16, 252, 183, 17, 252, 178, 18, 253, 174, 19, 253, 171, 19, 254, 168, 20, 254,
165, 21, 254, 164, 21, 255, 163, 22, 255, 161, 22, 255, 159, 23, 255, 157, 23, 255, 155, 24, 255, 149, 25, 255, 143,
27, 255, 139, 28, 255, 135, 30, 255, 131, 31, 255, 127, 32, 255, 118, 34, 255, 110, 36, 255, 104, 37, 255, 101, 38,
255, 99, 39, 255, 93, 40, 255, 88, 42, 254, 82, 43, 254, 77, 45, 254, 69, 47, 254, 62, 49, 253, 57, 50, 253, 53, 52,
```

```
252, 49, 53, 252, 45, 55, 251, 39, 57, 251, 33, 59, 251, 32, 60, 251, 31, 60, 251, 30, 61, 251, 29, 61, 251, 28, 62,
250, 27, 63, 250, 27, 65, 249, 26, 66, 249, 26, 68, 248, 25, 70, 248, 24, 73, 247, 24, 75, 247, 25, 77, 247, 25, 79,
247, 26, 81, 247, 32, 83, 247, 35, 85, 247, 38, 86, 247, 42, 88, 247, 46, 90, 247, 50, 92, 248, 55, 94, 248, 59, 96,
248, 64, 98, 248, 72, 101, 249, 81, 104, 249, 87, 106, 250, 93, 108, 250, 95, 109, 250, 98, 110, 250, 100, 111, 251,
101, 112, 251, 102, 113, 251, 109, 117, 252, 116, 121, 252, 121, 123, 253, 126, 126, 253, 130, 128, 254, 135, 131,
254, 139, 133, 254, 144, 136, 254, 151, 140, 255, 158, 144, 255, 163, 146, 255, 168, 149, 255, 173, 152, 255, 176,
153, 255, 178, 155, 255, 184, 160, 255, 191, 165, 255, 195, 168, 255, 199, 172, 255, 203, 175, 255, 207, 179, 255,
211, 182, 255, 216, 185, 255, 218, 190, 255, 220, 196, 255, 222, 200, 255, 225, 202, 255, 227, 204, 255, 230, 206,
255, 233, 208]

    colourmap_ironblack = [
        255, 255, 255, 253, 253, 253, 251, 251, 251, 249, 249, 249, 247, 247,
        247, 245, 245, 245, 243, 243, 243, 241, 241, 241, 239, 239, 239, 237,
        237, 237, 235, 235, 235, 233, 233, 233, 231, 231, 231, 229, 229, 229,
        227, 227, 227, 225, 225, 225, 223, 223, 223, 221, 221, 221, 219, 219,
        219, 217, 217, 217, 215, 215, 215, 213, 213, 213, 211, 211, 211, 209,
        209, 209, 207, 207, 207, 205, 205, 205, 203, 203, 203, 201, 201, 201,
        199, 199, 199, 197, 197, 197, 195, 195, 195, 193, 193, 193, 191, 191,
        191, 189, 189, 189, 187, 187, 187, 185, 185, 185, 183, 183, 183, 181,
        181, 181, 179, 179, 179, 177, 177, 177, 175, 175, 175, 173, 173, 173,
        171, 171, 171, 169, 169, 169, 167, 167, 167, 165, 165, 165, 163, 163,
        163, 161, 161, 161, 159, 159, 159, 157, 157, 157, 155, 155, 155, 153,
        153, 153, 151, 151, 151, 149, 149, 149, 147, 147, 147, 145, 145, 145,
        143, 143, 143, 141, 141, 141, 139, 139, 139, 137, 137, 137, 135, 135,
        135, 133, 133, 133, 131, 131, 131, 129, 129, 129, 126, 126, 126, 124,
        124, 124, 122, 122, 122, 120, 120, 120, 118, 118, 118, 116, 116, 116,
        114, 114, 114, 112, 112, 112, 110, 110, 110, 108, 108, 108, 106, 106,
        106, 104, 104, 104, 102, 102, 102, 100, 100, 100, 98, 98, 98, 96, 96,
        96, 94, 94, 94, 92, 92, 92, 90, 90, 90, 88, 88, 88, 86, 86, 86, 84, 84,
        84, 82, 82, 82, 80, 80, 80, 78, 78, 78, 76, 76, 76, 74, 74, 74, 72, 72,
        72, 70, 70, 70, 68, 68, 68, 66, 66, 66, 64, 64, 64, 62, 62, 62, 60, 60,
        60, 58, 58, 58, 56, 56, 56, 54, 54, 54, 52, 52, 52, 50, 50, 50, 48, 48,
        48, 46, 46, 46, 44, 44, 44, 42, 42, 42, 40, 40, 40, 38, 38, 38, 36, 36,
        36, 34, 34, 34, 32, 32, 32, 30, 30, 30, 28, 28, 28, 26, 26, 26, 24, 24,
        24, 22, 22, 22, 20, 20, 20, 18, 18, 18, 16, 16, 16, 14, 14, 14, 12, 12,
        12, 10, 10, 10, 8, 8, 8, 6, 6, 6, 4, 4, 4, 2, 2, 2, 0, 0, 0, 0, 0, 9,
        2, 0, 16, 4, 0, 24, 6, 0, 31, 8, 0, 38, 10, 0, 45, 12, 0, 53, 14, 0,
        60, 17, 0, 67, 19, 0, 74, 21, 0, 82, 23, 0, 89, 25, 0, 96, 27, 0, 103,
        29, 0, 111, 31, 0, 118, 36, 0, 120, 41, 0, 121, 46, 0, 122, 51, 0, 123,
        56, 0, 124, 61, 0, 125, 66, 0, 126, 71, 0, 127, 76, 1, 128, 81, 1, 129,
        86, 1, 130, 91, 1, 131, 96, 1, 132, 101, 1, 133, 106, 1, 134, 111, 1,
        135, 116, 1, 136, 121, 1, 136, 125, 2, 137, 130, 2, 137, 135, 3, 137,
        139, 3, 138, 144, 3, 138, 149, 4, 138, 153, 4, 139, 158, 5, 139, 163,
        5, 139, 167, 5, 140, 172, 6, 140, 177, 6, 140, 181, 7, 141, 186, 7,
        141, 189, 10, 137, 191, 13, 132, 194, 16, 127, 196, 19, 121, 198, 22,
        116, 200, 25, 111, 203, 28, 106, 205, 31, 101, 207, 34, 95, 209, 37,
        90, 212, 40, 85, 214, 43, 80, 216, 46, 75, 218, 49, 69, 221, 52, 64,
        223, 55, 59, 224, 57, 49, 225, 60, 47, 226, 64, 44, 227, 67, 42, 228,
        71, 39, 229, 74, 37, 230, 78, 34, 231, 81, 32, 231, 85, 29, 232, 88,
        27, 233, 92, 24, 234, 95, 22, 235, 99, 19, 236, 102, 17, 237, 106, 14,
        238, 109, 12, 239, 112, 12, 240, 116, 12, 240, 119, 12, 241, 123, 12,
        241, 127, 12, 242, 130, 12, 242, 134, 12, 243, 138, 12, 243, 141, 13,
        244, 145, 13, 244, 149, 13, 245, 152, 13, 245, 156, 13, 246, 160, 13,
        246, 163, 13, 247, 167, 13, 247, 171, 13, 248, 175, 14, 248, 178, 15,
        249, 182, 16, 249, 185, 18, 250, 189, 19, 250, 192, 20, 251, 196, 21,
        251, 199, 22, 252, 203, 23, 252, 206, 24, 253, 210, 25, 253, 213, 27,
        254, 217, 28, 254, 220, 29, 255, 224, 30, 255, 227, 39, 255, 229, 53,
        255, 231, 67, 255, 233, 81, 255, 234, 95, 255, 236, 109, 255, 238, 123,
        255, 240, 137, 255, 242, 151, 255, 244, 165, 255, 246, 179, 255, 248,
        193, 255, 249, 207, 255, 251, 221, 255, 253, 235, 255, 255, 24]

    def chunk(
            ulist, step): return map(
        lambda i: ulist[i: i + step],
        range(0, len(ulist),
              step))
    if (colorMapType == 1):
        chunks = chunk(colormap_rainbow, 3)
    elif (colorMapType == 2):
        chunks = chunk(colormap_grayscale, 3)
    else:
        chunks = chunk(colourmap_ironblack, 3)

    red = []
    green = []
    blue = []

    for chunk in chunks:
        red.append(chunk[0])
        green.append(chunk[1])
        blue.append(chunk[2])

    lut[:, 0, 0] = blue

    lut[:, 0, 1] = green

    lut[:, 0, 2] = red

    return lut

def startStream():
  global devh
  ctx = POINTER(uvc_context)()
  dev = POINTER(uvc_device)()
  devh = POINTER(uvc_device_handle)()
  ctrl = uvc_stream_ctrl()

  res = libuvc.uvc_init(byref(ctx), 0)
  if res < 0:
    print("uvc_init error")
    #exit(1)

  try:
    res = libuvc.uvc_find_device(ctx, byref(dev), PT_USB_VID, PT_USB_PID, 0)
    if res < 0:
      print("uvc_find_device error")
      exit(1)

    try:
      res = libuvc.uvc_open(dev, byref(devh))
      if res < 0:
        print("uvc_open error")
        exit(1)

      print("device opened!")
```

```
      print_device_info(devh)
      print_device_formats(devh)

      frame_formats = uvc_get_frame_formats_by_guid(devh, VS_FMT_GUID_Y16)
      if len(frame_formats) == 0:
        print("device does not support Y16")
        exit(1)

      libuvc.uvc_get_stream_ctrl_format_size(devh, byref(ctrl), UVC_FRAME_FORMAT_Y16,
        frame_formats[0].wWidth, frame_formats[0].wHeight, int(1e7 / frame_formats[0].dwDefaultFrameInterval)
      )

      res = libuvc.uvc_start_streaming(devh, byref(ctrl), PTR_PY_FRAME_CALLBACK, None, 0)
      if res < 0:
        print("uvc_start_streaming failed: {0}".format(res))
        exit(1)

      print("done starting stream, displaying settings")
      print_shutter_info(devh)
      print("resetting settings to default")
      set_auto_ffc(devh)
      set_gain_high(devh)
      print("current settings")
      print_shutter_info(devh)

    except:
      #libuvc.uvc_unref_device(dev)
      print('Failed to Open Device')
  except:
    #libuvc.uvc_exit(ctx)
    print('Failed to Find Device')
    exit(1)

toggleUnitState = 'F'

def ktof(val):
    return round(((1.8 * ktoc(val) + 32.0)), 2)

def ktoc(val):
    return round(((val - 27315) / 100.0), 2)

def display_temperatureK(img, val_k, loc, color):
    val = ktof(val_k)
    cv2.putText(img,"{0:.1f} degF".format(val), loc, cv2.FONT_HERSHEY_SIMPLEX, 0.75, color, 2)
    x, y = loc
    cv2.line(img, (x - 2, y), (x + 2, y), color, 1)
    cv2.line(img, (x, y - 2), (x, y + 2), color, 1)

def display_temperatureC(img, val_k, loc, color):
    val = ktof(val_c)
    cv2.putText(img,"{0:.1f} degC".format(val), loc, cv2.FONT_HERSHEY_SIMPLEX, 0.75, color, 2)
    x, y = loc
    cv2.line(img, (x - 2, y), (x + 2, y), color, 1)
    cv2.line(img, (x, y - 2), (x, y + 2), color, 1)

def raw_to_8bit(data):
    cv2.normalize(data, data, 0, 65535, cv2.NORM_MINMAX)
    np.right_shift(data, 8, data)
    return cv2.cvtColor(np.uint8(data), cv2.COLOR_GRAY2RGB)

camState = 'not_recording'
tiff_frame = 1
maxVal = 0
minVal = 0

fileNum = 1
@pyqtSlot(QImage)
def startRec():
    global camState
    global saveFilePath
    global mostRecentFile
    if camState == 'recording':
        print('Alredy Recording')
    else:
        file_nameH = str(('Lepton HDF5 Vid ' + QDateTime.currentDateTime().toString()))
        file_nameH = file_nameH.replace(" ", "_")
        file_nameH = str(file_nameH.replace(":", "-"))
    try:
        filePathAndName = str(saveFilePath + '/' + file_nameH)
        #saveFilePathSlash = str(saveFilePath + '/')
        startRec.hdf5_file = h5py.File(filePathAndName, mode='w')
        #startRec.hdf5_file = h5py.File(os.path.join(saveFilePathSlash, file_nameH))
        camState = 'recording'
        print('Started Recording')
    except:
        print('Incorrect File Path')
        camState = 'not_recording'
        print('Did Not Begin Recording')

def getFrame():
    global tiff_frame
    global camState
    global maxVal
    global minVal
    data = q.get(True, 500)
    if data is None:
        print('No Data')
    if camState == 'recording':

        startRec.hdf5_file.create_dataset(('image'+str(tiff_frame)), data=data)
        tiff_frame += 1
    #Cannot you cv2.resize on raspberry pi 3b+. Not enough processing power.
    #data = cv2.resize(data[:,:], (640, 480))
    minVal, maxVal, minLoc, maxLoc = cv2.minMaxLoc(data)
    img = cv2.LUT(raw_to_8bit(data), generate_colour_map())
    #display_temperature only works if cv2.resize is used
    #display_temperatureK(img, minVal, minLoc, (255, 0, 0)) #displays min temp at min temp location on image
    #display_temperatureK(img, maxVal, maxLoc, (0, 0, 255)) #displays max temp at max temp location on image
    #display_temperatureK(img, minVal, (10,55), (255, 0, 0)) #display in top left corner the min temp
    #display_temperatureK(img, maxVal, (10,25), (0, 0, 255)) #display in top left corner the max temp
    return img

def readTemp(unit, state):
    if state == 'max':
        if unit == 'F':
            return (str(ktof(maxVal)) + ' ' + unit)
```

```
        elif unit == 'C':
            return (str(ktoc(maxVal)) + ' ' + unit)
        else:
            print('What are you asking for?')
    elif state == 'min':
        if unit == 'F':
            return (str(ktof(minVal)) + ' ' + unit)
        elif unit == 'C':
            return (str(ktoc(minVal)) + ' ' + unit)
        else:
            print('What are you asking for?')
    elif state == 'none':
        if unit == 'F':
            return (str(ktof(cursorVal)) + ' ' + unit)
        elif unit == 'C':
            return (str(ktoc(cursorVal)) + ' ' + unit)
        else:
            print('What are you asking for?')
    else:
          i)   print('What are you asking for?')

def updateMaxTempLabel():
    if toggleUnitState == 'F':
        return ktof(maxVal)
    elif toggleUnitState == 'C':
        return ktoc(maxVal)
    else:
        print('No Units Selected')

class MyThread(QThread):
    changePixmap = pyqtSignal(QImage)

    def run(self):
        print('Start Stream')
        while True:
            frame = getFrame()
            rgbImage = cv2.cvtColor(frame, cv2.COLOR_BGR2RGB)
            convertToQtFormat = QImage(rgbImage.data, rgbImage.shape[1], rgbImage.shape[0], QImage.Format_RGB888)
            p = convertToQtFormat.scaled(300, 260, Qt.KeepAspectRatio)
            self.changePixmap.emit(p)


thread = "unactive"
saveFilePath = ""
fileNamingFull = ""
bFile = ""
class App(QMainWindow, Ui_MainWindow):
    def __init__(self):
        QMainWindow.__init__(self)
        Ui_MainWindow.__init__(self)
        self.setupUi(self)
        self.initUI()
        print('Always Run This Script as ADMIN')

    @pyqtSlot(QImage)
    def setImage(self, image):
        self.displayFrame.setPixmap(QPixmap.fromImage(image))

    def initUI(self):
        global fileNamingFull
        self.startRec.clicked.connect(self.startRec2)
        self.stopRec.clicked.connect(self.stopRecAndSave)
        self.startRec.clicked.connect(self.displayRec)
        self.stopRec.clicked.connect(self.displayNotRec)
        self.displayC.clicked.connect(self.dispCDef)
        self.displayF.clicked.connect(self.dispFDef)
        self.runPost.clicked.connect(self.runPostScript)
        self.startStreamBut.clicked.connect(self.startThread)
        self.displayFrame.mousePressEvent = self.on_press

        self.w = QWidget()
        self.filePathBut.clicked.connect(self.getFiles)

        # time display
        self.timer = QTimer(self)
        self.timerFast = QTimer(self)
        self.timer.setInterval(1000)
        self.timerFast.setInterval(10)
        self.timer.timeout.connect(self.displayStorage)
        self.timerFast.timeout.connect(self.displayTempValues)
        self.timer.start()
        self.timerFast.start()

        defaultName = 'IR_HDF5'
        fileNamingFull = defaultName
        self.lineEdit.setText(defaultName)
        self.lineEdit.textChanged.connect(self.fileNaming)
        self.ffcBut.clicked.connect(self.ffcFunction)
        self.comboGain.currentTextChanged.connect(self.gainFunction)
        self.comboFFCmode.currentTextChanged.connect(self.FFCmodeFunction)

        self.cmIronBut.clicked.connect(self.cmIronFunc)
        self.cmGrayBut.clicked.connect(self.cmGrayFunc)
        self.cmRainBut.clicked.connect(self.cmRainFunc)
        self.printShutterBut.clicked.connect(self.printShutterInfoFunc)
        self.AI.clicked.connect(self.ActuateIn)
        self.AO.clicked.connect(self.ActuateOut)
        self.LON.clicked.connect(self.LampOn)
        self.LOFF.clicked.connect(self.LampOff)
        #self.connect(self, SIGNAL('triggered()'), self.closeEvent)
    def LampOn(self):
        GPIO.setmode(GPIO.BCM)
            # init list with pin numbers
        pinList1 = [17, 27]
        # loop through pins and set mode and state to 'high'
        for i in pinList1:
            GPIO.setup(i, GPIO.OUT)
            GPIO.output(i, GPIO.HIGH)
        try:
            GPIO.output(27, GPIO.LOW)
            GPIO.output(17, GPIO.HIGH)
            print ("Halogen Lamp ON")
        except KeyboardInterrupt:
            print ("  Quit")
            # Reset GPIO settings
            GPIO.cleanup()
```

```
def LampOff(self):
    GPIO.setmode(GPIO.BCM)
        # init list with pin numbers
    pinList1 = [17, 27]
    # loop through pins and set mode and state to 'high'
    for i in pinList1:
        GPIO.setup(i, GPIO.OUT)
        GPIO.output(i, GPIO.HIGH)
    GPIO.output(27, GPIO.HIGH)
    GPIO.output(17, GPIO.LOW)
    print ("Halogen Lamp OFF")
    GPIO.cleanup()
def ActuateOut(self):
    GPIO.cleanup()
    GPIO.setmode(GPIO.BCM)
        # init list with pin numbers
    pinList1 = [2, 3]
    # loop through pins and set mode and state to 'high'
    for i in pinList1:
        GPIO.setup(i, GPIO.OUT)
        GPIO.output(i, GPIO.HIGH)
    try:
        GPIO.output(2, GPIO.LOW)
        GPIO.output(3, GPIO.HIGH)
        print ("Actuated out - camera in laser range")
    except KeyboardInterrupt:
        print ("  Quit")
        # Reset GPIO settings


def ActuateIn(self):
    GPIO.cleanup()
    GPIO.setmode(GPIO.BCM)
        # init list with pin numbers
    pinList1 = [2, 3]
    # loop through pins and set mode and state to 'high'
    for i in pinList1:
        GPIO.setup(i, GPIO.OUT)
        GPIO.output(i, GPIO.HIGH)
    GPIO.output(2, GPIO.HIGH)
    GPIO.output(3, GPIO.LOW)
    print ("Actuated camera system in - camera out of laser range")
def printShutterInfoFunc(self):
    global devh
    if thread == 'active':
        print_shutter_info(devh)

def cmIronFunc(self):
    global colorMapType
    colorMapType = 0
    self.history.insertPlainText('Changed Color Map\n')
    self.history.moveCursor(QTextCursor.End)

def cmRainFunc(self):
    global colorMapType
    colorMapType = 1
    self.history.insertPlainText('Changed Color Map\n')
    self.history.moveCursor(QTextCursor.End)

def cmGrayFunc(self):
    global colorMapType
    colorMapType = 2
    self.history.insertPlainText('Changed Color Map\n')
    self.history.moveCursor(QTextCursor.End)

def gainFunction(self):
    global devh
    global thread
    if thread == 'active':
        if (self.comboGain.currentText() == 'LOW'):
            set_gain_low(devh)
        elif (self.comboGain.currentText() == 'HIGH'):
            set_gain_high(devh)
            #print('Cannot set to back to HIGH yet')
        else:
            set_gain_auto(devh)
            #print('Cannot set to AUTO')

def FFCmodeFunction(self):
    global devh
    global thread
    if thread == 'active':
        if (self.comboFFCmode.currentText() == 'MANUAL'):
            set_manual_ffc(devh)
        elif (self.comboFFCmode.currentText() == 'EXTERNAL'):
            set_external_ffc(devh)
        else:
            set_auto_ffc(devh)
            #print('Cannot set to back to AUTO yet. Unplug USB from Raspberry Pi to reset lepton.')
    print_shutter_info(devh)

def ffcFunction(self):
    global devh
    global thread
    if thread == 'active':
        perform_manual_ffc(devh)

def startRec2(self):
    global thread
    global camState
    global saveFilePath
    global fileNamingFull
    if thread == 'active':
        if camState == 'recording':
            print('Already Recording')
        else:
            if fileNamingFull != "":
                dateAndTime = str(QDateTime.currentDateTime().toString())
                dateAndTime = dateAndTime.replace(" ", "_")
                dateAndTime = dateAndTime.replace(":", "_")
                filePathAndName = str(fileNamingFull + '_' + dateAndTime + '.HDF5')
                print(filePathAndName)
                self.filePathDisp.setText(filePathAndName)
                try:
                    startRec.hdf5_file = h5py.File(filePathAndName, mode='w')
                    camState = 'recording'
```

```
                        print('Started Recording')
                        if saveFilePath == "":
                            self.history.insertPlainText('Saved ' + str(filePathAndName) + ' to ' +
os.path.dirname(os.path.abspath(__file__)) + '\n')
                            self.history.moveCursor(QTextCursor.End)
                        else:
                            self.history.insertPlainText('Saved to ' + str(filePathAndName) + '\n')
                            self.history.moveCursor(QTextCursor.End)
                    except:
                        print('Incorrect File Path')
                        camState = 'not_recording'
                        print('Did Not Begin Recording')
                else:
                    print('No FileName Specified')
        else:
            print('Remember to Start Stream')
            self.history.insertPlainText('Remember to Start Stream\n')
            self.history.moveCursor(QTextCursor.End)

    def stopRecAndSave(self):
        global fileNum
        global tiff_frame
        global camState
        global dataCollection
        if tiff_frame > 1:
            print('Ended Recording')
            camState = 'not_recording'
            try:
                startRec.hdf5_file.close()
                print('Saved Content to File Directory')
                #fileNum += 1
            except:
                print('Save Failed')
            tiff_frame = 1
        else:
            camState = 'not_recording'
            print('Dont Forget to Start Recording')
            self.history.insertPlainText('Dont Forget to Start Recording\n')
            self.history.moveCursor(QTextCursor.End)

    def fileNaming(self):
        global fileNamingFull
        bFile = str(self.lineEdit.text())
        if saveFilePath == "":
            fileNamingFull = bFile
            self.filePathDisp.setText('/' + bFile + ' ... Date & Time Will Append at Recording Start')
        elif saveFilePath != "":
            fileNamingFull = saveFilePath + '/' + bFile
            self.filePathDisp.setText(saveFilePath + '/' + bFile + ' ... Date & Time Will Append at Recording Start')
        else:
            print('I am Confused')

    def startThread(self):
        global thread
        try:
            if thread == "unactive":
                try:
                    startStream()
                    self.th = MyThread()
                    self.th.changePixmap.connect(self.setImage)
                    self.th.start()
                    thread = "active"
                    print('Starting Thread')
                except:
                    print('Failed!!!!')
                    exit(1)
            else:
                print('Already Started Camera')
        except:
            msgBox = QMessageBox()
            reply = msgBox.question(self, 'Message', "Error Starting Camera - Plug or Re-Plug Camera into Computer,
Wait at Least 10 Seconds, then Click Ok and Try Again.", QMessageBox.Ok)
            print('Message Box Displayed')
            if reply == QMessageBox.Ok:
                print('Ok Clicked')
            else:
                event.ignore()


    def runPostScript(self):
        try:
            def thread_second():
                 call(["python3", postScriptFileName])
            processThread = threading.Thread(target=thread_second())  # <- note extra ','
            processThread.start()
        except:
            print('Post Processing Script Error - Most Likely Referencing Incorrect File Name')

    def dispCDef(self):
        global toggleUnitState
        toggleUnitState = 'C'
        self.history.insertPlainText('Display ' + str(toggleUnitState) + '\n')
        self.history.moveCursor(QTextCursor.End)

    def dispFDef(self):
        global toggleUnitState
        toggleUnitState = 'F'
        self.history.insertPlainText('Display ' + str(toggleUnitState) + '\n')
        self.history.moveCursor(QTextCursor.End)

    def displayTempValues(self):
        #global fileSelected
        global toggleUnitState
        #if fileSelected != "":
        self.maxTempLabel.setText('Current Max Temp: ' + readTemp(toggleUnitState, 'max'))
        #self.maxTempLocLabel.setText('Max Temp Loc: ' + str(maxLoc))
        self.minTempLabel.setText('Current Min Temp: ' + readTemp(toggleUnitState, 'min'))
        #self.minTempLocLabel.setText('Min Temp Loc: ' + str(minLoc))

    def displayTime(self):
        self.timeStatus.setText(QDateTime.currentDateTime().toString())

    def grabTempValue(self):
        global frame
        global lastFrame
        global fileSelected
```

```
        global xMouse
        global yMouse
        global thread
        if thread == 'active':
            data = q.get(True, 500)
            data = cv2.resize(data[:,:], (320, ))
            return data[yMouse, xMouse]
        else:
            self.history.insertPlainText('ERROR: Please Start IR Camera Feed First\n')
            self.history.moveCursor(QTextCursor.End)

    def on_press(self, event):
        global xMouse
        global yMouse
        global cursorVal
        #print('you pressed', event.button, event.xdata, event.ydata)
        try:
            xMouse = event.pos().x()
            yMouse = event.pos().y()
            cursorVal = self.grabTempValue()
            self.cursorTempLabel.setText('Cursor Temp (On Mouse Click): ' + readTemp(toggleUnitState, 'none'))
        except:
            self.history.insertPlainText('ERROR: Please Start IR Camera Feed First\n')
            self.history.moveCursor(QTextCursor.End)

    def displayStorage(self):
        usage = psutil.disk_usage('/')
        oneMinVid = 20000000
        timeAvail = usage.free/oneMinVid
        self.storageLabel.setText('Recording Time Left: ' + str(round(timeAvail, 2)) + ' Minutes')

    def displayRec(self):
        if camState == 'recording':
              self.recLabel.setText('Recording')
        else:
           self.recLabel.setText('Not Recording')

    def displayNotRec(self):
        if camState == 'not_recording':
            self.recLabel.setText('Not Recording')
        else:
            self.recLabel.setText('Recording')

    def getFiles(self):
        global saveFilePath
        saveFilePath = QFileDialog.getExistingDirectory(self.w, 'Open File Directory', '/')
        self.filePathDisp.setText(saveFilePath)
        self.fileNaming()

    def closeEvent(self, event):
        print("Close Event Called")
        if camState == 'recording':
            reply = QMessageBox.question(self, 'Message',
                                         "Recording still in progress. Are you sure you want to quit?",
QMessageBox.Yes, QMessageBox.No)
            print('Message Box Displayed')
            if reply == QMessageBox.Yes:
                print('Exited Application, May Have Lost Raw Data')
                event.accept()
            else:
                event.ignore()
        else:
            print('Exited Application')
            event.accept()

def main():
    app = QApplication(sys.argv)
    window = App()
    window.show()
    sys.exit(app.exec_())

if __name__ == '__main__':
    main()
```

Part sizing code:

```
import cv2
import numpy as np
from matplotlib import pyplot as plt
from scipy.spatial import distance as dist
from imutils import perspective
from imutils import contours
#import numpy as np

import imutils
import glob
import sys
from PIL import Image

image = glob.glob('./Defects_100_to_500/Layer*.jpg')

#print(img.shape[0:2])
i = 0
for fname in image:
        def midpoint(ptA, ptB):
```

```
        return ((ptA[0] + ptB[0]) * 0.5, (ptA[1] + ptB[1]) * 0.5)
image = cv2.imread(fname)

cv2.imshow("Orignal image", image)


imgbgr = cv2.cvtColor(image, cv2.COLOR_RGB2BGR)

gray = cv2.cvtColor(imgbgr, cv2.COLOR_BGR2GRAY)

edged = cv2.GaussianBlur(gray, (9, 9), 0)


edged = cv2.Canny(gray, 150, 255)
kernel = np.ones((2,2),np.uint8)
edged = cv2.dilate(edged, None, iterations=3)
edged = cv2.erode(edged, None, iterations=1)


cv2.imshow("edged", edged)
        # find contours in the edge map
cnts = cv2.findContours(edged.copy(), cv2.RETR_EXTERNAL,
        cv2.CHAIN_APPROX_SIMPLE)
cnts = imutils.grab_contours(cnts)
        # sort the contours from left-to-right and initialize the
# 'pixels per metric' calibration variable
(cnts, _) = contours.sort_contours(cnts)
pixelsPerMetric = None
        # loop over the contours individually
for c in cnts:
        # if the contour is not sufficiently large, ignore it
        if cv2.contourArea(c) < 500:
                continue
                # compute the rotated bounding box of the contour
        orig = image.copy()
        box = cv2.minAreaRect(c)
        box = cv2.cv.BoxPoints(box) if imutils.is_cv2() else cv2.boxPoints(box)
        box = np.array(box, dtype="int")
                # order the points in the contour such that they appear
        # in top-left, top-right, bottom-right, and bottom-left
                # order, then draw the outline of the rotated bounding
                # box
        box = perspective.order_points(box)
        cv2.drawContours(orig, [box.astype("int")], -1, (0, 255, 0), 2)
                # loop over the original points and draw them
        for (x, y) in box:
                cv2.circle(orig, (int(x), int(y)), 5, (0, 0, 255), -1)
                # unpack the ordered bounding box, then compute the midpoint
        # between the top-left and top-right coordinates, followed by
        # the midpoint between bottom-left and bottom-right coordinates
        (tl, tr, br, bl) = box
        (tltrX, tltrY) = midpoint(tl, tr)
        (blbrX, blbrY) = midpoint(bl, br)
                # compute the midpoint between the top-left and top-right points,
        # followed by the midpoint between the top-righ and bottom-right
        (tlblX, tlblY) = midpoint(tl, bl)
        (trbrX, trbrY) = midpoint(tr, br)
                # draw the midpoints on the image
        cv2.circle(orig, (int(tltrX), int(tltrY)), 5, (255, 0, 0), -1)
        cv2.circle(orig, (int(blbrX), int(blbrY)), 5, (255, 0, 0), -1)
        cv2.circle(orig, (int(tlblX), int(tlblY)), 5, (255, 0, 0), -1)
        cv2.circle(orig, (int(trbrX), int(trbrY)), 5, (255, 0, 0), -1)
                # draw lines between the midpoints
        cv2.line(orig, (int(tltrX), int(tltrY)), (int(blbrX), int(blbrY)),
                (255, 0, 255), 2)
        cv2.line(orig, (int(tlblX), int(tlblY)), (int(trbrX), int(trbrY)),
                (255, 0, 255), 2)

                # compute the Euclidean distance between the midpoints
        dA = dist.euclidean((tltrX, tltrY), (blbrX, blbrY))
        dB = dist.euclidean((tlblX, tlblY), (trbrX, trbrY))
                # if the pixels per metric has not been initialized, then
        # compute it as the ratio of pixels to supplied metric
        # (in this case, inches)
```

```
if pixelsPerMetric is None:
        pixelsPerMetric = 27
        # compute the size of the object
dimA = dA / pixelsPerMetric
dimB = dB / pixelsPerMetric
        # draw the object sizes on the image
cv2.putText(orig, "{:.4f}mm".format(dimA),
        (int(tltrX - 15), int(tltrY - 10)), cv2.FONT_HERSHEY_SIMPLEX,
        0.65, (255, 255, 255), 2)
cv2.putText(orig, "{:.4f}mm".format(dimB),
        (int(trbrX + 10), int(trbrY)), cv2.FONT_HERSHEY_SIMPLEX,
        0.65, (255, 255, 255), 2)
        # show the output image
cv2.imshow("Image", orig)
cv2.imwrite('./Defects_100_to_500/Trial/size_detection%02i.jpg' %i, orig)
#cv2.waitKey(0)
i = i + 1
cv2.waitKey(0)
```

Cropping just the detected part out of the image:

The following code was applied into the for lop after the contour corner points are detected. Code was written in to save the images in a new folder to be processed for defect detection.

```
Ox = int(tl[0])
        Oy = int(tl[1])
        lx = int(br[0])
        ly = int(br[1])
        cropped = image[Oy:ly,Ox:lx]
```

Grayscale:

To make it simpler for the edge detector to distinguish between the real and synthesized defects the pixels considered to be a defect was set to black and the pixels part of the melted part to be white using the following code. The second purpose of this code was designed to create a black and white image used to trace the bitmap of the image and create a DXF file in Inktrace.

```
imgbgr = cv2.cvtColor(image, cv2.COLOR_RGB2BGR)

gray = cv2.cvtColor(imgbgr, cv2.COLOR_BGR2GRAY)
# Open the input image


# Use numpy to convert the PIL image into a numpy array
npImage=np.array(gray)

# Make a LUT (Look-Up Table) to translate image values. Default output
value is zero.
LUT=np.zeros(256,dtype=np.uint8)
LUT[0:120]=0
LUT[120:255]=255

# Transform pixels according to LUT - this line does all the work
pixels=LUT[npImage];

# Save resulting image
Result = Image.fromarray(pixels)
```

```
result.save('result.jpg')
```

Defect sizing code:

After the cropped and grayscale code was applied, the same code as the part sizing code was applied with two exceptions, the threshold of the canny edge detector and the following line. This line was included after the edge detection to inverse the pixel colours and ensure the find contour function focused on the change of colour for the defective edges instead of the part edges.

```
edged = 255 - edged
```

APPENDIX D – CHAPTER 5 – PART SIZING EXAMPLES

Layer	Part size	Cropped Part based on part size contours	
1	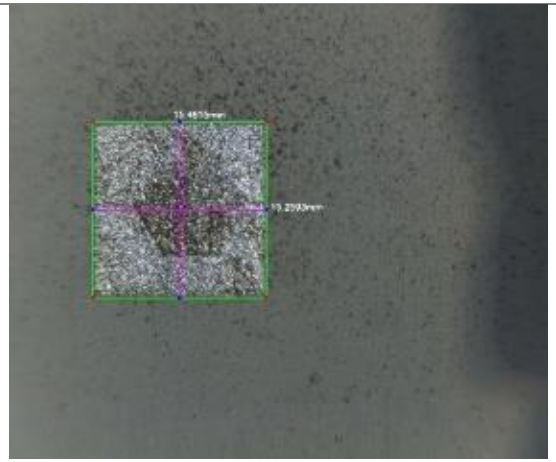	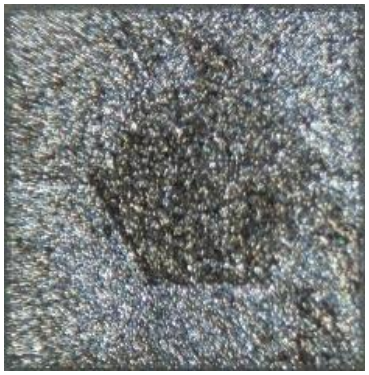	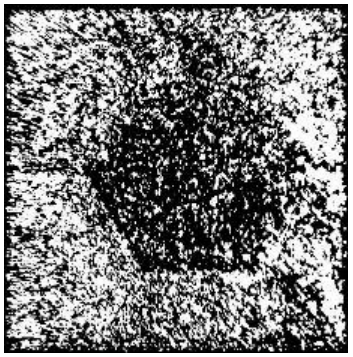
2	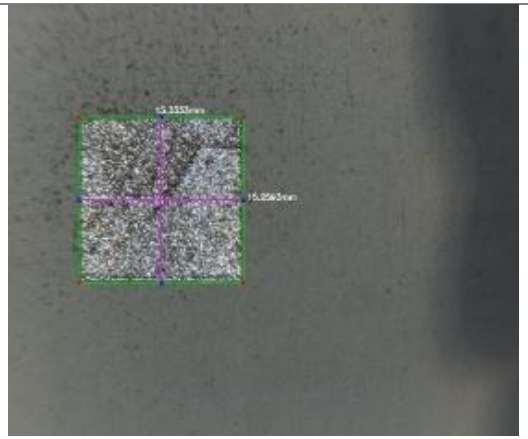	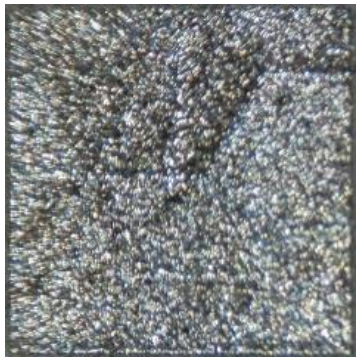	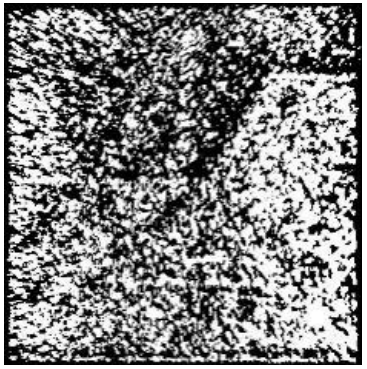

3	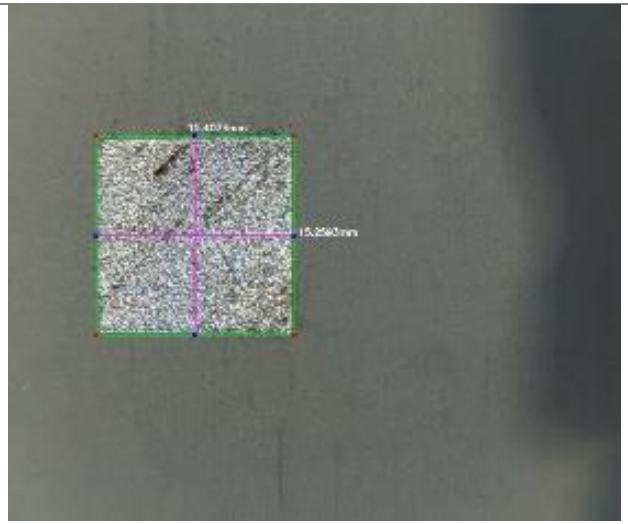	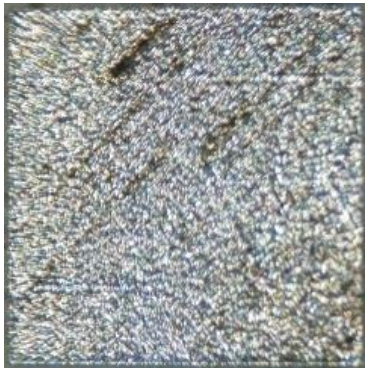	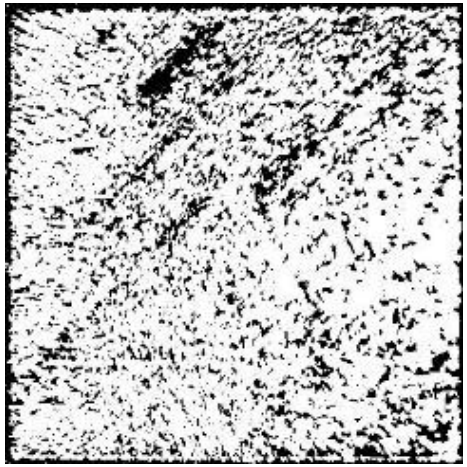
4	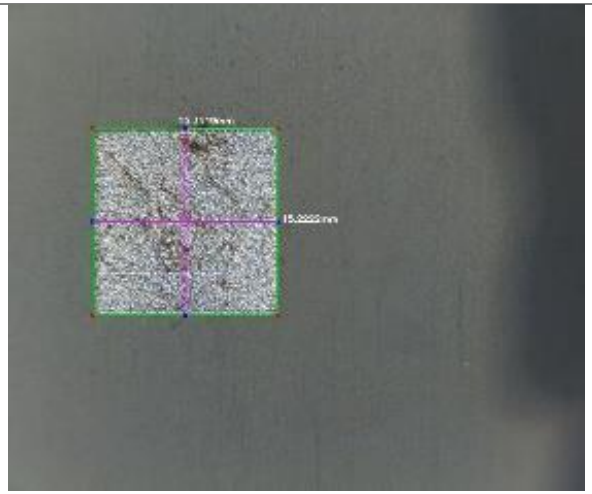		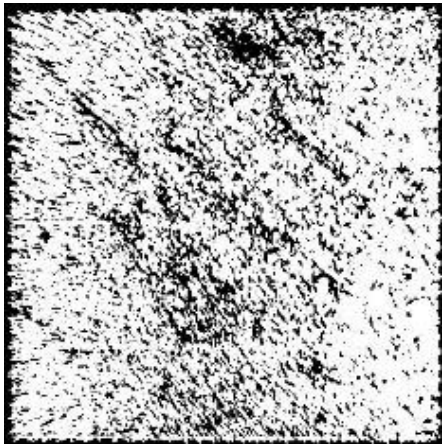

Layer	Part size	Cropped Part based on part size contours	
1	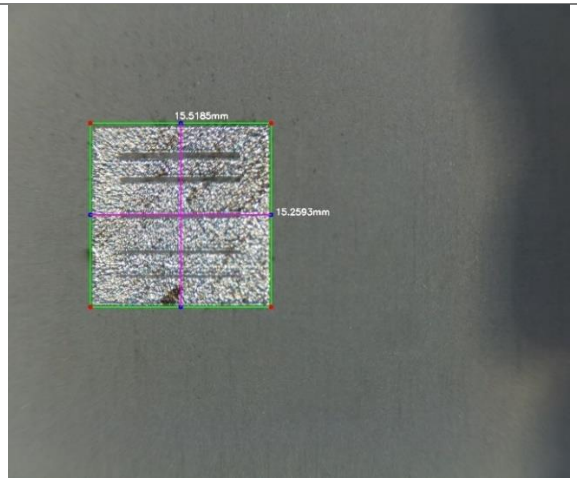	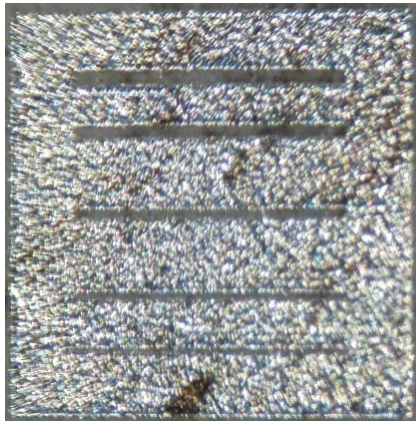	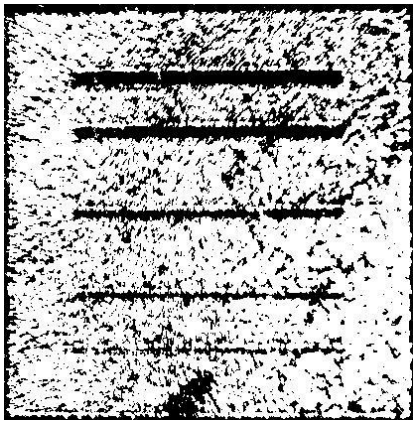
2	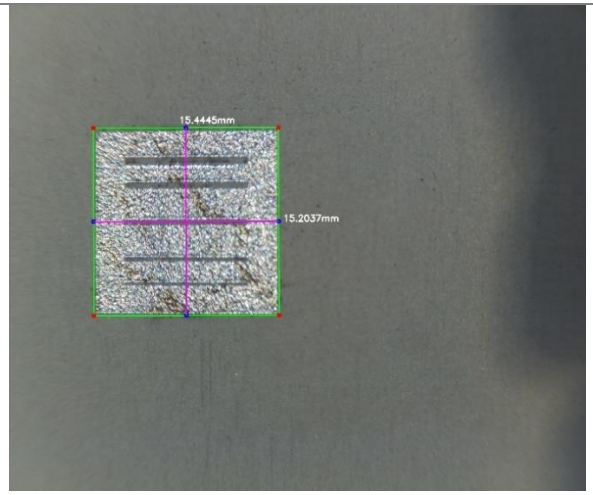	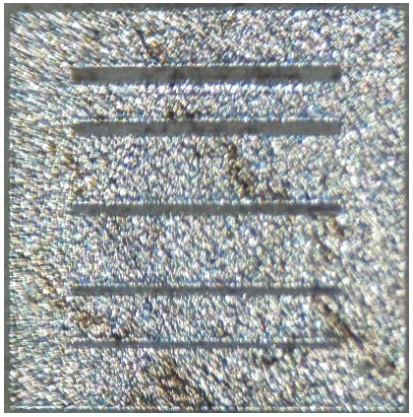	

3	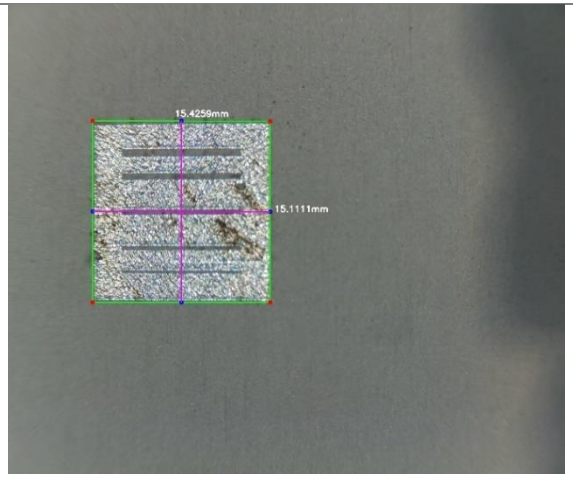	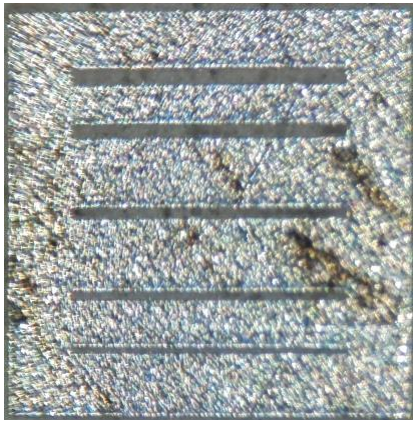	
4	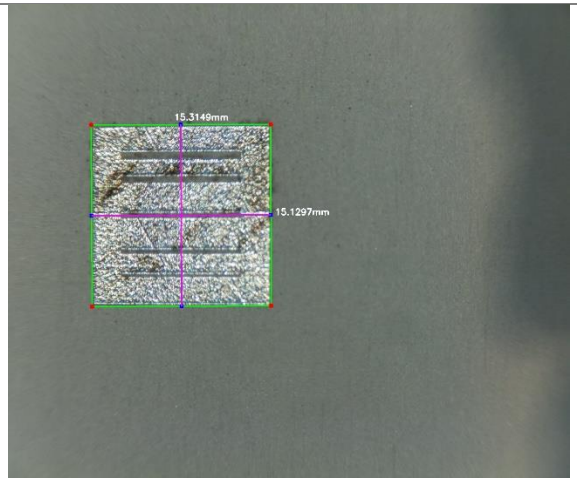	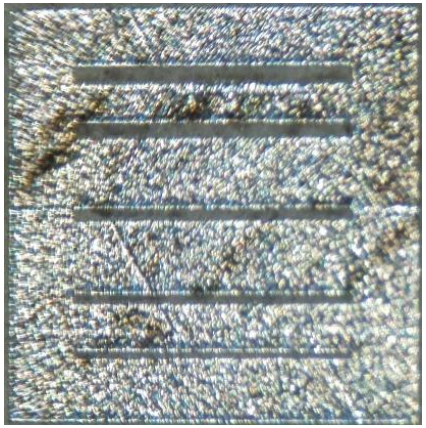	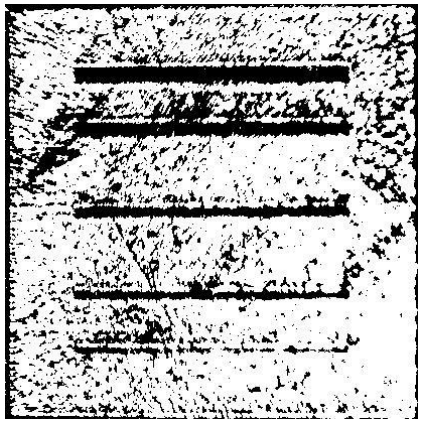

APPENDIX E – CHAPTER 3 – 3D TEXTURE APPLICATION EXAMPLE

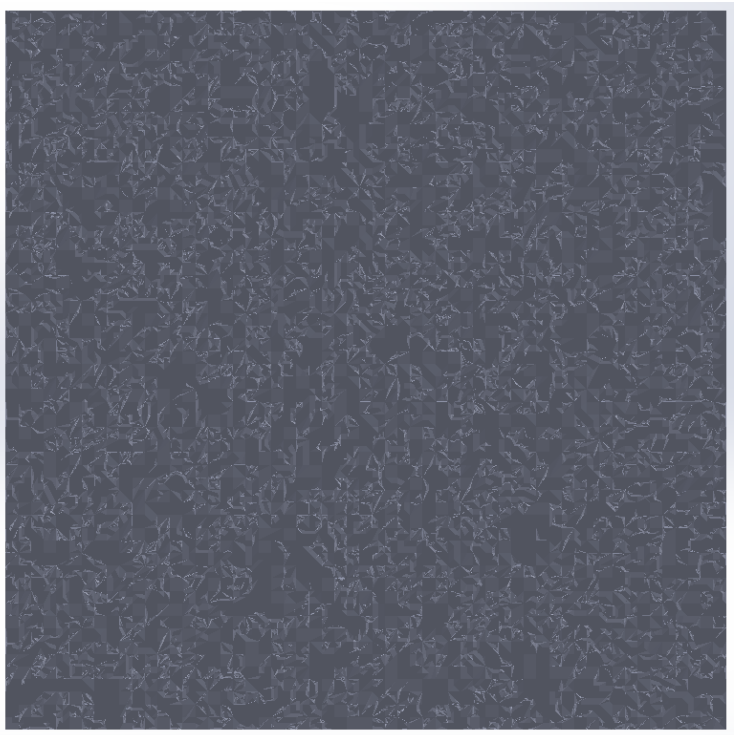

APPENDIX F – CHAPTER 5 – DEFECT DETECTION ATTEMPTS

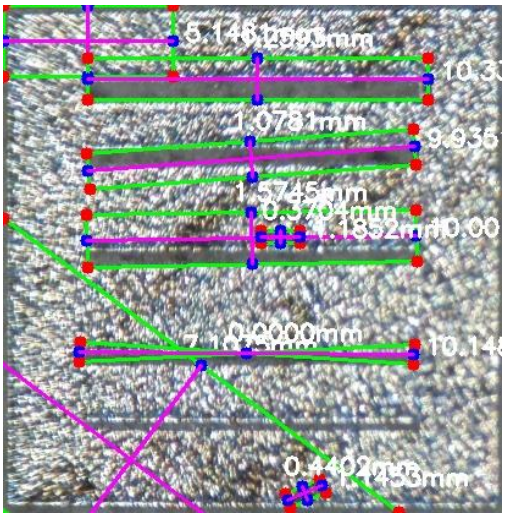

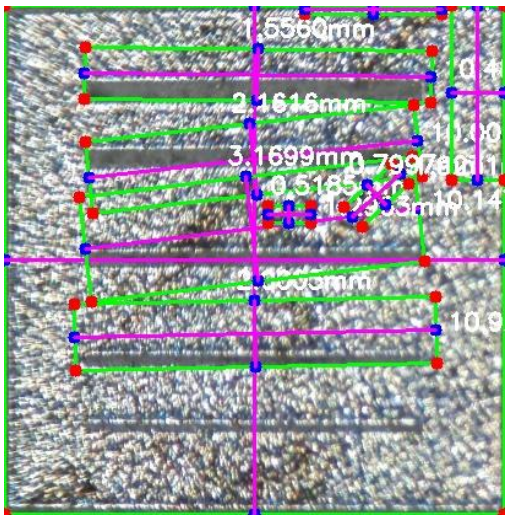

APPENDIX G – CHAPTER 1 – INDUSTRY SURVEYING

Company	Production Description AM Technology and Materials	Key Points derived from discussion
RAM 3D	Commercial Metal 3D printing company based in Tauranga. Produce AM parts using Inconel 718, Stainless Steel 316, Titanium 64 and Stainless Steel 155. Have several contracts with companies in New Zealand.	• Residual stress within parts created by laser technology printers is a major problem. Suggested using the laser to re-melt sections as a solution to stress relieve, but that it is important to consider the residual stress that may spread to what's known as the heat affected zone. • Laser quality, repetition, the power may drop, a lens shift could cause a change in the laser beam. • Surface Finish is a major issue, internally and externally. Cannot access complex flow chambers or valves which is a beneficial feature AM offers in comparison to traditional manufacturing features. • Leading NZ industries interested in AM, require parts with a method to improve internal surface finish. Furthermore, they would require a method to model it. These industries include the Food Processing industry, Geothermal and Marine industries.
TiDA	Commercial research and testing facility who have done some work with metal 3D printing but do not do any production work. Based in Tauranga. They are currently studying a laser-based machine using Stainless Steel 440C powder.	• Key issues they have identified, key issue is residual stress and powder quality after recycling. • They recommended using an optical tomography method for monitoring system and then integrating a feedback system. Such as using the laser to reheat the part to relieve residual stresses. • Metal AM machines with a powder feed, are capable of recycling material not used in the parts support material or the parts print. With each recycle the power degrades, with the integration of the chambers inerted gas (Oxy, Nitrogen etc), splattered particulates with a larger particle size than the ASTM specification.

Zenith Technica	Commercial Auckland based 3D metal 3D printing manufacturer. Produce metal parts using EBM AM machines, primarily the ARCAM brand. Work only with Titanium Alloys – ASTM grades 2, 5, 23. Have major contracts to produce AM parts with international entities (Confidential).	• Zenith relies on traditional mechanical tests for QA. They do question the reliability of this method. Especially for tensile test pieces printed in the Z axis vs the X axis. • They have a LAYER-CAM to manually monitor each layer, however it is a tedious process for someone to review every layer. Only AM experts can use this method for visual inspection. They would prefer a better monitoring system, current products on the market are too expensive. • Common problems in EBM include, the laser focus, speed of the system. They do worry that further processing time could increase production time, where commercial value is in a faster system. • Current QA is specific for machine-by-machine certification. • Surface Finish is a major issue, but the company lets the client handle the post-processing
Fuji Xerox	Well-established printing company interviewed an Auckland based office. They sell 3D systems AM machines, with commercial knowledge on printing specifications for quality achieved on the best printer and where the value is in QA research.	• 3D systems are working to reduce the oxygen content down to 25 parts per million. The lower the oxygen content, the better the part quality (less oxidization). • Suggested looking into Aerospace products, and even helicopters (Aim Altitude in NZ). • Indicated current monitoring systems on the market are too expensive and still cannot be integrated into every machine. • Recommended looking at critical defects in metals and confirmed that while it could be useful to apply a monitoring system for Plastic Laser Sintering processes, metal is in greater need of the technology.

APPENDIX H – STATEMENT OF CONTRIBUTION FOR PUBLICATIONS

DRC 16

MASSEY UNIVERSITY
GRADUATE RESEARCH SCHOOL

STATEMENT OF CONTRIBUTION
DOCTORATE WITH PUBLICATIONS/MANUSCRIPTS

We, the candidate and the candidate's Primary Supervisor, certify that all co-authors have consented to their work being included in the thesis and they have accepted the candidate's contribution as indicated below in the *Statement of Originality*.

Name of candidate:	Tanisha Pereira
Name/title of Primary Supervisor:	Prof. Johan Potgieter
Name of Research Output and full reference:	
A fundamental study of 3D printing testing methods for the development of new quality management strategies	
In which Chapter is the Manuscript /Published work:	Chapter 1
Please indicate:	
• The percentage of the manuscript/Published Work that was contributed by the candidate:	100%
and	
• Describe the contribution that the candidate has made to the Manuscript/Published Work:	
The candidate has written the majority of the manuscript. The candidate has conducted the experimentation and provided the analysis required for this publication.	
For manuscripts intended for publication please indicate target journal:	
Candidate's Signature:	Tanisha Pereira Digitally signed by Tanisha Pereira Date: 2021.12.05 20:18:16 +13'00'
Date:	5/12/2021
Primary Supervisor's Signature:	Johan Potgieter Digitally signed by Johan Potgieter Date: 2021.12.06 11:38:43 +13'00'
Date:	6/12/2021

(This form should appear at the end of each thesis chapter/section/appendix submitted as a manuscript/ publication or collected as an appendix at the end of the thesis)

GRS Version 4– January 2019

2017 24th International Conference on Mechatronics and Machine Vision in Practice (M2VIP)

A fundamental study of 3D printing testing methods for the development of new quality management strategies

Tanisha Pereira, Johan Potgieter, John V Kennedy
of *School of Engineering and Advanced Technology*, Massey University
Auckland, New Zealand
T.Pereira@massey.ac.nz

***Abstract*— A leading area of research in Additive Manufacturing, studies the quality of 3D prints using several testing strategies. This paper reviews two testing technologies: tensile testing (mechanical testing) and Scanning Electron Microscopy (SEM). The aim of this experiment was to provide a comparative study to better understand quality management processes in the 3D printing space. Additionally, this research study was performed to establish a good fundamental groundwork on which future Non-Destructive Testing research can be conducted. The study revealed the advantages of the tensile and SEM testing methods, whilst highlighting a need for better technologies to cover the disadvantages.**

Keywords—Additive Manufacturing; Quality Management; Tensile Testing; 3D Printing; SEM analysis

I. Introduction

Additive Manufacturing (AM) continues to revolutionize the manufacturing industry, with its capability to model a multitude of shape structures. AM refers to those shapes produced by a variety of gradual layering techniques [1]. It is popularly recognized as 3D Printing (3DP), a rapidly proliferating manufacturing technique, contributing essential data reviewed in this paper. The extensive range of 3DP technologies has gained significant academic and industry interest from its ability to form complex geometries with customizable material properties [2]. Due to the fast advancement of 3DP technologies, there is a growing necessity for testing technologies, to provide Quality Assurance (QA) and Quality Control (QC). There is incentive to explore possible methodologies to implement better testing strategies for QA and QC. To do this, existing methods must first be reviewed to better understand the problem space. This paper provides a comparative review of two 3DP testing technologies analyzing specimens from several 3DP samples generated utilizing a variety of 3DP technologies.

A. 3DP Technologies:

The rapid proliferation of 3DP technologies has resulted in several advancements and unique manufacturing methods. Due to the use of several of these technologies for the testing stage of this paper, a brief overview on 3DP technologies is provided. 3DP methodologies are often categorized by 3 main depositions; solid, liquid and powder based depositions [3]. Common solid based deposition 3D printing technologies include Fused Deposition Modelling (FDM) and Multi-Jet Printing (MJP). Few commercial 3D printing technologies use Powder Based deposition, the most common are the Binder Jet, Selective Laser Sintering (SLS) and Electron Beam Melting (EBM). Liquid based 3D printing primarily utilizes two methods; using a laser beam to cure the liquid or injecting the liquid through a micro nozzle. The liquid based deposition technologies that exist include; Stereolithography (SLA), Digital Light Projection (DLP) and inkjet techniques. To analyze the 2 testing strategies, 3DP specimens from a variety of these technologies have been generated.

B. Quality Assurance and Quality Control

QA/QC are quality management processes, with slightly different purposes. QA relates to the capability to guarantee the product is fit for purpose and meets the standard [4]. QC is the quality management process that inspects the part to determine its rating against the standard. Precision manufacturing requires rigorous QA and QC standards and procedures. One of the largest restrictions regarding the implementation of such strategies in the 3DP industry is the high variability in the processes utilized to manipulate differing types of material.

C. Testing Methods

Several testing strategies/technologies exist to quality manage 3DP parts; Chemical analysis, Mechanical Testing, Performance Evaluation, Metallurgical Analysis, Powders Evaluation and Non-Destructive Testing (NDT) [5]. Within this study, results from one mechanical testing method (Tensile testing) and one topographical/NDT microscopic analysis method (Scanning Electron Microscopy) are taken. The Instron Universal Testing Machine [6] is rated the most fundamental mechanical test for a breadth of applications to determine the mechanical performance/ properties of a material/part [7]. The Scanning Electron Microscopy (SEM) machine, provides a surface level analysis for solid specimens [8]. The micro level topographical image provides insight into the parts layer bonding, defects and any other anomalies that could contribute to inconsistencies found from the specimen's mechanical performance.

978-1-5090-6546-2/17/$31.00 ©2017 IEEE
Authorized licensed use limited to: Massey University. Downloaded on December 05,2021 at 07:28:17 UTC from IEEE Xplore. Restrictions apply.

MASSEY UNIVERSITY
GRADUATE RESEARCH SCHOOL

STATEMENT OF CONTRIBUTION
DOCTORATE WITH PUBLICATIONS/MANUSCRIPTS

We, the candidate and the candidate's Primary Supervisor, certify that all co-authors have consented to their work being included in the thesis and they have accepted the candidate's contribution as indicated below in the *Statement of Originality*.

Name of candidate:	Tanisha Pereira
Name/title of Primary Supervisor:	Prof. Johan Potgieter
Name of Research Output and full reference:	
A comparison of traditional manufacturing vs additive manufacturing, the best method for the job.	
In which Chapter is the Manuscript /Published work:	Chapter 2
Please indicate:	
• The percentage of the manuscript/Published Work that was contributed by the candidate:	100%
and	
• Describe the contribution that the candidate has made to the Manuscript/Published Work:	
The candidate has written the majority of the manuscript. The candidate has conducted the experimentation and provided the analysis required for this publication.	
For manuscripts intended for publication please indicate target journal:	
Candidate's Signature:	Tanisha Pereira Digitally signed by Tanisha Pereira Date: 2021.12.05 20:18:16 +13'00'
Date:	5/12/2021
Primary Supervisor's Signature:	Johan Potgieter Digitally signed by Johan Potgieter Date: 2021.12.06 11:40:24 +13'00'
Date:	6/12/2021

(This form should appear at the end of each thesis chapter/section/appendix submitted as a manuscript/ publication or collected as an appendix at the end of the thesis)

Available online at www.sciencedirect.com

ScienceDirect

Procedia Manufacturing 30 (2019) 11–18

Procedia MANUFACTURING

www.elsevier.com/locate/procedia

14th Global Congress on Manufacturing and Management (GCMM-2018)

A comparison of traditional manufacturing vs additive manufacturing, the best method for the job

Tanisha Pereira[a], John V Kennedy[b],Johan Potgieter *

[a]Massey University, North Shore, Auckland 0745, New Zealand
[b]GNS Science, 1 Fairway Drive, Lower Hutt 5040, New Zealand

Abstract

Manufacturing industries and investors are always seeking to improve techniques to lower cost, energy and expand their capability. Additive manufacturing, started in the 1960s, has since had a rapid and continuous growth, bringing to light novel techniques to expand manufacturing capability and reinvent the wheel. At this stage, research and industry interest lie in determining where AM can replace or create new manufacturing systems. Traditional manufacturing refers to subtractive and long-established manufacturing methods, quality assured and implemented in the commercial space.

This paper reviews the capability of AM and its current development to compete or add to established traditional manufacturing regions. Literature reveals the capability of AM to fit into established manufacturing regions for low and high production volume products. The paper comparison focuses on the similarities, differences, advantages and disadvantages found in AM vs SM studying the economic and quality management status of the industry today.

© 2019 The Authors. Published by Elsevier Ltd.
This is an open access article under the CC BY-NC-ND license (https://creativecommons.org/licenses/by-nc-nd/4.0/)
Selection and peer-review under responsibility of the scientific committee of the 14th Global Congress on Manufacturing and Management (GCMM-2018).

Keywords: Manufacturing, AM vs Traditional Manufacturing, Defects in Manufacturing, Quality Assurance Progression, Manufacturing Regions for AM, Part Characterization

* Corresponding author. Tel +64 (9) 414 0800 ext 41492;
E-mail address: J.Potgieter@massey.ac.nz

2351-9789 © 2019 The Authors. Published by Elsevier Ltd.
This is an open access article under the CC BY-NC-ND license (https://creativecommons.org/licenses/by-nc-nd/4.0/)
Selection and peer-review under responsibility of the scientific committee of the 14th Global Congress on Manufacturing and Management (GCMM-2018).
10.1016/j.promfg.2019.02.003

MASSEY UNIVERSITY
GRADUATE RESEARCH SCHOOL

STATEMENT OF CONTRIBUTION
DOCTORATE WITH PUBLICATIONS/MANUSCRIPTS

We, the candidate and the candidate's Primary Supervisor, certify that all co-authors have consented to their work being included in the thesis and they have accepted the candidate's contribution as indicated below in the *Statement of Originality*.

Name of candidate:	Tanisha Pereira
Name/title of Primary Supervisor:	Prof. Johan Potgieter
Name of Research Output and full reference:	
Development of quality management strategies for 3D printing testing methods – A Review	
In which Chapter is the Manuscript /Published work:	Chapter 1
Please indicate:	
• The percentage of the manuscript/Published Work that was contributed by the candidate:	100%
and	
• Describe the contribution that the candidate has made to the Manuscript/Published Work:	
The candidate has written the majority of the manuscript. The candidate has conducted the experimentation and provided the analysis required for this publication.	
For manuscripts intended for publication please indicate target journal:	
Candidate's Signature:	Tanisha Pereira Digitally signed by Tanisha Pereira Date: 2021.12.05 20:18:16 +13'00'
Date:	5/12/2021
Primary Supervisor's Signature:	Johan Potgieter Digitally signed by Johan Potgieter Date: 2021.12.06 11:39:05 +13'00'
Date:	6/12/2021

(This form should appear at the end of each thesis chapter/section/appendix submitted as a manuscript/ publication or collected as an appendix at the end of the thesis)

2017 4th Asia-Pacific World Congress on Computer Science and Engineering

Development of quality management strategies for 3D printing testing methods – A Review

Tanisha Pereira, Johan Potgieter, John V Kennedy
of *School of Engineering and Advanced Technology*, Massey University
Auckland, New Zealand
T.Pereira@massey.ac.nz

***Abstract*— Industrial progression in the Additive Manufacturing sector awaits novel quality management strategies to verify 3D printed parts are fit for purpose. A review of literature shows industrial entities are now moving their research focus to develop new non-destructive technologies. This paper reviews the Additive Manufacturing quality space, the new research focus to develop quality management strategies for this space and justify this need through a study of two existing technologies. The two testing technologies (tensile testing and Scanning Electron Microscopy [SEM]), were judged on their ability to detect defects in 3D printed parts. The experiment performed aimed to provide a comparative study, of the testing technologies, to better understand current quality management processes in the 3D printing space. This research study was conducted to provide the fundamental groundwork on which future Non-Destructive Testing research progress past. The study revealed the advantages of tensile and SEM testing methods, whilst highlighting a need for better technologies to cover the disadvantages.**

Keywords—Additive Manufacturing; Quality Management; Tensile Testing; 3D Printing; SEM analysis

I. Introduction

A major division in the Mechatronics Engineering research field, studies the development, characterization and refinement of technologies in Additive Manufacturing (AM). However, new research is moving into quality management and certification of the technologies in AM, to move the technology from a research/prototyping technique to an industrial standard manufacturing technology for high impact industries [1].

AM commonly referenced as 3D Printing (3DP), is a rapidly thriving manufacturing technique. This revolutionary technology works by constructing a variety of complex shapes via gradual layering techniques. [2]. This paper presents a study of different 3DP technologies. The extensive range of 3DP technologies has gained significant academic and industry interest from its ability to form complex geometries with customizable material properties [3]. Due to the fast advancement of 3DP technologies, there is a growing necessity for testing technologies, to provide Quality Assurance (QA) and Quality Control (QC). There is incentive to explore possible methodologies to implement better testing strategies for QA and QC. To do this, existing methods must first be reviewed to better understand the problem space. Additionally, the identification, recognition and understanding of defects within the technology is equally important. This paper draws conclusions on the ability of tested 3DP quality testing technologies, to determine the advantages and limitations of these technologies in relation to the AM field. Existing studies and reviewed literature reveals a vast number of defects/impurities that effect the mechanical properties of 3DP part; for each technology different defects exist.

The following subsections breakdown the research area to highlight the contribution and importance of each factor in relation to the current research and future research to be conducted.

A. Additive Manufacturing – 3DP Technologies

The vast and rapid development of 3DP technologies has produced several unique AM manufacturing methods. Appendix A illustrates this progression, displaying the types of 3DP, materials used, and the characterization summary of existing research performed to optimize the 3DP space. It is also a good indicator that the highly developed space needs to focus on quality assurance. The technologies are often categorized into 3 main depositions: Solid, Liquid and Powder based depositions [4]. This study examines samples from a variety of these technologies, to better visualize all related defects and the technologies ability to identify them.

B. Industry Interest and Progression

Extensive Research has now been performed in the Additive Manufacturing (AM) space to help standardize and certify each part of the manufacturing process. This includes machine, part, and material standardization [1]. Numerous testing strategies now exist to ensure each of these parameters meet the standard. However, it is now essential to certify the process as a whole. Industries such as General Electric (GE), who are working to integrate 3D Printing into their manufacturing procedures to create some of their commercial airline components need a new testing method to ensure their 3DP parts are all certified. Currently, samples from each batch are mechanically tested to determine whether they meet the standard. However, commonly known, inconsistencies exist within each batch and therefore they cannot state all samples meet the standard [5]. To do so, new quality strategies that can study the mechanical,

0-7695-6358-9/17/$31.00 ©2017 IEEE
DOI 10.1109/APWConCSE.2017.00047

Authorized licensed use limited to: Massey University. Downloaded on December 05,2021 at 07:28:21 UTC from IEEE Xplore. Restrictions apply.

MASSEY UNIVERSITY
GRADUATE RESEARCH SCHOOL

STATEMENT OF CONTRIBUTION
DOCTORATE WITH PUBLICATIONS/MANUSCRIPTS

We, the candidate and the candidate's Primary Supervisor, certify that all co-authors have consented to their work being included in the thesis and they have accepted the candidate's contribution as indicated below in the *Statement of Originality*.

Name of candidate:	Tanisha Pereira
Name/title of Primary Supervisor:	Prof. Johan Potgieter
Name of Research Output and full reference:	
The effect of reheating layers in metal additive manufacturing on the external surface finish of a printed part	
In which Chapter is the Manuscript /Published work:	Chapter 4
Please indicate:	
• The percentage of the manuscript/Published Work that was contributed by the candidate:	100%
and	
• Describe the contribution that the candidate has made to the Manuscript/Published Work:	
The candidate has written the majority of the manuscript. The candidate has conducted the experimentation and provided the analysis required for this publication.	
For manuscripts intended for publication please indicate target journal:	
Candidate's Signature:	Tanisha Pereira Digitally signed by Tanisha Pereira Date: 2021.12.05 20:18:16 +13'00'
Date:	5/12/2021
Primary Supervisor's Signature:	Johan Potgieter Digitally signed by Johan Potgieter Date: 2021.12.06 11:41:19 +13'00'
Date:	6/12/2021

(This form should appear at the end of each thesis chapter/section/appendix submitted as a manuscript/ publication or collected as an appendix at the end of the thesis)

2018 25th International Conference on Mechatronics and Machine Vision in Practice (M2VIP)

The effect of reheating layers in Metal Additive Manufacturing on the external surface finish of a printed part

1st Tanisha Pereira
School of Engineering and Advanced Technology
Massey University
Auckland, New Zealand
T.Pereira@massey.ac.nz

2nd Johan Potgieter
School of Engineering and Advanced Technology
Massey University
Auckland, New Zealand
J.Potgieter@massey.ac.nz

3rd John V Kennedy
GNS Science
Wellington, New Zealand
J.Kennedy@gns.cri.nz

4th Aamir Mukhtar
TiDA Ltd
Tauranga, New Zealand
aamir.mukhtar@tida.co.nz

5th Mike Fry
TiDA Ltd
Tauranga, New Zealand
mike.fry@tida.co.nz

***Abstract*— Additive Manufacturing (AM) is expanding out of the Rapid Prototyping space to an end user product manufacturing technology. The commercial interest in industry, has created research opportunities to study how quality assurance can be provided for AM end user parts. There are several concerns lacking solutions at this stage, one of which is the surface finish quality on a metal AM part. The unmodified printed part extracted from an AM metal printer, often has a rough finish on the exterior surface. When the support material is removed from the part, a rough texture from the prongs bonding the support layers and part layers often leaves an even rougher texture in associated areas. For this reason, AM parts require further maintenance, often media polishing, to achieve the parts required surface finish. In cases where structural and mechanical quality is required, the surface finish can have a detrimental impact.**

While there are several beneficial methods employed in Subtractive, Formative and Joining manufacturing processes to improve metal surface finish, the method of interest in this study is laser reheating. More specifically, the scope of this paper studies effect laser reheating has on the surface finish of AM prints. A review of similar processes for other AM metals is studied to determine testing parameters of interest. The experimental work performed focuses on testing specimens printed in a Direct Metal Printer (DMP), applied to Stainless Steel 17-4 PH powdered material. The aim of this experiment is to determine, through stronger bonding and further melting, whether a smoother and more polished surface can be achieved. The results of the experiment performed showed high laser power and scan speed result in a better polish with each repetition, but increased reheating on just one layer caused an inward collapse. Several quality inspection techniques are compared to determine which proves the most fruitful in a studying the surface finish of the samples. Testing methods utilized, include visual inspection techniques (human eye and Scanning Electron Microscopy (SEM)), mechanical tests (compression and micro-hardness testing) and NDE roughness profiling techniques (dye-penetrant, AFM and Surface Profilometer testing).

Keywords*— *Additive Manufacturing, Surface Finish improvement, DMP printing, SEM analysis, Quality Inspection, Layer reheating

I. Introduction

The Additive Manufacturing (AM) industry, commonly known for rapid prototyping, has now penetrated the commercial market, monopolizing on the complexity and customizability offered by the layer manufacturing technologies [1]. The unique layer by layer part production, enables manufacturers to produce complex product shapes, impossible to achieve through traditional (subtractive, formative or joining) manufacturing methods [2]. AM technologies have been developed to generate products using a range of materials; polymers, metals, ceramics and composites [3, 4]. The material classification of interest in this paper is metals, specifically Stainless Steel (SS). There are several metal AM machines [5-8], differentiated by their power source (laser or EBM), power deposition (sintering, melting etc.) and feedstock type (powder, wire etc.). Direct Metal Laser Sintering (DMLS) or Direct Metal Printing (DMP) [9] is a common metal AM process that can print complex metal parts from a 3D CAD (Computer Aided Design) file. Within the DMP printer, a powerful fiber laser is directed at a layer of fine metal powder (SS), where it selectively melts the powder particles to bind them together on a build plate. Following this a new layer of powder is added to the build plate and the process is repeated till the part is completed. This process has been proven to have a dense and homogenous material structure, with a more consistent quality in higher generation models. While industries such as Aerospace, Medical, Rapid Tooling, Automotive etc. have integrated metal printing into their manufacturing processes [10], there are still issues in AM that require further research to increase its capability. One of these issues is surface finish improvement [7].

Surface finish in AM is generally rough, and the layered manufacturing often exhibits a staircase effect. Reducing layer thickness could improve this issue [11]. However, it would require an accelerated scan speed, which could introduce undesirable defects with an increased build time (uneconomical). Literature documents several research methods that have been employed post print to improve the external surface finish of a part. Techniques include subtractive polishing and grinding methods, laser re-melting, laser polishing, shot peening etc. Dadbakhsh et al [12], creates a reference for laser polishing parameters for Laser

978-1-5386-7544-1/18/$31.00 ©2018 IEEE

Authorized licensed use limited to: Massey University. Downloaded on December 05,2021 at 07:28:24 UTC from IEEE Xplore. Restrictions apply.

MASSEY UNIVERSITY
GRADUATE RESEARCH SCHOOL

STATEMENT OF CONTRIBUTION
DOCTORATE WITH PUBLICATIONS/MANUSCRIPTS

We, the candidate and the candidate's Primary Supervisor, certify that all co-authors have consented to their work being included in the thesis and they have accepted the candidate's contribution as indicated below in the *Statement of Originality*.

Name of candidate:	Tanisha Pereira
Name/title of Primary Supervisor:	Prof. Johan Potgieter
Name of Research Output and full reference:	
. In-Situ low-power-laser-polishing of Direct-Metal-Printed specimens for an improved surface finish.	
In which Chapter is the Manuscript /Published work:	Chapter 4
Please indicate:	
• The percentage of the manuscript/Published Work that was contributed by the candidate:	100%
and	
• Describe the contribution that the candidate has made to the Manuscript/Published Work:	
The candidate has written the majority of the manuscript. The candidate has conducted the experimentation and provided the analysis required for this publication.	
For manuscripts intended for publication please indicate target journal:	
Candidate's Signature:	Tanisha Pereira Digitally signed by Tanisha Pereira Date: 2021.12.05 20:18:16 +13'00'
Date:	5/12/2021
Primary Supervisor's Signature:	Johan Potgieter Digitally signed by Johan Potgieter Date: 2021.12.06 11:41:41 +13'00'
Date:	6/12/2021

(This form should appear at the end of each thesis chapter/section/appendix submitted as a manuscript/ publication or collected as an appendix at the end of the thesis)

In-situ low-power-laser-polishing of Direct-Metal-Printed specimens for an improved surface finish

Author: Tanisha Pereira, Year: 3rd year PhD Candidate, Affiliation: Massey University
Co-Authors: Prof. Johan Potgieter, Dr John Kennedy , Dr Jonathan Zyzalo,

Introduction

The surface quality of Laser-Powder-Bed-Fusion (LPBF) [Figure 3] Metal Additive Manufactured (MAM) parts, is an established issue, with the staircase like effect created on the surface from the layered nature of the process. The rough texture leaves an undesirable finish that is not only visually unappealing but can cause geometric inaccuracies and serve as defect initiation (cracks etc.) sites. Surface finish in LPBF AM as-built parts exhibit considerable surface roughness, ranging from 5µm to 25µm. Additionally, different faces of a LPBF part exhibit different surface textures/roughness; [Figure 1a] the top face always has the best surface finish, [Figure 1b] faces that have support material are the roughest, [Figure 1c] the sides of a part, effected also by its angle of lean, have a varying surface roughness dependent on the staircase effect caused by the layering build procedure.

This research study characterizes the effect of laser re-melting [Figure 2] the external surface of Direct-Metal-Printed parts to determine if an improvement in surface roughness and texture can be achieved. Previous studies using laser polishing have proven the method to be successful, however the application commonly utilizes a high-powered laser (above 200W) instead and is performed after the part is removed from the printer.

The DMP printer used in this experiment is equipped with a low-powered laser (50W). This study examines taken into account the varying surface texture and roughness of each side of the printed part. Improving the surface finish with the DMP printer during print, will reduce the post-processing time required using subtractive machining tools and become a viable method to target internal channels inaccessible by conventional surface improvement tools.

Figure 1: Surfaces in a LPBF printed part; (a) the topmost flat (180°) surface, (b) surface connected to the support material and (c) leaned surface affected by its angle of lean (0-90°)

Surface Finish

Surface finish, alternatively known as surface texture or the surface topography, is the nature of a surface as defined by its characteristics (lay, surface roughness and waviness). Manufacturers often desire a specific surface finish for 1 of these 3 reasons; to visually improve its appearance or texture, remove perturbations to better fit between/into another part, and to control the process that results in the surface required. The key categories into which surface texture is often categorized are roughness, waviness, spacing and hybrid. Surface finish is popularly categorized by its surface roughness value (Ra), used to determine friction, wear, surface contact, lubrication, fatigue strength and tightness of joints.

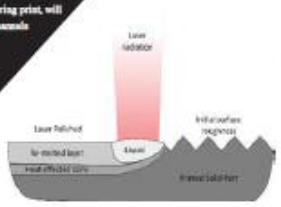

Figure 2: Laser Polishing/Re-melting process

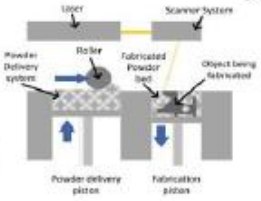

Figure 3: Laser-Powder-Bed-Fusion Process

Methodology

Figure 4: Top surface re-melting samples

Figure 5: 90° external e re-melting samples

Figure 6: 20°, 40°, 60°, 80° lean external surface re-melting samples

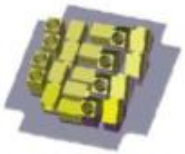

Figure 7: 0°,45°, and 90° internal surface re-melting samples

Figure 8: Curved external surface re-melting samples [sin(x), 2*sin(x) and 3*sin(x)]

This study examines the effect of varying laser power, laser speed and repetition, applied to the topmost surface (Figure 4) and different angled surfaces (Figure 5 & 6), for the external (Figure 4,5,6 &8) and internal walls (Figure 7) of a Direct Metal Printed part. The study applies several Taguchi method Design of Experiment studies, using an L9 (3x3) Taguchi Array design, for each surface studied with the same range of laser settings [laser power (30W, 35W and 40W), laser speed (100 mm/s, 500 mm/s and 1000 mm/s) and repetition (1,3 and 5 times). Only the outline (Figure 9) of the printed surface applies these settings to each layer; all printed specimens created in this experiment were manufactured in the DMP printer (inerted with Nitrogen gas), using Stainless Steel 17-4 PH, at its most optimized print settings, with 98% (49W) laser power and 340mm/s laser speed. The printed specimens (15mm x 15mm) were removed from the build plate using a Horizontal bandsaw. A surface roughness Gauge (Stylus parameters: material – Diamond, measurement angle - 90°, 5µmR), Optical Microscope, Scanning Electron Microscope (Hitachi TM3030Plus) and Vickers Hardness Tester were used to characterize the changes produced in each test specimen. Further testing is currently being performed. An initial study with a L16 (8^1, 2^2) Taguchi array was performed to study the laser power (LP) ranging from 10% to 90%, with varying hatch spacing (HP) (50µm & 100µm) and repetition (RP) (1/2) the results are shown below.

Summary and Future Work

To date this research study has shown the laser power ranging from 10-50% has minimal/negative effect on the surface roughness (Ra and Rz) profiles of the re-melted specimens. Laser power set at 60%, 70% and 80% demonstrated a higher potential to decrease the roughness of the samples, and were therefore chosen as the key settings in the Taguchi experiments described in the methodology. Testing for the other parameters and surfaces is still underway to study the effect of speed and repetition of the laser power and speed settings.

Outline Profile

The layer image on the right illustrates the difference between the entire part being melted and just the outline. For the outer angled and curved surfaces just the outline is selected for re-melting. For the top most surface the entire part layer as shown in the left image is selected for re-melting.

Results – Top Surface

This section provides a summary of results from the initial study mentioned at the end of the methodology for the laser polishing performed on the top surface of the samples. As shown in Figure 10, Sample 13 (70% LP, 50 HP and 2 RP), showed the most improvement, with the highest decrease in roughness (Ra) compared to sample 0 (Original – not re-melted). Because Samples 11 through to 15 also exhibited a significant improvement in surface roughness, the LP at 60%, 70% and 80% was chosen for the outline experiments detailed above. The hardness (HV) average of each specimen is illustrated in Figure 11, ranging from 308 HV - 363 HV. The typical hardness of Stainless Steel 17-4 PH according to printer datasheet, states the hardness should be ~300 ± 40 HV. Figure 9 provides one examples of the microscopic topography of one of the specimens in Sample 13's trials, it illustrates the thickness of weld lines after re-melting. The weld line thickness average of a perfectly printed sample should average around 70 µm, shown in the Sample 13 specimen shown in Figure 9. This initial test provides confidence that the surface texture and roughness of a DMP printed sample can be improved during print.

Figure 9: Optical microscope capture of weld lines (most improved sample (13)).

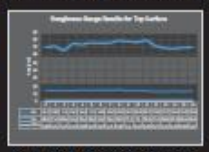

Figure 10: Surface profile parameter average for top surface experiment (all samples)

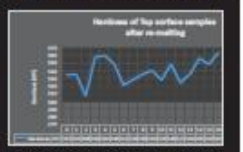

Figure 11: Average Hardness values for each test in the top surface re-melting study

References

[1] Pereira, T., et al. The effect of remelting layers in Metal Additive Manufacturing on the external surface finish of a printed part. In 2018 28th International Conference on Mechatronics and Machine Vision in Practice (M2VIP). 2018. IEEE.
[2] Ghorbani, L., E. Carrell, and C. Stanford. Tricycle laser polishing: effect of laser path and model gap. In CIRP ICME'14-6th CIRP Conference on Intelligent Computation in Manufacturing Engineering. 2014. Gardone.
[3] Yang, L., H. Ou, and A. Lassell. Surface treatment of Ti6Al4V parts made by powder bed fusion additive manufacturing processes using electropolishing. In Proceedings of the Solid Freeform Fabrication (SFF) Symposium, Austin, TX, USA. 2014.
[4] Gadelmawi, S., L. Hao, and C.K. King. Surface finish improvement of SLM samples using laser polishing. Virtual and Physical Prototyping, 2010. 5(4): p. 219-221.
[5] Erikinan, A. and Y. Fang. Review on mechanism and process of surface polishing using lasers. Frontiers of Mechanical Engineering, 2010. p. 1-10.

MaDe Manufacturing, Design, Entrepreneurship New Zealand